CRPP

CENTRE DE RECHERCHES EN PHYSIQUE DES PLASMAS
FACULTÉ DES SCIENCES DE BASE - EPFL
ASSOCIATION EURATOM – CONFÉDÉRATION SUISSE

ÉCOLE POLYTECHNIQUE
FÉDÉRALE DE LAUSANNE

ANNUAL REPORT

2004

Table of contents

1 INTRODUCTION

1.1 The political scene in the field of magnetic fusion in 2004

The ITER project will be the next major step in fusion research. In 2004, the siting of ITER remained the primary issue, with both the EU and Japan continuing to defend their candidate sites. Since June 2004, the negotiations between the ITER Parties, China, the EU, Japan, Russia, South Korea and the USA, have considered a "Broader Approach" which includes all the programmatic elements necessary to progress towards the ultimate goal, namely the construction of the first fusion reactor. This Broader Approach involves jointly constructing and operating ITER itself, research on smaller devices to prepare for the operation of ITER and research for the DEMO reactor including materials research centered around the International Fusion Material Irradiation Facility. In November 2004 the EU Council of Ministers stressed its strong support for the European ITER site and for maintaining, if possible, the involvement of all six Parties. Switzerland independently confirmed its vigorous support for the European ITER site. As a further positive sign, India and Brazil are now discussing entering the ITER agreement.

Discussions are going on concerning the extension of the working life of JET, the world's flagship experiment in tokamak research, by increasing its heating power and improving the power handling of the components which face the plasma by incorporating some of the concepts being developed for ITER. Enhancements to the measurement and control systems are also envisaged.

It is now vital to prepare the "Accompanying Programme" which will guide European fusion R&D during the construction of ITER. A document describing the elements of this "Accompanying Programme" is nearing completion. It will underline the commitment of the European fusion programme to keeping an active research base in preparation for the operational phase of ITER, and it will provide a basis for planning activities under the 7th Euratom Framework Programme, which will start in 2007.

1.2 The CRPP in 2004

2004 has been highly productive scientifically, both within the domestic programme and within international collaborations. As traditional, we highlight our major achievements this year.

- On the TCV tokamak, the most significant advance was to maintain the absorption of our Electron Cyclotron heating power at three times the resonance frequency, by careful control of the orientation of the high-power microwave beam.
- Electron Cyclotron power at twice the resonance frequency creates a strong thermal barrier inside the plasma. This barrier is created very quickly but is not linked with particular values of the magnetic field line helicity, contrary to other tokamak experiments.
- Studies on turbulence in the edge plasma, which surrounds the hot core of TCV, have shown a remarkable statistical property. The turbulence belongs to

a single family of distribution functions in all measured conditions, providing a strong constraint on theoretical modelling.

- The development of a non-linear "gyrokinetic" model of plasma turbulence remains a priority goal of the CRPP theory group. In 2004, simulations included the whole toroidal coupling of so-called "zonal flows" for the first time and illustrated the complexity of the turbulence evolution.
- A new code for Alfvén and ion cyclotron frequency plasma waves has been developed for tokamaks and stellarators and runs orders of magnitude faster than the few similar codes worldwide. Mode conversion has been studied in stellarators for the first time using this new tool.
- The TORPEX experiment was fully operational in 2004 and a large effort was devoted to identifying the mechanisms of microwave plasma production and to characterising plasma instabilities, including their non-linear evolution.
- Techniques have been developed for the production of dense, mm-thick tungsten coatings by chemical vapour deposition for protecting steel against the aggressive first wall fusion reactor conditions of erosion, thermal shocks, high temperatures and high thermal loads.
- In the field of superconductivity, a joint with the lowest resistance ever obtained for an ITER conductor (0.7nano-Ohm) was developed and tested in SULTAN.
- The first physical signs of the future ITER gyrotron test stand are now visible in the CRPP technical halls, showing the way forwards over the next few years.
- The CRPP plasma processing group has been working with industry for several years. A new company, UNAXIS solar, now exploits the fruits of one particular collaboration, underlining the spin-off content of such collaborations which are often linked to improved quality control or improved production rates.

This wealth of results from CRPP scientists is once again reflected in a large number of overview, invited and contributed papers in major international conferences on both physics and technology, as well as in over 70 papers appearing in refereed journals in 2004.

Collaborations continue to play an important role in the activities of the CRPP, especially in the operation and exploitation of the JET tokamak and in the preparation of ITER. Scientific and technical links are being maintained and strengthened with national and international research institutions and industries.

A detailed description of all the results and activities can be found in the following pages. Almost all of these activities are carried out within the frame of the Euratom Contract of Association although the plasma processing research is funded outside this contract. Finally, the CRPP wishes to thank all the funding bodies, listed in Appendix G, which support its long-term research goals.

1 INTRODUCTION

1.1 La situation politique dans le domaine de la fusion magnétique en 2004

La prochaine étape majeure, dans la recherche en fusion, sera le projet ITER. En 2004, la question du choix du site pour ITER est restée centrale, l'UE et le Japon continuant de défendre leur candidature. Depuis le mois de juin 2004, les négociations entre les partenaires d'ITER - la Chine, l'UE, le Japon, la Corée du Sud et les USA - portent sur une approche plus large, incluant tous les éléments programmatiques nécessaires à progresser vers le but ultime, à savoir la construction du premier réacteur de fusion. Cette approche plus large implique la construction et l'exploitation conjointe d'ITER proprement dit, la recherche sur des machines plus petites pour préparer le fonctionnement d'ITER, ainsi que les études pour le réacteur DEMO, y compris la recherche sur les matériaux, qui est centrée sur l' «International Fusion Material Irradiation Facility». En novembre 2004, le Conseil des Ministres de l'UE a souligné qu'il supportait fermement le site européen d'ITER et s'est prononcé pour le maintien, si possible, de l'implication des six partenaires. La Suisse a confirmé indépendamment son soutien vigoureux pour le site européen d'ITER. Un signe positif supplémentaire a été donné par l'Inde et le Brésil qui discutent maintenant la possibilité d'entrer dans l'accord ITER.

Les discussions continuent à propos de l'extension de la période d'activité du tokamak JET (Joint European Torus), le « vaisseau amiral » de la recherche en fusion magnétique au niveau mondial. Il s'agirait d'augmenter la puissance de chauffage et d'améliorer la capacité des composants qui font face au plasma à soutenir la puissance, tout en incorporant quelques-uns des concepts développés pour ITER. Des améliorations des systèmes de mesure et de contrôle sont également envisagées.

Il est maintenant vital de préparer le « Programme d'Accompagnement » qui guidera la Recherche et Développement européenne en fusion pendant la construction d'ITER. La rédaction d'un document, décrivant les éléments de ce « Programme d'Accompagnement », est près d'être terminée. Il soulignera l'engagement du programme de fusion européen à maintenir une base de recherche active, en préparation de la phase opérationnelle d'ITER. Il fournira une base pour la planification des activités du 7^{e} Programme Cadre de l'Euratom qui commencera en 2007.

1.2 Le CRPP en 2004

L'année 2004 a été fortement productive, à la fois dans le programme national et dans le cadre de collaborations internationales. Nous résumons ici les hauts faits de l'année écoulée.

- Sur le tokamak TCV (Tokamak à Configuration Variable), une percée significative a été de maintenir une bonne absorption de la puissance micro-ondes à la 3ème harmonique cyclotronique électronique, grâce à un contrôle soigné de l'orientation du faisceau micro-ondes de haute puissance.

- L'application de puissance micro-ondes à la 2ème harmonique permet la création de fortes barrières de transport dans le plasma de TCV. La création

de ces barrières est très rapide, mais elle n'est pas corrélée à des valeurs particulières de l'hélicité des lignes de champ magnétique, contrairement à certaines expériences menées sur d'autres tokamaks.

- Des études de la turbulence dans le plasma de bord, qui entoure le cœur chaud de TCV, ont montré une propriété statistique remarquable. La turbulence appartient à une famille unique de distributions de probabilité, dans toutes les conditions mesurées, ce qui fournit une forte contrainte sur la modélisation théorique.

- Le développement d'un modèle « gyro-cinétique » non linéaire de la turbulence du plasma reste une priorité du groupe théorique du CRPP. En 2004, des simulations tenant compte du couplage torique des écoulements zonaux ont été réalisées pour la première fois et ont illustré la complexité de l'évolution de la turbulence.

- Un nouveau code de calcul numérique pour les ondes aux fréquences d'Alfvén et cyclotroniques ioniques, applicable aux tokamaks et aux stellerateurs, a été développé. Il est des ordres de grandeur plus rapide que les quelques autres codes similaires existant au monde. Grâce à ce nouvel outil, la conversion de modes a été étudiée pour la première fois dans les stellerateurs.

- L'expérience TORPEX a été complètement opérationnelle en 2004, et un important effort a été dédié à identifier les mécanismes de production de plasma par micro-ondes et à caractériser les instabilités du plasma, y compris leur évolution non linéaire.

- Des techniques ont été développées pour la production de couches denses de tungstène, ayant des épaisseurs de l'ordre du millimètre, par déposition chimique en phase vapeur. Ces couches sont destinées à protéger l'acier de la paroi interne d'un futur réacteur contre l'érosion, les chocs thermiques, les hautes températures et les charges thermiques élevées.

- Dans le domaine de la supraconductivité, une jonction ayant la plus faible résistance jamais obtenue pour un conducteur d'ITER (0.7 nano Ohm) a été développée et testée dans l'installation SULTAN.

- Les premiers signes concrets du stand de test pour les futurs gyrotrons d'ITER sont maintenant visibles dans les halles techniques du CRPP, ouvrant la voie aux activités des prochaines années.

- Le groupe des procédés à plasmas du CRPP travaille depuis de nombreuses années avec l'industrie. Une nouvelle entreprise, UNAXIS Solar, exploite actuellement les fruits des retombées technologiques résultant d'une de ces collaborations qui portent souvent sur l'amélioration du contrôle de qualité ou de la productivité.

Cette abondance de résultats obtenus par les chercheurs du CRPP se reflète une nouvelle fois dans un grand nombre de papiers de revue, de papiers invités et contribués dans les conférences internationales majeures de physique et de technologie, ainsi que dans plus de 70 articles parus en 2004 dans des revues avec arbitrage.

Les collaborations continuent à jouer un rôle important dans les activités du CRPP, particulièrement en ce qui concerne l'opération et l'exploitation du tokamak JET et les préparatifs pour ITER. Les liens scientifiques et techniques sont maintenus et

renforcés avec les institutions de recherche nationales, internationales et l'industrie.

Une description détaillée des résultats et des activités est donnée dans les pages suivantes. Pratiquement toutes ces activités ont été exécutées dans le cadre du contrat d'association avec Euratom, à l'exception de la recherche sur les procédés plasmas, qui est financée en dehors de ce contrat.

Pour terminer, le CRPP exprime ses remerciements à tous ses bailleurs de fonds, énumérés dans l'appendice G, qui soutiennent ses buts de recherche à long terme.

1 EINLEITUNG

1.1 Die kontrollierte Kernfusion im Jahr 2004 aus politischer Sicht

Das Projekt ITER ist der nächste bedeutende Schritt auf dem Weg zum Fusionsreaktor. Im Jahr 2004 sollte in erster Linie über den Standort von ITER entschieden werden; in dieser Frage verteidigten sowohl die Europäische Union (EU) als auch Japan weiterhin jeweils die eigene Kandidatur. Seit Juni 2004 wurde zwischen den ITER Partnern China, EU, Japan, Russland, Südkorea und den USA, auf einer „erweiterten Basis" verhandelt. Dabei wurden alle Programmpunkte mit einbezogen, die von Bedeutung sind, um das gesetzte Ziel eines Fusionreaktors zu erreichen. Diese „erweiterte Basis" umfasst die gemeinsamen Aktionen zum Bau und Betrieb von ITER, die Forschung an kleineren Maschinen zur Vorbereitung von ITER, Forschungsaktivitäten im Hinblick auf den DEMO Reaktor und Materialforschung, die an einer internationalen Anlage zur Bestrahlung mit Neutronen (IFMIF) durchgeführt werden soll.

Im November 2004 bestätigte der Ministerrat der EU seine Unterstützung für den europäischen Standort von ITER, sowie den Wunsch einer Verwirklichung unter Beteiligung aller sechs Partner. Unabhängig davon setzte sich auch die Schweiz nachdrücklich für den europäischen ITER Standort ein. Zusätzliche positive Zeichen wurden von Indien und Brasilien gesetzt, die ihre Absicht bekundet haben, der ITER Partnerschaft beizutreten.

Die Diskussionen um eine Verlängerung des JET Experiments, das zur Zeit als Flagschiff der Fusionsforschung betrachtet werden kann, gehen weiter. Die Pläne für die Zukunft umfassen die Erhöhung der Heizleistung und Verbesserungen in der Belastbarkeit von dem Plasma zugewandten Komponente der Gefässwand unter Berücksichtigung von Konzepten, die auch für ITER vorgesehen sind. Darüber hinaus sind Verbesserungen an den Einrichtungen zur Diagnostik und Kontrolle des Plasmas geplant.

In der gegenwärtigen Situation ist es äusserst wichtig, ein „begleitendes Programm" auszuarbeiten, mit dem die Leitlinien für die europäischen Aktivitäten in Forschung und Entwicklung während der Bauphase von ITER gesetzt werden. Die Ausarbeitung dieses Begleitprogramms ist nahezu abgeschlossen. Damit soll die Absicht des europäischen Fusionsprogramms hervorgehoben werden, im Hinblick auf die Vorbereitung und den Betrieb von ITER, die Basis einer aktiven Forschungstätigkeit zu erhalten. Es wird auch als Grundlage für die Planung der Forschung innerhalb des 7. Rahmenprogramms von EURATOM dienen, das im Jahr 2007 in Kraft treten wird.

1.2 Das CRPP im Jahr 2004

Sowohl im Hinblick auf die Forschungstätigkeit am eigenen Institut als auch bei der internationalen Zusammenarbeit war das Jahr 2003 äusserst erfolgreich. Traditionsgemäss geben wir im folgenden einen Ueberblick der herausragenden Ergebnisse :

- Der bedeutenste Fortschritt in Zusammenhang mit dem Tokamak TCV war die Verbesserung der Absorption von Elektronzyklotronwellen bei der

3.Harmonischen zur Heizung des Plasma. Die Schlüsselrolle spielte dabei die genau kontrollierte Ausrichtung des Mikrowellenstrahls .

- Die Plasmaheizung mit Elektronenzyklotron-Wellen bei der 2. Harmonischen ermöglicht die Erzeugung einer Transportbarriere im Innern des Plasmas. Im Gegensatz zu anderen Tokamaks wurde am TCV beobachtet, dass sich diese Barriere sehr rasch aufbaut und dass sie offensichtlich nicht an bestimmte Werte des Sicherheitsfaktors geknüpft ist, der die helische Verschraubung der Feldlinien beschreibt.

- Untersuchungen der Turbulenz im Plasmarandbereich haben interessante statistische Eigenschaften erkennen lassen. Gemäss den Beobachtungen lässt sich die Turbulenz für alle untersuchten Bedingungen durch eine einzige Klasse von Verteilungsfunktionen beschreiben. Daraus ergibt sich eine stark einschränkende Randbedingung für die Modelrechnungen.

- Die Entwicklung eines nicht-linearen gyro-kinetischen Models zur Beschreibung der Plasmaturbulenz ist weiterhin das vorrangige Ziel der Theorie-Gruppe. Im Jahre 2004 gelangen erstmals Simulationen unter Einbeziehung toroidaler Kopplung von sogenannten 'zonal flows' und zeigten damit die volle Komplexität in der zeitlichen Entwicklung von turbulenten Phenomenen.

- Zur Beschreibung von Alfvén- und Ionenzyklotronwellen wurde ein neuer Komputercode entwickelt, der sich sowohl auf Tokamaks als auch auf nicht-axial symmetrische Anordnungen, wie z.B. Stelleratoren, anwenden lässt. Dieser Code ist um Grössenordnungen schneller als vergleichbare Programme, die zur Zeit international verfügbar sind. Mit diesem Code konnte zum ersten Mal die Modenkonversion in einer Stelleratorkonfiguration untersucht werden.

- Die TORPEX Maschine war im Jahr 2004 in vollem Betrieb . Die Experimente waren in erster Linie Untersuchnungen zur Plasmaerzeugung mittels Mikrowellen, sowie der Charakterisierung von Instabilitäten und deren zeitlicher Entwicklung gewidmet.

- Auf dem Gebiet der Materialforschung wurden am CRPP spezielle, dichte Beschichtungen aus mm-dickem Wolfram entwickelt. Diese Schichten, die in einem chemischen Prozess in der Gasphase aufgebracht werden, sollen Stahlbauteile gegen die Aggression durch Erosion, thermische Schocks und hohe thermische Belastungen schützen, denen sie in der ersten Wand eines Fusionsreaktors ausgesetzt sein werden.

- Ein bedeutender Fortschritt auf dem Gebiet der supraleitenden Anschlüsse war die Entwicklung eines Leiterstücks für ITER mit einem bisher unerreichtenWiderstand von 0.7 NanoOhm. Dieses Leiterstück wurde auf dem Prüfstand SULTAN des CRPP getested.

- Am zukünftigen Gyrotron-Prüfstand wurde mit ersten vorbereitenden Arbeiten begonnen. Damit wird eine für die nächsten Jahre bedeutsame Aktivität erkennbar.

- Die Gruppe Plasmatechnologie des CRPP hat bereits während der vergangenen Jahre eine enge Zusammenarbeit mit der Industrie gepflegt. Inzwischen ist mit der Firma UNAXIS SOLAR ein neuer Partner hinzugekommen. Bei dieser Zusammenarbeit werden Erkenntnisse aus früheren Projekten ausgenutzt, wodurch die Bedeutung von ‚spin-offs' unter Beweis gestellt wird, die sich aus Gemeinschaftsprojekten mit der Industrie

ergeben, die häufig auf eine Verbesserung der Qualitätskontrolle und der Produktionsraten ausgerichtet sind.

Die Fülle von Ergebnissen, die von Wissenschaftlern am CRPP erzielt wurden, findet Ausdruck in zahlreichen Beiträgen zu bedeutenden internationalen Konferenzen auf den Gebieten von Physik und Technologie. Insbesondere wurden im Jahr 2004 mehr als 70 Artikel in renommierten Fachzeitschriften veröffentlicht.

Der internationalen Zusammenarbeit , insbesondere beim Betrieb von JET und bei den Vorbereitungen für ITER, wird am CRPP ein hoher Stellenwert eingeräumt. Die Verbindungen zu Partnern in Forschung und Industrie, im wissenschaftlichen und technischen Bereich, konnten erweitert und verstärkt werden.

Der folgende Bericht enthält eine detaillierte Zusammenstellung der Forschungstätigkeit und der daraus hervorgegangenen Ergebnisse. Der grösste Teil der Arbeiten fand im Rahmen des Assoziationsvertrags mit EURATOM statt, lediglich die Aktivitäten auf dem Gebiet der Plasmatechnik sind davon nicht betroffen und werden aus anderen Quellen finanziert.

Abschliessend möchten sich Leitung und Mitarbeiter des CRPP bei all denen bedanken (Liste der Förderer im Anhang G), die durch ihre Unterstützung diese auf lange Sicht angelegten Forschungsarbeiten ermöglichen.

1 INTRODUZIONE

1.1 Il panorama politico nel campo della fusione magnetica nel 2004

Il progetto ITER (Reattore Internazionale Sperimentale di tipo Tokamak) costituirà il prossimo grande traguardo della ricerca sulla fusione. Nel 2004, la collocazione geografica di ITER è rimasta la questione primaria, e sia l'Unione Europea che il Giappone hanno continuato a sostenere i propri rispettivi siti candidati. Dal giugno 2004 i negoziati tra i partecipanti, ovvero Cina, U.E., Giappone, Russia, Corea del Sud e Stati Uniti, hanno preso in considerazione un programma globale più vasto (noto come "Broader Approach"), comprendente tutti gli elementi programmatici necessari per il progresso verso il traguardo finale, che consiste nella costruzione del primo reattore a fusione. Tale programma globale comprende la costruzione e l'operazione congiunta di ITER, la ricerca condotta su dispositivi più piccoli per preparare l'operazione di ITER e la ricerca condotta in previsione del reattore DEMO, che comprende la ricerca sui materiali affidata al progettato Centro Internazionale di Irradiazione dei Materiali per la Fusione. Nel novembre 2004 il Consiglio dei Ministri dell'U.E ha espresso un forte sostegno al sito europeo per ITER e al mantenimento, nel limite del possibile, della partecipazione dei sei attuali membri. La Svizzera ha indipendentemente confermato il proprio massimo appoggio al sito europeo per ITER. Un ulteriore segnale positivo viene da India e Brasile, che stanno attualmente discutendo la possibilità di partecipare all'accordo su ITER.

Sono in corso discussioni sulla possibile estensione della vita del JET, l'esperimento di punta della ricerca mondiale sui tokamak, con piani di aumentare la potenza di riscaldamento e di migliorare la resistenza al calore dei componenti a contatto con il plasma, incorporandovi alcuni dei concetti in via di elaborazione per ITER. Sono inoltre previste ulteriori aggiunte ai sistemi di misura e di controllo del plasma.

La preparazione del "Programma di Supporto", che guiderà le attività di ricerca e sviluppo europee nella fusione durante la costruzione di ITER, è attualmente di vitale importanza. Un documento che precisa i diversi elementi del Programma di Supporto è in via di completamento. Questo documento sottolineerà l'impegno del programma di fusione europeo di mantenere una capacità di ricerca attiva in preparazione alla fase operativa di ITER; su di esso si baseranno le attività di pianificazione del settimo Programma Quadro dell'Euratom, che inizierà nel 2007.

1.2 Il CRPP nel 2004

Il 2004 è stato altamente produttivo dal punto di vista scientifico, nel contesto sia del programma nazionale sia delle collaborazioni internazionali. Come è d'uso, riportiamo di seguito i principali traguardi conseguiti quest'anno.

- Il più importante passo in avanti per il tokamak TCV è stato il conseguimento di un buon assorbimento della potenza di riscaldamento mediante onde di ciclotrone elettroniche (ECH) lanciate alla terza armonica della frequenza di ciclotrone, impiegando un preciso sistema di controllo dell'orientamento angolare del fascio di microonde ad alta potenza.
- Il riscaldamento mediante ECH alla seconda armonica permette di creare una forte barriera termica all'interno del plasma. La barriera si forma su una scala di tempo molto breve, ma non è legata a valori particolari dell'elicità

delle linee di campo magnetico, in contrasto con esperimenti su altri tokamak.

- Studi sulla turbolenza nel bordo del plasma, la regione che circonda il nucleo ad alta temperatura di TCV, hanno rivelato una notevole proprietà statistica: la turbolenza è descritta da una sola famiglia di funzioni di distribuzione in tutte le condizioni di misura, permettendo di vincolare fortemente la modellizzazione teorica.
- Lo sviluppo di un modello girocinetico non lineare della turbolenza nel plasma rimane un progetto prioritario per il gruppo di teoria del CRPP. Simulazioni effettuate nel 2004 hanno incluso per la prima volta il completo accoppiamento toroidale dei flussi zonali, illustrando la complessità dell'evoluzione della turbolenza.
- Un nuovo programma di calcolo è stato scritto per descrivere la fisica delle onde di Alfvén e di ciclotrone ioniche in tokamak e stellarator. Questo programma è più rapido di svariati ordini di grandezza rispetto ai pochi simili programmi esistenti nel mondo. Grazie a questo nuovo strumento, la conversione di modo è stata studiata per la prima volta negli stellarator.
- TORPEX è stato pienamente operativo nel 2004, con un forte impegno nello studio dei meccanismi di produzione di plasma per mezzo di microonde e nella caratterizzazione delle instabilità del plasma fino alla loro evoluzione non lineare.
- Sono state sviluppate tecniche per produrre densi rivestimenti millimetrici di tungsteno mediante deposizione chimica di vapore, allo scopo di proteggere l'acciaio contro le condizioni inospitali della prima parete di un reattore a fusione, ossia l'erosione, gli sbalzi termici, le alte temperature e i forti carichi termici.
- Nel campo della superconduttività, è stata sviluppata, e sottoposta a prove in SULTAN, una giunzione dalla più bassa resistenza mai ottenuta per un conduttore per ITER (0.7nano-ohm).
- I primi elementi fisici del futuro banco di prova dei girotroni di ITER sono ora presenti nei laboratori del CRPP, illustrazione visibile dell'orientamento del Centro per i prossimi anni.
- Il gruppo specializzato nei processi al plasma collabora con l'industria ormai da diversi anni. Una nuova società, UNAXIS solar, raccoglie ora i frutti di una specifica collaborazione, a sottolineare le potenzialità di spin-off di tali collaborazioni, spesso legate a un miglioramento del controllo di qualità o della produzione.

La ricchezza di questi risultati ottenuti dai ricercatori del CRPP si riflette una volta di più in un numero elevato di relazioni di compendio e invitate o ancora di contributi spontanei a congressi internazionali, sia di fisica che di tecnologia, e in oltre 70 articoli apparsi in riviste scientifiche internazionali nel corso del 2004.

Le collaborazioni esterne continuano a costituire un elemento importante delle attività del CRPP, soprattutto nell'operazione e utilizzazione del tokamak JET e nella preparazione di ITER. I legami scientifici e tecnici con istituti di ricerca e industrie nazionali e internazionali vengono continuamente mantenuti e rafforzati.

La descrizione dettagliata di tutti i nostri risultati e delle nostre attività è contenuta nelle pagine che seguono (solo in inglese). Quasi tutte queste attività si svolgono nel quadro del Contratto di Associazione Euratom, mentre la ricerca sui processi al plasma è finanziata da fonti esterne a tale contratto. Concludiamo infine questa introduzione ringraziando tutti gli organi, elencati nell'appendice G, da cui

riceviamo finanziamenti, per il loro sostegno dei nostri obiettivi di ricerca a lungo termine.

2 RESEARCH ACHIEVEMENTS OF THE CRPP IN 2004

2.1 The TCV tokamak

2.1.1 Overview of the experimental programme

The CRPP contributions to the field of experimental fusion physics are concentrated on the *Tokamak à Configuration Variable*, TCV, characterised by a major radius R=0.88m, a minor radius a<0.255m, a toroidal magnetic field B_t<1.54T and a vessel elongation of three. The injection of waves in the Electron Cyclotron frequency range constitutes the primary method to heat (ECH) and drive current non-inductively (ECCD) in the TCV plasma. The ECH and ECCD systems provide to a total power of up to 4.5MW, 3MW at the second harmonic (X2) and 1.5MW at the third harmonic (X3) of the electron cyclotron frequency.

The exceptional flexibility in its configuration, control and auxiliary heating systems makes TCV a unique tool worldwide to contribute to a number of crucial areas of research, of interest both for the next generation of burning plasma experiments, such as ITER, and for longer term developments towards an improvement of the magnetic confinement concept for fusion reactors. The TCV scientific programme aims at maintaining a balance between these two approaches, consolidating the knowledge of the presently developed tokamak scenarios and their operational limits on one hand, and exploring new plasma regimes and fundamental aspects of the physics that plays a role in obtaining, sustaining, heating, and confining them, on the other. Such an investigation of possible optimisations of the plasma performance beyond standard modes of operation for tokamaks relies on an adequate degree of control of a large variety of plasma shapes, pressure and electrical current profiles.

The scientific programme for the 2004 campaign was concentrated on five main themes:

- investigation of methods for improving the plasma performance in term of the plasma β, including studies of electron heat transport in shaped plasmas, of plasma rotation, of methods to heat high density plasmas and to control edge localised instabilities;
- physics of the interaction between waves and particles in the EC frequency range, for the optimisation of ECH and ECCD, in particular for the recently installed top-launched third harmonic ECH;
- physics of enhanced confinement regimes, in particular in the presence of internal transport barriers, investigating the barrier formation, the plasma response to an inductive current perturbation, and MHD activity;
- physics of energy and particle transport, including detailed studies of particle pinch mechanisms;
- divertor and edge physics, including a characterisation of density and potential fluctuations in the plasma scrape of layer, and investigations of the mechanisms behind the anomalous plasma detachment observed on TCV.

The experimental campaign in 2004 resumed at the end of May, after a shutdown that lasted about 6 months, and continued, with an interruption of one month, through September 2004. Investigations were conducted in ohmic and ECH-ECCD plasmas, with both X2 and X3. Although the analysis of the data collected during

the 2004 campaign is still ongoing, preliminary results are illustrated in the following Sections, whose structure essentially reflects that of the five main research themes of this year's programme.

2.1.2 Enhancement of Plasma Beta Using X2 and X3 ECH-ECCD

This section describes the TCV studies and developments aimed at understanding the conditions for improving the plasma β using Electron Cyclotron Heating and Current Drive (ECH and ECCD), in second and third harmonic mode (X2 and X3) and operation at high density. These include the study of electron transport over an extremely broad range of values for the temperature gradient as a function of plasma shape, a characterisation of the bulk plasma rotation profile and its relation with MHD and transport, the use of additional heating allowing access to different H-mode ELM regimes at X3 accessible high densities, and the experimental study of Electron Bernstein Emission (EBE) or EB Heating (EBH) to develop heating scenarios for densities above EC cut-off values.

Electron heat transport in shaped plasmas: electron temperature gradient variation experiments using ECH

Electron heat transport experiments were performed in 2003 in L-mode plasmas at two values of plasma triangularity, δ=0.2 and δ=0.4, using radially localised ECH to vary the normalised electron temperature gradient R/L_{Te} (with $L_{Te}=\nabla T_e/T_e$) over an unusually large range, Fig. 2.1.1. These experiments have been analysed in detail in 2004. Local gyro-fluid (GLF23) and global collisionless gyro-kinetic (LORB5) simulations have been performed to determine the micro-instabilities responsible for anomalous heat transport in these plasmas. Ion temperature gradient (ITG) and trapped electron (TE) modes are found to be unstable. This is summarised in Fig. 2.1.2, which shows that TE modes are the most unstable modes, except at the lowest R/L_{Te} values where they are stabilised and where ITG modes dominate. In all these plasmas, the high $Z_{eff}T_e/T_i$ values in these plasmas lead to a complete stabilisation of the electron temperature gradient (ETG) modes.

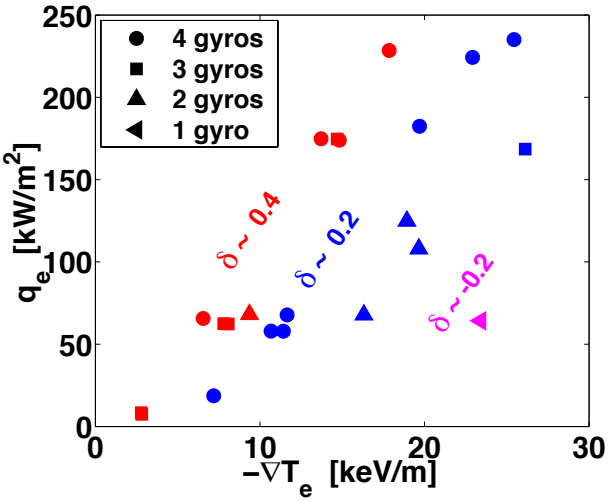

Fig. 2.1.1 *A large range of heat fluxes q_e and electron temperature gradients ∇T_e is explored at different triangularities. At constant heat flux, larger gradients are generated at lower triangularity.*

Experimentally, a strong dependence of the electron heat diffusivity χ_e on the electron temperature is observed, Fig. 2.1.3. On the other hand, in contrast with the results of GLF23 simulations, no clear dependence of χ_e on R/L_{Te} or R/L_{ne} is

observed. The plasma collisionality ν_{eff} is found to strongly reduce the electron heat transport, which is consistent with the stabilisation of TE modes while increasing ν_{eff} in the simulations. However, the variation of ν_{eff} with δ prevents us from quantifying the dependence of χ_e on δ. To answer this question, new experiments have been designed to keep ν_{eff} constant while δ varies from –0.4 to 0.4 and these are being analysed at present.

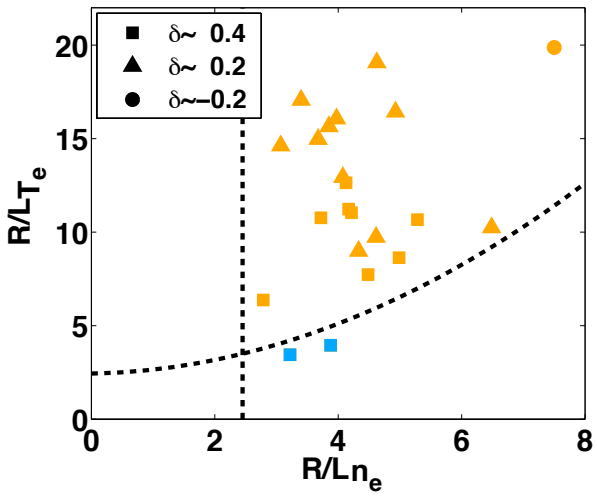

Fig. 2.1.2 *Experimental values of the two driving gradients for TE modes: R/L_{Te} and R/L_{ne}. When TE modes are dominating in GLF23 simulations, experimental points are shown in yellow, whereas when ITG modes dominate, they are shown in blue. The dashed lines indicate the pure TE threshold for a fluid model.*

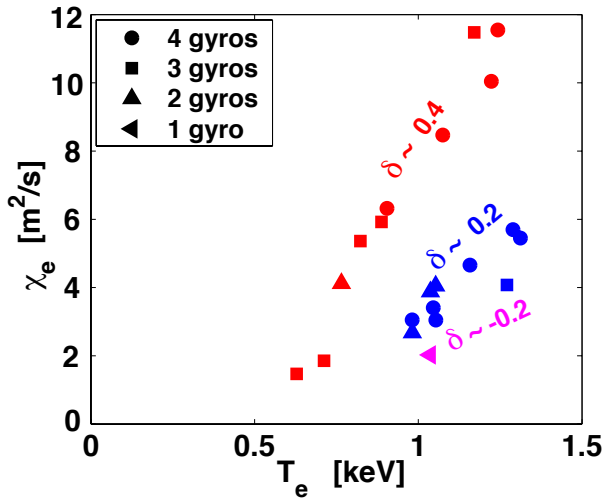

Fig. 2.1.3 *Electron heat diffusivity versus electron temperature, showing a clear step-linear dependence for δ=0.4*

Rotation measurements

In TCV the toroidal velocity profile of fully stripped carbon is measured by active Charge eXchange Recombination Spectroscopy (CXRS) with a temporal resolution of typically 100ms and a spatial resolution of 2-3cm. During the last campaign a series of experiments were explicitly designed and performed to systematically study the dependence of the toroidal rotation profiles on major plasma parameters, like the direction and intensity of the plasma current, electron density and plasma shape. All experiments were performed in quasi-stationary Ohmic L-mode, as this regime constitutes a unique test for any momentum transport theory.

Experiments with positive and negative plasma current clearly show that the carbon impurities flow at all radii in the counter-current direction and that the

profile symmetrically flips around zero when changing the sign of I_p, as can be seen in Fig. 2.1.4.

The rotation velocity profiles grow from the edge monotonically up to a certain region in the plasma close to the location of the sawtooth instability inversion radius ρ_{inv} (see Fig. 2.1.5). Inside ρ_{inv} the profile is flat or even hollow. As a result, increasing the plasma current flattens the toroidal rotation profile.

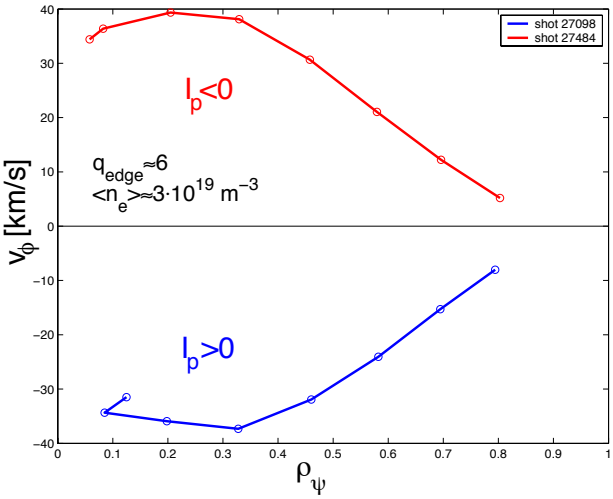

Fig. 2.1.4 *Toroidal rotation velocity profiles for positive and negative current for discharges with otherwise similar parameters*

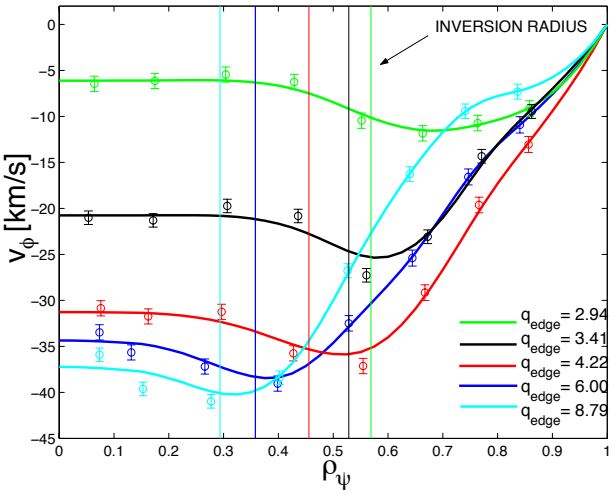

Fig. 2.1.5 *Toroidal rotation profiles in a plasma current scan for discharges with otherwise similar parameters. The location of ρ_{inv} is displayed with a vertical line of the same colour of the corresponding profile*

Additional Heating of ELMy H-mode Plasma

Experiments use additional heating to access ELMy H-mode regimes not accessible by Ohmic heating only. In typical Ohmic H-modes on TCV, ELMs have many characteristics of Type III. Previous attempts to use top launch X3 electron cyclotron heating have ended in a transition to ELM-free H-mode, and eventually in a disruption at high density.

Recent experiments using the full power (1.5MW) of the X3 heating system and an optimised target plasma have resulted in a change of ELMy H-mode regime. Figure 2.1.6 shows the transition from small ELMs to large ELMs at the introduction of X3 heating. The ELMs in the additionally heated phase exhibit a lower frequency and much larger (~10 times higher than the Ohmic phase) energy loss per ELM. Data from these experiments is still being analysed in an attempt to verify the ELM type in both the Ohmic and additionally heated phases.

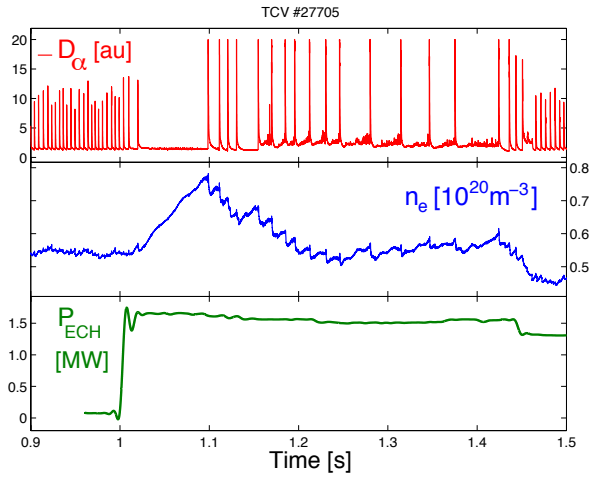

Fig. 2.1.6 *Transition to different ELM regimes with additional X3 heating power, as shown by the D_α emission (top trace). An initial ELM-free phase induces a density rise (middle trace), stabilised by the occurrence of large ELMs.*

Electron Bernstein Wave Emission and Heating (EBE & EBH)

Initial experiments have been performed in TCV to detect emission of electron cyclotron waves from overdense plasmas. Emission is expected to occur in O-mode with a specific wave vector determined by full mode conversion from an inward propagating X-mode at the O-mode cut-off. Such an inward propagating X-mode wave can in turn be generated by conversion from an electron Bernstein wave at the upper hybrid resonance. Not being subject to density cut-offs, electron Bernstein waves are emitted throughout the second harmonic electron cyclotron resonance surface. This scheme can thus be used to diagnose the electron temperature of overdense plasmas.

In this experiment an EC launcher was used in reverse as a receiver and connected to an ECE radiometer. The optimal emission angle was sought through angular sweeps of the launcher mirror. The signal had to be discriminated against a sizable polarization-independent background, which is believed to be random radiation reflected multiple times by the vacuum vessel walls. A significant excess signal, varying with the angle, is indeed measured in O-mode, as expected, and not in X-mode. The O-mode signal is shown in Fig. 2.1.7 as a function of time and frequency, along with the parallel wave number at the receiver. A preliminary comparison with conversion calculations performed by a ray tracing code suggests good qualitative agreement on the location of the signal maximum. Analysis of these data is in progress.

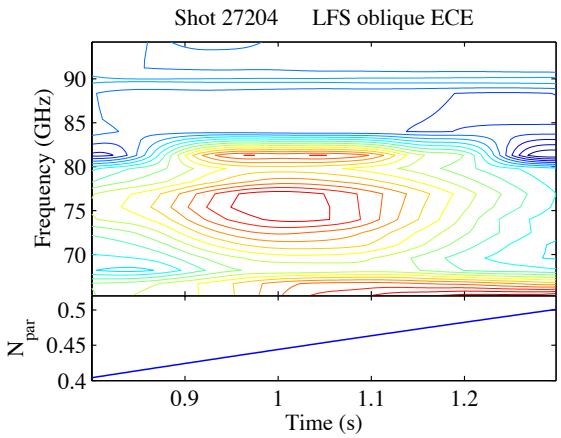

Fig. 2.1.7 *Electron cyclotron emission measured from a toroidaly swept ECH mirror launcher used in reception mode, showing a clear maximum of emission at N_{par}~0.45 and attributed to EBE*

ELM control

A few experimental sessions were devoted in 2004 to the investigation of the method to control ELMs based upon a perturbation of the plasma vertical position. The major goal of these sessions was to determine whether the magnetic perturbation triggers ELMs through a prompt or a cyclic mechanism. Since the sawteeth are also known to play a role in the ELM triggering, the interaction between sawteeth, magnetic perturbations and ELMs was addressed.

In previous experiments the perturbation frequency was smoothly ramped to measure the frequency range over which ELM triggering can be achieved. In the 2004 experiments, the time delay between perturbations was randomly set, within a predefined range. Figure 2.1.8 shows a fraction of a long pulse train in which three successive ELMs are in phase with the perturbation. In this example, the instantaneous frequency of the perturbation moves from 180Hz to 250Hz. Since the ELMs remain in phase with the perturbation despite the large change in frequency, the action of the perturbation onto the ELM seems to be prompt. In another experiment, a series of pulse trains were used as perturbation. The number of synchronisations found on the first pulse of a train seems to confirm the prompt character of the perturbation.

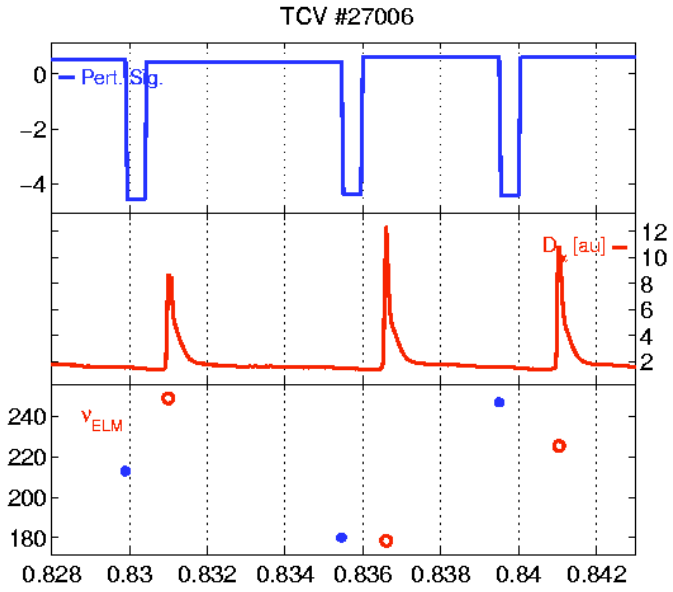

Fig. 2.1.8 *Example of synchronisation between the externally imposed perturbation (top trace) and the ELMs. The bottom plot shows the instantaneous frequency for the ELMs (red) and the external perturbation (blue)*

In the plasma target used in these experiments, the sawtooth frequency was approximately half the natural ELM frequency. When applying a constant perturbation frequency slightly higher than the natural ELM frequency, the pattern of the time delay between the perturbation and ELMs revealed the influence of the sawtooth on the ELM. For instance, the synchronisation of the ELM with the magnetic perturbation is lost when the perturbation occurs soon after a sawtooth

crash. On the other hand, the time delay between the magnetic perturbation and the ELM is decreasing with the phase within the sawtooth cycle.

2.1.3 Studies of EC wave-particle interaction

As a result of several years of intense study on TCV, EC heating and current drive has now become a highly reliable, versatile, and mostly well-understood tool that can be employed in a variety of studies of plasma confinement and stability, particularly in advanced tokamak regimes. The high degree of confidence with which this tool can be wielded is reflected in a shift of emphasis during this past year from fundamental ECH studies to ECH applications, as documented in this report. Nevertheless, the topic of EC wave-particle interaction is far from exhausted, and work has continued in particular on the physics of third harmonic ECH, following the recent commissioning of real-time launcher control.

Absorption of top-launched third harmonic ECH

The investigation of third harmonic (X3) ECH absorption was significantly simplified by real-time control of the launcher. This study was performed on L-mode plasmas with the main goal of determining the absorbed fraction as a function of plasma density at different levels of injected power. With mirror feedback control, the measurement was performed only after the mirror angle reached a stationary state. The absorbed power was measured during a modulated phase of the X3 pulse (full-power modulation of one gyrotron at 273Hz) using a diamagnetic loop. The diamagnetic flux modulation is related to the plasma energy modulation, which in turn, via a global power balance equation, yields the absorbed power fraction.

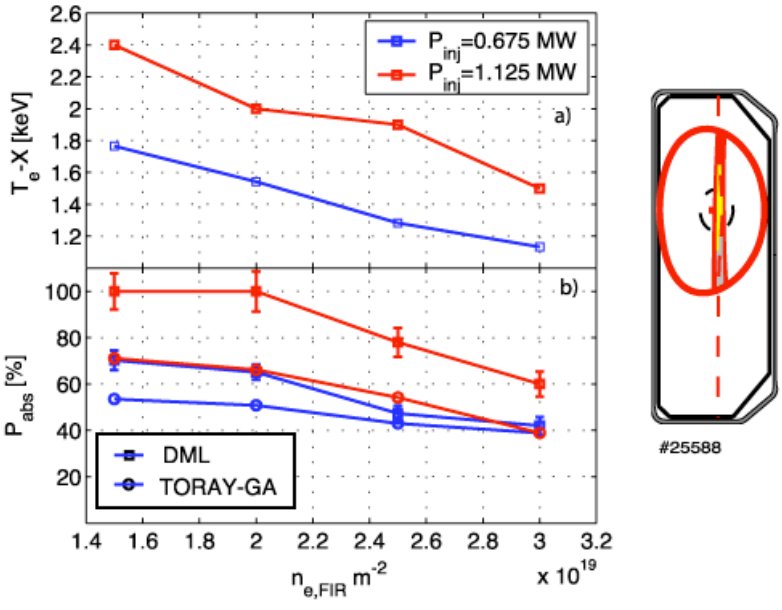

Fig. 2.1.9 *a) Central temperature versus line integrated density for two levels of X3 injected power. For the target plasma used, the value of the central density [m^{-3}], is twice the value of the line integrated density. The central temperature during the Ohmic heating phase (before the EC power injection) is 0.9 keV.*
b) Absorbed fraction measured with the DML (squares) and predicted by TORAY-GA (circles) versus line-integrated density for two levels of X3 injected power.

The absorbed fraction versus plasma density is shown in Fig. 2.1.9b for two different levels of average injected power, for a target plasma with a cross section as shown on the right of the figure (R_0=0.9m, a=0.26m, κ=1.55, δ=0.12, B_T=1.45T, I_p=230kA). The two levels of average injected power correspond to the sum of the average power of a fully square-wave modulated gyrotron (P_{av}=225kW) plus the power of one (450kW) or two (900kW) additional gyrotrons.

The difference between the measured absorbed fraction (DML) and the value predicted by the TORAY-GA ray tracing code is ascribed to the existence of a suprathermal population generated by the X3 wave itself. At higher electron densities this difference is lower since the increased collisionality causes a more rapid thermalisation of the suprathermal population.

Typical density and temperature profiles measured with the Thomson scattering diagnostic are shown in Fig. 2.1.10 for a central electron density of 4.10^{19} m^{-3}, which on Fig. 2.1.9 corresponds to a line integrated density of 2.10^{19} m^{-2}. The Ohmic profiles (squares) are time averaged during 100ms before the X3 is turned on and the profiles during the ECH phase are time averaged from the start of the ECH pulse until the modulation phase is started. At the X3 power switch on, a clear flattening of the density profile is observed. This "pump out" phenomenon has also been observed in X2 ECH and ECCD experiments on TCV as well as on ASDEX Upgrade.

Further studies of the X3 absorption properties at higher elongations and triangularities, along with a study of the coupling to the ions at high density, will be performed in the near future.

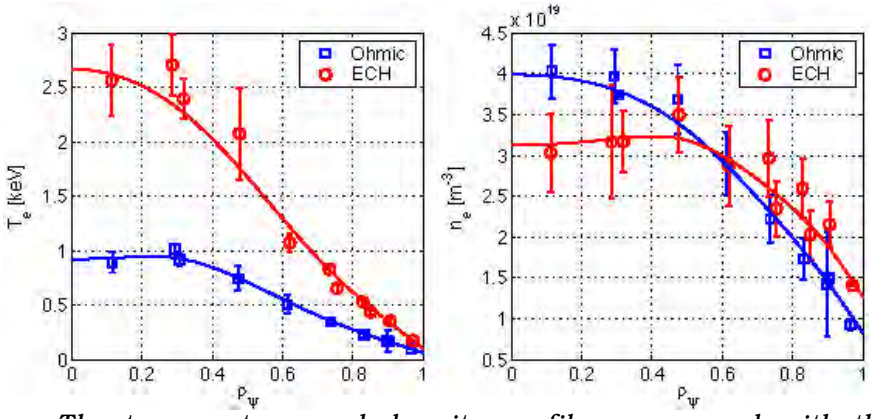

Fig. 2.1.10 *The temperature and density profiles measured with the Thomson scattering diagnostic for both Ohmic and ECH phases. This shot corresponds to a point in Figure 2.1.9 with P_{inj} =1.125MW and line integrated density of 2.10^{19} m^{-2}.*

2.1.4 Enhanced Confinement Regimes

Up until the end of the year, only a few designated experiments have been conducted on regimes with internal confinement barriers (experiments are scheduled for the beginning of 2005). However, analyses of plasma discharges from previous years have led to further understanding of the mechanisms behind the barrier formation, the confinement enhancement with ohmic current perturbations and the limitations imposed by MHD activity.

Barrier Formation

The procedure for obtaining non-inductively driven eITBs starts with an ohmic plasma in stable conditions. Then co-ECCD is applied off-axis, which sustains the plasma current and, coupled with the bootstrap current, generates a hollow current and a reversed shear profile leading to the barrier formation. The current profile evolution from a peaked (ohmic phase) to a hollow profile (enhanced confinement phase) occurs on a relatively slow timescale (~200ms) governed by the plasma internal inductance. Despite the slow evolution, a rapid formation of the electron internal transport barrier (eITB) is observed, while all external parameters remain constant as seen for example on the integrated soft X-ray emission chords Fig. 2.1.11a. The time constant for the barrier formation appears to be shorter than the electron energy confinement time (~2ms) and influences only the region inside the barrier position r=0.44 (Fig. 2.1.11b).

The contours of Fig. 2.1.11 indicate that an improvement in confinement is observed throughout the plasma core, although the soft X-ray intensity is integrated along a chord viewing the plasma cross section and cannot distinguish local effects. Recent improvements to the MPX diagnostics have enabled the inversion of the soft X-ray signal. Figure 2.1.12a shows several inverted soft X-ray emission profiles during the barrier formation. The barrier appears to form locally, with the increase in local emissivity first observed near ρ~0.3. Afterwards the barrier influences neighbouring flux surfaces both inside and outside ρ~0.3 as seen when plotting the time evolution of the local emissivity for different radial locations (Fig. 2.1.12b).

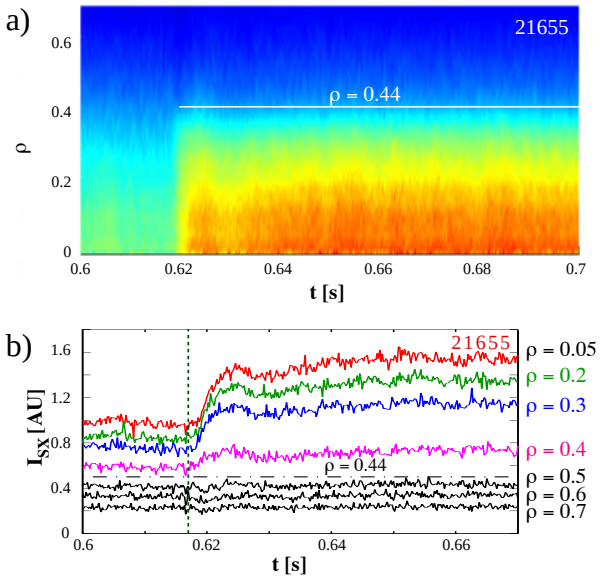

Fig. 2.1.11 *Temporal evolution of the line-integrated soft X-ray emission across the plasma cross section. The eITB forms near 0.62s during a gradual evolution from a peaked to a hollow current density profile while keeping all external actuators constant. (b) Lne-integrated soft X-ray emission viewed at selected values of ρduring the eITB transition; the barrier improves the confinement inside of ρ~0.44 (horizontal dashed-dotted line).*

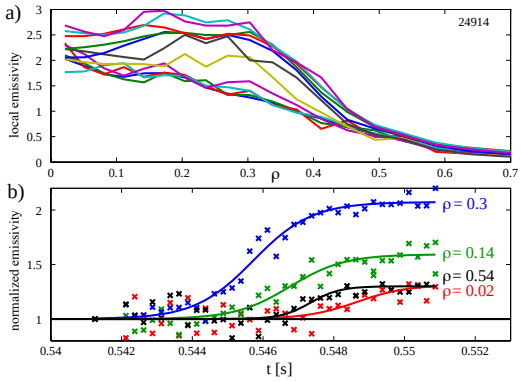

Fig. 2.1.12 *(a) Reconstructed local soft X-ray emission profiles averaged over 0.25s and plotted every 0.75ms during the barrier formation. (b) Temporal evolution of local soft X-ray emission normalized and plotted for selected radial locations. The barrier forms first at ρ ~0.3.*

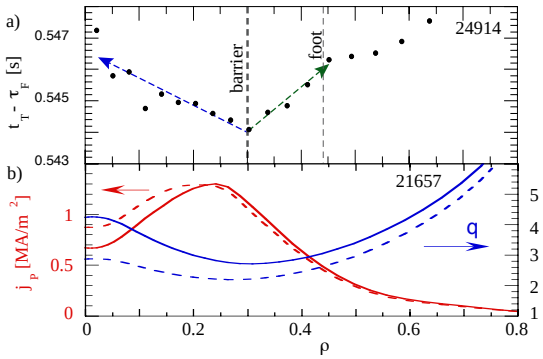

Fig. 2.1.13 *(a) The fitted rise time (t_T-τ_F) of the X-ray emissivity: the barrier forms at ρ~0.3 (vertical dashed line) and the effects then propagate inward (blue line) and outward (green line).*
(b) Calculated j_P and q-profile from the CQL3D code for shot #21657 (equivalent to #21655 and 24914 but in equilibrium conditions).

The barrier occurs rapidly and in a localised region. Using CQL3D (a Fokker-Planck code) the current density and q-profiles were calculated for a similar discharge under steady state conditions, Fig. 2.1.13. The location at which the barrier forms corresponds to the minimum in the q-profile (or the zero shear point). This comparison suggests that the barrier forms when and where the q-profile becomes inverted, and that the barrier formation is triggered by the appearance of a zero shear flux surface in the plasma.

Inductive current perturbation of eITB

After the barrier is formed, central heating or counter-current drive can be added to further enhance the confinement. The additional heating increases the central temperature leading to a steeper pressure gradient off-axis and to an increased bootstrap current. The counter-ECCD also increases the temperature and decreases the central current. Both effects tend to improve the confinement by increasing the hollowness of the current profile, resulting in a more inverted shear profile. ECCD alone cannot provide a current source without also heating the plasma. Instead, this can be accomplished using co- or counter-inductive current perturbations using a preprogrammed variation of the ohmic transformer current.

Inductive current perturbations have been performed during the central heating phase of the non-inductively driven eITB, with inductive current contributions varying from –50 to +50kA (I_P~90kA) adding a negligible source of ohmic heating of ~5kW (P_{ECH} ~1.5MW). The inductive current perturbation is introduced at 1.4s approximately 0.5s after the start of the central heating phase and the magnitude of the perturbation is varied on a pulse-to-pulse basis. Correspondingly, a significant improvement (degradation) is observed with the addition of a counter- (co-) inductive current as shown in Fig. 2.1.14. Since the inductive current profile is proportional to $T_e^{3/2}$ once steady state has been reached, the majority of the inductive current is in the core of the plasma where the temperature is the highest. In the case of a counter- inductive current perturbation the depth of the hollow current profile is increased and results in a more reversed shear profile and a confinement enhancement.

With the co- inductive current perturbation, the hollow current profile is partially filled, decreasing the reversed shear and the enhanced confinement performance, see Fig. 2.1.15. These experiments demonstrate that the confinement enhancement can be controlled by the current profile alone.

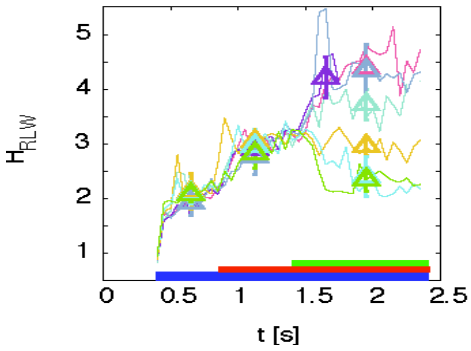

Fig. 2.1.14 *H_{RLW} factors for a series of shots in which inductive current perturbations are added at 1.4s. Confinement degrades with co-inductive current and improves with counter-inductive current relative to the heated eITB level of H_{RLW} ~ 3.*

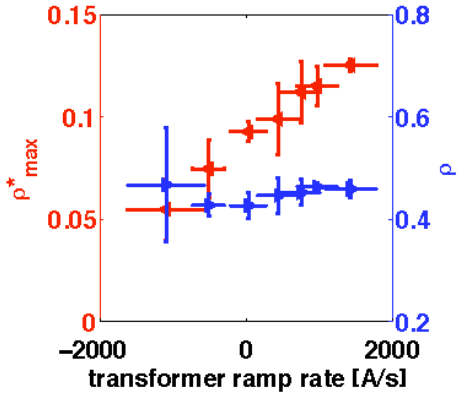

Fig. 2.1.15 *The barrier strength (green) and location (blue) for the same seven discharges as the previous figure. A ramp rate of 1000A/s corresponds to a loop voltage of 64.5mV in steady-state. Thus, the H_{RLW} increases as the barrier is strengthened by a reduction in the central current density and an increase in the bootstrap current off-axis near the barrier. The barrier location remains roughly constant.*

MHD activity in ohmic eITB

The regime of improved energy confinement in EC heated plasmas with formation of an eITB is characterised by a strong increase of the central electron temperature and usually only small changes of the electron density profile. As a consequence peaked pressure profiles are formed, in particular in cases with high power deposited in the centre, which are typical for scenarios using central counter ECCD to compensate the inductive current component. Furthermore large pressure gradients build up near the barrier location. This may lead to unfavourable of MHD stability.

During eITB scenarios on TCV, two basic types of MHD activity have been observed: tearing modes (TM) and kink-like modes near low order rational q-surfaces. The growth of a TM is usually correlated with a collapse in the central temperature and are seen as a rapid drop of the soft X-ray emission (SXR) (Figs 2.1.16a,b). Analysis of the signals from magnetic probes has allowed us to reconstruct the magnetic island associated with the TM, which in the case shown in Fig. 2.1.17 consists of two coupled modes (m/n=2 and m/n=3) localised near q=2 and q=3 in the region of positive shear outside the eITB. These large amplitude TMs destroy the ITB and lead to a significant decrease in energy confinement.

The kink-like modes can be identified in the SXR signals as periodic relaxation oscillations with a sawtooth-like signature. They are driven by high local pressure gradients, in particular in regions with low shear. Compared with TMs, their influence on the eITBs and the energy confinement is less pronounced when averaged over several oscillation periods. In Fig. 2.1.18, the sawtooth-like oscillations have an average period of about 25ms and disappear when the current profile is modified by an increase of central counter ECCD.

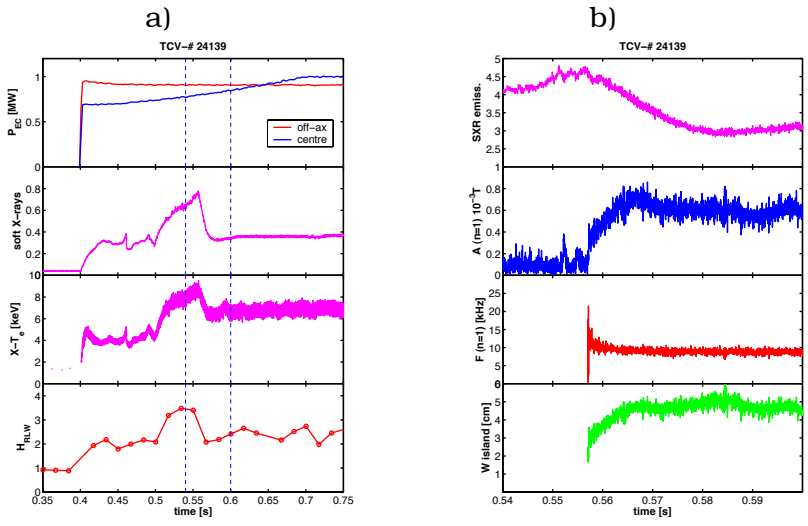

Fig. 2.1.16 *(a) Collapse event caused by the growth of tearing modes during a ramp of central counter ECCD for #24139. SXR reveals a rapid decrease of the central temperature. The decrease of the H-factor, calculated from Thompson scattering data, which are taken every 50ms, indicates a degradation of energy confinement. (b) Collapse event on an enlarged time scale (interval 0.54 to 0.60s), showing the decrease in the SXR signal and the evolution of the n=1 mode amplitude and frequency from magnetic measurements. The bottom trace shows the growth of the width of the island associated with the TM.*

The analysis of a series of eITB discharges has confirmed the existence of an experimental beta limit, associated with the peaking of the pressure profile (Fig. 2.1.19). Maximum beta values can be maintained with careful control of the pressure profile via an optimisation of the EC power levels and deposition locations.

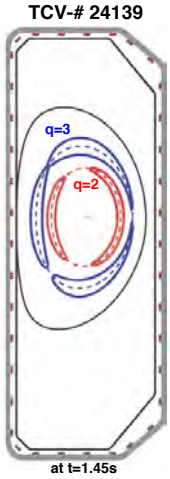

Fig. 2.1.17 *Reconstruction of the magnetic islands associated with TMs m/n=2/1 and 3/1 located near the q=2 and q=3 surfaces.*

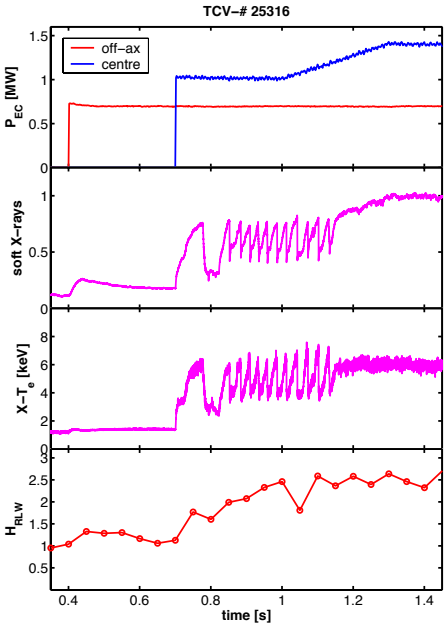

Fig. 2.1.18 *Example of sawtooth-like MHD activity near q=2, which is stabilised when the central counter ECCD is increased (#25316).*

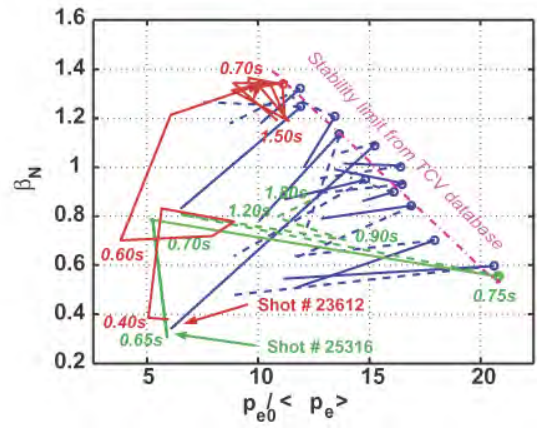

Fig. 2.1.19 *Experimental beta limit as a function of the pressure profile peaking factor. The data are obtained from a series of TCV discharges with eITB and with an inductive current component.*

2.1.5 Particle transport

Characterisation of particle pinches

Work carried out on TCV in previous years has demonstrated the existence of inward particle convection not attributable to the Ware pinch, especially in fully electron cyclotron current driven (ECCD) plasmas. These observations are in good agreement with expectations from Turbulent EquiPartition (TEP) theories or their fluid counterpart, the curvature pinch, in the collisionless limit. A puzzling finding is that peaked density profiles, indicating an inward pinch, are observed throughout the entire collisionality range accessible to TCV, not just in low collisionality plasmas where full ECCD is achieved. Experiments with modulation of the plasma density and current have been undertaken recently in Ohmic plasmas, to check whether density peaking at higher collisionality could be accounted for by the Ware pinch. Remarkably, even in discharges with fast current modulation, the density profiles appear to follow, with no or little delay, the evolution of the current profile, irrespective of the strongly varying parallel electric field (Fig. 2.1.20). These results are unambiguously incompatible with any model in which the Ware pinch is assumed to be the main cause of the inward pinch. Experiments where the density (and hence the collisionality) is varied show that beyond the dominant effect of the current profile, collisionality has a weak but measurable influence on the peakedness of the density profile. Density profiles are slightly more peaked at high average density than at low density for the same current and temperature profiles. Although the experimental data are still being analysed, they may reflect a weak collisionality dependence of the convection-to-diffusivity ratio due to anomalous transport, or may be a consequence of the Ware pinch.

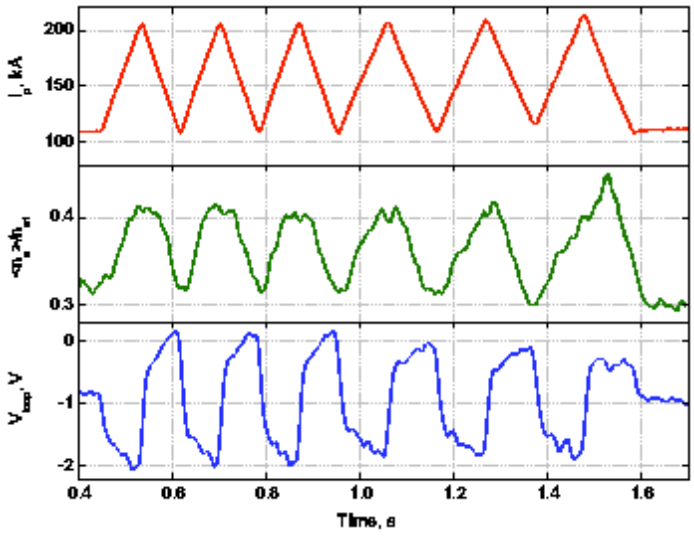

Fig. 2.1.20 *Current modulation experiment. Evolution of plasma current, width of density profile and loop voltage.*

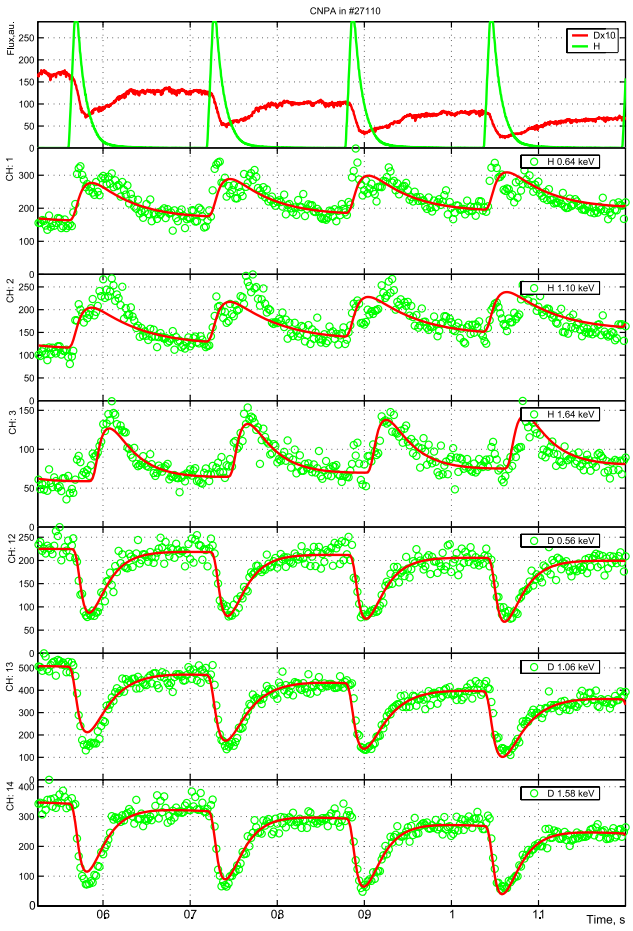

Fig. 2.1.21 *H and D fluxes from gas valves and CNPA count rates at three different energies in a TCV discharge with H-gas puff. (D flux is multiplied by 10). Experimental points – green circles, Fit – red lines.*

Isotope substitution experiments

The diffusion of plasma and impurity ions is to a large extent decoupled from the overall behaviour of the plasma electrons. Reactor operation will be influenced by the cross-diffusion of fuel, ash and impurity ions. The recent installation of the Compact Neutral Particle Analyser (CNPA), which is capable of simultaneously measuring neutral fluxes from two ion species (H and D or D and He) has permitted us to start ion transport investigations in isotope substitution experiments. In these experiments brief puffs of hydrogen were introduced into the discharge and their penetration into the plasma was assessed by measuring the changes in the fluxes of H and D neutrals, in the energy range 0.6-3keV. During the H-puff, the flux of hydrogen atoms from the plasma increases by a factor of 2-4, while the flux of deuterium neutrals decreases by a factor of 2-3 (Fig. 2.1.21). The time evolution of the fluxes can be modelled (red lines) using an effective confinement time (10-40ms, depending on conditions). Similar times are required for the H fluxes to establish Maxwellian spectra of the same temperature as the D background. Initial modelling of the data suggests diffusion coefficients for H in a D background in the range 0.3-1m^2/s. Systematic investigations of the effect of plasma parameters on ion transport have been initiated. A detailed analysis of these experiments will require the inclusion of a model for neutral and ion transport.

Impurity transport

Radially resolved measurements of CV K-α and CVI Lyman-α emission profiles using a four-channel multilayer mirror spectrometer operated jointly with IPP Prague have been modelled using the ionisation equilibrium code STRAHL, demonstrating that transport coefficients for intrinsic carbon in the plasma periphery (r/a>0.7) can be obtained from an analysis of the ionisation equilibrium. Because of the small number of chords, these experiments relied on a radial compression of the plasma in order to increase the resolution. Recent experiments have shown that, at least for the measurement of CVI profiles, a promising CV charge exchange line is available. If confirmed, this should expedite the measurement of impurity transport coefficients in the plasma periphery. The new method is expected to complement data obtained by the injection of medium Z impurities, such as laser ablated Si, in collaboration with KFKI, Budapest.

2.1.6 Edge and Divertor Physics

SOL density and potential fluctuations

Measurement and characterisation of density and potential fluctuations in the TCV scrape-off layer (SOL) has continued to be a main theme of edge physics research in 2004. Data collected in 2003 have been augmented in 2004 with an expansion towards a greater range of discharge conditions. Detailed analysis has continued with the result being some important new findings, in particular with regard to the statistical nature of density fluctuations. These results are summarised in Fig. 2.1.22, which demonstrates how SOL density turbulence on TCV is, as observed in other tokamaks, progressively more “bursty” with increasing distance from the separatrix, or last closed flux surface (LCFS). In the separatrix vicinity, the probability density function (PDF) of the turbulence is near Gaussian, becoming progressively more skewed as the plasma-wall interface is approached. At the wall, the PDF closely approximates a negative exponential distribution and is characterised by long correlation times and a power spectrum showing scale-free (self-similar) behaviour over more than two frequency decades. In fact, for a wide range of discharge conditions in TCV, including forward and reversed toroidal magnetic field, low and high density, D and He plasmas, ohmic L-mode and (inter-ELM) H-mode, the PDF of density turbulence at all radii within the SOL can be well described by a Gamma process. The latter has been observed to govern the statistics of many natural turbulent systems exhibiting clustering of events and intermittency.

Already at relatively short distances from the LCFS, the “cluster” parameter, $A=\langle n\rangle/\sigma$ describing the distribution, $\langle n\rangle$ being the mean density and σ the standard deviation) is observed to saturate at low values for all plasma conditions. One consequence of this behaviour is that fluctuations in the turbulent driven radial (i.e. cross-field) particle flux near the plasma-wall interface scale solely with the mean density there. This observation may have important practical applications for the estimation of expected ion fluxes at the main chamber walls of next step devices. The result that PDF’s are well matched by a Gamma process throughout the SOL may also provide a key observational parameter to be matched by numerical simulations of two-dimensional fluid turbulence.

Divertor detachment studies

Efforts have continued in 2004 to understand, through SOLPS5 code simulations, the anomalous divertor detachment regularly observed in TCV single-null lower ohmic discharges. Research during 2003 eliminated two suspected candidates: geometry effects and D_2 molecularly enhanced recombination (MAR). Further refinement has now allowed the inclusion of CD_4 molecules, representing the first ever attempt to include hydrocarbon MAR in a full fluid-Monte Carlo simulation of the SOL. This mechanism has also proved unable to account for the observed strong detachment.

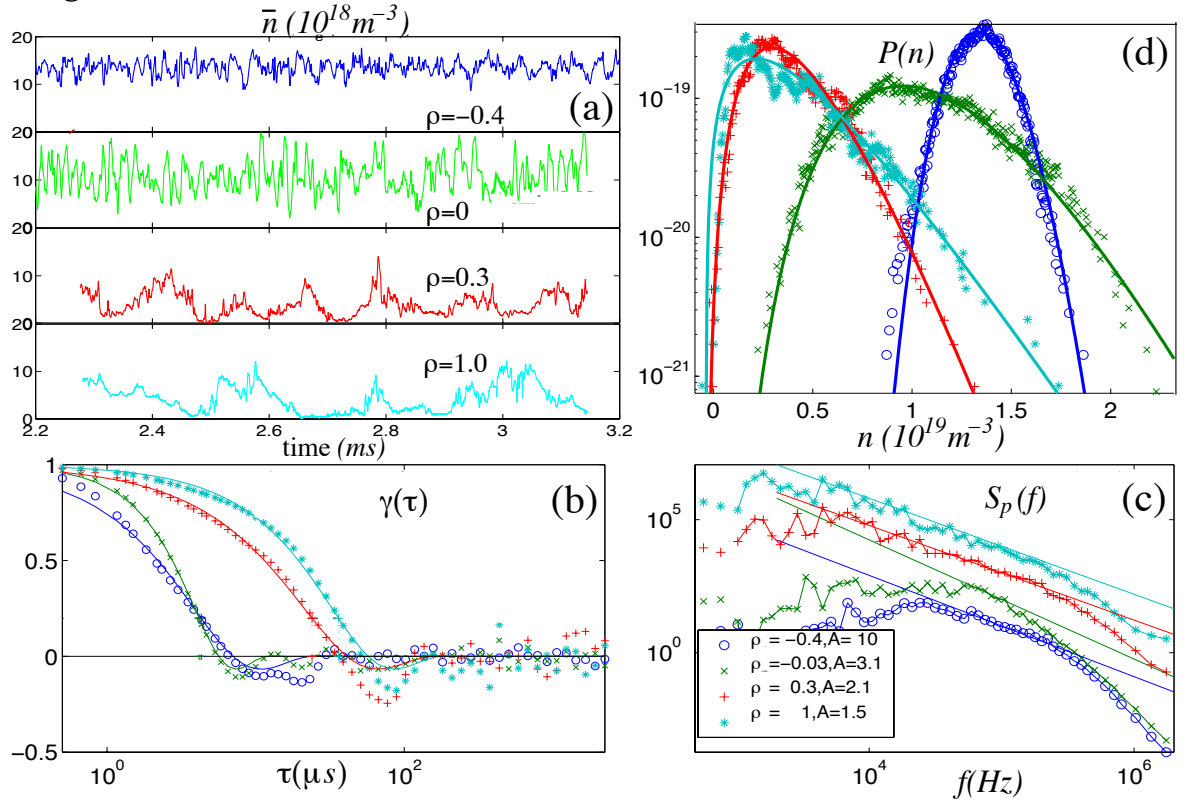

Fig. 2.1.22 *Characteristics of density fluctuations in the TCV SOL for a single-null lower, medium density ohmic discharge. (a) The SOL density at four radial positions (ρ is a normalised distance, with ρ =0 at the separatrix and ρ=1 at the wall) for short time intervals during which the fast reciprocating probe moves only a short distance. (b) The turbulence autocorrelation function at each location showing the increased correlation time with increasing distance into the SOL. The lines are a fit to the data using a modified functional form consistent with a turbulent process, which is self-similar or "scale-free". (c) The power spectrum, PS(f) and comparison with the scaling $S(f) \propto f^{-\beta}$ with β the cascade index which would be obtained in a scale-free cascade model. (d) PDF's of the density turbulence at the three radial locations showing the transition from a near Gaussian to a strongly skewed distribution as the wall is approached. The lines are Gamma distributions with the only fitting parameters being <n> and σ.*

One remaining candidate is the effect of anomalous transport processes in the main SOL. To date, TCV SOLPS5 simulations have employed a "standard" diffusive *ansatz* for the cross-field particle flux. Inspired by the strongly intermittent nature

of the density fluctuations, seen experimentally to drive a large cross-field flux, especially at high density, an anomalous convective transport term has been added, activated only in the low field side region of the plasma equilibrium. Whilst the introduction of such a term does not in itself enhance detachment, it turns out that the increased plasma-wall interaction that it provokes on the main chamber walls leads to increased impurity production which strongly influences the SOL energy balance (through radiation) and hence the power flux into the outer divertor. This establishes parallel temperature and density profiles along the outer divertor leg that make particle and momentum removal and hence early detachment possible. There are, in addition, indications that ion conversion processes (MAR) through both D_2 and CD_4 molecules can, under these conditions, contribute to the total reduction in particle flux.

Measurements of parallel flow in the TCV SOL have continued through 2004 with the addition to the database of matched discharges with reversed toroidal field, a study of the influence on the flow of X-point location (upper or lower) and a poloidal scan of the flow magnitude around the outboard ballooning region. Strong flow is present in TCV, as elsewhere, with magnitude dependent on density and direction on magnetic field direction. There is evidence for a correlation between the magnitude of cross-field turbulent transport and parallel flow, as observed recently in JET during similar measurements. Further analysis is required to determine if the measurements can prove that enhanced ballooning transport is a strong contributor to the anomalously high parallel flow.

A new array of tile embedded Langmuir probes has been installed during the recent shutdown on the outboard side of the vessel wall and symmetrically disposed above and below a vertical height corresponding to the magnetic axis of many single null lower diverted configurations used to study ELM physics. This diagnostic has operated successfully and shows that the ELM event does indeed propagate outward in the SOL, with sizeable ion currents being detected at the wall at the level of the magnetic axis, even for relatively small Type III ELMs. The signal amplitude decreases in amplitude with increasing distance from the axis. Acquisition speeds for this new array are up to 125kHz and, in conjunction with divertor target probe arrays, will allow the detailed study the relationship between parallel and perpendicular particle transport during the ELM.

2.2 Theory and numerical simulation

CRPP theory group follows its tradition of improving our understanding of basic magnetically confined plasmas, developing models of the stability and transport of axi-symmetric and 3D configurations. As this work progresses, each year sees more detailed comparisons between the predictions of theoretical models and the observations made in experiments, both at the CRPP and elsewhere.

2.2.1 Physics underlying anomalous transport

Numerical global gyrokinetic simulations

Ion temperature gradient (ITG)-driven instabilities evolve nonlinearly to a turbulent state characterised by the presence of a strong axisymmetric component called the zonal ExB flow. These ExB flows have the effect of reducing the turbulent fluctuation energy level. In toroidal systems, the zonal flows are coupled by geometrical effects. We have implemented in our gyrokinetic, global, finite element, PIC code ORB5 the correct formulation in the field equations, which require the resolution of an integral-differential system of equations. This new version has been successfully tested and first results indicate that this toroidal coupling term modifies the evolution of zonal flows and their sidebands (n=0, m=+-1), but has a relatively small effect on the level of turbulence for late nonlinear time evolution.

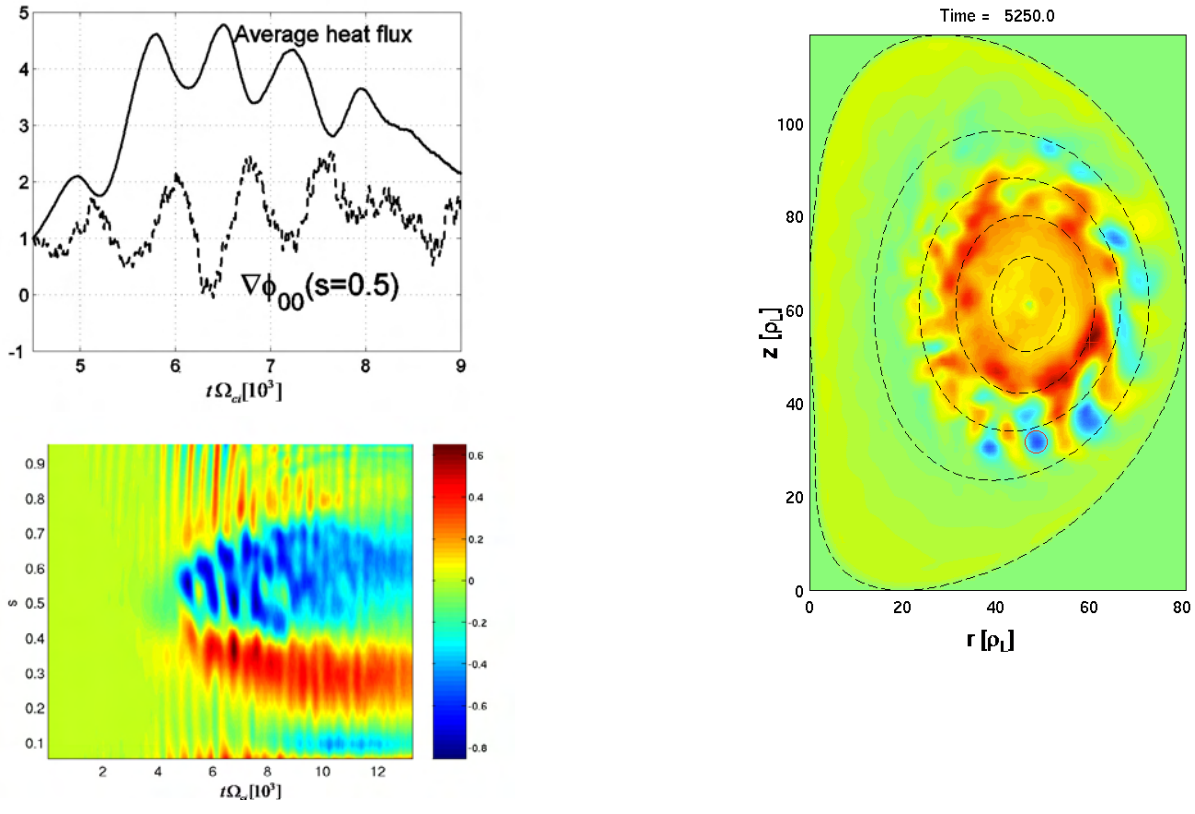

Fig. 2.2.1 *Global nonlinear gyrokinetic simulation in a TCV-shaped equilibrium. Contours of zonal ExB flow vs time and radius (top left). Contours of electrostatic potential in a plasma cross-section (top right). Bursts of heat flux and zonal ExB flow vs time (bottom left).*

We have observed the occurrence of successive bursts of turbulent amplitude, in the early stages of the nonlinear phase, accompanied by fast local flattening of the effective temperature profile and followed by bursts in zonal flow amplitude (Fig. 2.2.1, bottom). This avalanche-like process results in a fast radial spreading of the turbulence on a timescale comparable to the typical ITG growth times, much faster than diffusive transport time scales. In the later nonlinear stage, the system establishes a quasi steady state characterised by much broader zones than in the cylindrical case. Unlike in cylindrical simulations, we have observed oscillations of

the zonal component (Fig. 2.2.1, top) and attributed these to the excitation of Geodesic Acoustic Modes (GAM). A comparison with results obtained from another global gyrokinetic code (GT3D) has confirmed these observations. We have performed nonlinear simulations of ITG turbulence in TCV shaped plasmas given by MHD equilibria reconstructed from experimental data, in order to demonstrate this unique capability of the nonlinear code ORB5 (Fig. 2.2.1, right!. Another improvement has been made by implementing a new algorithm that avoids the need to perform a time integration of the perturbed part of the distribution function, δf, thus reducing the noise level, saving computing time and avoiding unphysical contributions to the drive of GAMs.

In another development, progress has been made on the global semi-Lagrangian numerical scheme which consists of solving for the full distribution function on a fixed grid in phase space and tracing the particle orbits back in time. Finite Larmor radius has been introduced. First results indicate that this has the effect of reducing the problem of small scales appearing in the solution. The next step will be to extend the code to toroidal axisymmetric geometry.

Linear gyrokinetic simulations

The global spectral gyrokinetic electromagnetic numerical code EM-GLOGYSTO has been upgraded to include the contribution of finite mass (non adiabatic) electrons to the electrostatic density fluctuations. For toroidal-ITG modes at zero β, the growth rate and real frequency with finite mass electrons remain unaffected compared with the case with zero mass (adiabatic) electrons. However, the eigenmode structure drastically changes with the inclusion of finite-mass electrons: sharp radial structures due to electron dynamics are introduced near the resonant magnetic surfaces (Fig. 2.2.2a,b), which affects the linear mixing length estimates of transport coefficient (Fig. 2.2.2c,d). In the electromagnetic studies (finite β) on Alfvén ITGs (AITGs) or Kinetic Ballooning Modes (KBMs), it is demonstrated that a combination of the pressure gradient parameter (α_{mhd}) and particle nonadiabaticity plays a central role in determining the properties of AITGs/KBMs. For example, it is shown that in the absence of trapped electrons, AITGs are unstable to Reverse Shear L-mode-like and H-mode-like plasmas. In the case of weak or zero shear, a new mode called low-n global Kinetic Infernal Mode (analogous to the MHD Infernal mode) has been found (Fig. 2.2.3). It is suggested that this new global mode with a large real frequency and an MHD-like growth rate may prove dangerous for some tokamak equilibria.

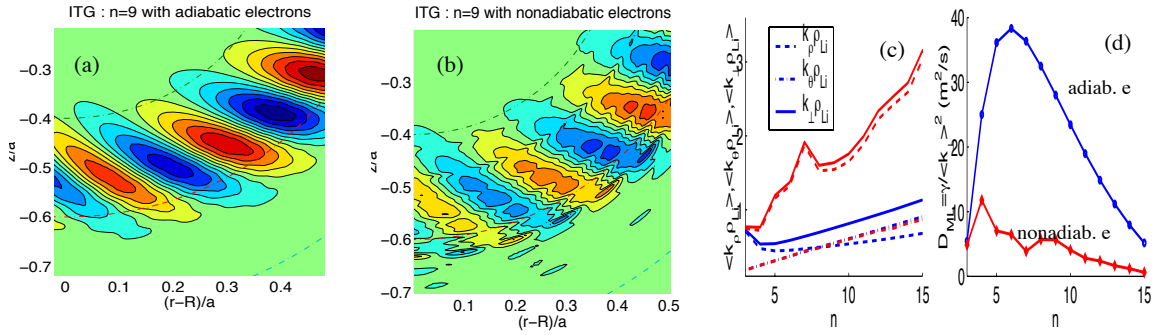

Fig. 2.2.2 *Eigenmode structures of toroidal ITGs with adiabatic (a) and nonadiabatic passing electrons (b). Averaged wavevectors (c) and coresponding mixing length estimates of diffusion coefficient (d).*

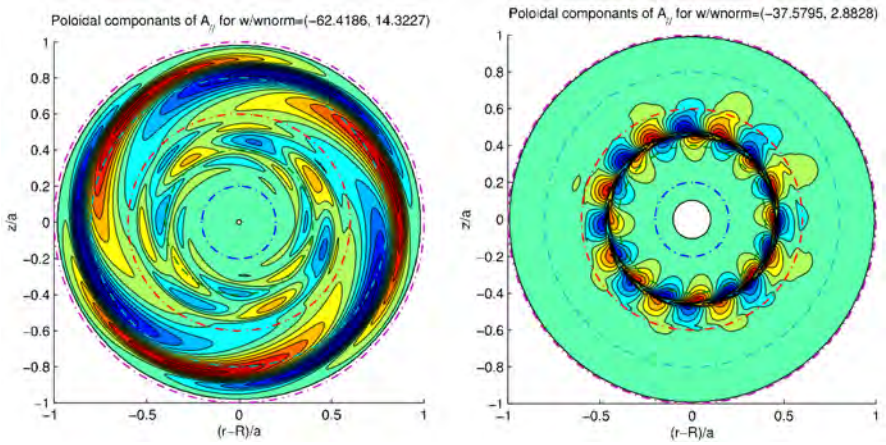

Fig. 2.2.3 *Eigenmode structures of low shear global Kinetic Infernal mode, n=3 (left) and AITG at finite positive shear, n=7 (right).*

The global gyrokinetic electrostatic linear code LORB5 has been upgraded to include the resolution of all equations (i.e. particle motion, evolution of the distribution function and quasi-neutrality equation) in a magnetic system of coordinates which is more appropriate to the study of low frequency microinstabilities. It completely avoids the use of two different grids and the associated back and forth interpolations. The coordinates are straight-field-line, i.e. a magnetic field line is a straight line in coordinate space. The new scheme also completely avoids the singularity problem on the magnetic axis, which is inherent to this type of coordinates. The result is a code which is up to 30% faster than the previous version. It opens the way for further improvements to the PIC codes, including for the nonlinear case.

2.2.2 RF waves

Electron Cyclotron Heating and Current Drive

The calculations of electron cyclotron current drive (ECCD) using the code CQL3D have been extensively compared with experimental results, in standard L-mode scenarios and in scenarios with internal transport barriers. The best method to be used and suitable radial diffusion coefficients have been determined, so that CQL3D is now a routine tool for calculating the RF driven current density j_{CD} for TCV discharges. These systematic studies coupled with equilibrium reconstruction using these j_{CD} profiles and the bootstrap current have shown that the internal transport barriers on electrons (eITBs) with strong electron confinement improvement occur with discharges having significantly reversed shear q profiles. They have also shown that the radial diffusion coefficient to be used decreases when improved confinement occurs, as expected. Figure 2.2.4a shows the electron temperature profile obtained in a TCV eITB plasma. The barrier is clearly seen around ρ=0.4. Fig. 2.2.4b shows the ECCD current density profiles (dashed lines) as calculated with the CQL3D code. We have to adjust the radial diffusion coefficient to match the expected total ICD driven in the discharge, within the experimental error bars. This leads to some variations in the j_{CD} profiles. However the total current profile, obtained with j_{CD} + j_{BS}, where j_{BS} is the bootstrap current density calculated from the experimental measurements, is clearly non-monotonic. These discharges are fully non-inductive, therefore the only current contributions are the bootstrap current and ECCD. These simulations provided the first demonstration that eITBs in TCV are related to reverse shear q profiles.

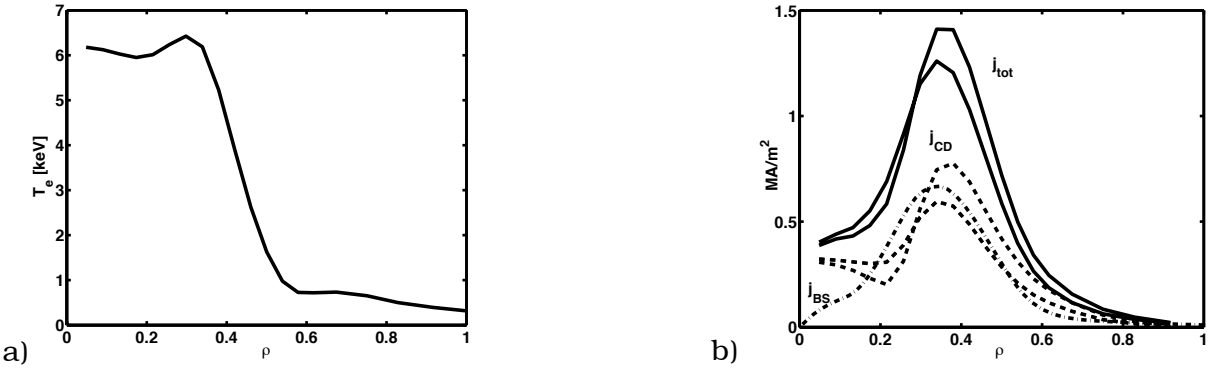

Fig. 2.2.4 *(a) Te profile in a TCV fully non-inductively sustained electron internal transport barrier scenario (eITB); (b) Bootstrap current density (dash-dotted line), CQL3D calculated ECCD current density (dashed lines) and total current density, within the experimental error bars of the total driven current I_{CD}.*

Alfvén Waves in 3D Plasma Configurations

The newly developed LEMan code for resolving of full wave equations in 3D configurations has been applied to various configurations in the Alfvén and ion cyclotron (ICRF) frequencies. The continuous spectrum of shear Alfvén resonant surfaces was independently computed by solving the corresponding partial differential equation with a 2D Fourier technique. Detailed comparisons with LEMan results show a remarkable and detailed agreement, even for complex 3D configurations such as the LHD stellarator. They show that the MHD shear Alfvén resonances lie on magnetic surfaces, and that their position coincides with mode conversion surfaces to quasi-electrostatic modes obtained with LEMan for which finite electron mass, hence finite parallel electric field, is included. For ICRF, mode conversion and fast wave heating scenarios have been studied with high field side (HFS) and low field side (LFS) excitation. An example of the wave field structure in a JET tokamak equilibrium is shown in Fig. 2.2.5. The results confirm earlier results obtained with the LION code but now with a much improved accuracy. In magnetic mirror configurations the “magnetic beach” scenario has been studied. The present version of the LEMan code uses the cold plasma dielectric tensor. Work is underway to include parallel kinetic effects of finite electron temperature, thus enabling the study of kinetic Alfvén waves, albeit without finite Larmor radius effects.

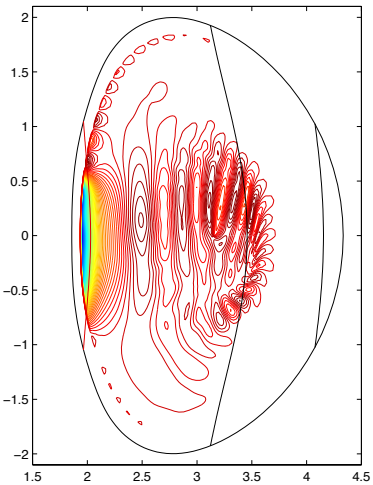

Fig. 2.2.5 *Spatial structure of the perturbed magnetic field component, high-field side antenna, f=37.8MHz, JET equilibrium. Vertical lines, from left to right: deuterium cyclotron resonance, ion-ion hybrid resonance, hydrogen cyclotron resonance.*

2.2.3 Operational Limits and Comparison with Experimental Results

Kinetic effects on MHD modes

Studies continue to identify kinetic modifications to modes which are essentially of magnetohydrodynamic (MHD) origin. In general it is found that kinetic effects can strongly affect the growth rates of MHD modes, while the structure of such modes (eigenfunction) is unaltered to leading order. This latter observation permits the kinetic effects to be added to the analysis perturbatively, thus enabling a tractable approach to the stability analysis. The kinetic effect of finite orbit widths on MHD modes has recently been analysed via a Lagrangian approach to obtain a generalised drift kinetic equation. Research continues into the stability of interchange modes and ballooning modes, while a detailed analysis now exists for the case of the m=n=1 internal kink mode. In particular, the effects on the internal kink mode of energetic asymmetrically distributed circulating ions with finite orbit effects have been analysed (Fig. 2.2.6). Circulating ions which intersect the q=1 resonant surface due to finite radial excursion contribute to the mode either in the region of favourable or unfavourable curvature depending on the sign of $v_{||}$ Internal kink mode stabilisation for predominantly co-circulating ion populations is consistent with the observation of long sawteeth using tangential co-injection of neutral beams in JT-60U. Off-axis neutral beam heating emerges as a possible means of assisting sawtooth control in future fusion grade experiments.

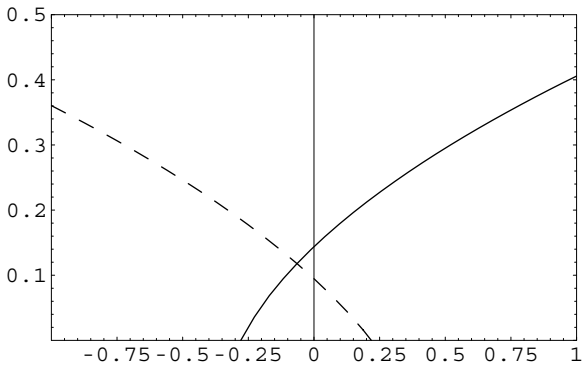

Fig. 2.2.6 *Marginal poloidal β as a function of injection asymmetry for two different energetic ion pressure profiles. The solid curve is relevant to central heating and the dash curve to off axis heating.*

Another way in which kinetic effects can modify both the equilibrium and stability of tokamaks is through velocity anisotropy. This is particularly relevant for plasmas employing radio frequency (RF) heating whereby the velocity of the heated population in the direction perpendicular to the magnetic field is typically an order of magnitude larger than the parallel velocity. Such kinetic effects can be analysed in the MHD framework by employing a pressure tensor rather than a scalar pressure. Analytical but realistic (Fig. 2.2.7) models have been employed to represent the anisotropic velocity distribution function. It is found that anisotropy can significantly distort the magnetic flux surfaces. This is expected to influence the stability of a variety of MHD modes. For example, as discussed in the next section, it is well known that toroidal effects and shaping effects (elongation and triangularity) strongly modify the stability of the internal kink mode and sawteeth in tokamaks, Fig. 2.2.7.

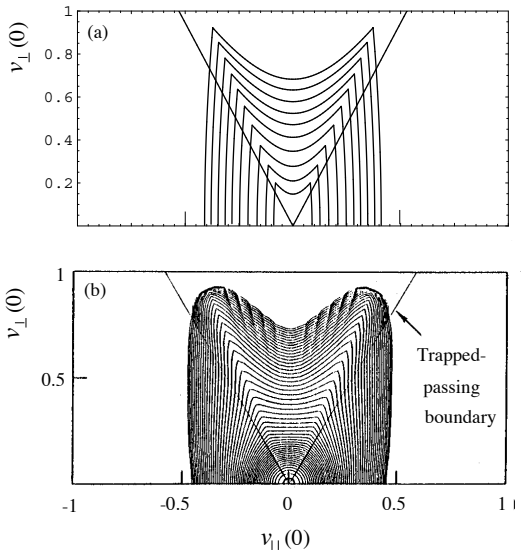

Fig. 2.2.7 *RF distribution function contours versus velocity coordinates from (a) an analytically tractable model distribution and (b) from a steady-state Fokker Planck calculation.*

Sawtooth behaviour and internal kink mode

A review of the analytical calculations of the internal kink growth rates has been made and an analytical formula has been derived combining all the relevant published contributions. It has been shown that this is still not sufficient to predict adequately the internal kink growth rate in typical present tokamak discharges and even more so for tight aspect ratio tokamaks. A formula based on a fit to the results from the KINX code is found to be superior. The results of the KINX code predict much larger growth rates at slightly negative triangularity and stabilisation with still more negative values. This has been tested experimentally and a strong dependence of the sawtooth period has been observed, with a minimum at slightly negative triangularity, this is consistent with a more unstable plasma. The KINX calculations, using the experimental equilibria, confirm the dependence of the growth rate on plasma triangularity and yield values of the same order as the ion diamagnetic frequency, in agreement with the assumption that the sawtooth crash is due to ideal internal kinks.

High-n edge kink/ballooning modes

The KINX code developed at CRPP in collaboration with the Keldysh Institute in Moscow is the only ideal MHD stability code that consistently takes into account the plasma up to the magnetic separatrix. This unique feature is crucial for the study of Edge Localized Modes (ELMs). A simple current density limit for the edge stability has been found: $\langle j_{sx} \rangle / (Ip/S) = 1$, above which mid- to high-n external kink modes are destabilised. The limit appears to be practically identical for several shapes (TCV, ITER) and is roughly independent of the edge pressure gradient up to the ballooning limit. This is in sharp contrast with the so-called “peeling” mode stability criterion derived by other research groups, which is inconsistent because it considers limiter plasmas, whereas it is well known that ELMs only occur in plasmas with separatrix. Another result is the scaling $w\ n\ q_{95}$ = constant for the most unstable mode toroidal wavenumber n, with varying pedestal width w and q_{95}. The KINX code results have been used to derive a semi-empirical model for ELM

relaxation phenomena. TCV discharges in which edge current perturbations induced by external coils were used to control the ELM sequence were analysed with KINX. Results confirm the picture of edge current driven instabilities as triggers of the ELM relaxation.

Current hole

The computation of equilibria with current density reversal in the plasma core have been extended to finite pressure gradient cases. The shape of axisymmetric magnetic islands which necessarily form in such cases has been shown to be sensitive to the plasma pressure. A change in topology is observed and solutions with multiple magnetic axes appear with increasing pressure in the region between the negative current density and the internal separatrix. This poses challenges for the numerical formulation of the stability problem: traditional methods assume nested flux surfaces, which is not the case anymore here.

MHD limits in eITB reversed shear discharges

The strength of eITBs, i.e. the maximum local T_e gradient, can be controlled in TCV with counter current drive in the centre in order to create stronger reversed shear and/or more central heating. If the local gradients become too strong the discharge can disrupt or a minor disruption occurs, which annihilates the barrier. Detailed analysis of these discharges has shown that the profiles are close to the ideal limit of the n=1 kink mode. The β_N limit depends on both the current density and pressure profiles, as expected with non-monotonic q profiles. Because of the large gradients created in TCV, the ideal limit for these cases is relatively low, $\beta_N \sim 1$. As expected the limit is lower for q_{min} near integer values.

2.2.4 Optimisation of 3D magnetic configurations

4-period Helias reactor with finite bootstrap current

The most effective method to optimise a stellarator system is through the variation of the parameters that control the plasma shape to achieve the targeted physics properties. The boundary obtained, however, constitutes a single point in the phase space of the physics properties that are aimed. A reverse engineering procedure is applied to obtain a filament coil model by discretising the distributed current on a control surface that would generate the optimal plasma boundary surface. The physics properties with the discrete coils must be then verified and the sensitivity to variations of plasma pressures, currents and profiles must be ascertained. We have examined the impact of a self consistent bootstrap current (BC) in the collisionless $1/\nu$ regime is examined on the equilibrium and global ideal MHD stability properties of a 4-period Helias stellarator reactor under free boundary conditions with a volume of ~1500m^3 (Fig. 2.2.8). The BC at β=4.5% reaches 300kA, causes the rotational transform to approach unity in the outer 40% of the plasma volume and provides free energy to destabilise an external m/n=1/1 mode. Using a model current profile that simulates the effect of counter electron cyclotron current drive to globally (but not locally) suppress the bootstrap current, we find that a slight overcompensation of about 50kA suffices to reduce the edge transform well below unity and stabilise the kink mode. Rotational transform profile control with current drive techniques may be required in advanced stellarator systems.

$J_{//}$ optimised quasi-isodynamic stellarators with poloidal quasisymmetry

The optimisation of stellarator systems with respect to poloidally closed contours of the second adiabatic invariant $J_{//}$ has included a subsidiary minimisation of the structural factor of the bootstrap current in the collisionless regime. The study of a 6-period optimised configuration that is MHD stable at β=8.9% has been completed. Investigations of 3-period and 9-period systems are still underway with MHD stable configurations already obtained at β=3.9% and β=11% for 3 and 9 periods, respectively. These configurations also satisfy the condition of pseudo-symmetry which manifests itself through almost constant mod-B lines closing poloidally, thus satisfying poloidal quasi-symmetry (Fig. 2.2.9). The possibility of advanced fuel cycles becomes promising when large stable β values can be achieved.

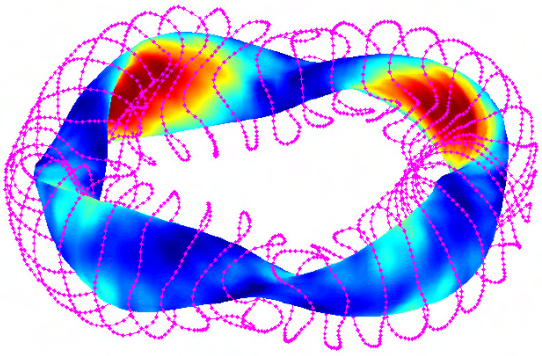

Fig. 2.2.8 *The filament coil model, the shape of the plasma boundary surface and the B^2 distribution on that surface for a 4-period Helias reactor with finite bootstrap current at β=4.5%.*

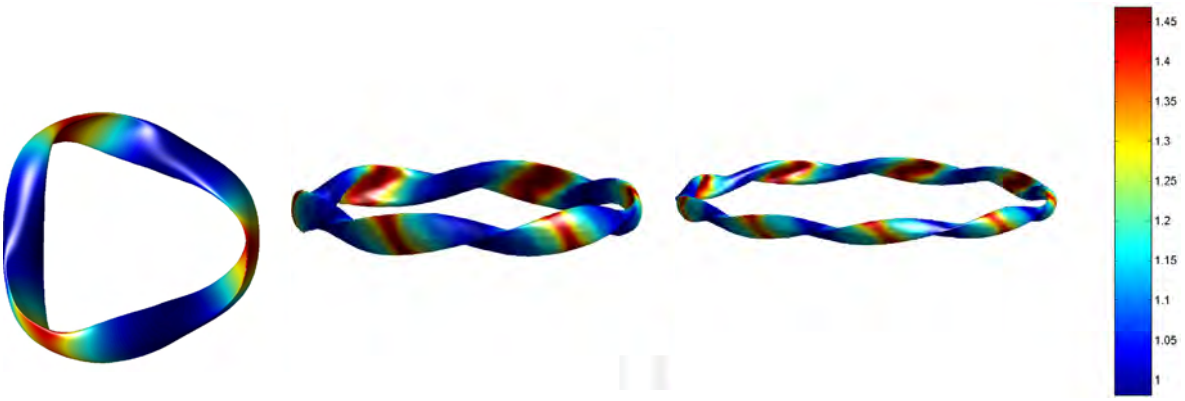

Fig. 2.2.9 *Boundary magnetic surfaces of the optimised N=3, β=3.9%; N=6, β=8.9% and N=9, β=11% configurations. The colour identifies the magnetic field strength on the boundary magnetic surfaces.*

2.2.5 Full tokamak simulations using the DINA-CH code

The DINA-CH code simulates all the details of the evolution of a tokamak discharge, including plasma transport, free-boundary equilibrium evolution and the control system for plasma shape, current and position. A general interface to the data required to model different tokamaks has been developed for 5 tokamaks (TCV, ITER, MAST, AUG, GLOBUS-M). A new module to simulate diagnostic

measurements during the simulation has been developed to allow the creation of more detailed feedback on kinetic variables, Fig. 2.2.10

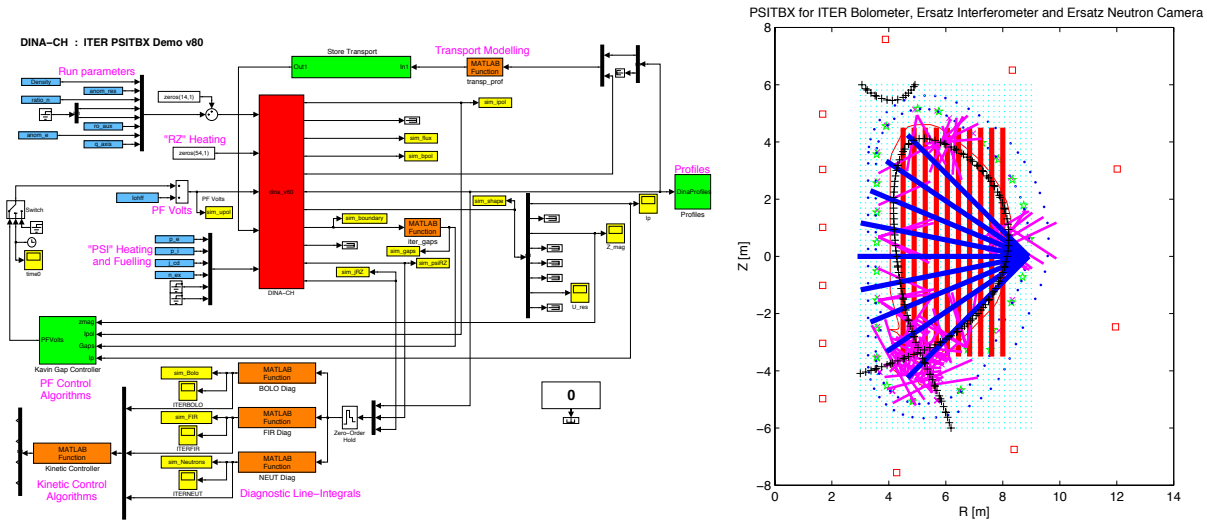

Fig. 2.2.10 *Incorporation of a general diagnostic module in DINA-CH, allowing the development of realistic kinetic control feedback algorithms with free-boundary evolution ; left - the simplicity of uniting the profile information and the plasma equilibrium as input to the module ; right – the implementation of the present bolometer design plus an illustrative neutron camera and an imaginary interferometer*

2.2.6 EU Integrated Tokamak Modelling Task Force

This task force has been formed this year and CRPP is an active member. While the task force is being organised, collaboration with UKAEA on suitable representation of the different tokamak databases has been started. Universal definitions of the physical description of a tokamak have been prototyped for ITER, TCV, MAST, AUG and GLOBUS-M for use with DINA-CH with the aim of determining suitable structures.

2.3 Operation of a specialised basic plasma physics device, TORPEX

Basic investigations of electrostatic turbulence and its effects on the transport of energy and particles across the magnetic field are conducted on the TORoidal Plasma EXperiment, TORPEX. Low plasma densities and temperatures make it possible to obtain high-resolution measurements of plasma parameters and wave fields throughout the plasma cross-section. Plasmas are confined by a primarily toroidal magnetic field up to B_T=0.1T, and a smaller vertical component, $B_v \leq 50$mT, the simplest configuration incorporating the main ingredients for drift wave instabilities and turbulence, namely pressure gradients and field line curvature.

Highly reproducible discharges of Argon and Hydrogen with density and electron temperatures in the range $n_e \sim 10^{16}$-10^{17}m^{-3} and T_e~5-10eV are driven for 100ms by microwaves at 2.45GHz, corresponding to the electron cyclotron (EC) range of frequencies. Up to 50kW of microwave power is injected from the low field side in the ordinary mode and can be modulated at frequencies up to 60kHz (sinusoidal).

Parameters such as the neutral gas pressure, the location of the EC resonance and the amount of injected power can be varied to control density and electron temperature profiles.

The first plasmas were obtained in TORPEX in 2003. The experimental campaigns in 2004 have been devoted to identifying the mechanisms involved in the microwave plasma production, to obtaining the plasma source profile, to completing the study of the effect of the vertical field on the plasma equilibrium and confinement, to characterising drift waves in the coherent regime and weak turbulence, and to observing their nonlinear evolution, linked to the plasma temperature and density profiles. The results of these investigations are summarised in the following sections, while the completion of the TORPEX installation, including new power supply connections, the introduction of easily removable mobile sectors for diagnostic installation, and upgrade to the diagnostic systems are described separately in the technical achievements Section 3.5.

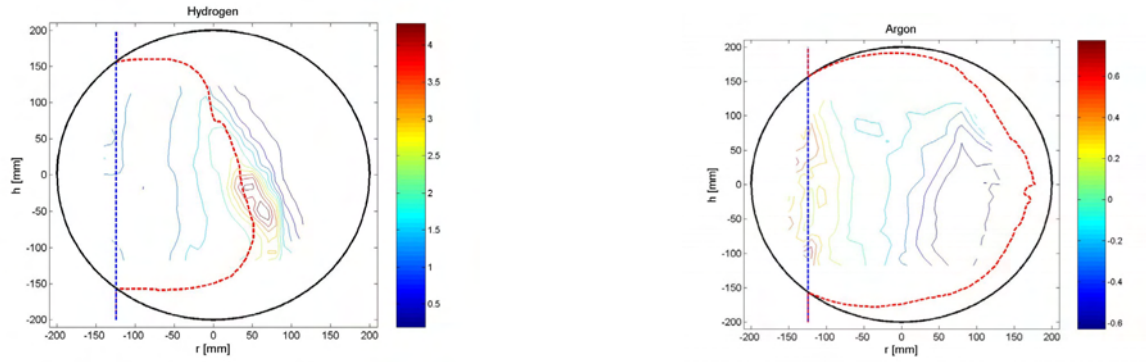

Fig. 2.3.1 *Measured fractional density variation with modulated EC power (square pulses, modulation frequency 500Hz, duty cycle 20%) in Hydrogen and Argon. The absorbed power (taken as the difference between the injected and reflected power measured in the transmission line) changes from 0.2kW to 1.8kW. The EC (blue) and UH (red) resonant locations are extrapolated to the whole poloidal section.*

2.3.1 Plasma production and characterisation

A knowledge of the spatial profile and the dynamical behavior of the particle and heat sources as a function of magnetic field, background gas pressure and microwave injected power is needed is to establish the link between these control parameters and the resulting plasma characteristics. In particular, it is important to characterise the response of the plasma to different levels of absorbed power, to use EC modulation techniques and to control typical gradient lengths for transport studies. For these reasons, the mechanisms responsible for the ionisation of the neutral gas by means of EC waves have been investigated in TORPEX. The main contributions to the global ionisation rate come from the thermal electron population and the electrons accelerated at the EC and upper hybrid (UH) resonant layers. The contribution of the thermal population can be directly estimated from the experimental profiles of density and electron temperature. The role of the two resonances has been investigated experimentally in discharges in which the microwave source was modulated with short square pulses, allowing a separation of the fast time scale that characterises the ionisation processes from the slower time scale linked to the mechanisms that lead to the stationary background profiles.

In Fig. 2.3.1 for Hydrogen plasmas, as the EC power is increased the density rises suddenly at a location coinciding with the position of the resonant UH layer estimated from the measured density profile. On the basis of the three wave absorption and ionisation mechanisms discussed above, an equation relating the total number of particles, N_{tot}, to the absorbed microwave power P_{abs} was derived and used to fit the experimental data $N_{tot}=N_{tot}(P_{abs})$. The experimental data and the results of the fit for Ar and H plasmas are shown in Fig.2.3.2.

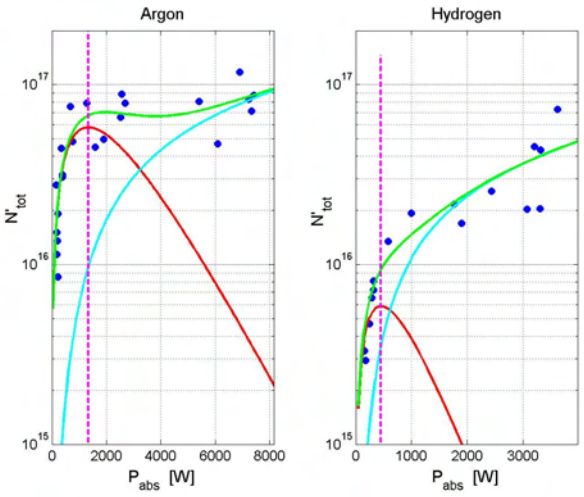

Fig. 2.3.2 *Total number of plasma particles vs. absorbed microwave power. Full circles: experimental data. Green: fit of the data. Red: contribution of the EC layer. Cyan: contribution of the UH layer. The vertical dashed line indicates the power at which the contribution of the UH layer starts dominating the ionization rate.*

From this analysis it appears that for absorbed power P_{abs}<2kW the EC channel in Argon is much more efficient than in Hydrogen, where the dominant contribution to the ionisation rate comes from the UH resonant layer even for very low power. This interpretation is supported by the results shown in Fig. 2.3.1, where the opposite behaviour in terms of ionisation location is observed for the two gases for a modulation of the injected power between the same values of 0.2kW up to 1.8kW.

2.3.2 Optimisation of magnetic configuration: vertical field

A systematic study of the plasma confinement mechanism obtained by superimposing a small vertical magnetic field on the dominant toroidal field was performed. The spiral-shaped field lines allow particles to partially short-circuit the vertical electric field E_z driven by charge dependent grad B and curvature drifts. Coulomb collisions are responsible for an equilibrium determined by $E_z \propto \nu B_z^{-2}$ being reached, causing **ExB** particle loss. Accounting also for the particle loss where the field lines intersect the vacuum vessel ($\propto |B_z|$), the particle confinement time τ can be estimated. We find that there is an optimal value

$$|B_{z,opt}| = \left[\frac{4\nu |B_\varphi| m_e \sqrt{m_i T_e}}{e^2 R}\right]^{1/3}, \qquad \tau_{\max} = \frac{\pi}{3}\frac{a}{c_s}\frac{|B_\varphi|}{|B_{z,opt}|},$$

for which τ is maximal. Experimentally, estimates for τ are obtained from the local exponential decays of Langmuir probe measurements of ion saturation current after the plasma production is stopped. The results (Fig. 2.3.3) indicate a good qualitative agreement, in particular in terms of the optimal value for the vertical magnetic field. On the other hand, τ is quantitatively overestimated by about a factor of three.

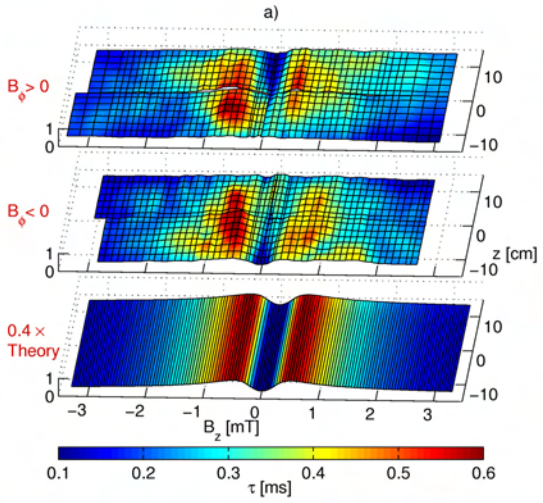

Fig. 2.3.3 *Comparison of theoretical model predictions with experimental data on particle confinement time as a function of vertical magnetic field and vertical position.*

2.3.3 Spectral properties of electrostatic instabilities

The power spectra of density fluctuations exhibit peaks at low frequency (*i.e.* much lower than the ion cyclotron frequency), whose width and amplitude depend on the density gradient. The phase velocity of density fluctuations in the poloidal direction, v_ϕ=1km/s, is comparable to the drift velocity evaluated from background parameters, corrected for the Doppler shift caused by ExB drift caused by the radial electric field. An example of the experimental reconstruction of the phases of the wave at different poloidal locations, and of the associated k-spectrum is shown in Fig. 2.3.4.

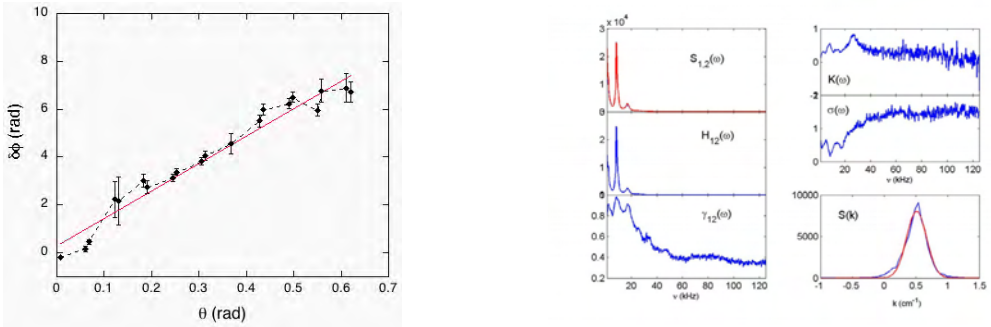

Fig. 2.3.4 *Left: phase shift of density fluctuations along poloidal direction, measured at r=16cm, z=[-5,5]cm, for Ar plasma, with p_{gas}=2.5×10^{-5} mbar, B_T=80mT and B_v=1mT. The peak density is n_e≈4×10^{17} m^{-3} and temperature T_e≈4eV. All the phases are referred to the first tip of the array. Right: wave number spectrum evaluated from two tips 1cm apart (pairs 5 and 6 in figure at left). The broadening of the spectrum gives an estimate of the scale length of turbulence (L≈σ^{-1}).*

A complete, unambiguous identification of the nature of instability will be obtained from measurements of the phase shift between density and potential fluctuations, for which a new Langmuir probe for the measurement of flux is being developed. The direct comparison between density fluctuation spectra and flux spectra in *k*-space will allow deeper insight into the identification and characterisation of instabilities excited on TORPEX and their driving mechanisms.

To investigate the origin of the instability, we looked at the plasma response to variations in the microwave power. When the microwave power is reduced, the density peak moves towards the centre of the poloidal cross-section and the radial density gradient in the low field side region decreases. The power density spectra for the plasma density are also computed over the whole cross-section. For the region, where ∇n and ∇B are in the same direction, the amplitude of the density fluctuations is larger on a more extended range of frequencies than in the case in which ∇n and ∇B are in opposite direction. This is the signature of a ballooning instability due to the toroidal curvature, which cannot be present in a slab geometry.

2.3.4 Characterisation of nonlinear wave behaviour

The conditional average sampling technique was used to identify nonlinear structures in space resolved electrostatic fluctuation data. This technique is based on measuring the local response of the plasma to a naturally occurring perturbation, detected on an arbitrarily chosen reference channel. The response is averaged over many repetitions of such a perturbation (identified according to a condition on its amplitude), and averaged over a time interval τ_w. The role of the choice of τ_w was studied. The first test was performed on data from a Hydrogen plasma with a highly coherent mode at 4kHz. Here, we chose $\tau_w/\tau_c<<1$, where τ_c is the typical auto-correlation time of the reference signal. In this case, the conditional sampling technique provides a simple way to filter and visualize the signal, including its main oscillatory character, if present. This is illustrated on Fig. 2.3.5. Here the results of the conditional average sampling on density fluctuations are represented along a 9cm radius circle centred at (r,z)=(0,0). Wave fronts propagating in the electron diamagnetic direction appear very clearly. The phase velocity is given by an estimation of the slope, as shown on the figure: $v_{ph}=R.\Delta\theta/\Delta\tau=400m.s^{-1}$. An estimate of the diamagnetic velocity $v_{d,e}=T_e/B|\nabla n_e|/n_e$ from the local gradient gives $v_{de}=240m.s^{-1}$, i.e. the observed phase velocity is of the same order as the diamagnetic velocity.

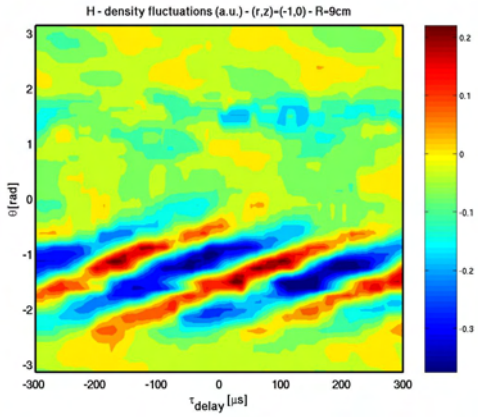

Fig. 2.3.5 *Conditional average sampling applied to density fluctuations in a Hydrogen plasma with P_{rf}=500W with $\tau_w<<\tau_c$. The results are represented along a 9cm radius circle centred at (r,z)=(0,0).*

A different choice of the parameter τ_w, namely τ_w/τ_c ~1, is necessary to visualise structures in the fluctuation data other than the wave itself. We have done this with the same data as in the previous case but no significant structures were observed corresponding to the highly coherent mode at 4kHz. The technique was then applied to a different set of data from a typical Argon plasma. In this case, the plasma density spectrum shows a peak at a frequency around 8kHz but this peak is less coherent compared with the Hydrogen case, probably due to a stronger instability drive caused by a stronger density gradient. The conditional average sampling applied to density fluctuations gives indeed a very different result (Fig. 2.3.6). Density structures or "blobs" moving in the poloidal cross section can be observed in the time sequence. The direction of propagation for these blobs is not that of the electron diamagnetic velocity but could correspond to the ExB direction. The velocity of these density structures can be estimated to be v_{blob}=320ms^{-1}. This velocity is quite different from both the diamagnetic velocity and the phase velocity estimated from the data of the 3-array LPs for this case, which are of the order 1km.s^{-1}.

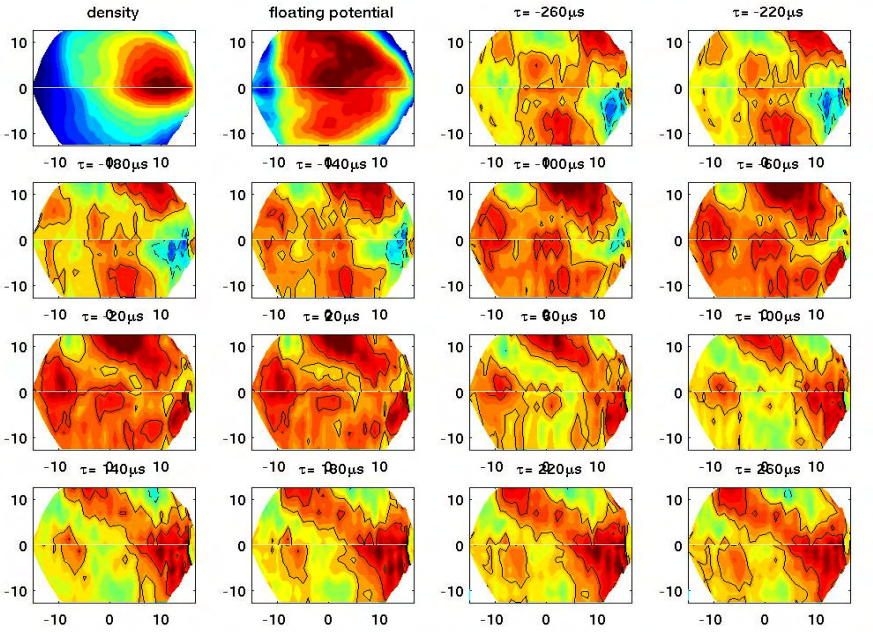

Fig. 2.3.6 *Conditional average sampling of density fluctuations with τ_w~τ_c applied to a typical Argon plasma. Density blobs propagating in the poloidal cross-section are visible*

2.4 Materials for a fusion reactor

The main objective of the Fusion Technology Materials (FTM) group is to investigate the effects of the damage produced by radiation in a variety of materials, in particular candidate materials for structural components of the future fusion reactors but also pure metals and model alloys. This group is located at the Paul Scherrer Institute (PSI) in Villigen. It used the high-energy (590MeV) proton beam of the PSI accelerator, through the Proton Irradiation Experiment (PIREX) until December 2003 and uses the Swiss Spallation Neutron Source (SINQ) facilities from April 2004, to simulate experimentally the effects of the 14MeV neutrons that are the product, together with helium nuclei, of fusion reactions between deuterium and tritium nuclei. Some activities of decommissioning PIREX also started in 2004.

Key parameters for the first wall in fusion power reactors with a fusion power of 3 to 4GW and in quasi-continuous operational mode include a total neutron flux of 10 to $15x10^{14}n/cm^2.s$, a neutron wall loading of 2 to $3MW/m^2$, an integrated wall load of 10 to $15MWy/m^2$, a surface heat load of 0.1 to $1MW/m^2$ and a volume power density of 20 to $30W/cm^3$. The accumulated dose will amount to 100-150dpa/year in steels, while the gas produced by transmutation nuclear reactions will amount to 10-15appm He/dpa and 40-50appm H/dpa, also in steels. From the technological point of view, the temperature window of operation of fusion reactors is mainly limited by the mechanical properties of the structural materials.

Just like 14MeV neutrons, 590MeV protons produce atomic displacement cascades and transmutation nuclear reactions within the irradiated materials. From the point of view of materials science, atomic displacement cascades induce the formation of point structure defects, i.e. vacancies and interstitial atoms, while transmutation nuclear reactions yield the production of impurities, such as helium or hydrogen gas atoms. The final microstructure of the irradiated material results from reactions between these different defects. It may be formed of defect clusters, dislocation loops, dislocation networks, precipitates, stacking-fault tetrahedra (SFT's), voids and/or helium bubbles (Fig. 2.4.1). This microstructure has important effects on the physical and mechanical properties of the material. It can engender important hardening, loss of ductility (Fig. 2.4.2) and fracture toughness, as well as macroscopic swelling of the material. Those effects are the main factors limiting the choice of candidate materials. The residual radioactivity of a large amount of exposed material is also a concern and will govern the handling methods, dictate the storage periods and the overall waste management and recycling scenarios. The development strategy that takes into account these limitations has led to the development of the class of low activation materials.

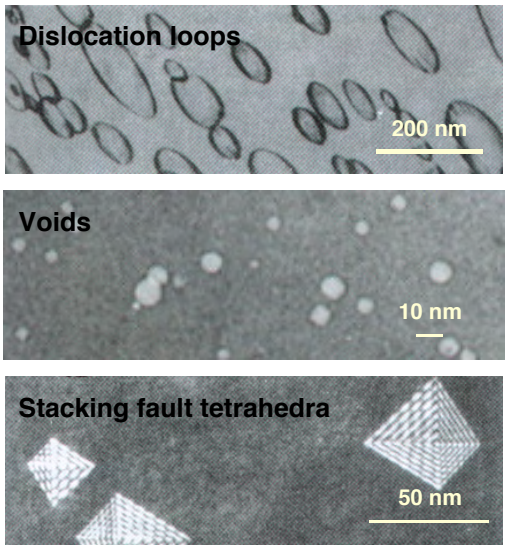

Fig. 2.4.1 *Examples of transmission electron microscopy images of irradiation-induced structure defects.*

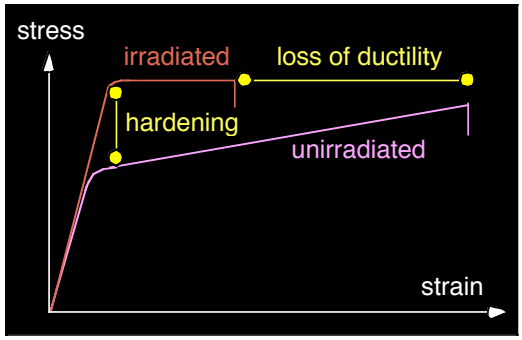

Fig. 2.4.2 *Schematic of irradiation-induced hardening and loss of ductility, as measured in tensile tests on irradiated specimens.*

One of the main advantages of the 590MeV protons is to generate high impurity production rates, which cannot be achieved with any other current irradiation source. While proton irradiations in PIREX were producing about 130appm He/dpa and 800appm H/dpa (in steels), irradiations in SINQ with a mixed spectrum of neutrons and protons produce about 50appm He/dpa and 450appm H/dpa (in

steels). However, in order to investigate the material property changes and degradation under different irradiation conditions, the FTM group is also involved in specific neutron irradiations performed in reactors in the U.S.A., the Netherlands and Hungary.

Candidate structural materials for first wall and breeding-blanket applications include mainly reduced activation ferritic/martensitic (RAFM) steels, vanadium alloys and fibre reinforced SiC/SiC ceramic composites. Each alternative alloy class exhibits some specific problems arising from radiation damage. For the time being, the most promising class of alloys is the RAFM steels for which the greatest technology maturity has been achieved. Qualified fabrication routes, welding technology and a general industrial experience are already available.

The design of materials with properties adequate for use in an irradiation environment requires an understanding of the effects of irradiation on their physical and mechanical properties. The FTM group has been active in this field for several years within the framework of the European Fusion Development Agreement (EFDA) and collaborates with many research institutes and industries in Switzerland as well as abroad. The research activities of the FTM group include basic research on radiation damage in pure metals and alloys, characterisation and development of low activation materials for fusion power reactor applications and characterisation of materials destined to ITER. The scientific approach adopted by the FTM group to understand the fundamentals of radiation damage in metals and alloys is based on investigating the structure/mechanics relationships at different length scales (micro-, meso-, and macroscopical). A range of experimental and numerical tools is used to reach these objectives. The main experimental tools include mechanical testing on sub-sized and standard specimens, scanning and transmission electron microscopy (SEM, TEM) and small angle neutron scattering (SANS). The main numerical tools include molecular dynamics (MD), Monte-Carlo (MC) and dislocation dynamics (DD) simulations and finite element (FE) calculations.

2.4.1 Irradiation Experiments

The definitive shutdown of the PIREX facility took place on December 22, 2003. Decommissioning of the PIREX facility was started in March 2004. It will be pursued in a continuous way until September 2006. Technically, the PIREX facility is mainly composed of four irradiation heads, referred to as targets, a rectangular port allowing the heads to be inserted into the proton beam line, a Helium loop with its compressor (for cooling the heads and specimens during irradiation), and electrical connections. The targets are strongly radioactive and the Helium loop is slightly contaminated with tritium. Most of the dismantling will have to be performed in hot cells using remote handling. Irradiation experiments are being continued with high-energy protons by means of the SINQ facility, as well as with neutrons in fission reactors in Petten (the Netherlands) and Budapest (Hungary).

2.4.2 Underlying Technology Tasks

In Beam Fatigue of RAFM Steels

This work was aimed at investigating the behaviour of the EUROFER 97 RAFM steel in the condition of in beam fatigue using an in situ testing facility specially designed for the PIREX facility. A number of in beam fatigue experiments have been

conducted at two different temperatures, namely 150 and 250°C, with or without pre-deformation. The irradiation dose at the end of experiment was in the range 0.3-0.4dpa. For comparison, two fatigue tests have been also performed at the same temperatures of 150 and 250°C but without beam. Results are reported in Table 2.4.1.

Test temperature [°C]	Pre-deformation [number of cycles]	Imposed fatigue strain [%]	Frequency [Hz]	Period [sec]	Number of cycles at fracture	Irradiation dose [dpa]
150	-	0.8	0.005	200	1488	0.42
250	-	0.8	0.005	200	1252	0.34
250	250	0.8	0.005	200	1505	0.30
150	300	0.8	0.005	200	1468	0.31
150	-	0.8	0.0166	60	2881	-
250	-	0.8	0.0166	60	2900	-

Table 2.4.1 *Results of in beam fatigue tests on the EUROFER 97 RAFM steel.*

In the in beam condition the fatigue life decreases with increasing irradiation temperature. This is an indication of the limited role of hydrogen produced by spallation nuclear reactions, since hydrogen embrittlement effects should be more severe at low temperatures. In previous experiments on the MANET RAFM steel, it had been found that pre-deformation was drastically reducing the endurance. Obviously, this is not the case for the EUROFER 97 material, as the fatigue life is not reduced following pre-deformation, due to a different evolution of the microstructure under simultaneous deformation and irradiation. However, comparison with unirradiated specimens indicates that the fatigue life is reduced by a factor of approximately two as a result from the in beam condition.

Modelling of radiation damage in fcc and bcc metals

The irradiation-induced damage in Ni and Cu face centred cubic (fcc) metals was simulated by molecular dynamics (MD). The aim was to produce a data set of atomic displacement cascade-induced defects to be used as input for kinetic Monte Carlo (kMC) calculations that allow prediction of the long-term evolution of the defect microstructure at a mesoscale. The MD code has been improved to control the time-step adjustment better. It is now adapted to displacement and energy jumps as well.

Ni was first considered, as a large experimental dataset is already available from our own proton irradiations in the PIREX facility. Series of atomic displacement cascades were produced in Ni, for PKA (primary knock-on atom) energies of 5, 10, 20, 30 and 40keV, and temperatures of 10, 100 and 300K. The cascades were created with four different interatomic potentials (Farkas1, Farkas2, Cleri-Rosato, modified Cleri-Rosato) in order to understand the role of the material properties on the defect configuration. The main parameter of interest here is the stacking fault energy (SFE). The first three potentials provided SFE's of 70, 140 and 300mJ/m^2, respectively, while the fourth potential provided also a SFE of 300mJ/m^2, but with a refined high-energy part, in order to obtain a better response for a high PKA energy. Dramatic differences have been observed in the final damage (Fig. 2.4.3), showing its sensitivity to the choice of the interatomic potential. It appears that the key parameter in the production of defects is the displacement threshold energy and, up to this point of our study, not the SFE.

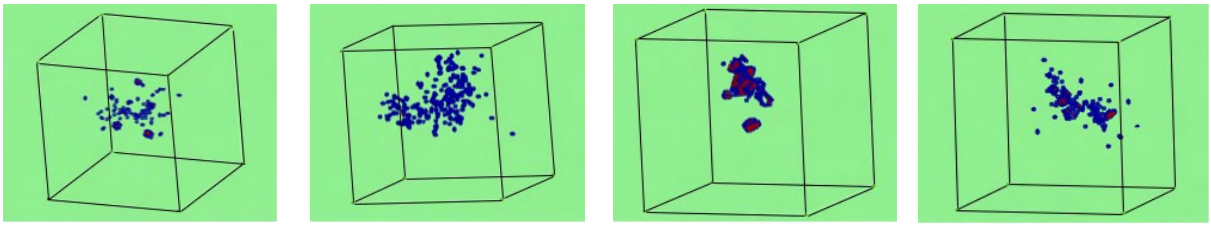

Fig. 2.4.3 *MD simulation of the damage following a 20keV cascade in Ni with various interatomic potentials. Colour reflects atomic coordination. Blue atoms: non-fcc, nor bcc nor hcp atoms. Red atoms: hcp atoms. From left to right the stacking fault energy is 70, 140, 300 and 300mJ/m^2, respectively.*

In body centred cubic (bcc) pure metals series of atomic displacement cascades were produced by MD in Fe with the Ackland interatomic potential (1997) and in Fe-He with the interatomic potentials derived by Morishita and Wirth (2003). Cascades were generated for PKA energies of 1, 5, 10 and 20keV and temperatures of 10, 300 and 523K, in order to compare the results obtained with the experimental ones arising from irradiations and ion implantations. The resulting defects will then be used to define the defects that will have to be accounted for in dislocation dynamics simulations. These will allow the calculation of the strength of these defects as obstacles to mobile dislocations. Figure 2.4.4 illustrates the case of a 10keV atomic displacement cascade at 10K in the Fe-He system. It should be noted that the Fe-He interatomic potentials do not reproduce the appropriate energies for the He interstitial and substitutional locations and for the He migration energy in bcc Fe, as compared with values obtained by ab-initio techniques. However, there is at present no other set of potentials available.

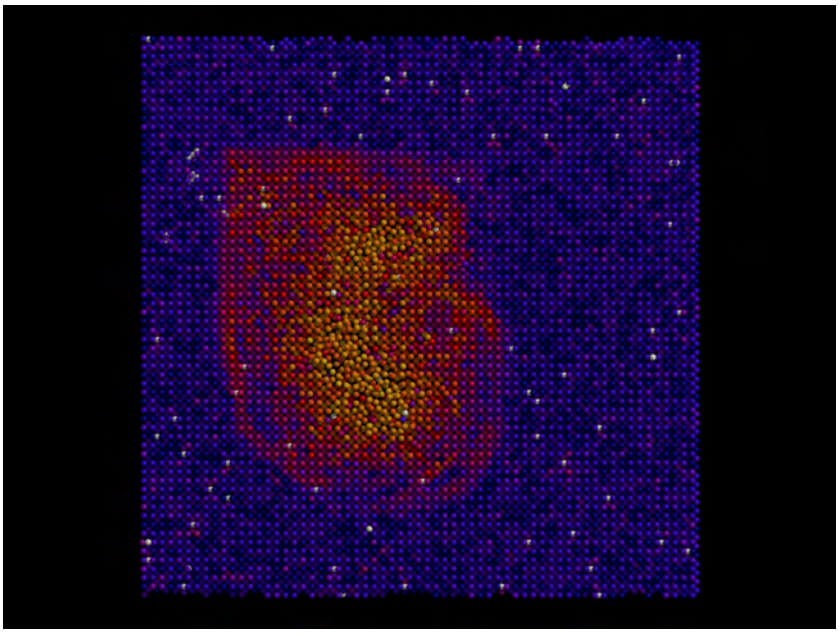

Fig. 2.4.4 *MD simulation of a 10keV atomic displacement cascade at 10K in Fe containing 1.0at.% interstitial He. Colour represents kinetic energy (temperature). White: He atoms. Note the disordered region in the centre of the atomic displacement cascade and the shock wave that starts to propagate outwards.*

Development and characterization of nanocrystalline materials for fusion applications

Polycrystalline tungsten has been obtained with a purity of 99.95wt.% in the form of two square plates, 50x50mm^2, 0.5mm thick, for a total weight of 53.1g. Figure 2.4.5 (left) shows a transmission electron microscopy (TEM) bright field micrograph of the as-received material. It exhibits well-developed equiaxed grains of about 1μm in size, which contain a low density of dislocations.

Neutron-irradiation of pure, polycrystalline tungsten in the HFR reactor in Petten (The Netherlands) at 600-650°C and 900-950°C to a dose of about 2.5dpa, has been completed. The cooling down phase is in progress and the irradiated specimens will be transported back to Switzerland at the end of 2004. Investigation of the microstructure and mechanical properties of neutron-irradiated pure W will be performed in 2005.

Discs with a diameter of 8mm and a thickness of 0.5mm have been cut out by spark erosion from the as-received tungsten plates. The discs have been sent to the Institute of Physics of Advanced Materials at the Ufa State Aviation Technical University, Russia. There, the tungsten discs were submitted to severe plastic deformation by performing high-pressure torsion (SPD-HPT) in order to obtain a nanostructured texture. A pressure of 6GPa was applied and the upper anvil was rotated five times through 360° during the compression. The resulting microstructure is shown in Fig. 2.4.5 (right). The deformed discs exhibit a strongly textured, inhomogeneous microstructure with grain sizes between 40 and 100nm. There is a strong gradient in the grain size from the centre to the edge of the SPD-HPT discs, the smaller grains appearing at the edge of the discs.

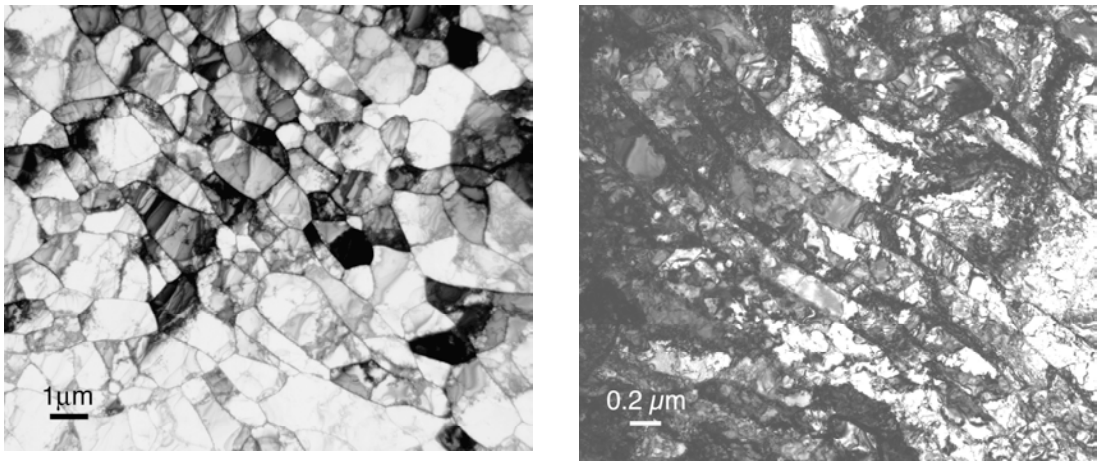

Fig. 2.4.5 *Left: TEM bright field micrograph of the as-received pure W. Right: TEM bright field micrograph of the SPD-HPT deformed W.*

On the constitutive behaviour at low temperatures of the tempered martensitic alloys

The strain-hardening law for a tempered martensitic Fe-9wt%Cr-0.1wt%C model alloy was examined in terms of dislocation mechanics. The alloy was normalised at 980°C for 1 hour followed by air-cooling producing a fully martensitic structure. After normalization, the alloy was tempered at 760°C for 80 minutes. Tensile DIN specimens 3mm in diameter and 18mm in calibrated length were machined. Tensile tests were carried out in an electro-mechanical Schenck testing machine at several temperatures ranging from -196°C to -100°C. The tests were carried out at a constant crosshead displacement speed of 0.1mm/min that corresponds to a nominal strain rate of 9.25x10^{-5}s^{-1}.

In the case of face centred cubic (fcc) or body centred cubic (bcc) materials at temperatures above approximately $0.2T_m$, where T_m is the melting temperature, it is well established that the flow stress is proportional to the square root of the dislocation density:

$$\sigma = M\alpha\mu b\sqrt{\rho} \tag{1}$$

where M is the Taylor factor, μ is the shear modulus, b is the Burgers vector, α is a numerical constant and ρ is the dislocation density. This equation holds as long as the flow stress is controlled only by dislocation-dislocation interactions. When other strengthening mechanisms are considered, for example solid solution strengthening, carbide distribution or precipitates, it is common to assume that the contributions to the flow stress coming from these different mechanisms, which we refer to as $\tilde{\sigma}$, are additive:

$$\sigma = \tilde{\sigma} + M\alpha\mu b\sqrt{\rho} \tag{2}$$

Equation 2 describes the simplest approach, where the component $\tilde{\sigma}$ of the flow stress is independent of the dislocation density and weakly dependent on temperature. For the bcc materials at $T<0.2T_m$, the usual relationship between the flow stress and the square root of the dislocation density is no longer valid. Actually, the origin of this change relates to the micro-mechanisms controlling the motion of dislocations. It is well established that in bcc metals the mobility of the dislocation screw segments is strongly reduced at low temperatures owing to the non-planar character of the dislocation core, which results in a strong lattice friction. Consequently, screw dislocations tend to arrange themselves in straight segments aligned along the <111> directions under the presence of a stress field. The movement of these segments occurs by a thermally activated mechanism of kink-pair formation followed by the propagation of the kinks.

For the bcc materials at low temperatures, there exists a simple model (Rauch's model), based upon energy balance considerations, where a new relationship between the applied stress and the dislocation density is proposed. In this model, the motion of moving screw segments is analysed in terms of a concomitant lattice friction and interaction with the forest of dislocations. First, we expressed the applied shear stress, τ_a, of Rauch's model as a function of the measured applied stress, σ_a, by using a Taylor factor M equal to 3 ($\sigma_a = M \cdot \tau_a$). Second, we considered a $\tilde{\sigma}$ component for the flow stress, which can certainly not be neglected in the case of tempered martensitic alloys and which accounts at least for the high density of boundaries decorated by carbides. In this context, the modified Rauch's relationship between the applied stress and the plastic strain can be written as follows:

$$\sigma = \frac{\tilde{\sigma} + \sigma^*}{2} + \frac{1}{2}\sqrt{(\tilde{\sigma} + \sigma^*)^2 + 4(M\alpha\mu b)^2\rho} \tag{3}$$

where σ^* is the effective stress required to nucleate a double-kink at the imposed strain rate, which sharply increases with decreasing temperature. In the framework of this model, σ^* is considered to be independent of the actual state of the structure (dislocation density), i.e. $\sigma^* = \sigma^*(T)$.

In order to write a plastic strain hardening expression, it is necessary to establish the strain dependence of the dislocation density. This dependence was derived by

following the phenomenological approach of Kocks who proposed the following expression for the dislocation evolution with plastic strain, ε_p:

$$\frac{d\rho}{d\varepsilon_p} = M\left(\frac{1}{b\Lambda} - k_2\rho\right) \qquad (4)$$

The first term in the bracket represents the storage of dislocations in the microstructure. For the tempered martensitic alloys, we already showed that the mean free path is limited to a few microns, suggesting that the numerous boundaries of this typical microstructure control the mean free path. Consequently, a characteristic length, Λ, can be associated with the microstructure, and it is postulated that the average displacement of the dislocations responsible for the plastic strain is mediated by Λ. Therefore, Λ should be interpreted as a constant, whose value is unequivocally determined by the microstructure and is independent of the temperature. The second term of equation (4) takes into account all the dynamical recovery processes, e.g. annihilation of screw dislocations in parallel planes following cross slip. Here, the dynamical recovery is assumed to be linear with ρ, and it is characterised by a recovery coefficient, k_2, which is temperature dependent.

Equation 3 can be differentiated with respect to the plastic strain, ε_p, to obtain an expression for the plastic strain hardening, θ_p:

$$\theta_p = \frac{d\sigma}{d\varepsilon_p} = \frac{\left(M\alpha\mu b\right)^2}{\left[(\tilde{\sigma} + \sigma^{*2}) + 4(M\alpha\mu b)^2\rho\right]^{1/2}}\frac{d\rho}{d\varepsilon_p} \qquad (5)$$

Combining Equation 5 with Equation 4, we obtain:

$$\theta_p = \frac{M}{b\Lambda}\frac{\left(M\alpha\mu b\right)^2}{2\left(\sigma - \left(\frac{\sigma^* + \tilde{\sigma}}{2}\right)\right)} + \frac{Mk_2\left(\sigma^* + \tilde{\sigma}\right)^2}{8\left(\sigma - \left(\frac{\sigma^* + \tilde{\sigma}}{2}\right)\right)} - \frac{Mk_2}{4}\left[2\left(\sigma - \left(\frac{\sigma^* + \tilde{\sigma}}{2}\right)\right)\right] \qquad (6)$$

Equation 6 describes the plastic strain hardening evolution at constant plastic strain rate and temperature. In practice, $(\sigma^* + \tilde{\sigma})$ can be considered as a single parameter to be fitted, as σ^* and $\tilde{\sigma}$ are assumed to be independent of the dislocation density. $\tilde{\sigma}$ was taken as the value of the athermal component of the yield stress and σ^* was deduced from the temperature dependence of the yield stress. As a typical example, the $\theta_p(\sigma_p)$ dataset obtained at -130°C was fitted with Equation 6, Fig. 2.4.6. It appears that the predictions of Equation 6 agree rather well with the experimental data.

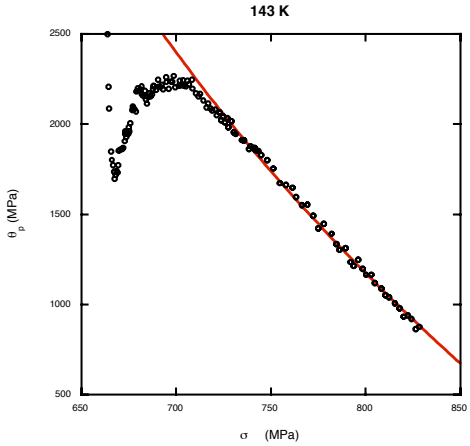

Fig. 2.4.6 *Example of fit of Equation 6 to a dataset obtained at -130°C.*

Small angle neutron scattering analysis of irradiation-induced defects in pure metals and alloys

Nano-scale irradiation-induced defects are believed to contribute significantly to the irradiation hardening in metals along with the microscopic defects. Transmission electron microscopy (TEM) allows direct observations of defects whose size is larger than about 1nm in weak beam imaging but other techniques have to be used to reveal ultra-fine scale microstructures. It is well established that small angle neutron scattering (SANS) is an effective technique to characterise nano-scale distributions of features in terms of number density, size distribution and chemical composition. Therefore, SANS experiments have been undertaken on the EUROFER 97 RAFM steel following proton irradiations at 250°C and 350°C to doses of 0.3 and 1dpa.

The SANS measurements were carried out at the Paul Scherrer Institute. Neutron scattered intensities were obtained with a neutron wavelength of 0.5nm and a specimen-detector distance of 2m, which allows measurements over a range of (q) from 0.35 to 2.6nm^{-1}, with q being the scattering vector. The measurements were performed in a strong saturating magnetic field perpendicular to the incident neutron beam. The raw data counts on the detector were corrected by subtracting off the background, the parasitic scattering and the scattered intensity of an unirradiated specimen. Finally, the anisotropy of the detector was accounted for by normalising the corrected scattered signal with the signal obtained for a water reference specimen with a known isotropic cross-section. In order to characterise the distribution of irradiation-induced scattering features, we used the equation relating the differential coherent small angle cross-section, $d\Sigma/d\Omega$, which is proportional to the scattered intensity, to a dilute distribution of a single type of scattering features:

$$\frac{d\Sigma}{d\Omega}(q) = \Delta\rho^2 \int N(R) V_p^2(R) P(q,R) dR \qquad (7)$$

where N(R)dR is the number of particles per unit volume having a diameter between R and R+dR, $V_p(R)$ is the volume of such a particle, P(q,R) is the form factor of the particles, and $\Delta\rho$ is the difference between the scattering length density of the particles and that of the matrix (it is the so-called contrast). $d\Sigma/d\Omega$ is proportional to the corrected scattered intensity. In the following, we present the corrected scattered intensities. So, all the results must be considered qualitative.

The scattered intensity of the specimens irradiated at 250°C to the two doses of 0.3 and 1dpa are presented in Fig. 2.4.7 (left) as a function of q along with that of an unirradiated reference specimen. The intensities are presented in arbitrary units and have been determined in a 10° wide vertical sector, centred at 90° from the magnetic field direction, where the scattered intensity is maximal. The additional scattered intensity arising from the irradiation-induced defect microstructure becomes detectable for q values larger than 0.7nm^{-1}. The scattered intensity for the specimen irradiated to 1dpa is clearly larger than that of the specimen irradiated to 0.3dpa. For the sake of clarity, the scattered intensity of the specimen irradiated at 350°C to 1dpa only is shown in Fig. 2.4.7 (right) in addition to that of an unirradiated reference specimen.

Fig. 2.4.7 *Left: scattered intensities after irradiation at T=250°C, for doses of 0.3 and 1dpa, along with the scattered intensity of an unirradiated specimen. Right: scattered intensity after irradiation at T=350°C, for a dose of 1dpa, along with the scattered intensity of an unirradiated specimen.*

The amplitude of the scattered intensity of the specimen irradiated at 350°C to 1dpa is much weaker than that of the specimen irradiated at 250°C to the same dose. Actually, the same observation holds for the specimens irradiated to 0.3dpa. A variety of small irradiation-induced defect clusters may contribute to the scattered intensity; these include nanometer-sized voids and helium bubbles and small dislocation loops. In the following, and in order to proceed with a qualitative discussion, we assume that we deal with a single distribution of spherical nano-features. This last assumption constitutes a simplification of the more complex real distribution of different types of nanometer-sized defects but allows assessment of the general trend of the evolution of the nanometer-sized defect distribution with dose and irradiation temperature. We recall that the distribution function is reflected in Equation (7) by N(R). A log-normal function is used for the distribution, which is written as:

$$N(R) = \frac{N}{\sqrt{2\pi}sR}\exp\left(-\frac{(\log(R/R_o))^2}{2s^2}\right) \qquad (8)$$

where R_o and s are the so-called scale and shape parameters and N is the number density. In order to better assess the evolution trend of N and R_o with irradiation dose and irradiation temperature, a value of 0.2 was selected for s. With these assumptions, it has been possible to satisfactorily fit the scattered intensities of the irradiated specimens by adjusting two parameters of the log-normal distribution function, namely R_o and N. The distribution functions obtained are reported in

Fig. 2.4.8 (left), where it can be seen that all the distributions peak below 1nm. Interestingly, the number density at a given irradiation temperature increases with dose but the number densities after the irradiations at 350°C are much lower than those at 250°C. The dose dependence of N for both irradiation temperatures is shown in Fig. 2.4.8 (right). Clearly, the nanometer-sized irradiation-induced defects tend to disappear with increasing irradiation temperature by enhanced recombination of point defects and possible coarsening of the clusters. It is also important to emphasise that the features described by these distributions have a size well below the TEM resolution limit.

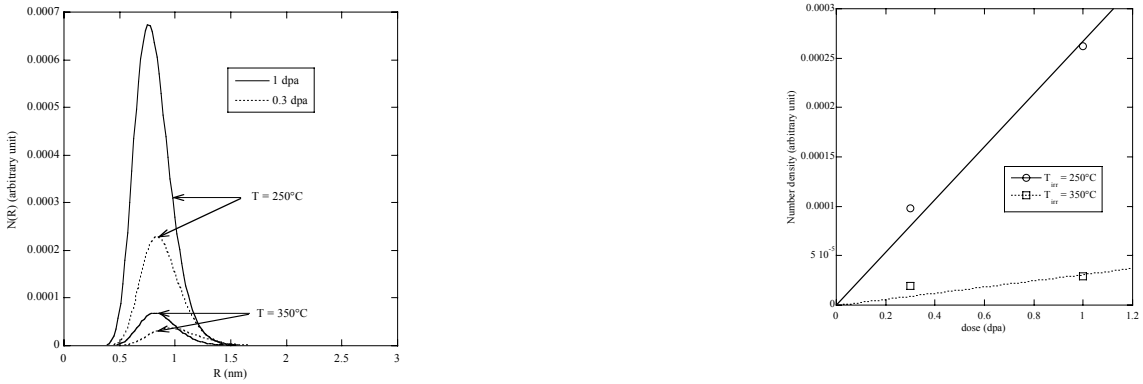

Fig. 2.4.8 *Left: size distribution of the scattering features for the different irradiation conditions investigated. Right: Number density N of the nano-features as a function of dose for both irradiation temperatures.*

2.4.3 EFDA Technology Tasks

Tasks Long Term

TW0-TTMI-003 deliverable 3: Small specimen test technology - Development of experimental fracture testing devices to be used in a hot cell environment and constraint loss assessment on sub-sized compact specimens of EUROFER 97

This work was aimed at developing experimental and modelling tools to ultimately model the temperature dependence of the fracture toughness in the ductile-to-brittle transition, to understand the effects of irradiation on the general degradation of the fracture properties, reflected by a shift of the transition to higher temperature and by a decrease of the fracture toughness in the ductile region, and finally to assess the specimen size and geometry effects on the measured fracture toughness. Hot cells have been built (Fig. 2.4.9, upper) that will allow us to work with irradiated specimens as big as 0.4T, such as compact tension specimens. All the necessary equipment, such as the remote handlers (Fig. 2.4.9, middle left), the drawer (Fig. 2.4.9, middle right) and the transport container (Fig. 2.4.9, bottom left), have been designed and manufactured, and the work procedures identified and adapted to fulfil the radioprotection requirements of the PSI. Furthermore, special techniques using remote handling had to be defined for the transfer of radioactive specimens between the hot cell and the storage place. A testing machine was modified and equipped with a self-aligned system (Fig. 2.4.9, bottom right) for flat and round tensile specimens, for notched-round tensile specimens and for compact specimens of different thicknesses. The development was done in such a way that the set-up of the different kinds of specimens in the testing machine is

easily manageable in the hot cell environment. An environmental chamber was mounted around the load train that allows us to cover a temperature range between -196°C and 250°C. Tensile tests and fracture tests were successfully carried out with this new load train, on standard DIN specimens and 0.4T CT specimens, respectively, of tempered martensitic steels and model alloys at temperatures between -196°C and 200°C.

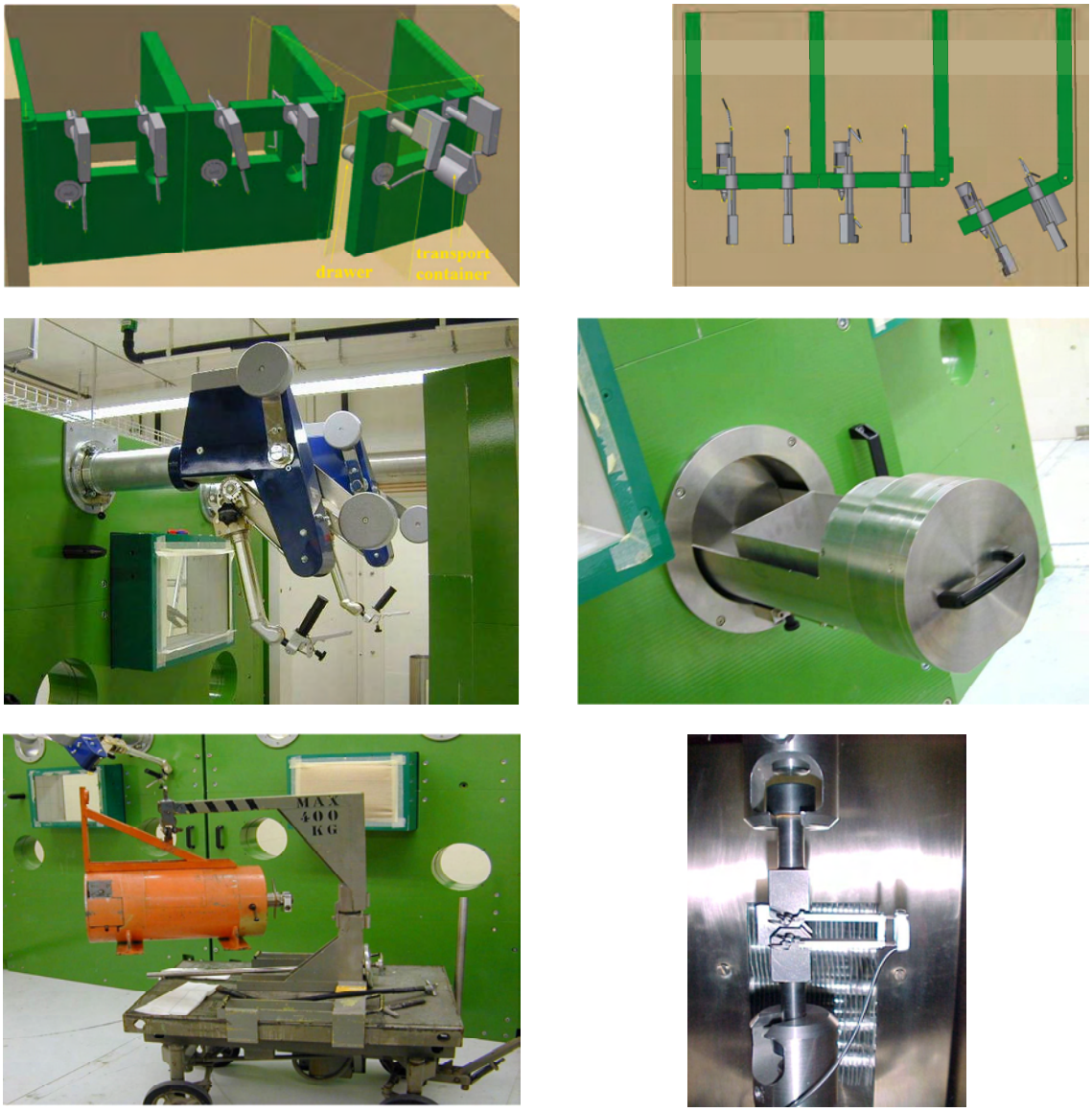

Fig. 2.4.9 *Up left: Schematic front view of the three hot cells. The drawer and transport container can be seen at the right cell. Up right: Schematic top view of the three hot cells. Middle left: Close-up view of the remote handles and the shielded front window. Middle right: Close-up view of the drawer for the transfer of weakly radioactive specimens. Bottom left: transport container on the pushcart for the transfer of strongly radioactive specimens. Bottom right: self-aligned load train with a 0.4T CT specimen and a clip gage attached directly to the pins, aside the clevises.*

TW1-TTMS-001 deliverable 3 : Proton irradiation of plate EUROFER 97 up to 1 dpa, for He effect testing

Series of tensile flat specimens (8mm in gauge length, 2.5mm in width, 0.3mm in thickness) of the EUROFER 97 RAFM steel have been irradiated with high-energy protons in the PIREX facility at 50°C, 250°C and 350°C to doses of 0.3, 1 and 2dpa. Tensile testing is in progress. Series of mini-bend bars (1mm x 1mm x 12mm) of EUROFER 97 RAFM steel have been irradiated with high-energy protons in the PIREX facility at 300°C to a dose of about 0.5dpa. Characterisation of the fracture toughness-temperature curve of irradiated EUROFER 97 will take place at the end of 2004, via 3-point bend testing of the irradiated mini-bend bars, following the usual cooling down period.

TW1-TTMS-002 deliverable 20 : Tensile and fracture toughness of EUROFER 97, punch testing

The small ball punch test (SPT) has been developed to extract tensile and fracture properties, to assess the so-called ductile-to-brittle transition temperature and even the fracture toughness properties. The ball punch test experimental device is presented in Fig. 2.4.10 (left). It consists of deforming a centre-loaded clamped disk with a spherical puncher. The load-displacement curve is then recorded. The spherical puncher is a 0.5mm radius (R1) hard steel ball. The ball is pushed with a rod through a 1mm hole in the upper die (D1) (a small tolerance of 0.05mm and oil lubrication are necessary). The diameter of the hole in the lower die is 1.5mm (D2), having a machined round billet radius of 0.2mm (R2). The sample (in black) is a disc with a diameter of 3mm (D3) and a thickness varying between 0.23 and 0.27mm (T).

A finite element model (FEM) for the SPT was developed using ABAQUS 6.4-1 standard code. The model is shown in Fig. 2.4.10 (right) and includes the ball, the upper and lower dies, and the sample disc. Taking advantage of the rotational symmetry of the experimental set-up, an axisymmetric FEM was developed. The ball and dies were implemented as rigid bodies. The disc was modelled with 2000 axisymmetric linear reduced integration elements (CAX4R). A force was applied between the upper die and the lower die during the deformation in order to prevent the specimen from slipping away. Friction between the dies and the disc constrains the latter in the same way as in the actual experimental device. The calculations were run by imposing the vertical displacement of the ball. Calculations with frictionless contact interactions as well as with a friction coefficient of 0.05 between the ball and the disc were considered. Such a friction coefficient is the upper value characterising the interaction between lubricated polished metal pieces. Finally, a constitutive behaviour had to be defined for the disc. The elastic properties are the Young's modulus, E, the Poisson's ratio, ν, and the yield stress, $\sigma_{0.2}$, defined at 0.2% plastic strain. For the plastic behaviour, the ABAQUS code also requires the plastic behaviour to be represented by the flow stress, σ, as a function of the plastic strain, ε_p, which is written as:

$$\sigma = \sigma_{0.2} + \sigma_{pl}(\varepsilon_{pl}) \qquad (1)$$

The $\sigma_{pl}(\varepsilon_{pl})$ relationship is derived from the uniaxial tensile behaviour. This can only be easily obtained up to the strain at which the necking starts. However, the equivalent plastic strain at certain locations of the punch disc can reach about 80% in the final stage of the SPT, i.e. a strain much larger than the true uniform strain. Hence, it is necessary to extrapolate the tensile curves beyond necking to have the appropriate constitutive behaviour to be used as input to the FEM calculations.

Five true stress–true strain relationships are shown in Fig. 2.4.11 (left), among which two deal with the constitutive behaviour of the F82H-mod reduced activation ferritic/martensitic (RAFM) steel in the unirradiated condition and three relate to possible constitutive behaviour that may result from irradiation-induced changes. A typical experimental SPT load-deflection curve obtained at room temperature for the F82H-mod RAFM steel in the unirradiated state is shown in Fig. 2.4.11 (right). Along with this experimental curve, five simulated curves are presented in Fig. 2.4.11 (right), which have been calculated using the five true stress–true strain relationships reported in Fig. 2.4.11 (left).

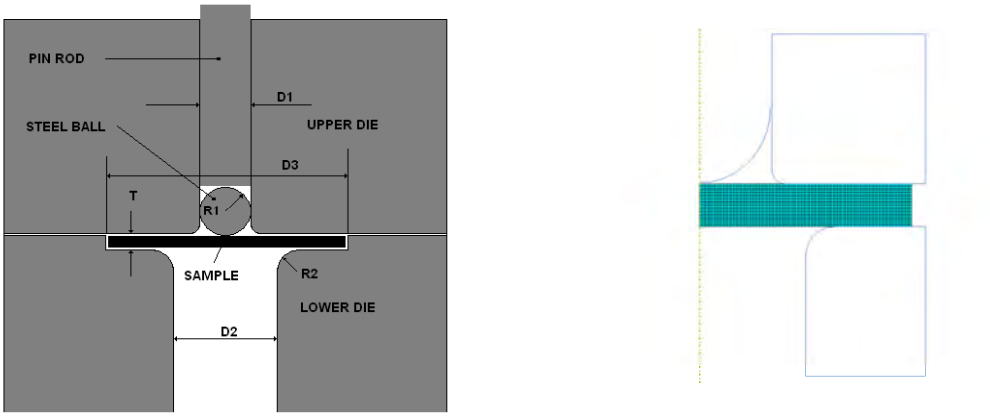

Fig. 2.4.10 *Left: experimental ball punch test device. Right: sketch of the axisymmetric FEM model implemented in ABAQUS for the ball punch tests.*

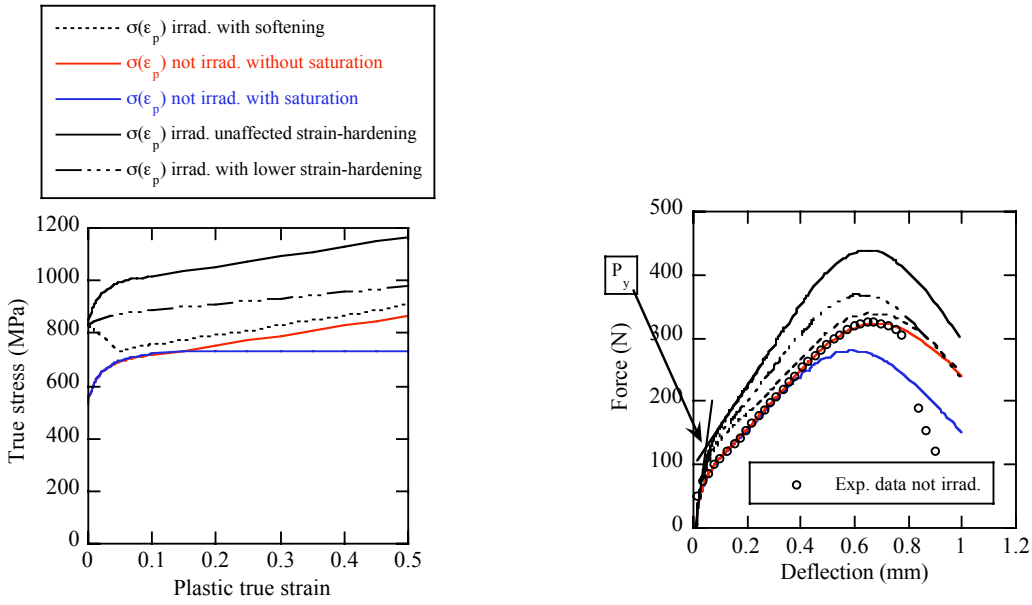

Fig. 2.4.11 *Left: five different constitutive behaviours used as input to simulate SPT load-deflection curves. Right: five simulated SPT load-deflection curves and one experimental curve obtained at room temperature for the unirradiated F82H-mod steel. The colours correspond to those used on the left for simulation inputs.*

The two $\sigma(\varepsilon_p)$ curves for the unirradiated case were constructed by extrapolating the experimental standard tensile curve, whose true uniform strain is limited to 5%. Two kinds of extrapolation have been made, one by extending the curve beyond necking with a linear slope (red curve in Fig. 2.4.11, left) and another one with a saturation stress (blue curve in Fig, 2.4.11, left). Excellent agreement between the simulated and experimental SPT curves was obtained when using the $\sigma(\varepsilon_p)$ curve without saturation. It was concluded that a linear strain-hardening stage beyond necking exists for the RAFM steels.

We have also studied the potential effect of irradiation hardening on the shape of the SPT curves by constructing three different true-stress true strain curves representing three possible constitutive behaviours for the irradiated F82H-mod RAFM steel. We arbitrarily selected an irradiation hardening (difference between the yield stress of the irradiated alloy and the one of the unirradiated alloy) of 300MPa and constructed three different post-yield behaviours. For the first one, the same strain-hardening as that of the unirradiated material was chosen, the second one accounts for a decrease of strain-hardening and the third one considers an initial softening of 100MPa over the initial 5% of plastic strain followed by a moderate strain-hardening regime identical to that of the unirradiated case above 5%. In Fig. 2.4.11 (left) these three curves are referred to as 'unaffected strain–hardening' curve, 'lower strain-hardening' curve, and 'with softening' curve, respectively. The SPT curves calculated after having assigned these three constitutive behaviours to the punch disc are plotted in Fig. 2.4.11 (right). It can be seen that the load P_y, determined by the intersection of the two slopes of the load-deflection curve drawn on both sides of the yielding zone, is practically independent of the post-yield behaviour. This fact confirms a previous observation we made, that P_y is mainly mediated by the yield stress, $\sigma_{0.2}$. Furthermore, this also supports the use of a simple and direct calibration between P_y and $\sigma_{0.2}$. Consequently, it is quite reasonable to estimate the irradiation hardening from the P_y increase itself provided a good calibration is made. As far as the post-yield behaviour is concerned, its major role is reflected in the slope of the load-deflection curves beyond 0.2mm. Actually, it was found that the slope of the SPT load-deflection curves beyond 0.2mm tends to scale with the averaged flow stress over the strain range 0.1-0.6. Thus, these slopes can be seen as the signature of the averaged strain-hardening capacity of the materials, defined as the difference between the averaged flow stress and the yield stress.

TW2-TTMS-006a deliverable 3 : Creep testing at RT-750°C on the two improved ODS batches

The reduced activation ferritic/martensitic (RAFM) steel EUROFER 97 and the oxide dispersion strengthened (ODS) EUROFER 97 steels, with the EUROFER 97 as matrix material and 0.3wt.% Y_2O_3 particles as reinforcement material, are expected to be used as structural materials in fusion power reactors at temperatures up to about 550°C and 650°C, respectively. Their creep behaviour is one of the key issues for their future application. Thermal creep tests have been conducted on the EUROFER 97 RAFM steel and two kinds of ODS EUROFER 97 steels, which were manufactured using powder metallurgy techniques (ball milling and hot isostatic pressing) at the CRPP and the CEA-Grenoble (France), respectively. Thermal creep experiments were conducted under constant stress at temperatures between 450°C and 750°C, in an argon flow, up to rupture.

It was found that the creep strength of the CRPP ODS batch is quite similar to that of the CEA ODS batch. The creep strength of both ODS steels is much higher than that of the EUROFER 97 alloy. In particular, for a given applied stress value, the

Larson-Miller parameter is larger by about 1.5 for both ODS steels with respect to the EUROFER 97 alloy (Fig. 2.4.12), which corresponds to a temperature increase of about 65 degrees for a given rupture time and indicates that both ODS steels could be used up to a maximum temperature that is about 65 degrees higher than for the EUROFER 97 alloy. Creep exponents in the range 3.9-5.5 were found for both ODS steels and an activation energy of 0.38eV was measured for the CRPP ODS batch. These values are characteristic of a dislocation creep mechanism associated with dislocation climb at obstacles, i.e., the Y_2O_3 particles. A creep exponent of about 14 was measured for the EUROFER 97 alloy, which indicates that the strain rate sensitivity to the applied stress is much lower for both ODS EUROFER 97 steels than for the EUROFER 97 alloy, which is beneficial to their future use.

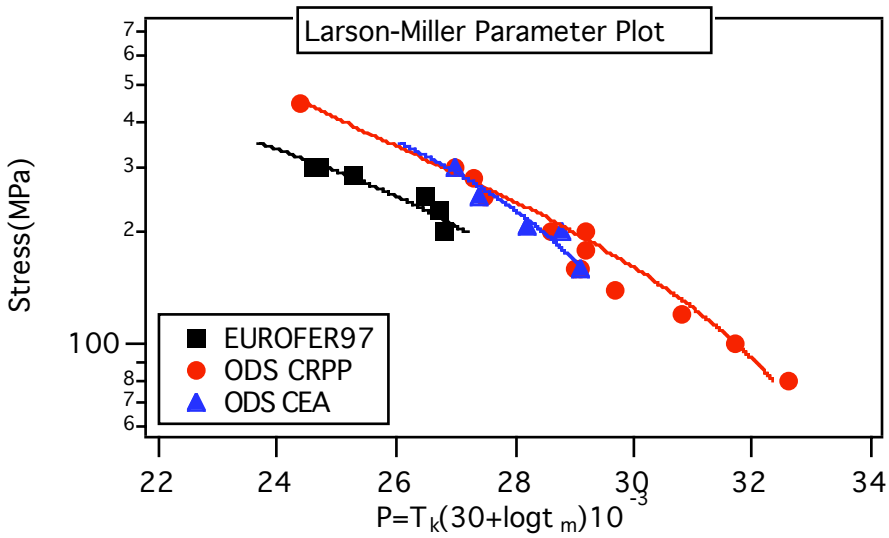

Fig. 2.4.12 *Larson-Miller parameter plot for the EUROFER 97 RAFM steel and both ODS EUROFER steels; T is the test temperature (in Kelvin), t_m is the creep life (in hours).*

TW2-TTMS-006a deliverable 6 : Tensile testing at RT-750°C on the two improved ODS batches

This work was aimed at characterising the tensile properties of two ODS (oxide dispersion strengthened) EUROFER 97 steels, with the reduced activation ferritic/martensitic (RAFM) steel EUROFER 97 as matrix material and 0.3wt% Y_2O_3 particles as reinforcement material, which were manufactured using powder metallurgy techniques (ball milling and hot isostatic pressing) at the CRPP and the CEA-Grenoble (France), respectively.

Tensile tests were performed in a Zwick Z010 testing machine on tensile flat specimens (2.5mm in width, 0.3mm in thickness, 8mm in gauge length) of both ODS steels, in an argon flow, at various temperatures ranging between room temperature and 700°C, up to rupture. The strain rate was about $5x10^{-4}s^{-1}$. As expected, it was found that both ODS steels present a much higher tensile strength than the EUROFER 97 RAFM steel alone in the temperature range RT-550°C (Fig. 2.4.13). However, the tensile strength of both ODS steels shows a strong drop in the range 550-600°C, like the one for EUROFER 97. As a result, the gain in high temperature strength by both ODS steels remains quite small. As also expected, the total elongation of both ODS steels is significantly lower than the one of the

EUROFER 97, at all test temperatures. However, it can still be considered as reasonable. The tensile strength of the CRPP ODS batch is significantly higher than the one of the CEA ODS batch. However, its ductility is lower, as reflected by the absence of necking at all test temperatures. This could be due to the absence of heat treatment applied to the CRPP ODS batch following processing by powder metallurgy.

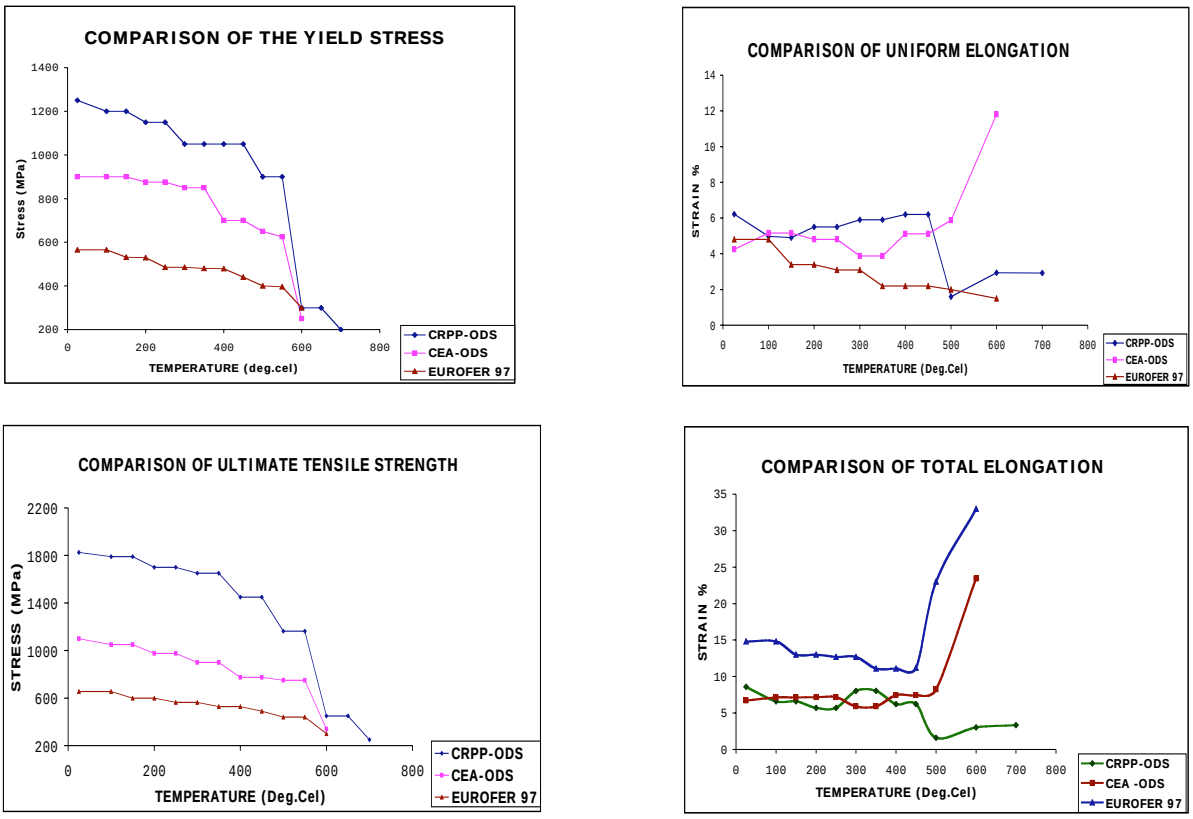

Fig. 2.4.13 *Tensile behaviour of both ODS EUROFER steels compared with the EUROFER 97 RAFM steel.*

TW2-TTMS-004b deliverable 3 : Development and testing of coatings to improve the corrosion resistance vs Pb17Li at T>450°C

Thirty cylindrical specimens (10mm in diameter, 50mm in length) have been cut by spark erosion from a plate of the reduced activation ferritic/martensitic (RAFM) steel EUROFER 97. Eighteen specimens have been sent to three different European companies for deposition of pure W coatings using three different techniques. Six specimens were coated with a 10μm-thick hard W coating using a galvanic technique (Fig. 2.4.14, left). Six specimens were coated with a 18-22μm-thick W coating using a physical vapour deposition (PVD) technique (Fig. 2.4.14, right). Six specimens were coated with a 120μm-thick W coating using a plasma spraying technique. All the coated specimens were received in spring 2004. On the other hand, design of a small corrosion device has been completed, which will allow us to test the resistance of the three types of W coatings as protection barriers for the EUROFE 97 RAFM steel against corrosion in molten Pb-17Li. In this device a cylindrical specimen is screwed to the bottom part of a rod that is connected to a small motor. The motor allows the specimen to rotate in a bath of molten Pb-17Li at a speed between 1mm/s and 5m/s and a bath temperature between 300°C and 800°C. A first mock-up has been manufactured and successfully tested

(Fig. 2.4.15). Ten such corrosion devices are being now manufactured. Corrosion experiments will be performed in 2005, at a specimen rotation speed of about 30cm/s and a bath temperature of 550°C, for various corrosion times ranging between 500 and 10'000 hours.

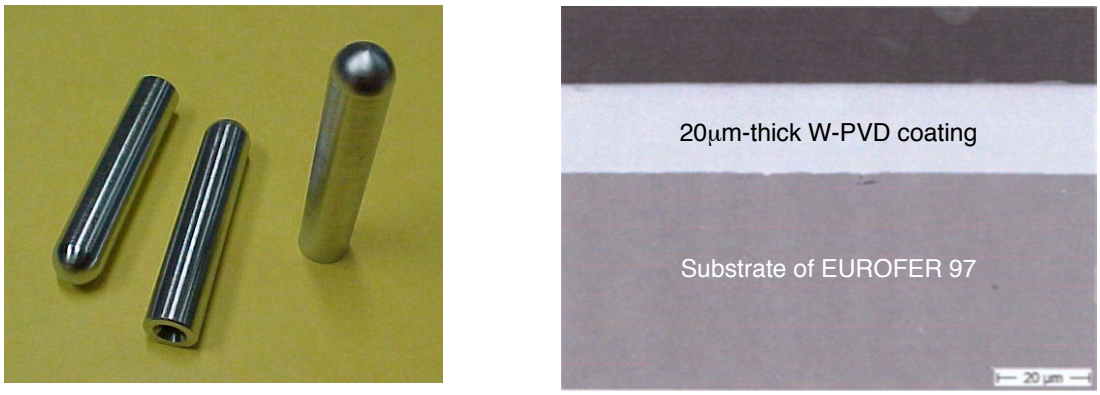

Fig. 2.4.14 *Left: Optical micrograph of cylindrical specimens of the EUROFER 97 RAFM steel coated with a 10-μm layer of Hardalloy W. Right: Scanning electron microscopy image of a cross-sectioned specimen of EUROFER 97 coated with a 20μm-thick layer of W-PVD; note the high density of the W-PVD coating.*

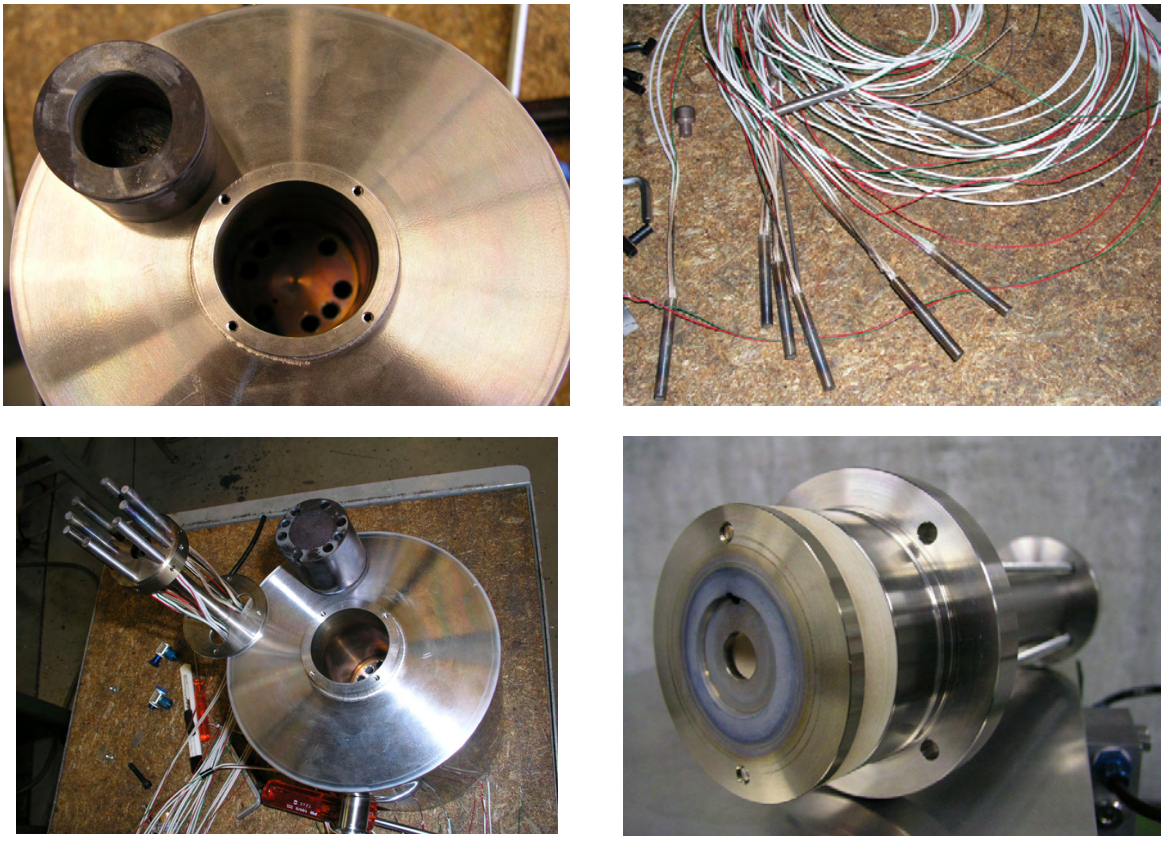

Fig. 2.4.15 *Optical micrographs of the Pb-17Li corrosion facility. Top left: Mo container and cooling chamber under vacuum. Top right: cylindrical thermo-elements. Bottom left: the thermo-elements are being inserted into the wall of the Mo container, from the bottom part of the vacuum chamber. Bottom right: upper part of the installation, mainly composed of a rotating central rod that is fixed to a small motor.*

TW2-TTMS-005b deliverable 6 : Small-scale fracture mechanics - Modelling of brittle and brittle to ductile transition behaviours using appropriated theories. Formation of rules for transferability to standards and fusion components

In order to assess the size/geometry effect on fracture toughness in the transition between the ductile and brittle modes, we developed one of the main modelling tools that we need. This tool consists of calculating the stress/strain fields at the crack tip by finite element analysis (FEA) and in establishing a cleavage criterion. Two-dimensional models were built with ABAQUS 6.4-1 to evaluate the in-plane constraint loss for bend bars and compact tension specimens. The 2D model for the bend bar is shown in Fig. 2.4.16 (left) as an example. The crack tip was modelled with an initial root radius ρ_o to allow blunting. In order to make the results independent of the initial root radius, the simulated specimens had to be loaded up to a load for which the crack tip opening displacement δ is at least five times as large as ρ_o. Iso-stress contours for the maximum principal stress at the crack tip are shown in Fig. 2.4.16 (right).

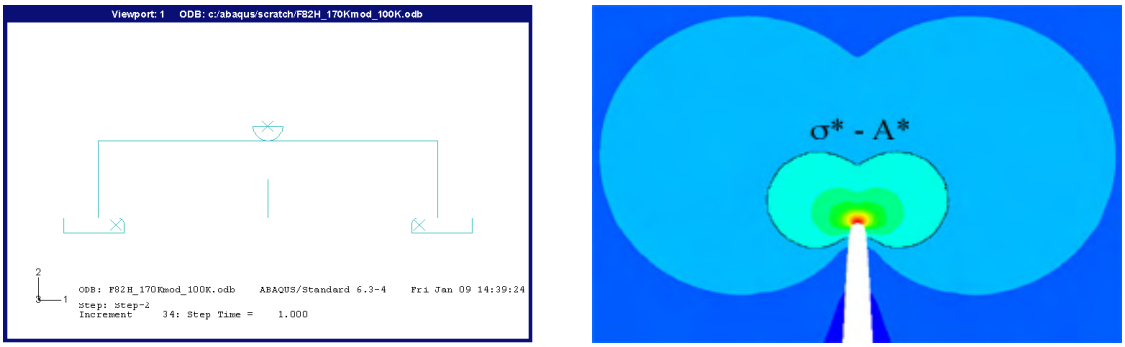

Fig. 2.4.16 *Left: 2D model of a bend bar, loaded in the standard configuration. Right: Details of the mesh refinement at the crack tip.*

The effect of specimen size/geometry on fracture toughness can be quantified in the transition, where the fracture mode remains cleavage, by defining a cleavage criterion related to the attainment of a critical stress σ^* encompassing a critical area A^*. When the σ^*-A^* criterion is reached, fast fracture by cleavage is triggered. The size/geometry effect on fracture means that for different sizes/geometries different critical applied stress intensity factors K_c (or critical energy release rates J_c) are required to reach the σ^*-A^* criterion. This criterion is illustrated in Fig. 2.4.16 (right). Only under special circumstances is fracture toughness a material property. In particular, the dimensions of the specimen have to be large with respect to those of the process zone in which cleavage is initiated. These special conditions are usually called small scale yielding SSY conditions.

Subsequently, we investigated the effects of irradiation hardening (irradiation-induced increase in yield stress) and the post-yield behaviour on the attainment of the critical conditions for cleavage. For the unirradiated F82H-mod RAFM steel, the fracture toughness in SSY conditions is about $100 MPa.m^{1/2}$ at -100°C, a temperature at which we chose to run a series of simulations. The corresponding experimental constitutive behaviour is shown in Fig. 2.4.17. The necking begins at 0.05 and then the curve is simply linearly extrapolated. We also selected three hypothetical true stress-true strain curves for the irradiated state (Fig. 2.4.17). All three curves exhibit an irradiation hardening of 100MPa but different post-yield behaviours. In the first case, the strain hardening is not affected by the irradiation.

In the second case, a Lüders-type strain region without strain hardening up to 0.03 is followed by the same strain-hardening law as that of the unirradiated material. In the third case, we considered a moderate softening (-50MPa) over a strain of 0.03 also followed by the same strain-hardening law as that of the unirradiated material.

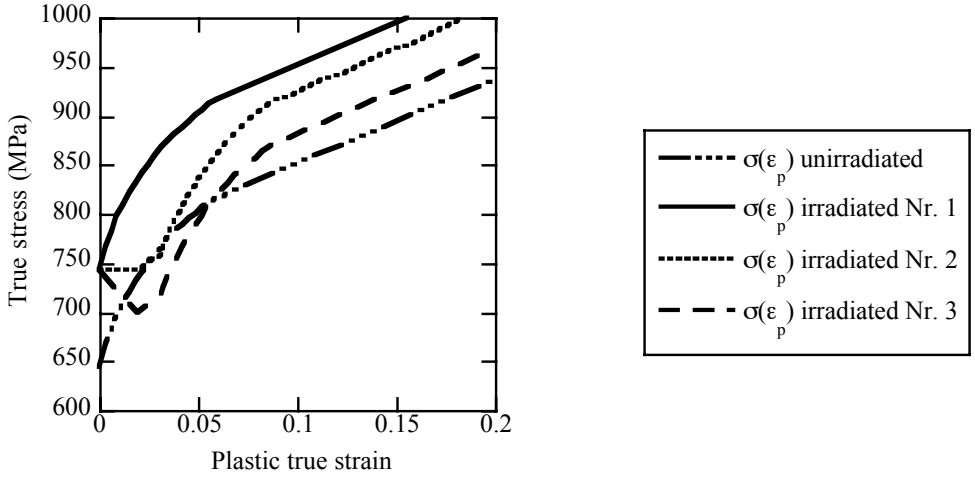

Fig. 2.4.17 *Four different constitutive behaviours used as inputs to simulate the stress field at a crack tip.*

We imposed the elastic displacement field at the outer boundary of the mesh and assigned the $\sigma(\varepsilon_p)$ unirradiated curve as the constitutive behaviour of the material. Then we assumed that the local critical condition for cleavage is given by σ^*=2000MPa acting over an area A*= $1x10^{-8}m^2$. These last values for the (σ^*-A*) criterion are quite similar to those already used for the F82H-mod steel to model the entire fracture toughness-temperature curve. Using this σ^*-A* criterion we simulated the stress field that develops at the crack tip when the three other constitutive behaviours for the irradiated material are selected and we searched the required applied stress intensity factor to reach the cleavage condition σ^*-A*. The results are summarized in Table 2.4.2, where the strong influence of the post-yield behaviour on the attainment of the σ^*-A* criterion can be seen. This is reflected in the strong dependence of K_c on the constitutive behaviour. It is therefore of prime importance to establish the true stress-true strain relationship over a significant strain range (about 0.05). This is particularly evident if one wants to predict the fracture toughness change under irradiation. Unfortunately, tensile testing of irradiated specimens does not allow us to obtain this information due to the necking phenomenon occurring at low strain. Consequently, compression or torsion specimens, which permit investigation of the true stress-true strain relationship over a significant strain range, should be used and included in future irradiation matrices.

Constitutive relationship	**Applied K_c to reach σ^*=2000MPa-A*=$1x10^{-8}m^2$**
$\sigma(\varepsilon_p)$ unirradiated	100 MPa $m^{1/2}$
$\sigma(\varepsilon_p)$ irradiated Nr. 1	56 MPa $m^{1/2}$
$\sigma(\varepsilon_p)$ irradiated Nr. 2	66 MPa $m^{1/2}$
$\sigma(\varepsilon_p)$ irradiated Nr. 3	85 MPa $m^{1/2}$

Table 2.4.2 *Critical applied stress intensity factor K_c to reach the selected cleavage criterion σ^*-A*.*

TW3-TTMA-002 deliverable 2 : W coating onto RAFM alloys

Eight cylindrical specimens, with a diameter of 25mm and a height of 10mm, have been cut out from a plate of the EUROFER 97 reduced activation ferritic/martensitic steel. A 50μm-thick layer of pure Cu has been deposited onto the surface of these eight specimens using a galvanic method. The pre-coated specimens have subsequently been sent for deposition of mm-thick W coatings using a chemical vapour deposition (CVD) technique. Note that pre-deposition of a Cu layer onto the EUROFER 97 substrates was necessary as the adherence of W-CVD coatings on steel substrates is known to be close to zero. The W-CVD coatings have been then characterized by means of Vickers microhardness and bond strength measurements, scratch tests and microscopic observations (optical microscopy, scanning electron microscopy). The quality of the W-CVD coatings was found excellent, especially in terms of high density (Fig. 2.4.18) and excellent adhesion to the steel substrates. The only drawback concerns the necessity to have an interlayer between the steel substrate and the W-CVD coating.

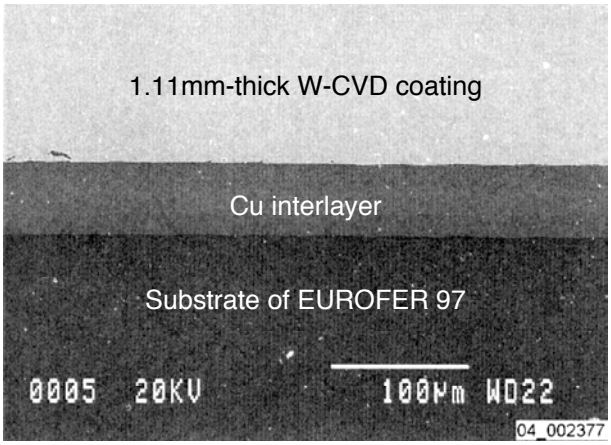

Fig. 2.4.18 *Scanning electron microscopy image (secondary electrons) of a cross-sectioned W-CVD coated specimen of the EUROFER 97 RAFM steel.*

TW3-TTMS-005 deliverable 1 : Low cycle fatigue testing of EUROFER 97

This work is aimed at testing the EUROFER 97 reduced activation ferritic/martensitic (RAFM) steel under low cycle fatigue (LCF). The fatigue will be strain controlled at room temperature, 150°C, 300°C and 550°C. The tests will be run in vacuum using strains of 0.5%, 0.8% and 1.4%. Tests with 500sec hold times will be also run, at the same temperatures and using the same imposed strains. The first step of this project consisted in the development of a new LCF mini-specimen, suitable for irradiations in reactors (small size, small mass) and compatible with our testing machine. Furthermore, the new design had to account for the available norms and designs already in use in other laboratories. Therefore, a visit to the Forschungszentrum Karlsruhe was made in January 2004. The specimen finally chosen is a cylindrical round specimen with a diameter of 2.7mm and a gauge length of 6mm (Fig. 2.4.19). This geometry should guaranty good stability, even at high temperatures, for imposed strains up to 2%. The specimen is gripped with two conical fittings screwed to the specimen extremities by a 5mm thread. Forty specimens were manufactured. The conical fittings were made of Inconel 718 and annealed. The chosen design is assumed to work up to 550°C. Only real tests will demonstrate the correctness of the design. Specimens were cut

out from a 25mm-thick plate of the EUROFER 97, in the rolling direction. They became available in May 2004. LCF testing is in progress.

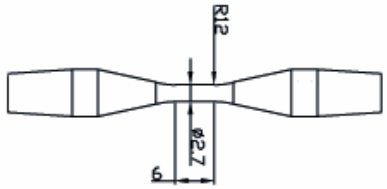

Fig. 2.4.19 *LCF mini-specimen geometry.*

TW3-TTMS-005 deliverable 2 : Investigation (tensile and Charpy testing) of PHT and PWHT to improve the design limits and to define the acceptable temperature range

No activity has been undertaken yet since the post-weld heat-treated plates are not available from the EFDA for the time being.

TW3-TTMS-006 deliverable 3 : Study of the influence of Ti addition on the mechanical properties (Charpy, tensile) with characterisation of the full fabrication process

This task is aimed at producing and characterising a batch of ODS EUROFER containing a small addition of Ti in an attempt to improve the fracture properties. A first ingot has been produced by powder metallurgy and characterised by means of transmission electron microscopy (TEM), tensile tests and Charpy impact tests. Atomised EUROFER 97 has been sieved to particles smaller than 45μm and mixed with 0.3wt.% Y_2O_3 particles, 10 to 30nm in size, and with 0.5wt.% Ti powder (99.99%), by ball milling for 24 hours in an Argon atmosphere. This work was performed in collaboration with the University Carlos III in Madrid (Spain). The resulting ODS powder was sent to the Haute Ecole Valaisanne in Sion (Switzerland) for compaction. There, the powder was pre-pressed uniaxially in a rough vacuum (150mbar), under 35MPa at 1100°C for about 7 minutes, to close the porosity as much as possible, using a matrix and a piston in graphite protected by boron nitride, and cooled down. Final compaction of the samples protected by a boron nitride coating was made in a hot isostatic press (HIP) under 180MPa at 1000°C for 1 hour. To reduce the excessive residual porosity obtained in previous processing experiments, the ingot geometry was changed to optimise the compactness. The ingots originally had a diameter of 30mm or 53mm and a height of 6-7mm. They have now a diameter of 30mm and a height of 30mm. The piston and the matrix had to be changed. Optical microscopy observations showed that the material is fully dense, to the exception of some regions at the edges of the HIPed specimens.
Transmission electron microscopy (TEM) observations revealed a martensitic morphology (Fig. 2.4.20, left), with lathes and a high dislocation density, and grain sizes in the range 1 to 5μm. Large particles, between 10 and 500nm in diameter, have also been observed (Fig. 2.4.20, right). Their distribution is heterogeneous, which is in principle detrimental to the mechanical properties. TEM chemical analyses revealed that the large particles are made of a titanium-yttrium oxide. Tensile tests showed that the material has an ultimate tensile strength in the GPa range from room temperature to about 400°C but with very limited plasticity (the total plastic strain is below 1%). Above 400°C, the strength starts to decrease and reaches 350MPa at 600°C, with a total plastic strain of 3 to 5%. Charpy impact tests revealed that the material is brittle from room temperature to 500°C.

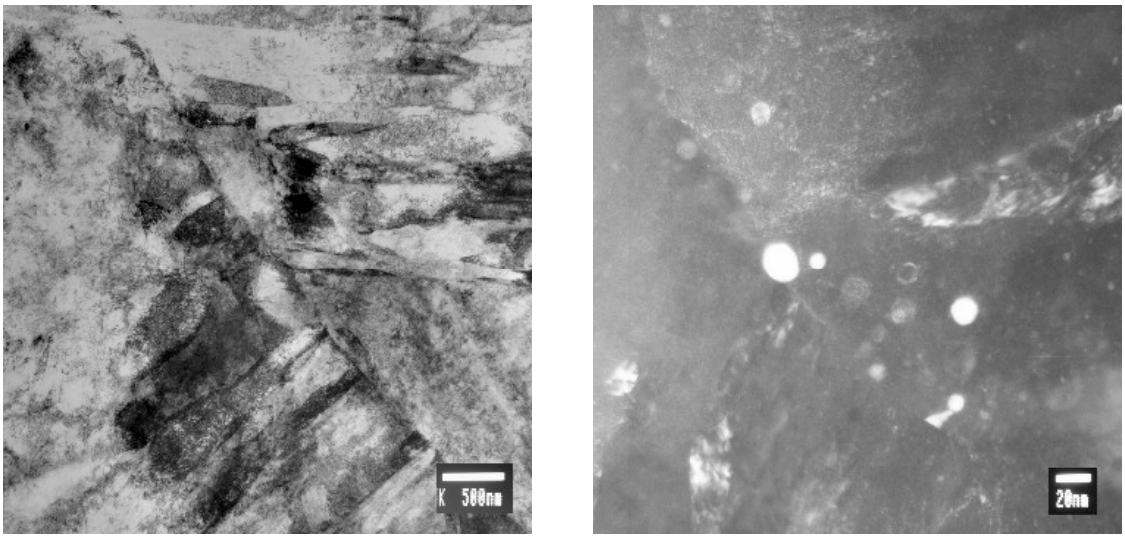

Fig. 2.4.20 *Left: TEM bright field image showing the martensitic-like microstructure of the as-prepared ODS EUROFER Right: TEM dark field image showing the inhomogeneous distribution of the Ti-Y-O particles.*

TW3-TTMS-007 deliverable 8 : Irradiation in SINQ

Specimens of the EUROFER 97 reduced activation ferritic/martensitic (RAFM) steel, the ODS EUROFER (EUROFER 97 reinforced with 0.3wt.% Y_2O_3 particles) and three Ti-base alloys (Ti-5Zr-2.4Sn, Ti-5Zr and Ti-22Zr), destined to be irradiated in 2004/2005 in the Swiss Spallation Neutron Source (SINQ), had been prepared by spark erosion at the end of 2003. They include mini-Charpy specimens ($3x4x27mm^3$), tensile flat specimens (5mm in gauge length x 1mm in width x 0.4mm in thickness), specimens for TEM observations and small punch testing (3mm in diameter x 0.25mm in thickness) and specimens for small angle neutron scattering measurements ($8x8x1mm^3$). Specimens were mounted into the irradiation tubes at the beginning of 2004. The tubes consist of 9mm internal diameter Zircaloy tubes inserted into the solid target. The specimens were packed with either Zircaloy or Al. Note that two or three thermocouples per tube are used to monitor the irradiation temperature. The irradiation campaign was started at the end of April 2004, following the usual 4-month winter shutdown of the PSI proton accelerator, and will last two years (about 16 full irradiation months). The irradiation spectrum is a mixture of high-energy protons (original energy: 570MeV) and 30 to 50% spallation neutrons, depending on the position of the tube inside the target. The dose and irradiation temperature, as well as the amount of impurities (e.g. He, H) produced as a result of spallation nuclear reactions, vary according to the position of the tube inside the target. The mounting was performed in such a way that enough specimens will be irradiated in a given irradiation condition, which will allow us to perform subsequently systematic, valuable mechanical tests on irradiated specimens. The doses and irradiation temperatures are expected to range between 5 and 10dpa, and 300 and 600°C, respectively.

TW3-TTMS-007 deliverable 10 rev.1 : MD simulations of effects of cavities

This task is aimed at identifying the defects that actually contribute to the hardening of Fe and Fe-Cr alloys in presence of irradiation-induced He. For this purpose, particular defect configurations have been created by means of molecular

dynamics (MD) simulations. Dislocation loops with a Burgers vector of the a/2<111> or <001> type and lying in {110} or {001} planes, respectively, were created in Fe. In addition, cavities with a radius of 0.5, 1.0, 2.0 and 5.0nm were created, also in Fe. They remained empty or were filled with He. In order to simulate the Fe-He interaction in MD, the interatomic potentials implemented by Morishita (2003) have been used. They are based on the interatomic potentials of Ackland (1997), Wilson-Johnson (1972) and Beck (1968), which describe the interactions of Fe-Fe, Fe-He and He-He, respectively. The MD code was adapted to these potentials.

A code has been written to generate dislocations for MD simulations with any Burgers vector in a face centred cubic (fcc) or body centred cubic (bcc) lattice. The displacement field is described in the frame of the anisotropic elasticity of the continuum. It can generate any type of dislocations, from edge, mixed to screw dislocations. Figure 2.4.21 shows the cores of an edge dislocation and a screw dislocation that were generated with this computer code and were relaxed by means of MD. The procedure was successful as it could reproduce the fact that the edge dislocation core presents a planar dissociation, or core spread, in the {011} glide plane, while the screw dislocation presents a three fold core dissociation in three {011} planes, 120° apart.

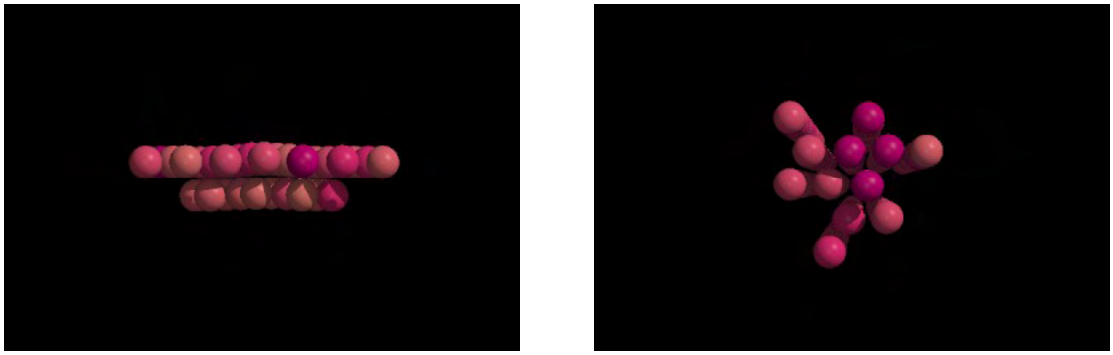

Fig. 2.4.21 *Left: edge dislocation core in bcc Fe, viewed along a <112> direction. Right: screw dislocation core in bcc Fe, viewed along a <111> direction. Only high potential energy atoms are displayed.*

The MD code has been adapted to apply a stress and/or strain to the simulation box containing the irradiation-induced defect configurations and one screw or edge dislocation. Figure 2.4.22 shows first results of a MD simulation of the interaction between an edge dislocation and a 2nm void in pure Fe. The dislocation moves under an applied strain rate at a speed of 60m/s. The resulting hardening is about 200MPa. In addition, the He effect has been investigated. First results showed very surprisingly that He bubbles seem to offer a weaker hardening than voids, presumably because their internal surface energy is reduced. The work is being continued to investigate the dependence of this hardening with temperature, strain rate and dislocation character (edge or screw).

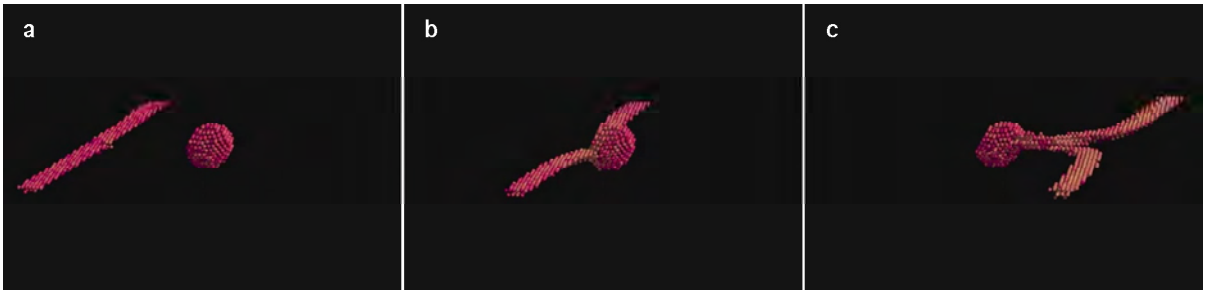

Fig. 2.4.22 *MD simulation of the interaction between an edge dislocation (left) flying at 60m/s and a 2nm void (centre): (a) dislocation approaching the void, (b) dislocation being attracted to the void, and (c) just before the dislocation escapes the void. Only high potential energy atoms are displayed.*

TW4-TTMA-002 deliverable 2 : Development of W-based materials for future divertor application using electrodeposition

It is proposed to use electro-deposition with the aim of producing nanostructured tungsten (W) with improved ductility and fracture toughness, due to the reduction in grain size,. A literature research has been made to find the optimum electro-deposition conditions. It appeared that it is not possible to deposit W alone, but W can be co-deposited with other metallic elements, such as Fe, Ni or Co. It was decided to deposit W with Fe, a relatively low activation element from the point of view of irradiation-induced radioactivity. The selected solution consisted of sodium tungstate, ammonia citrate, phosphoric acid, boric acid, 2-butene-4-diol and $FeSO_4$, diluted in water. The W-Fe alloy was deposited electrolytically over a Cu plate, 10mm wide and 0.5mm thick. The deposited alloy was 20μm thick and it appeared to be fully dense under optical microscopy. A carefully controlled experiment showed that the deposit is paramagnetic, indicating that it is rich in Fe. Transmission electron microscopy (TEM) observations revealed a nanostructured microstructure (Fig. 2.4.23). Grains are nicely equiaxed and their mean size is about 50nm. X-ray energy dispersive spectrometry showed that the deposit contains 85at.% Fe and only 15at.% W. In the next step, the electro-deposition solution will be tailored to enrich the material in W.

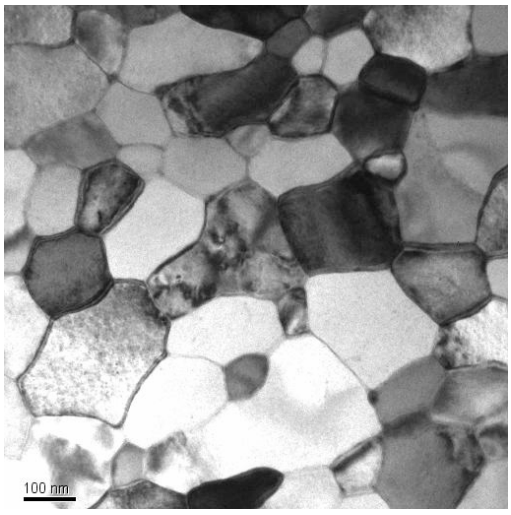

Fig. 2.4.23 *TEM bright field image of the electro-deposited W-Fe alloy.*

TW4-TTMS-005 deliverable 4 : Support in the development of design rules for structural materials with low ductility

Tensile tests were carried out at room temperature on flat and cylindrical tensile specimens of the EUROFER 97 reduced activation ferritic/martensitic steel. The tests were instrumented with a clip gauge fixed along the gauge length of the specimens. The uniform elongations measured for both geometries were very similar while, as expected, the post necking behaviour differs according to the tested geometry. During the testing, the elongation of the specimen was also measured with a linear variable differential transformer (LVDT) recording the displacement of the mobile traverse, and a well-calibrated compliance correction was applied, which allowed us to calculate the strain of specimens deformed at various temperatures without the clip gage. A series of scanning electron micrographs of fracture surfaces of the cylindrical specimens were taken to characterise the fracture mode. A new series of specimens with markers on the strain gauge has been machined to test the feasibility of the in-situ detection of necking.

TW4-TTMS-006 deliverable 2 : Literature study on ferritic ODS steels for HT application

Even though the alloys Fe(12-14)Cr-(2-3)W-(0.2-0.5)Ti-(0.2-0.5)Y_2O_3 already display excellent mechanical properties, ODS ferritic alloys for fusion applications are still at an early stage of development. Neither of these materials is at a commercial stage of development compared with conventional and reduced activation ferritic/martensitic steels, for which the technology (i.e. steel processing, final fabrication, welding, etc.) is advanced to the point that a fusion reactor could be constructed. Some of the problems still to be solved for ODS ferritic steels include: the impurity puck-up during mechanical alloying process, the elimination of the eventual elongated grain structure (deriving from the way most of these steels are processed) that produces anisotropic behaviour in the mechanical properties, the production of large section sizes, and the joining of ODS ferritic steels in a large structure. The mechanical behaviour of ODS ferritic steels depends on minor details of composition, milling method and conditions, consolidation path and conditions, and thermo-mechanical treatment. Finally, there is the question of irradiation resistance of ODS ferritic steels, for which limited information is available. In addition to the above-mentioned parameters, post-irradiation analyses indicate that the mechanical behaviour of irradiated ODS ferritic steels depends strongly on the reactor history (reactor type, irradiation conditions).

TW4-TTMS-007 deliverable 7 : Molecular dynamics simulations of grain boundaries

The role of grain boundaries (GBs) in the development of atomic displacement cascades in body centred cubic (bcc) Fe was studied using large-scale molecular dynamics (MD) simulations. Using the Ackland potential, simulations of cascades of 5-20keV primary knock-on atom (PKA) energy have been performed in 6nm, 12nm and 18nm grain-sized samples containing 1.4, also 1.4 and 7.25 million atoms, respectively. The nanocrystalline samples contained several GBs with structures varying from low to high angle, allowing us to study the role of the various GB structures as sinks for the self-interstitial atoms (SIAs). Comparison was also done to single crystalline samples of approximately the same size as that of nanocrystalline samples.

Preliminary results of the 12nm grain-sized single crystalline samples showed that the SIA clusters are mostly quite small and move in <111> directions. Vacancy

clusters are also small, the largest clusters containing only 4 vacancies. With the introduction of GBs, the large exodus of SIAs to the GBs leaves a larger number of vacancies in the interior of the grains. Within the 6nm grain-sized nc samples the irradiation was spread over several grains with some GBs situated in the midst of the cascade core. As a consequence not many vacancies formed, such that the damage was much smaller than in single crystals because of the GBs role during the displacement cascade. Within the 12nm grain-sized nanocrystalline samples many small clusters containing up to 3 vacancies formed as a result from displacement cascades up to 10keV. For 20keV displacement cascades, large voids containing as many as 35 vacancies were observed in addition to the small vacancy clusters. Within the 18nm grain-sized nanocrystalline samples the number of vacancies is of the order of that in single crystals. The size of these samples, however, limits the number of simulations possible because of computational constraints.

The GBs are made up of consecutive regions of high tensile and high compressive pressure. Detailed study of the path followed by the SIAs showed that they are attracted to regions of high tensile pressure. Therefore, as seen previously also in nanocrystalline face centred cubic (fcc) Ni, the GBs act as sinks for the SIAs with attraction of SIAs to regions of high tensile pressure within the GBs and their annihilation within the free volume.

Tasks Next Step

TW1-TVV/Titan : Titanium alloy irradiation testing

All experiments have been completed. The main obtained results are presented below together with the results obtained within the task TW3-TVM-TICRFA, also achieved.

TW3-TVM-TICRFA : Effect of low dose neutron irradiation on Ti alloy mechanical properties

The following reports on both the tasks TW1-TVV/Titan and TW3-TVM-TICRFA in which tensile and mini-Charpy specimens ($3x4x27mm^3$) of two titanium alloys, namely Ti-6Al-4V and Ti-5Al-2.5Sn, have been irradiated at 150°C to about 0.15dpa, with 590MeV protons in the PIREX facility and with neutrons in the KFKI reactor in Budapest (Hungary), respectively. Note that, in case of neutron irradiations one mini-Charpy specimen per material was initially loaded with 150wppm H and another one was annealed in order to remove most of the hydrogen content.

The Ti-5Al-2.5Sn alloy was found to be less affected by both the proton and neutron irradiations compared with the Ti-6Al-4V alloy. Following neutron irradiation, the radiation hardening measured at 150°C is only 14MPa for the Ti-5Al-2.5Sn alloy compared with 150MPa for the Ti-6Al-4V alloy. The stronger irradiation hardening evidenced for the Ti-6Al-4V alloy results probably from the irradiation-induced formation of vanadium precipitates. Fracture toughness tests have been performed on both alloys. Before irradiation, the fracture toughness values were found very similar for both alloys. They are equal to about $60kJ/m^2$ at room temperature and reach about $100kJ/m^2$ at 150°C. Following irradiation, both alloys show a large reduction in fracture toughness when tested at room temperature, while at 150°C the reduction in fracture toughness is more pronounced for the Ti-6Al-4V alloy. This holds for both the proton and neutron irradiations. The annealed Ti-6Al-4V

alloy resists the irradiation much better. Following neutron irradiation, the Ti-5Al-2.5V alloy initially loaded with 150wppm H still is still very ductile, whereas the Ti-6Al-4V alloy loaded with the same amount of hydrogen appears quite brittle. Nevertheless, the effect of hydrogen is not obvious and does not seem to be additive as the fracture toughness is of the same order of magnitude with or without hydrogen. As shown in our previous work, loading hydrogen by heat diffusion leads to a change in the microstructure. Therefore, the mechanical behaviour of an as-received material containing a certain amount of hydrogen is not comparable to that of a hydrogen-loaded material.

TW5-TVM-COMADA: Investigation of the effect of creep fatigue interaction on the mechanical performance and lifetime of CuCrZr

The CuCrZr alloy is a candidate heat sink material for the first wall of the ITER fusion reactor. Therefore, extensive research was conducted in the past on the fatigue properties of the CuCrZr alloy, under relevant ITER operating conditions. Unfortunately only few data exist on its creep-fatigue behaviour, mainly due to the very costly testing involved.

A collection of ITER data files, reports, reviews articles and papers on the fatigue and creep-fatigue of the CuCrZr alloy has been delivered to us by EFDA, to verify the suitability of the linear damage accumulation rule for life predictions in creep-fatigue tests. The time-based approach, proposed by the French RCC-MR design code, will be used to check the possibility of reliable life predictions, based on existing fatigue and creep data. This method assumes that fatigue and creep damage are linearly additive and that a life prediction can be made on the basis of the partition of pure creep and pure fatigue times. The method requires knowledge of the relevant fatigue life equations, the cyclic hardening curve and the creep equation. The method can be applied with more accuracy if the particular relaxation curve at the holding point is known, which of course requires the completion of at least a partial creep-fatigue test. The second part of the task will deal with the production of the experimental data points missing or necessary to validate the method.

2.5 Superconductivity

The activities of 2004 we focused on the SULTAN facility, with two full size NbTi conductors, namely tested in several campaigns, a test update of the CRPP full size Nb_3Sn conductor and two subsize Nb_3Sn conductor samples prepared in collaboration with MIT. Thermo-hydraulic test campaigns for SULTAN samples are underway.

Beside the SULTAN samples, the activity on HTS superconductors was maintained, with the current lead test completed and the bus-bar design started. The JORDI test facility is about to produce the first results on the resistance distribution on joints. Strand testing and pressure drop tests have produced interesting results.

2.5.1 Poloidal Field Insert Coil Conductor Sample (PFIS) test

A short sample of the NbTi cable-in-conduit conductor (CICC) manufactured for the ITER PF insert coil has been tested in the SULTAN facility. Based on a cable prepared in Russia, the insert coil is being manufactured in Europe and will be

tested in Japan. Two short lengths of the Insert Conductor have been assembled into a short sample for the SULTAN test facility. A testing group, including members of many European laboratories as well as ITER IT members, has been entrusted with the assessment of the test results. The main aim of the test, carried out in March-May 2004, is a broad characterisation of the NbTi CICC and a qualification of the joint layout for the Insert Coil.

The sample for SULTAN, named PFIS = Poloidal Field Insertconductor Sample, consists of one "regular" conductor section (PFISW) and one "de-wrapped" section (PFISNW), where the sub-cable wraps have been removed before jacketing, joined at one end by a hairpin joint, prepared by compacting the cable ends into CuCrZr sleeves and joining them by five copper saddles.

Although some parameters have been a priori dictated by the availability of material (e.g. Cu:non-Cu ratio and steel jacket size), the conductor layout for PFCI reflects the design of the ITER PF1&6 conductors see Table 2.5.1.

	$PFIS_W$	$PFIS_{NW}$	ITER PF1&6
NbTi strand diameter (Ni coated), mm	0.73	0.73	0.73
Cu:non-Cu	1.41*	1.41*	1.6
Number of strands (3x4x4x5x6)	1440	1440	1440
Total Cu cross section, mm^2	353	353	371
Total non-Cu cross section, mm^2	250	250	232
Sub-cable wraps cross section, mm^2	13.4	-	7.6
Outer wrap cross section, mm^2	22.3	-	19.8
Cable space diameter, mm	37.53	36.89	38.2
Cable pitches, mm	42/86/122/ 158/489	42/86/122/ 158/489	45/85/125 165/425
Estimated/retained cosθ	0.96	0.96	0.95
Steel spiral for central channel, mm	10 x 12	10 x 12	10 x 12
Void fraction, %	33.5**	34.3**	34.5
Outer conductor size, mm	50.35 x 50.45	49.82 x 49.78	53.8x53.8

* weighted average according to strand and cable QA sheets
** calculated assuming zero elongation of the strands during compaction

Table 2.5.1 *Layout of the PFIS Conductors, compared to ITER PF1&6 Design*

The two conductor lengths are cooled in parallel by independent circuits, with coolant flow from bottom to top. To avoid temperature gradients over the conductor cross section and improve the definition of the operating temperature, the central channel has been blocked in both conductor sections inserting a rubber pipe plugged at the outlet side. The instrumentation, Fig. 2.5.1, includes voltage taps, heaters, temperature and pressure sensors, mass flow meters, pick-up coils and six arrays of Hall sensors, attached to the conductors in high field, next to the joint and termination (symbol "H" in Fig. 2.5.1) to sense the self-field distribution. Each array includes 10 sensors.

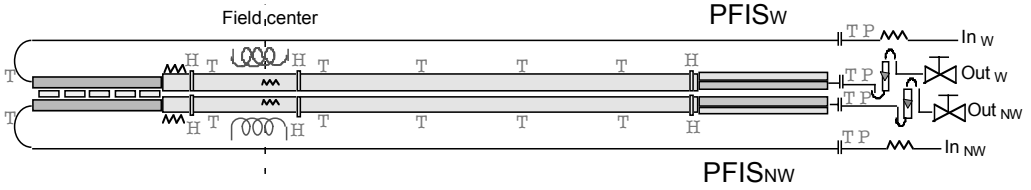

Fig. 2.5.1 *Instrumentation sketch of PFIS: "H" is for the Hall sensor arrays, "T" and "P" for temperature and pressure sensors (voltage taps are not shown).*

The test campaign for PFIS lasted from mid March to the end of April 2004, with 50 critical current and 20 current sharing temperature runs at various operating conditions and 100 bipolar load cycles (±45kA @ 7T background field). The ac test included loss curves vs. frequency by gas flow calorimetry and magnetization methods for both conductors in the background field of 2T, with ac field amplitude of ±0.2T, before and after cycling, at 4.5K and above T_c. The current distribution, monitored during all the runs, was also investigated for different current ramp rate and long holding time.

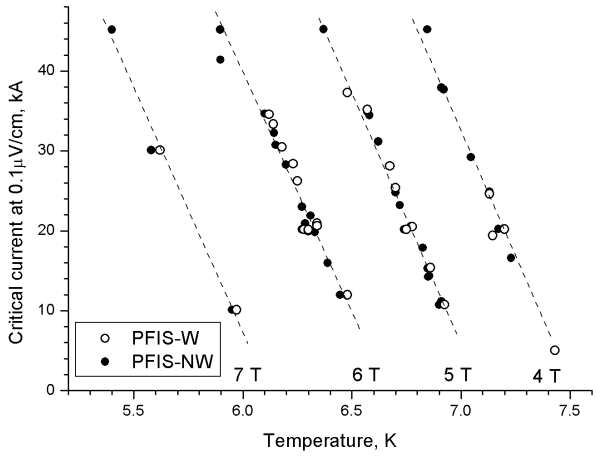

Fig. 2.5.2 *Summary of critical current and current sharing temperature at the electrical field criterion 0.1μV/cm at background field of 4, 5, 6 and 7T.*

The electric field at which the quench occurs, E_q, decreases at increasing current, as a result of the superposition of self-field and background field. The local electric field along a strand in the cable reaches very high values at the peak magnetic field, driving a quench, although the average electric field, sensed by the voltage taps on the conductor jacket remains very low. Such self-field induced, sudden take-offs are typical of large size NbTi CICC. The 0.1μV/cm criterion for I_c and T_{cs} test could only be measured for current below 45kA (PFISNW) and 35kA (PFISW), see Fig. 2.5.2. T_{cs} is the current sharing temperature and I_c is the current limit, both setting a limit to maintaining superconductivity. The behaviour vs. temperature is almost linear and the performance difference between the two conductors is marginal. The gap to the predicted performance is of the order of 0.1K.

The current at which the voltage take-off occurs, quench current I_q, is shown in Fig. 2.5.3. Above 35kA (PFISW) and 45kA (PFISNW), i.e. when the take-off is observed at very low electric field level, the behaviour of I_q vs. T deviates strongly from linearity and the performance is much poorer than expected from the strand. Despite some scattering observed in the high current I_q results, the performance of PFISNW is better than PFISW, i.e. the deviation from linearity is smaller and occurs at higher current. The large deviation from the linear behaviour is not an intrinsic feature of the self-field induced quenches. To understand the behaviour in Fig. 2.5.3, we must postulate some current imbalance among the strands. When enough voltage builds up along the strands, see I_c results in Fig. 2.5.2, current re-distribution from the overloaded strands is possible in both PFISNW and PFISW. In the condition of self-field induced quench, i.e. with high local electric field but very low average voltage, the overloaded strands are unable to transfer the excess current to the neighbouring strands and quench. The better behaviour of PFISNW

suggests that the sub-cable wraps play a negative role in the current re-distribution process. Indeed, for the same quench current, a higher E_q is observed at PFISNW compared to PFISW.

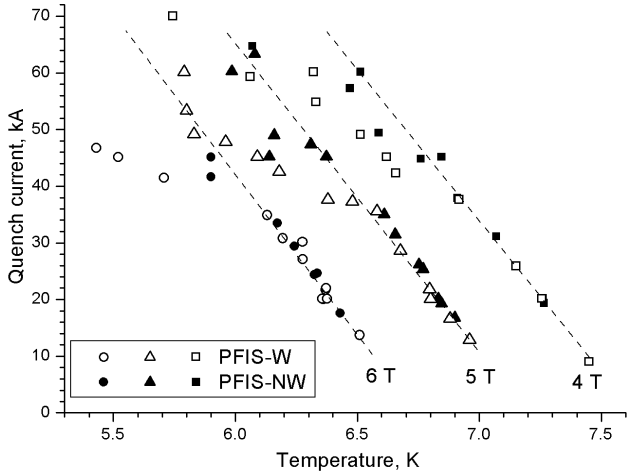

Fig. 2.5.3 *Summary of quench current results from all the critical current and current sharing temperature runs at 4, 5 and 6T*

In the ITER design, the PF1&6 conductors operate at 45kA, 6T peak field, with T_{cs}=6.5K, i.e. 1.5K above the operating temperature of 5K. The test conditions of PFIS are not identical to ITER-PF: the self-field gradient is higher in PFIS and the joint is closer to the high field. The NbTi strand fulfills the ITER spec at 4.2K, but the J_c interpolated at higher temperature is lower than retained in ITER. On the other hand, the non-Cu cross section of PFIS is 8% larger than in the ITER PF1&6 and the central channel is blocked. Interpolating the 45kA results of Fig. 2.5.2 and 2.5.3 for a peak field of 6T (background plus self-field), we obtain T_{cs}≈6.31K for PFISNW and T_q≈6.05K for PFISW. The PFISW, with no T_{cs} at 45kA, does not fulfill the ITER design (the same happened with the PF-FSJS conductor). In the region of self-field induced quench, the dc performance may be very sensitive to current unbalance. The PFISNW, with measurable T_{cs} at 45kA, comes closer to the ITER design, with the gap being partly due to the retained scaling for strand J_c.

An unexpectedly high resistance was observed in the joint (about 10nΩ) and in the termination (about 6/18nΩ). The high resistivity of the CuCrZr sleeve, $\rho=9.5\cdot10^{-9}\Omega$m, makes up to 5nΩ of the joint resistance. The remainder is likely due to the cable-to-sleeve contact (Ag coated strands pressed/heated to the tinned inner wall of the sleeve). A 28mm long slice was cut by electronic erosion from a conductor termination, prepared in the same way as for the PFIS joint. The resistance of the slice was measured at CRPP in liquid helium, with the holder shown in Fig. 2.5.4. The result, R_{slice}=240nΩ, perfectly scales to R_{joint}=10.6nΩ, providing an easy method to quickly assess the improvements that are planned at Tesla for the PFIC conductor termination.

The evolution of the Hall sensors signal during T_{cs} runs bring evidence of current re-distribution, more pronounced in PFISNW, for which a larger, initial current unbalance is also estimated.

The dc performance of the PF conductor without sub-cable wraps, PFISNW, is about 0.2K below the ITER design. A minor iteration on PF conductor design (non-Cu cross section and scaling law for J_c) is recommended. The conductor with sub-cable wrap suffers of self-field induced take-offs and has no measurable T_{cs} at 45kA.

The removal of sub-cable wraps helps to increase the threshold for instability. The quench temperature, T_q, of the self-field induced take-offs is very sensitive to current unbalance and cannot be predicted based on strand properties and cable geometry. The high joint resistance, ≈10nΩ, is not acceptable for ITER coils.

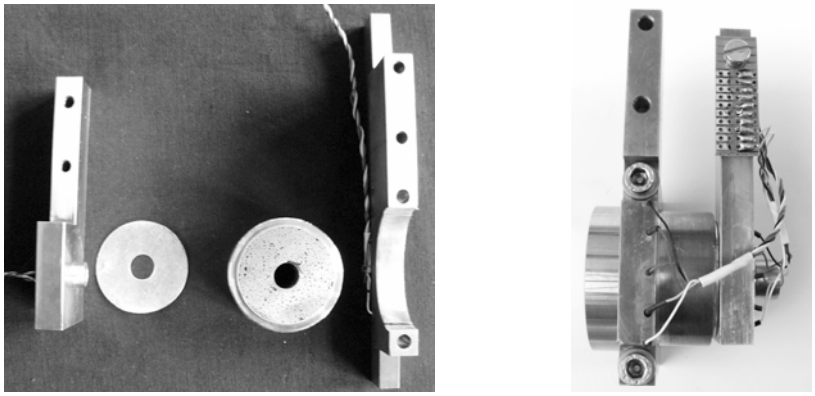

Fig. 2.5.4 *The slice of conductor termination and its holder: exploded view and assembled sample*

2.5.2 Test of two subsize Nb_3Sn samples with different jacket material

In the scope of a collaboration between MIT and CRPP, a cable with 144 Nb_3Sn strands was prepared in 2002 from left over material of the CS Model Coil (IGC strand). The cable was cut into two sections, which have been jacketed with stainless steel and titanium pipes respectively. CRPP received the conductors in December 2002, prepared the U-bend sections and sent them to MIT for heat treatment. The heat treated sections were back at CRPP in summer 2003 and were assembled into SULTAN samples, including termination, instrumentation and clamps. Finally, the test in SULTAN was carried out in spring 2004.

The only difference between the two conductors is the coefficient of thermal expansion of the jacket material, see Table 2.5.2. The conductor layout is also identical to the conductor SECRETS A, manufactured in 1999 by VNIIKP based on Nb_3Sn strand from Bochvar (TF insert coil production) for a stability experiment at CRPP.

	SS	T_i
Nb_3Sn strand Diameter	0.81 mm	
Cu:non-Cu	1.5 ± 0.05	
Cr plating	2 μm	
Cable configuration	3 x 3 x 4 x 4 = 144	
Cable pitches	10 / 51 / 79 / 136 / 166 mm right hand	
Outer cable wrap	stainless steel tape, 0.065 x 25 mm, 40-45 % overlap, left hand	
Non-Cu cross section	≈ 29.7 mm^2	
Cu cross section	≈ 44.5 mm^2	
Void fraction	≈ 33.1 %	
CICC diameter	14.51 – 14.57	14.56 – 14.59
Jacket material	Stainless steel 12X18H110T	Titanium (grade 2)

Table 2.5.2 *Conductor Layout*

At first, the two conductor sections had to be straightened and then formed into a hairpin shape, with the U-bend of about 50 mm radius. The final appearance of the U-bend is shown in Fig. 2.5.5. All the four conductor ends are dismantled from the jacket over a length of 550 mm. The Cr plating is removed by dipping the cable ends in a solution of HCl placed in an ultrasonic bath. A copper pipe is slid over the cable ends and swaged, reducing the void fraction in the cable space from ≈33.1% to ≈26%. Five ceramic spacers over the copper sleeve and a stainless steel (respectively Ti) pipe are slid over the conductor end and welded to the jacket. The hairpin conductors are fitted into a light stainless steel frame to maintain the shape during the heat treatment.

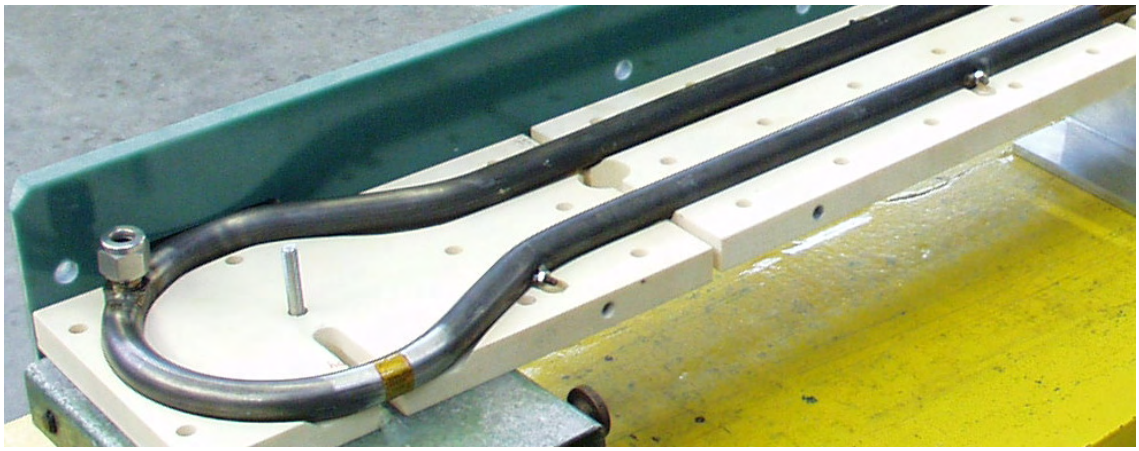

Fig. 2.5.5 *The U-bend of the hairpin at the final assembly of the sample*

After the heat treatment, the protective stainless steel/T_i sleeve are removed. The conductor end was filled with SnAg solder. The termination box is the standard CRPP design, consisting of a vacuum brazed assembly of a copper plate, a steel plate and a thin steel collar to be welded to the jacket. The copper body of the box is first tinned. Then the solder filled termination is slid into the box through the collar and a PbSn solder foil is interleaved between copper sleeve and copper plate. A moderate pressure is applied on the copper sleeve to enhance the contact to the copper plate and the assembly is heated to 200°C, till the PbSn melts.

The instrumentation scheme, shown in Fig. 2.5.6, includes one pick-up coil for magnetization ac loss. one heater for calorimetry calibration, four CERNOX temperature sensors on the jacket surface and fifteen pairs of voltage taps. Additional instrumentation is available from the facility. The four temperature sensors T1-T4 are used in the same location for SS and T_i, i.e. after testing one sample they are removed and attached to the other sample, to cancel any systematic error in the comparison of the test results

The test procedure has been drafted after iterations between CRPP and US team, according to the main aim of the action, i.e. the assessment of the degradation (including cool-down, transverse load and cyclic load) vs. coefficient of thermal expansion of the jacket material. The first test campaign of the SS sample, started on November 2003, had to be stopped because of the failure of one current lead. After a facility shut down to repair the current lead, the test of the SS sample was restarted by May 6th 2004. The test of the T_i sample was completed on July 23rd 2004.

The resistance of the connections between sample and transformer plates is within the range measured on termination of subsize conductor samples: 2.8/3.9nΩ (SS) and 5.7/4.8nΩ (T_i).

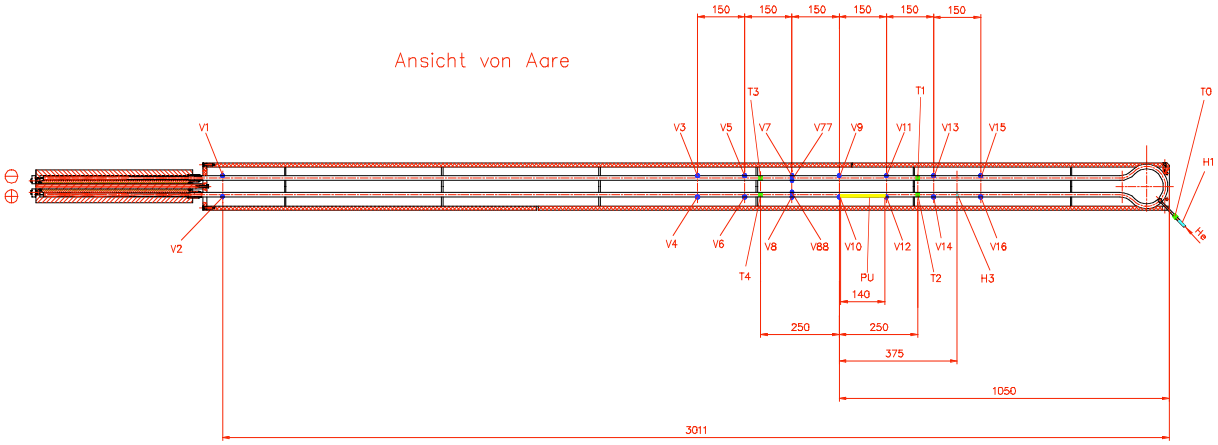

Fig. 2.5.6 *The instrumentation scheme*

A summary of the dc results at different B and T before the cyclic load is shown in Fig. 2.5.7, which includes the critical current and current sharing results at 0.1μV/cm. The T_{cs} results are in good agreement with the I_c data. As the strain affects both B_{c2} and T_c, the dc performance of SS sample is not a fixed fraction of the Ti sample. At higher temperature/field the Ti performance is much better than SS (up to a factor of 2), but a low field/temperature, i.e. far from B_{c2} and T_c, the SS performance is only 20% worse than Ti.

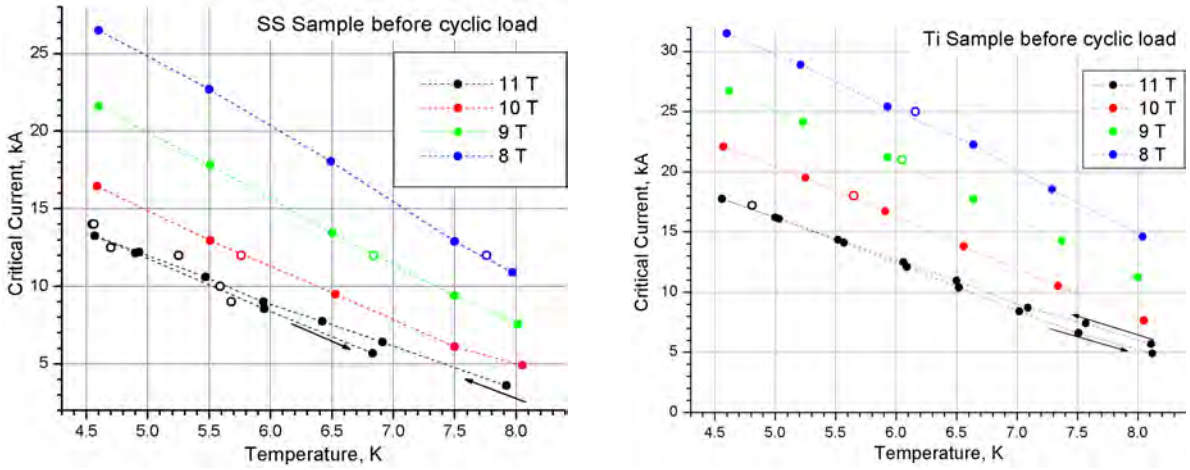

Fig. 2.5.7 *DC results of the SS and Ti samples before cyclic load. Full symbols are I_c, open symbols are T_{cs}*

The small hysteresis shown at 11T is due to the intentional progressive load applied to the sample (the 11T test is the first loading at all). It is the initial stage of the cyclic load degradation discussed below. The same load is applied to both samples, B=10T, I=0-17-0kA. The number of loads is 1000 for SS and 1600 for Ti. The dc test before cycling load makes up about 30 additional cycles. Every 200 cycles, an I_c test is carried out at 11T,≈4.5K. Occasionally, a test with reversed current direction is also made. The same series of test taken after 1000 cyclic loads is shown in Fig. 2.5.8. The extent of the cyclic load degradation ranges from 10 to 20%, being higher at higher field and temperature. The relative degradation after 1600 load cycles is at large in the same range as for the SS sample, i.e. 10-20%.

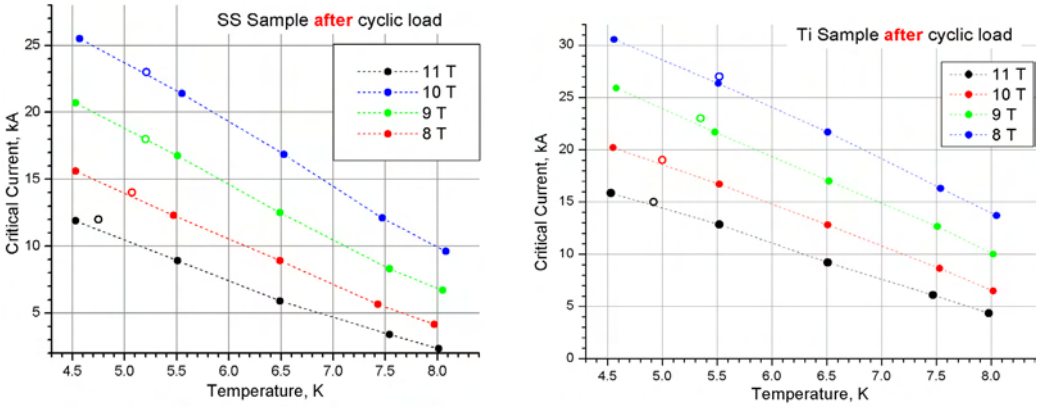

Fig. 2.5.8 *DC results of the SS and Ti sample after cyclic load. Full symbols are I_c, open symbols are T_{cs}*

A summary of the I_c results vs. number of load cycles is plotted in Fig. 2.5.9 (left), for both the SS and Ti samples. Where two points appear in the SS sample at 600 cycles, one reverse load was carried out between the two points (the difference is within the accuracy of the measurement). For the Ti sample, two points at the same number of cycles only means that the test has been carried out twice. To answer the question weather the relative sensitivity to cyclic load is higher (or lower) as a function of the coefficient of thermal expansion of the jacket material, the ratio of critical currents, I_c^{Ti}/I_c^{SS} is plotted vs. the number of cycles in Fig. 2.5.9 (right). The ratio stays constant between 1.32 and 1.36, which is a very tiny range considering the accuracy of the data, suggesting that the cyclic load degradation is at large independent on the contraction of the jacket material.

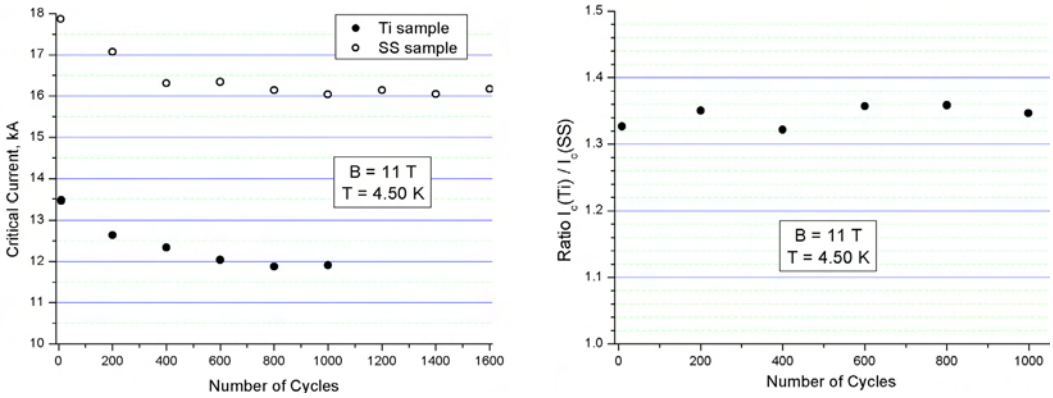

Fig. 2.5.9 *Critical current results of SS and Ti sample vs. number of cycles (left) and ratio of critical current results of Ti and SS sample vs. number of cycles.*

Further information on the dc behaviour is provided by the index *n* of the V-I characteristic. Fig. 2.5.10 (left) gathers all the index *n* results from I_c runs on strand test, SS and Ti sample, before and after cycling. The evidence that index *n* is smaller in cable than in single strand suggests that some degradation occurred. The worsening of the index *n* after cyclic load indicates that the degradation progresses. Due to the scattering in the series of points, it is not clear if there is a systematic difference between SS and T_i sample. A clearer picture is obtained comparing the evolution of the index *n* for the SS and T_i samples during cycling, see

Fig. 2.5.10. The index *n* is initially marginally higher (21 vs. 17) for the Ti sample and comes down to the same values (about 13) as the cycling progresses.

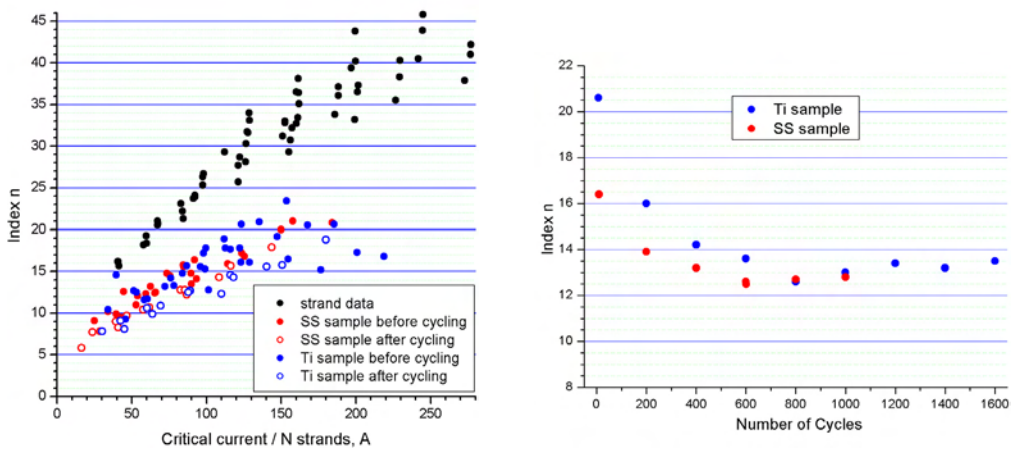

Fig. 2.5.10 *Summary of all the index n results for strand, SS and Ti samples, before and after cyclic load (left) and evolution of n index during cyclic load for SS and Ti*

2.5.3 Preparation of two Nb_3Sn subsize samples

To investigate the impact of the cable pattern on the transverse load degradation of Nb_3Sn CICC, two subsize samples were prepared and tested. The Nb_3Sn strand was procured at EAS (former VAC) from a left over batch of the TF Model Coil production, i.e. it has the same diameter, copper ratio as the OAS (former IGC) strand for the subsize samples described under 2.5.2. However, EAS is a "bronze" technique strand, while OAS is an "internal Sn" method.

Two cables have been prepared from the strand. The cable "T" (Triplet based) has the same layout and pitch sequence as the conductors in 2.5.2, i.e. 3x3x4x4=144 strands. The cable "B" (Braid based) consists of 5 braids of 29 strands, i.e. 29x5=145 strands. The jacket is a steel pipe, identical to the jacket of the SS sample in 2.5.2. The outer size and hence the void fraction are also the same as in Section 2.5.2. The braiding work was carried out at Marti Supratech (Zürich). The final cabling and jacketing work was contracted to VNIIKP (Moscow). The conductor sections were delivered to CRPP in summer 2004.

The test program for the two samples will be identical to the one for the samples in Section 2.5.2. As the sample SS is identical to the sample T of the new task except the strand manufacturing technique, comparing the relative cyclic load degradation of SS vs. T we will assess which strand is more sensitive to transverse load degradation. Comparing T vs. B (made of the same strand with the same void fraction) we will sort out which cable pattern is more tolerant to transverse load degradation.

The components for the sample assembly have been procured. The heat treatment, termination and instrumentation will be completed within the end of 2004. The test is planned in the beginning of 2005.

2.5.4 High temperature superconducting current leads

The CRPP and the Forschungszentrum Karlsruhe (FZK) are responsible for the design, construction and test of a 70kA high temperature superconductor (HTS) current lead for the toroidal field (TF) coil system of ITER. The work has been performed in the frame of the European Fusion Technology Programme. In the first half of 2004 the 70kA HTS current lead was installed and successfully tested in the TOSKA facility of FZK. The experiments covered the DC performance and the quench behaviour of the current lead.

The HTS current lead consists of a conduction-cooled HTS part (4.5-65K) and a conventional copper heat exchanger (65-300K) cooled by helium gas with a 50K inlet temperature. As required in the ITER design, the current lead is installed in a horizontal position. The modular design of the HTS, manufactured by American Superconductor Corporation, is schematically illustrated in Fig. 2.5.11. The main building blocks of the current lead module are 12 superconducting panels, supported by stainless steel carriers, arranged in a 12-fold prism.

The current lead was operated up to 70kA in steady state at the nominal operating conditions (helium inlet temperature: 50K, warm end of HTS module: 65K). At a reduced helium inlet temperature of 41K, leading to an HTS module warm end temperature of 57K, it was even possible to operate the current lead for more than 30 minutes at a current as high as 80kA. The measured contact resistances are listed in the following Table. The performance of all soldered contacts is as designed, while the resistance of the screw contact connecting the HTS module with the copper heat exchanger is much higher than expected from a previous similar contact. As a consequence the helium mass flow rate necessary to reach a HTS module warm end temperature of 65K was considerably enhanced.

Contact Resistance	Value
Soldered contact HTS module – NbTi bus bar	1.9 nΩ
Cold end cap of the HTS module (12 panels in parallel)	(0.86±0.1)nΩ
Warm end cap of the HTS module (12 panels in parallel)	(2.95±0.4)nΩ
Screw contact HTS module – heat exchanger	40-80nΩ

The tangential magnetic fields measured by 12 Hall probes, placed close to the centre of the outer side of each panel, were used to reconstruct the individual panel currents. The contact resistances at the cold and the warm end of each panel, obtained from the measured voltages and the reconstructed panel currents, are shown in Fig. 2.5.12. The reconstructed panel currents are presented in Fig. 2.5.13. A comparison of Figures 2.5.12 and 2.5.13 indicates that the panel currents are mainly determined by the sum of the warm and cold end contact resistances of the panels.

The heat load at 4.5K and zero current was determined by measuring the enthalpy change of the helium flowing in the NbTi bus bar. The background losses were found by the variation of the warm end temperature of the HTS module and extrapolation to vanishing temperature gradient. The heat load found for a warm end temperature of 65K is ≈13.5W, which is considerably larger than the design value of 5.7W. This result suggests that only 42% of the heat load at 4.5K is caused by the HTS module, whereas additional parasitic losses related to the installation of the current lead in the TOSKA facility are dominating. But even the heat load of

13.5W is lower by a factor of 6 than that caused by a conventional gas-cooled current lead.

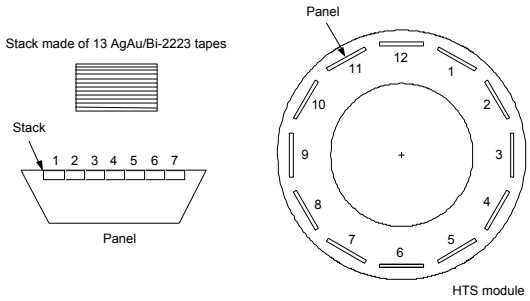

Fig. 2.5.11 *Sketch of the modular design of the HTS current lead module.*

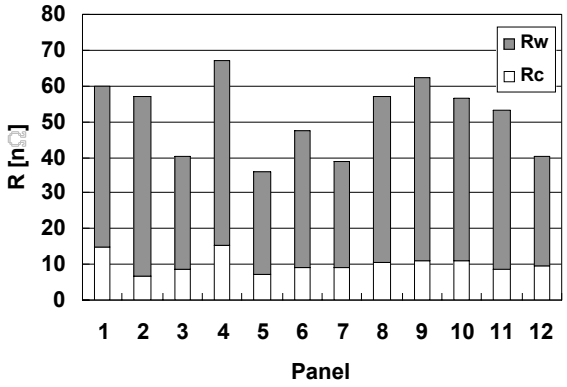

Fig. 2.5.12 *Contact resistances measured at the warm and cold ends of the panels.*

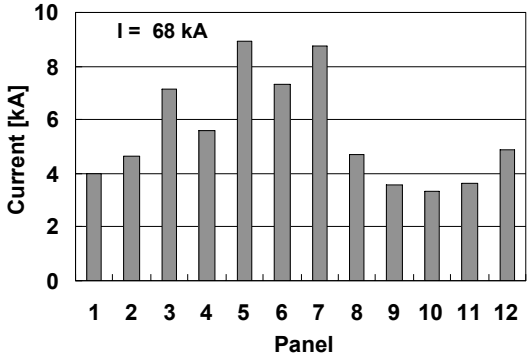

Fig. 2.5.13 *Current distribution among the panels at an operating current of 68kA reconstructed from the tangential magnetic fields measured by 12 Hall probes.*

At the nominal operating current of 68kA, the heat load at 4.5K is enhanced by 12.8W due to the Joule heating in the contact resistances at the cold end. Subtracting the excessive losses caused by the large resistance of the screw contact we find a reduction of the refrigerator power consumption by a factor of 3.7 at 68kA. In agreement with optimisation calculations performed at CRPP, it was found that for helium inlet temperatures between 40 and 59K the variation in the required refrigerator input power is only 5%.

Finally, the quench behaviour of the HTS current lead was investigated. The HTS module was quenched by carefully increasing its warm end temperature by means of a reduced helium mass flow rate through the heat exchanger. A voltage of 10μV/cm was used to define the current sharing temperature. Generally, this voltage level was first reached in panel 12. The current sharing temperatures found at currents of 50, 68 and 80kA are ≈79, 73.5-79 and ≈70K, respectively. During a quench the maximum temperatures and voltages increase linearly with a slope of 10K/s and 10mV/s, respectively. A voltage of 90mV is reached at a temperature of 160K. For safety reasons, the ITER current leads must be able to carry the full operating current at least for three minutes in the case of a loss of flow in the current lead. To study this aspect the helium mass flow through the heat exchanger part of the HTS current lead was stopped, while the current was kept at 68kA. A time of 6.3 minutes elapsed until the HTS current lead quenched.

The 70kA HTS current lead could be stably operated up to a current of 80kA. This is a new world record for the current carrying capacity of HTS current leads. The total power required by the refrigerator to cool an HTS current lead with a low resistance connection between the HTS module and the heat exchanger is by a factor of 5 smaller than that consumed by a conventional gas-cooled current lead. The test results indicate that HTS current leads can be used for ITER.

2.5.5 Further evaluation of the new Nb_3Sn full size conductor

In 2003 CRPP established a convincing experiment to assess how far local, mechanical support in the strand bundle affects the overall conductor performance. Two conductor sections were prepared from the same basic layout:

1) an as-manufactured cable-in-conduit conductor, with Cr plated strands, 37% void fraction in strand bundle and Ti spiral for the central channel, denoted **A** and

2) a solder-filled conductor, with bare strands, annular space filled with PbIn solder and Ti-pipe for the central channel, denoted **B**.

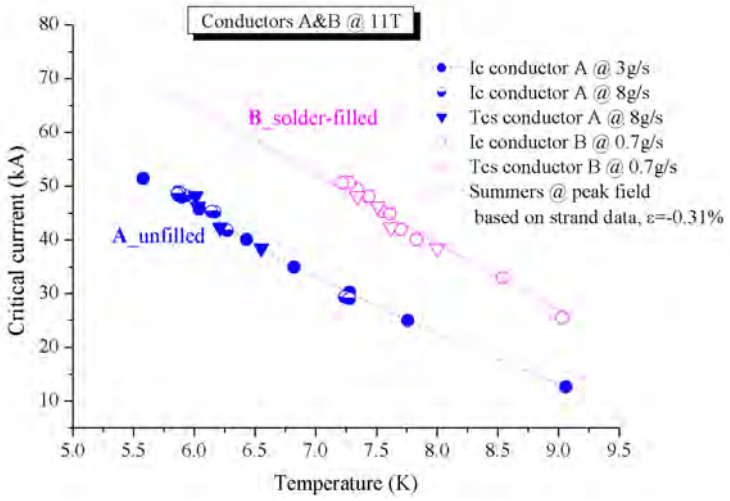

Fig. 2.5.14 *Critical currents for conductors A and B at 11T as a function of temperature. Both results of critical current measurements (solid and open circles) and of current sharing temperature measurements (solid and open triangles) are shown*

A direct comparison between conductors A and B, as illustrated in Fig. 2.5.14, shows a better performance of B in spite of a higher estimated residual strain of the Nb_3Sn filaments in the solder-filled conductor B. The thermal strain difference between the two conductors is due to the different history between 550K and 300K, where conductor B included the solder with a large coefficient of thermal expansion. The good performance of B indicate that solder filling leads to a mechanical stabilization of the cable in addition to a better distribution of the transverse magnetic force between the strands, thus reducing stress concentrations at crossover points.

An essential point to note in Fig. 2.5.14 is that part of the data were obtained after the conductors were exposed to 200 cycles of transverse magnetic load. The cyclic load was performed by ramping the sample current from 0 to 60kA and back to 0 in presence of a background magnetic field of 11T. This results in an electromagnetic transverse load of 18MPa. Obviously, neither in A nor in B, a measurable change of the critical current occurs after 200 cycles.

Before continuing the cycling test, technical reasons required a warm up of the SULTAN Facility while some modifications regarding the clamping of the sample unit have been done. In order to reduce the thermal coupling between conductors A and B, the saddle shaped stainless steel piece which fills the gap between conductors (and thus separates them), was replaced by a G10 similar piece. Evidently, to perform this operation, the whole clamping system had to be dismounted and reassembled again.

The cycling test was resumed after the subsequent cool down in the same manner as was done previously. After the next 375 cycles, the critical current of the conductors has been measured again using the same parameters like ramp- and mass flow rate. Fig. 2.5.15 summarises the results of critical current and current sharing temperature measurements before and after the modification of the clamping system.

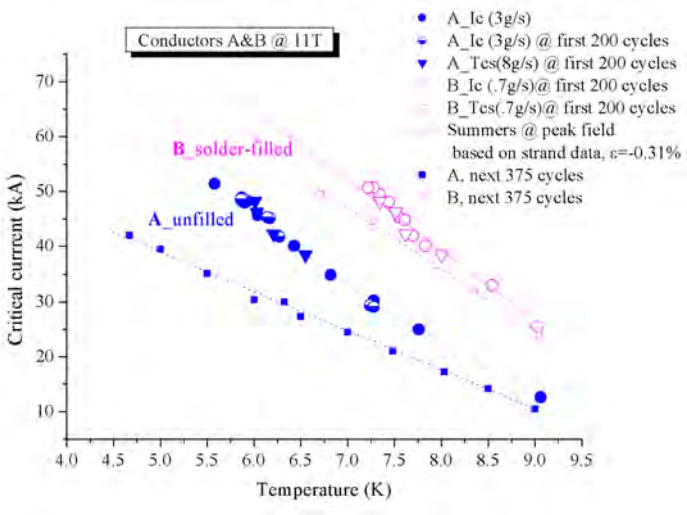

Fig. 2.5.15 *Test results of Ic and Tcs measurements for conductors A and B*

While the new cycling campaign caused a performance drop in both conductors, the decline of the critical current in conductor A is more pronounced than in B. This may be interpreted as evidence for the high sensitivity of the non-filled conductor to

transverse stress. However, the question immediately raised concerns the lack of response to transverse load in both conductors after the first 200 cycles. A possible explanation is that the performance drop observed after the second cycling campaign might be at least partly due to conductor handling problems during insertion of the G10 saddle shaped core between conductors. It should be mentioned that due to the failure of the core, the insertion had to be repeated with the consequence that the conductors have been straddled twice. In spite of the incertitude regarding the exact cause for the I_c degradation measured after the second cycling campaign, the different magnitude of the effect in conductors A and B shown in Fig, 2.5.15 confirms again that solder filling leads to a mechanical stabilization of the superconducting cable.

An interesting question raised by the present work is whether conductor A is irreversibly degraded and if not, how much of its performance would recover. To try to answer this question, the annular space of conductor A, still clamped together with B in the steel structure, has been filled with a low temperature solder. In this way, the conductor A has acquired the same local mechanical support within the cable bundle as revealed by conductor B. The re-measurement of conductor A in the filled condition is planned for October 2004.

2.5.6 Pressure Drop test on PFI conductor sections

The assessment of the maximum mass flow rate for CICC at a given inlet pressure (and hence the power load removal) requires the knowledge of the friction factor of the cable, which has been so far characterised mainly by its hydraulic diameter and void fraction. If experimental data are not available, usually less accurate friction factors can be predicted using correlations. This issue is particularly sensitive in dual-channel CICC where the knowledge of the two friction factors is important for assessing the repartition of the total mass flow rate.

Two straight sections of the same conductors used for the PFIS Sultan sample, see Section 2.5.1, have been tested for pressure drop. Figure 2.5.16 shows a cross section of the two conductors, with and without sub-cable wraps. The goal of the experiment was to determine the friction factor of the annular bundle region. Our experimental device uses pressurized water at constant temperature, a method applied in similar measurements of the ITER Central Solenoid conductor at CRPP. The central spiral is blocked using a silicon rubber tube, thus restricting the flow to the bundle area. The 10mm rubber pipe is pulled through the central channel over the whole conductor section and is plugged at the end of the pipe at the outlet side.

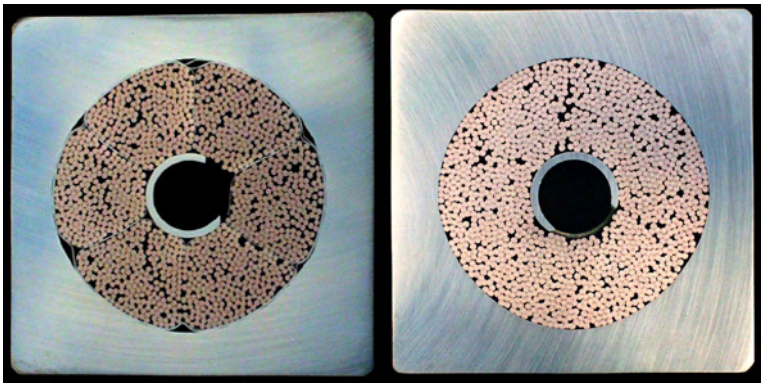

Fig. 2.5.16 *Conductor cross sections: the original PFI conductor (left) and the PFI conductor without subcable and outer wraps (right).*

The experimental set-up consists of a closed circuit of de-mineralized water at 0.8MPa (Fig. 2.5.17). The water temperature in the circuit remains constant during the experiment and therefore the measurements are very accurate since the water density (ρ) and dynamic viscosity (η) are also constant. The longitudinal friction factor of the annular bundle region is deduced from measurements of pressure drop (Δp) and mass flow rate (dm/dt). The pressure drop is measured by means of a differential pressure transmitter (signal Δp_d), as well as by two absolute pressure transmitter at inlet and outlet, from which $\Delta p_a = p_{in} - p_{out}$ is derived. The error of the differential and absolute manometers is ±0.2% of the full range, i.e. 0.15MPa and 3.0MPa respectively. The overlap between Δp_a and the more accurate signal Δp_d is in good agreement over a broad range. The water mass flow rate has been measured by four, parallel operated floating-ball flow meters having different ranges (100 l/h, 400 l/h, 630 l/h and 1600 l/h, respectively); the error is ±2% of the full scale. The circuit temperature is measured by a thermometer located in front of the sample inlet, whose accuracy (±0.5°C) results in a negligible error bar on the mass flow rate.

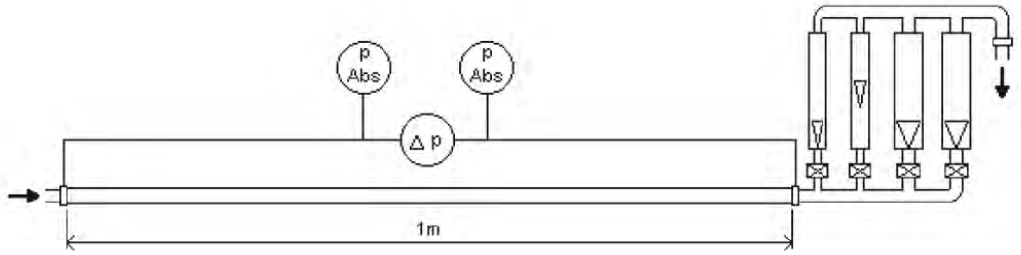

Fig. 2.5.17 *Schematic view of the experimental set up. The thermometer to derive the average thermodynamic properties is located in front of the sample inlet (not shown). The sample length is 1.0m (PFI_W) and 0.631m (PFI_{NW})*

The raw data, i.e. pressure drop per unit length ($\Delta p/L$) versus mass flow rates, show no discontinuity over the full range of dm/dt. Since the two conductors do not have exactly identical geometry, dimensionless analysis in terms of Reynolds number Re and friction factor *f* is needed to assess their behaviour. The results of *f*(Re) show that within the measurement accuracy, the conductors PFI_W and PFI_{NW} have approximately the same friction factor for Re>100. A comparison of these results with the measurements of the ITER Central Solenoid conductor (CS1, a CICC conductor with wraps which was tested in the same experimental set-up) shows that the pressure gradient in the annular bundle region of the wrapped conductors is approximately the same.

The experimental f(Re) in the annular bundle region has been compared with the correlation for CICC proposed by Katheder $f_{Katheder}=(1/v^{0.72})(0.051+19.5/Re^{0.88})$ (Fig. 2.5.18). The Katheder correlation overestimates the experimental f(Re) of both PFI conductors (e.g. +55% at Re=820). Ongoing work on ITER conductor samples (HECOL facility at CEA, Cadarache, France) qualitatively confirms this result. However, the PFI result is in disagreement with the CS1 result where $f_{Katheder}$ underestimates the experimental data (e.g. -22% at Re=820). It was argued that the presence of wrapping could be a possible reason for the disagreement since the Katheder correlation was obtained from samples without wraps, which is not confirmed by the measurements reported here.

In summary:

- The wraps have a negligible effect on the friction factor.
- The correlation by Katheder overestimates the PFI experimental friction factor whereas $f_{Katheder}$ underestimates the friction factor of the CS1.

To date, we cannot explain why the friction factor of the PFI conductor is considerably smaller than the friction factor of the CS1 conductor. For design purposes, the Katheder correlation can be retained with a ± 35% accuracy.

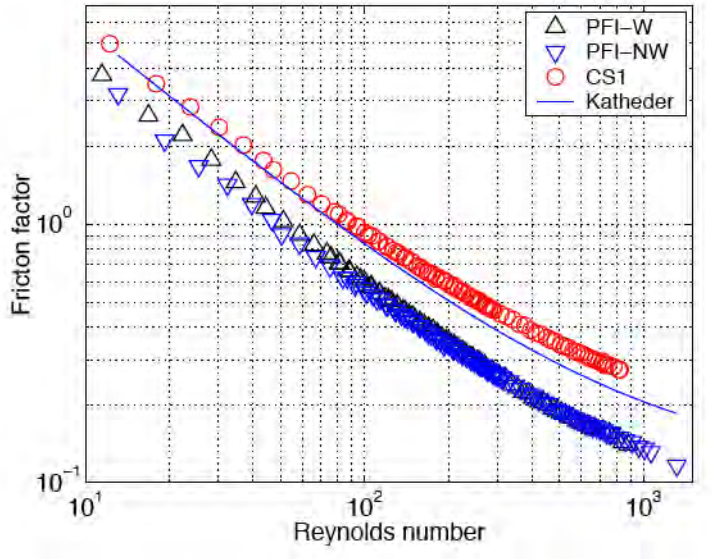

Fig. 2.5.18 *Comparison of experimental results of the PFI and CS conductors (open symbols) with the Katheder correlation. This correlation is only a function of the void fraction, which is only marginally different in PFIW (33.47%), PFINW (34.31%) and CS1 (36.50%). Therefore, only one curve is plotted to avoid unnecessary graphic confusion.*

2.5.7 High Temperature Superconductor Busbar

In collaboration with the Forschungszentrum Karlsruhe (FZK) we have started a new task considering the use of both HTS current leads and bus bars for ITER. This includes a conceptual design of HTS bus bars as well as the discussion of potential synergy effects of the use of both HTS current leads and bus bars. The complete work is performed in cooperation with FZK. CRPP focuses more on the ITER option with the use of HTS current leads and bus bars, while FZK works on the ITER option using only HTS current leads.

Based on the results of design studies and the measured performance of the 70kA EU HTS current lead the optimum operating conditions for ITER HTS current leads will be determined including an estimation of the savings in the refrigeration cost (see also Section 2.5.4). As a new option the use of HTS bus burs instead of the water-cooled aluminium bus bars will be considered. Potential advantages of the use of HTS bus bars could be a reduced space required for the bus bars and the considerably reduced electrical power losses.

First, design studies providing the optimum cooling concept and operating conditions need to be performed. As a basis for these studies the current design of the ITER feeder system will be used. The current carrying capacity of the HTS bus

bar is very sensitive to the operating temperature and the maximum magnetic field at the HTS superconductor. The anisotropy of the field dependence of the critical current of HTS superconductors with respect to the relative orientation of the textured HTS superconductor and the field direction has to taken into consideration. In addition to the results of the design studies, the conceptual design of the HTS bus bars must allow their industrial fabrication.

2.5.8 Test results of a low cost NbTi full size conductor

At an ITER meeting on the NbTi insert coil, the issue of the kind of joint to be adopted for the NbTi PF insert coil was discussed. Contrary to other proposals, which involved complex and expensive technology, as well as high manufacturing risk, CRPP proposed an easy design, adoptable at any workshop, promising low resistance, low ac loss, lowest leak risk and, most of all, low cost. The issue of the joint geometry was also raised at that meeting. It was argued that the “hairpin” geometry (praying hands), which is the standard geometry for joint samples to be tested in SULTAN, is different from the “lap” geometry (shaking hands), foreseen in the PF insert coil. To investigate the possible differences between the two joint geometries, CRPP offered to modify the layout of the SULTAN prototype sample, including two joints: one “bottom” joint with the usual hairpin geometry and an “intermediate” joint on one of the two legs, with the overlap geometry.

The conductor to be used for the prototype low cost joints has to be a “full-size” conductor, adequate for the ITER PF coils. On the other hand, some restriction on the conductor size is set by the SULTAN sample design, which includes an intermediate joint at mid-length. To design a suitable conductor without running into high cost for the RFPT, the following boundary conditions had to be retained:

- At the VNIIKP manufacturing facility, a set of rollers with ø=39.5mm was available to compact the jacketed conductor, imposing the outer conductor diameter of 39.5mm
- Few left over sections of the stainless steel jacket of the TFMC are available to sheath the cable. The wall thickness is ≈1.8 mm, before compaction. With an outer diameter of 39.5mm, the expected, final cable space diameter is ≈35.9mm
- The copper content and diameter of the NbTi strand is dictated by the stock material available at VNIINM, and used also for the PF insert coil conductor: strand diameter 0.73mm, Cu:non-Cu=1.32 (a higher copper fraction would be highly desirable)
- The same central spiral as for the PF insert coil conductor, 10x12mm, must be used.

To maintain the cable pattern at the higher cable stage as in the ITER design, the first cable stage has been selected as a copper core with 9NbTi strands cabled around. The overall cable pattern is a four stages bundle (1+9)x4x4x6, with 96 copper cores, ø=1.31mm, and 864NbTi strands, ø=0.73mm, see Fig. 2.5.19. The angle of the strands in cable is very close to the PF insert coil conductor. Ni plating has been selected as a strand coating. No sub-cable wraps are included. The manufacturer uses an outer wrap to protect the cable during the jacketing and compaction process. Even within the above restrictions, the selected conductor design can be considered to be of the class of the ITER PF1&6 conductors, see the following Table.

	ITER PF1&6	**PF Insert Coil**	**Low Cost Joint**
Steel jacket	53.8 x 53.8 mm	50.3 x 50.3 mm	Ø = 39.5 mm
Cable space	Ø = 38.2 mm	Ø = 38.0 mm	Ø = 35.9 mm
Total Cu	370.9 mm^2	342.9 mm^2 *	335.1 mm^2 *
Total non-Cu	231.8 mm^2	259.7 mm^2 *	155.8 mm^2 *
Central Channel	10 x 12 mm	10 x 12 mm	10 x 12 mm

* based on the nominal Cu:non-Cu value of 1.32

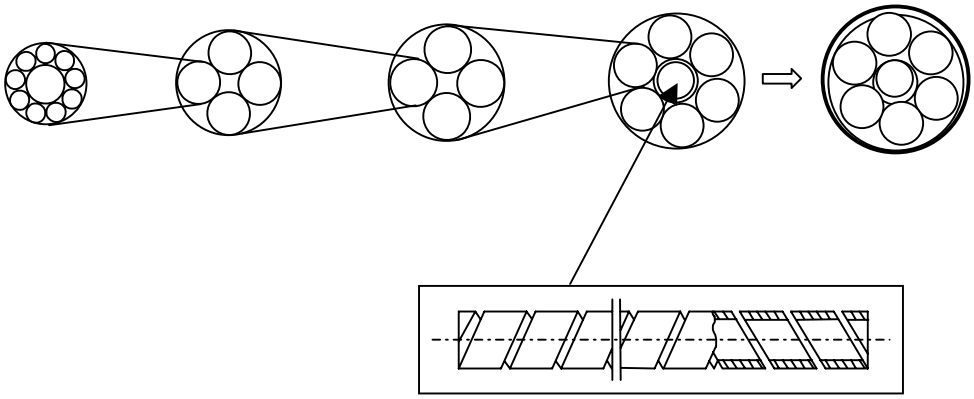

Fig. 2.5.19 *Schematic build up of the conductor for the low cost joint (a cross section is shown in Fig. 2.5.25)*

The conductor sections for the low cost joint have been supplied by the RFPT in the scope of an Task Agreement, which included, as a main object, the cable for the PF insert coil. Four straight sections, each 4.25m long, were delivered for a total of 17m. The sections are used for the SULTAN sample, for bending trials and for a joint sample to be tested in the JORDI test facility, see Section 2.5.9.

The main challenge of the sample design is to fit in the SULTAN test well cross section a joint (the intermediate joint) and the return conductor. All the existing ITER joint designs (CEA, US, JA and RF) would have been far too large to fit in the test well together with the return conductor. A second challenge is the joggling of the conductor sections, which is necessary as the axis of the conductors at the intermediate joint is shifted compared to the axis at the upper termination. A schematic view of the assembled sample is shown in Fig. 2.5.20.

The sample consists of two upper terminations, three conductor sections (≈3.4m, 2.6m and 1.3m long), a hairpin joint and a lap joint. The upper termination of the sample is designed according to the standard CRPP layout, with the compacted cable soldered into a slot machined in a steel/copper vacuum brazed box, with a welded lid. Below the upper termination, the two legs run straight and parallel, insulated by two glass-epoxy half shells and bolted by a single, 1.5m long steel clamp. Then, the two conductors are joggled, still running parallel, and moved to one end of the test well. Below the intermediate joint the two conductors are at the ends of the test well and must be joggled to be brought to the original axis. Eventually, the hairpin joint is placed at the bottom. The clamping of the sample is complex due to the changing cross sections. At the joggled sections, wedged fillers are prepared to fill the space between the conductors. At the intermediate joint, a single clamp on the side of the insulated return conductor, bolted directly to the joint box, replaces the standard clamping system.

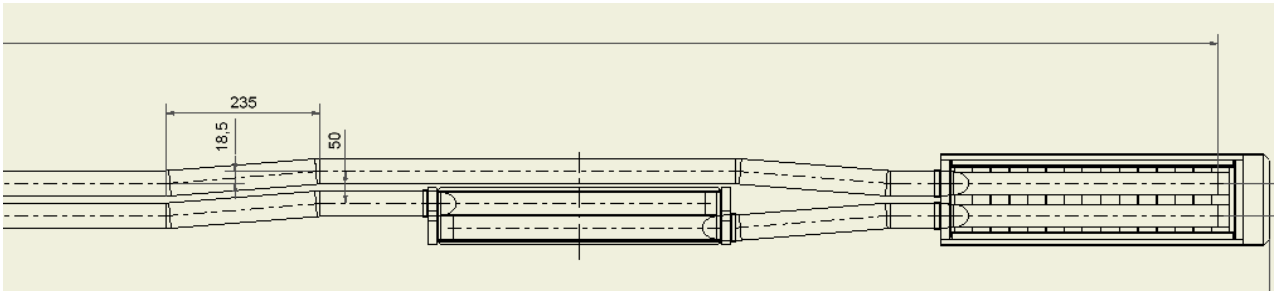

Fig. 2.5.20 *Schematic geometry of the sample, with the joggling and the two joints*

The two branches of the sample are cooled in parallel, with common inlet at the hairpin box. Two valves at the outlet, after the upper termination, control the flow rate in the two branches. In such a configuration, the intermediate joint is neither an inlet nor an outlet of the sample. Lowering the sample in the SULTAN test well, the center of the dc and ac coils is at the midpoint of the intermediate joint. In this position ("first test campaign") it is also possible to test the conductor, i.e. the return leg. In the second test campaign, the sample is lifted in the test well by 710mm, using two extensions of 670mm and 40mm. In this position ("second test campaign"), the hairpin joint is about at the center of the dc and ac coils.

A low resistance, low ac loss joint was developed in 1998 at CRPP for the ITER Nb_3Sn conductor. The basic concept is maintained for the NbTi low cost joint, with some further improvement and adjustment to the NbTi technology (no need of heat treatment). The design of the joint is driven by:

- Reliable leak tightness, by the use of a fully welded, steel box encasing the joint, avoiding cold, bimetallic joining (explosive bonding, brazing, friction welding)
- Reliable, low resistance contact between cable and copper by soft soldering, avoiding "pressure contacts"
- Low eddy currents loss, obtained by minimizing the volume of copper and segmenting it into smaller elements
- Easy tools and technology, available at any workshop, i.e. avoiding the use of advanced technology (laser, electron beam welding) and large machinery

The assembly procedure goes through following steps:

1. Dismantle the jacket with two longitudinal and one orbital cuts. Remove the outer cable wraps while clamping the end of the cable to prevent de-twist. Remove the Ni plating from the strands facing at the cable surface by mechanical abrasion.
2. Pre-tin the copper connecting elements with PbSn alloy and place half of them on the bottom of the pre-assembled body of the joint box. Re-fresh the cable surface with solder flux and wrap the cable with 0.2mm thick strips of SnAg5 alloy. Place the conductor ends in the joint box and cover with the other half of the copper connecting elements, see also Fig. 2.5.21.
3. Place the steel lid on the box and press it down to compact the cable and close the box (load ≈60t). Spot-weld the lid to the box to maintain the preload.
4. Heat the box up to 250°C to melt the SnAg strips and solder the cable to the copper elements (the pre-load is maintained to large extent).
5. Complete the weld of the lid to the box as well as the weld of the conductor jacket to the box.

Fig. 2.5.21 *The upper row of pre-tinned copper elements assembled in the hairpin joint. The cable length is 420mm, but only 380mm are electrically connected.*

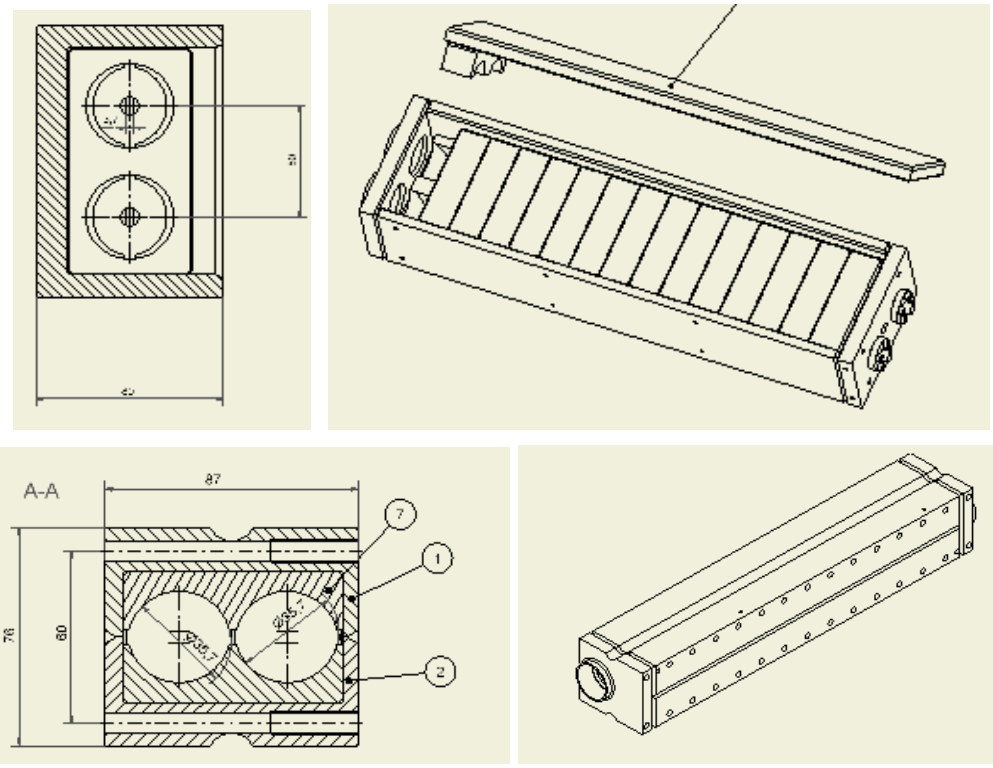

Fig. 2.5.22 *Elements of the hairpin joint (above) and lap joint box (below)*

Although the two joints have the same design, they are not fully identical. In the hairpin joint, the distance between the two conductor axes is limited by the minimum distance to be kept between the conductor jackets to carry out the welding of the joint box (eye glass piece). The distance between the conductors at the lap joint can be reduced to zero because no minimum requirement must be kept. The inter-axis distance is 50mm at the hairpin joint and 37mm at the

intermediate joint. The minimum distance between the compacted cables is 14.5mm and 1.5mm respectively. The contribution of copper bulk resistivity to the joint resistance is roughly estimated 0.2nΩ (hairpin) and 0.1nΩ (lap).

The sample has been tested in August 2004. The most spectacular result is the joint resistance, see Fig. 2.5.23. At the background field of 4T and operating current of 45kA, both joint have a resistance of about 0.7nΩ, dominated by the magnetoresistance of the copper blocks. So far. this is the lowest resistance joint developed for the NbTi ITER conductors.

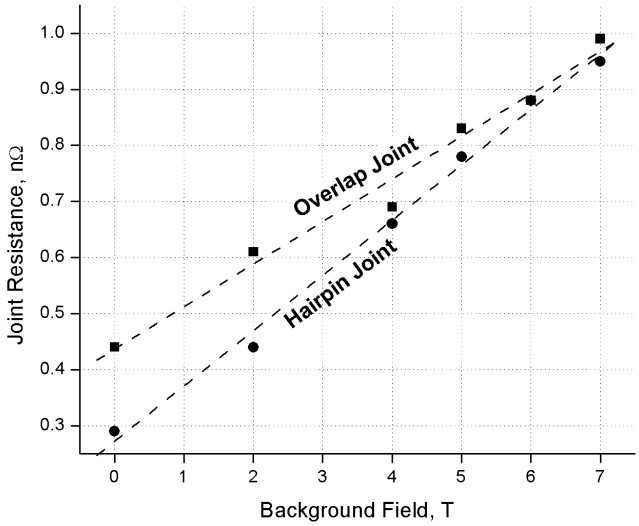

Fig. 2.5.23 *Resistance vs. background field of the two joints at I_{op}=45kA*

2.5.9 JORDI sample and test results

The first sample for the JORDI test facility, see Section 3.6, has been prepared and is being tested. The JORDI sample is in principle a highly instrumented typical ITER joint manufactured using the CRPP design and technology. A layout of the sample is shown in Fig. 2.5.24. To the right the joint itself can be seen, while to the left, 96 elements (superstrands composed of 9 superconducting wires wound around a central copper wire) are independently extracted from the joint and provided each with a calibrated shunt. The conductor for the sample is the same used for the low cost joint sample, see Section 2.5.8.

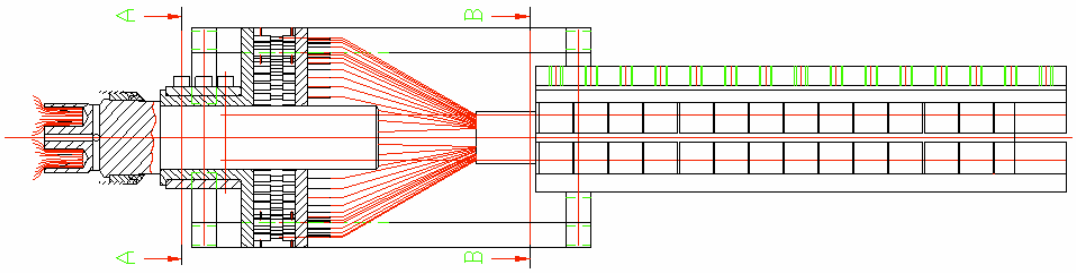

Fig. 2.5.24 *Layout of the JORDI contact resistance distribution sample.*

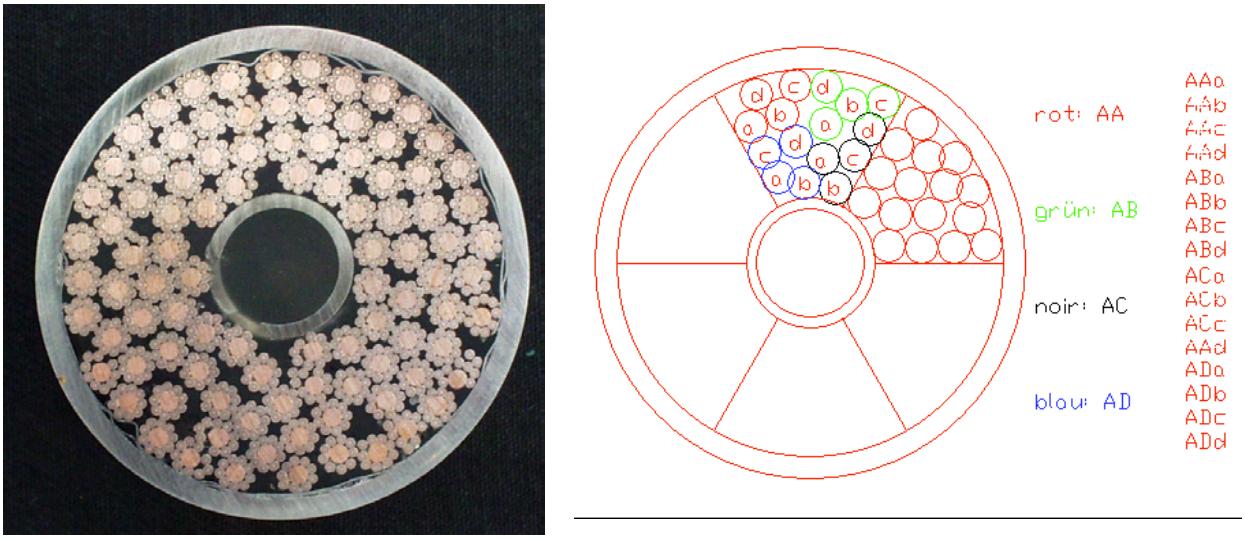

Fig. 2.5.25 *A cross section through the cable used to manufacture the joint together with the labelling of the superstrands.*

The cable used to prepare the joint is a NbTi cable with the structure (9+1)x4x4x6 provided with a central cooling channel. A cross sectional view of the cable is shown in Fig.2.5.25 together with the selection and the labelling of the position of the elements whose contact resistance will be measured.

In order to assess the contact resistance distribution, 2x200 copper sensing wires have to be extracted from the liquid helium bath to the laboratory at room temperature. A special low voltage feed through has been developed as shown in Fig. 2.5.26. The space between the two G10 plates is filled with STYCAST™ during the final assembly.

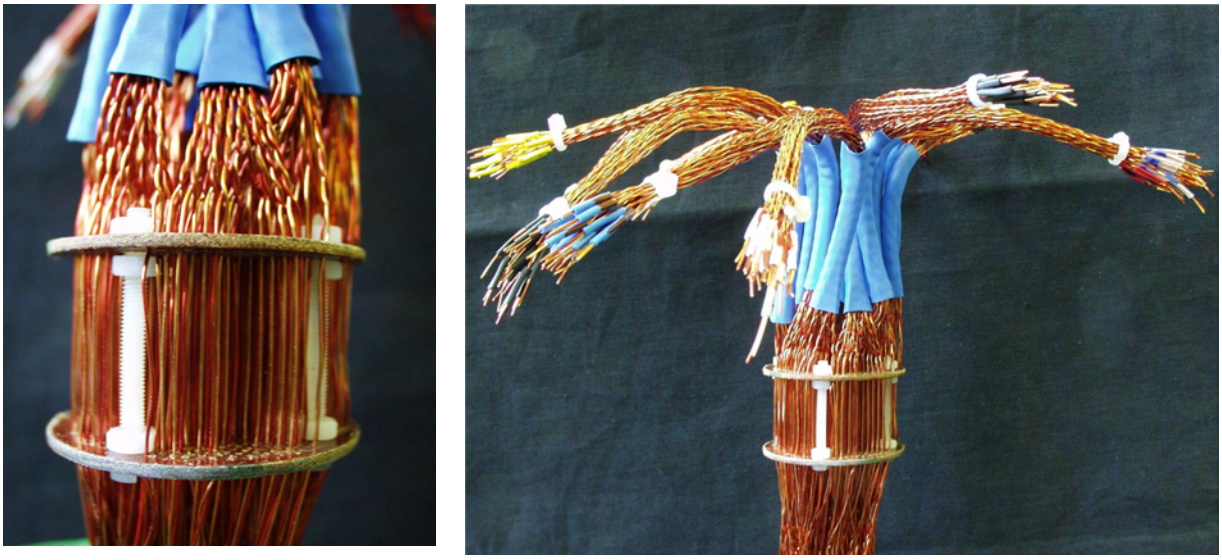

Fig. 2.5.26 *The low voltage home-made vacuum tight feedtrough for 2x200 wires before impregnation with STYCAST™*

2.5.10 Advanced Strand test

The objective of this task is to evaluate the shortly developed advanced strands procured by EFDA in the scope of manufacturing and testing new TF full-size prototype conductors. Prior to the cross-checking investigations aimed at verifying the results of the strand suppliers, benchmarking and calibration of the I_c test facilities have been performed using a Nb_3Sn Power-in-Tube (PIT) strand manufactured by SMI.

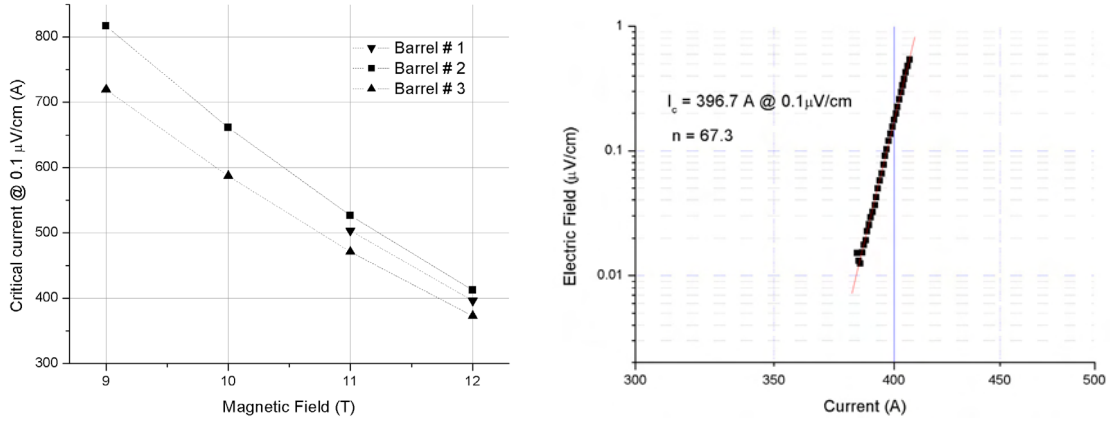

Fig. 2.5.27 *Critical current results vs. magnetic field (top) and evaluation of the n index (bottom)*

Three specimens wound on TiAlV grooved mandrels have been reacted in vacuum according to the schedule recommended by the manufacturer. To prevent accidental loss of tin along the active wire section, 4cm long wire pieces emerging from the copper rings have been left at both ends of the sample holder. These end pieces have been cut after the heat treatment. A pair of voltage taps with a separation of 48cm was soldered along the central region of the samples. The criterion for the I_c determination was $0.1\mu V/cm$. All results are from the first cool down. Due to enhanced voltage noise, some of the V-I curves were not be satisfactorily evaluated and have not been considered. The following table summarises the experimental results.

	Specimen #1		Specimen #2		Specimen #3	
B(T)	I_c(A)	*n*(-)	I_c(A)	*n*(-)	I_c(A)	*n*(-)
9	-	-	817	-	719.6	64
10	-	-	661.4	67.9	587.2	-
11	503.5	63.3	526.5	63.3	471.1	69.6
12	396.4	67.3	412.4	54	373	66.2

There is some variation in the critical current among the three specimens. The deviation of I_c from the overall average value is roughly within ±5% at 12T. This scattering of the I_c results could be associated with performance variation along the strand. The PIT strand reveals quite high *n*-value for a Nb_3Sn product. This may be interpreted as giving evidence for the absence of filament cross-sectional irregularities. Given the very high J_c of the present strand there is an additional possible contribution for a steep current-voltage characteristic. Although a good heat removal is assumed during I_c testing in liquid helium, the shape of the transition may be altered by excessive heat generation in the current contacts. However, within this measurement campaign it was not possible to substantiate the

one or the other contribution to the shape of the transition. The critical currents as a function of magnetic field for all specimens are given in Fig. 2.5.27, top. The bottom of the figure shows the index n of resistive transition for one specimen determined from the V-I characteristic.

2.6 Industrial process plasmas

Most of the research projects of the industrial plasma group of the CRPP are carried out in close collaboration with Swiss industries and are mainly funded by the CTI (Commission for Technology and Innovation. During 2004 several projects such as the design of a new large area high density RF plasma source and a high throughput coating system for mass production of silicon thin film solar cells have been finished. This latter project was of particular interest since it allowed UNAXIS, a Swiss equipment manufacturing industry, to enter the market for equipment for thin film solar cell production. In order to keep up with the market, further development of our present equipment is necessary. This close collaboration is underlined by the fact that during the whole year a process engineer from UNAXIS Display worked at the CRPP on the different projects where the company is involved.

During this year other, new projects have started and many projects are still under discussion with industry and the funding agent, in particular with CTI. Besides deposition plasmas, new research and development topics such as atmospheric plasmas, arcing and micro-discharges have emerged. Discharge plasma physics is the main topic in these interesting projects linked to successful industrial applications.

Modelling of process plasmas, not only for large area RF plasmas, is becoming more and more important. Modelling is also facilitated by new software such as partial differential equation solvers and multi-physics software for the modelling of the complex plasma environment and plasma sources.

2.6.1 Consequences of non-uniform RF plasma potential in RF reactors

Capacitively-coupled parallel plate radio frequency (rf) reactors are commonly used for plasma-enhanced chemical vapor deposition (PECVD) or dry etching of thin films such as amorphous silicon, silicon oxide or silicon nitride. Large area rectangular reactors exceeding $1m^2$ are used for the production of photovoltaic solar cells and thin film transistors for flat screens. These industrial applications typically require a uniformity in film thickness and composition of better than 10%. Several effects can give rise to non-uniform deposition in large area rf capacitive reactors, including inappropriate gas flow distribution, clouds of dust particles and non-uniform electrical power dissipation in the plasma due to finite wavelength effects associated with high frequencies in large area reactors, or due to electrical perturbations associated with the reactor edge design. The plasma non-uniformity considered in this project is due to the redistribution of rf current along the plasma near the edges of asymmetric electrodes. An asymmetry of the electrode edges causes a perturbation in the rf plasma potential, which propagates along the resistive plasma between capacitive sheaths. This perturbation propagation is analogous to the wave propagation along a lossy conductor in a transmission line and can be described by the telegraph equation.

The plasma reactor investigated is a modified version of the industrial UNAXIS KAI-S type Plasmabox reactor used for thin-film deposition. It consists of a rectangular grounded box, 57cm long by 47cm wide, installed inside a larger vacuum chamber. An rf electrode, which acts also as gas showerhead, is suspended above the reactor with a 25mm interelectrode gap. Two different reactor wall configurations have been used in this study: an asymmetric configuration where the plasma is confined by the lateral grounded walls of the box, corresponding to the standard configuration, and a symmetric configuration, where the plasma is confined by two vertical pieces of metal of equal height separated by a small vacuum gap, one connected to the rf electrode and the other connected to the grounded floor. Measurements for the argon plasma were performed using an array of 72 surface electrostatic probes installed in the grounded floor of the reactor. Figure 2.6.1a) shows measurements of the spatial variation of the probe floating potential along the longer axis of the reactor for the non-symmetric and symmetric wall configurations for an argon plasma with an excitation frequency of 40.68MHz. Figure 2.6.1b) shows the calculated spatial variation of the rf voltage amplitude across the ground sheath obtained from the telegraph model assuming a damping length of 3cm.

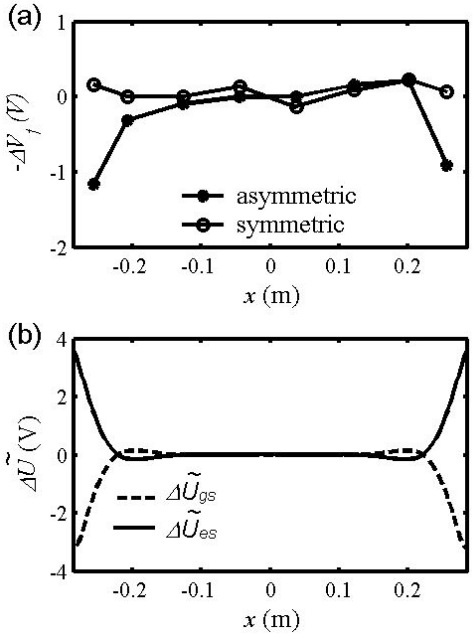

Fig. 2.6.1 *a) Spatial variation of the floating potential of the probes measured along the reactor longer axis; stars are for the non-symmetric wall configuration and open circles for the symmetric wall configuration; b) spatial variation of the rf voltage amplitude across the ground sheath calculated from the telegraph equation*

Electrostatic surface probes cannot be used to study a PECVD process plasma, since the thin film deposition on the surface of the probes will perturb the measurements. Therefore, in order to find possible influences of the plasma rf potential non-uniformity on the overall deposition uniformity, we have measured the deposited film thickness profile on both electrodes for the asymmetric and symmetric wall configurations. Figure 2.6.2 shows the amorphous silicon (a-Si:H) thin film thickness profile along the short axis of symmetry of the KAI-S reactor, deposited using pure silane. As can be seen in Fig. 2.6.2a), the film thickness for the asymmetric wall configuration is similar for both electrodes in the central part of the reactor, but at a distance of about 5cm from the reactor edge, the film thickness starts to strongly increase on the rf electrode while it continues to decrease on the grounded reactor floor. Contrarily, for the symmetric wall

configuration (Fig. 2.6.2b)), both film thickness profiles have similar shapes until the edge of the reactor. These two different behaviours for the symmetric and asymmetric wall configurations can be clearly seen by plotting, for each configuration, the difference between film thickness deposited on the rf electrode and the film thickness deposited on the grounded reactor floor (dotted lines in Fig. 2.6.2). For the asymmetric configuration, the difference is almost zero in the central part and then strongly increases towards the reactor edge, while for the symmetric case it remains close to zero along the whole electrode.

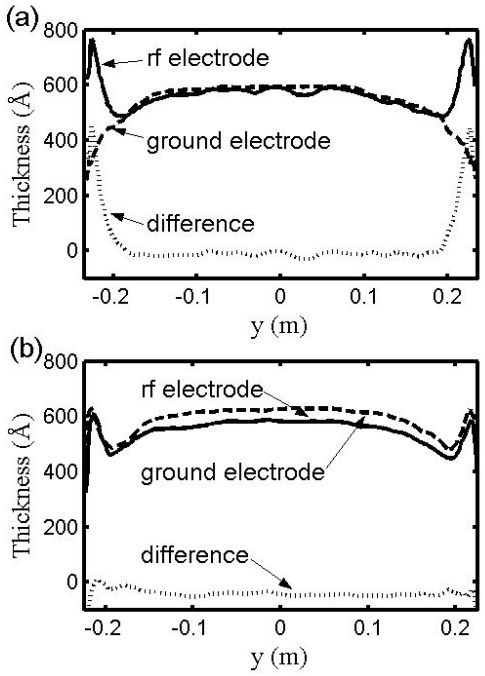

Fig. 2.6.2 *Deposited a-Si:H film thickness profiles on the rf electrode (solid line) and grounded reactor floor (dashed line) along the short axis of symmetry of the reactor for (a) the asymmetric and (b) the symmetric wall configurations. The dotted line represents for each case the difference between the film thickness on the rf electrode and the film thickness on the grounded reactor floor.*

2.6.2 Characterisation of supersonic low pressure plasma jets

Unlike atmospheric pressure plasma jets, which have been extensively studied experimentally and theoretically, the growth of interest in low pressure DC plasma jets only occurred recently. Low pressure plasma jets present unconventional properties such as their low collisionality, their large dimensions and their supersonic flow. Therefore specific diagnostics have to be adapted for these conditions. Studies of plasma jets using optical emission spectroscopy (OES) are mostly based on the assumption of local thermodynamic equilibrium (LTE) which is no longer satisfied at lower pressure. Enthalpy probe measurements in compressible supersonic plasma jets have been reported but were limited to a pressure range down to 200mbar. These limitations show the need to develop a diagnostic to characterize DC plasma jets covering a pressure range from 2 to 80mbar and which is independent of the LTE assumpton.

Electrostatic probes are widely applied in low density plasmas such as glow discharges to measure the electron temperature and density. Unlike other

diagnostics like optical emission spectroscopy (Boltzmann plot) or the enthalpy probe, this technique does not require the assumption of local thermodynamic equilibrium.

The investigated plasma jet is generated with a Sulzer Metco F4-VB gun with a conical nozzle. The double Langmuir probe is made of two parallel tungsten wires of 0.15mm diameter protruding 1.5mm from a thin ceramic sheath used as shield. The two wires are 1mm apart and the probe is quickly swept radially through the plasma jet by a rotating arm with calibrated position to obtain radial profiles. The current circulating between the electrically floating probes immersed in the plasma jet is measured as a function of the voltage difference. The Mach probe construction is similar to the double probe, except that the two probes are mounted with their axes perpendicular to each other. Therefore one probe is parallel to the plasma jet flow, the other perpendicular. Each probe is polarised at the same potential in the ion saturation current region of the Langmuir characteristic. The ratio of the currents collected by the two probes allows the Mach number of the plasma flow to be determined.

Measurements made at a chamber pressure of 10mbar are presented in Fig. 2.6.3 and show the typical trends of under-expanded jets for a pressure range of 6 to 40mbar. The torch parameters used here are a current of 400A and a gas flow of 40SLPM Ar. A compilation of the plasma jet properties presented in the previous section are summarised in Fig. 2.6.3 showing contour plots of the light emission a), Mach number b), electron density c) and temperature d). The shock wave structure presented in the plasma jet phenomenology is also added in the figure as part e).

The visible bright plasma plume which is created inside the nozzle by the hot and dense arc expands freely outside of the nozzle since there are only expansion waves at the nozzle exit and the surrounding gas density is low. Once the radial expansion has started, the plasma jet density and emission decrease to reach a minimum in region "c". The process afterwards between region "d" and "e" is similar to over-expanded jets at the nozzle exit. The local pressure is lower than the surrounding pressure, which leads to the creation of oblique shock waves. A compression zone is created in "e" corresponding to the visible bright zone in the image. The pressure of the jet at this location is increased above the chamber pressure and the flow is slowed down. A part of the kinetic energy from the expansion zone is converted into thermal energy in the compression zone.

The process of expansion and compression repeats until the pressure in the plasma jet is equal to the chamber pressure. At 10mbar and for these plasma conditions, the total visible length of the plasma jet can be as long as 1m.

The mappings confirm the previous analysis made by means of the axial and radial profiles of the plasma jet properties. The maximum of light emission at z=60mm does not correspond to a special zone of the plasma jet. The region of minimum Mach number is centered at about z=50mm, which is also the region where the electron density and temperature are maximum. Note that the electron temperature contour plot reveals two local maxima at z=45 and z=50mm. The region of maximum electron temperature corresponds to the zone where the shock waves meet on axis and the center of cell "e" of Fig. 2.6.3e).

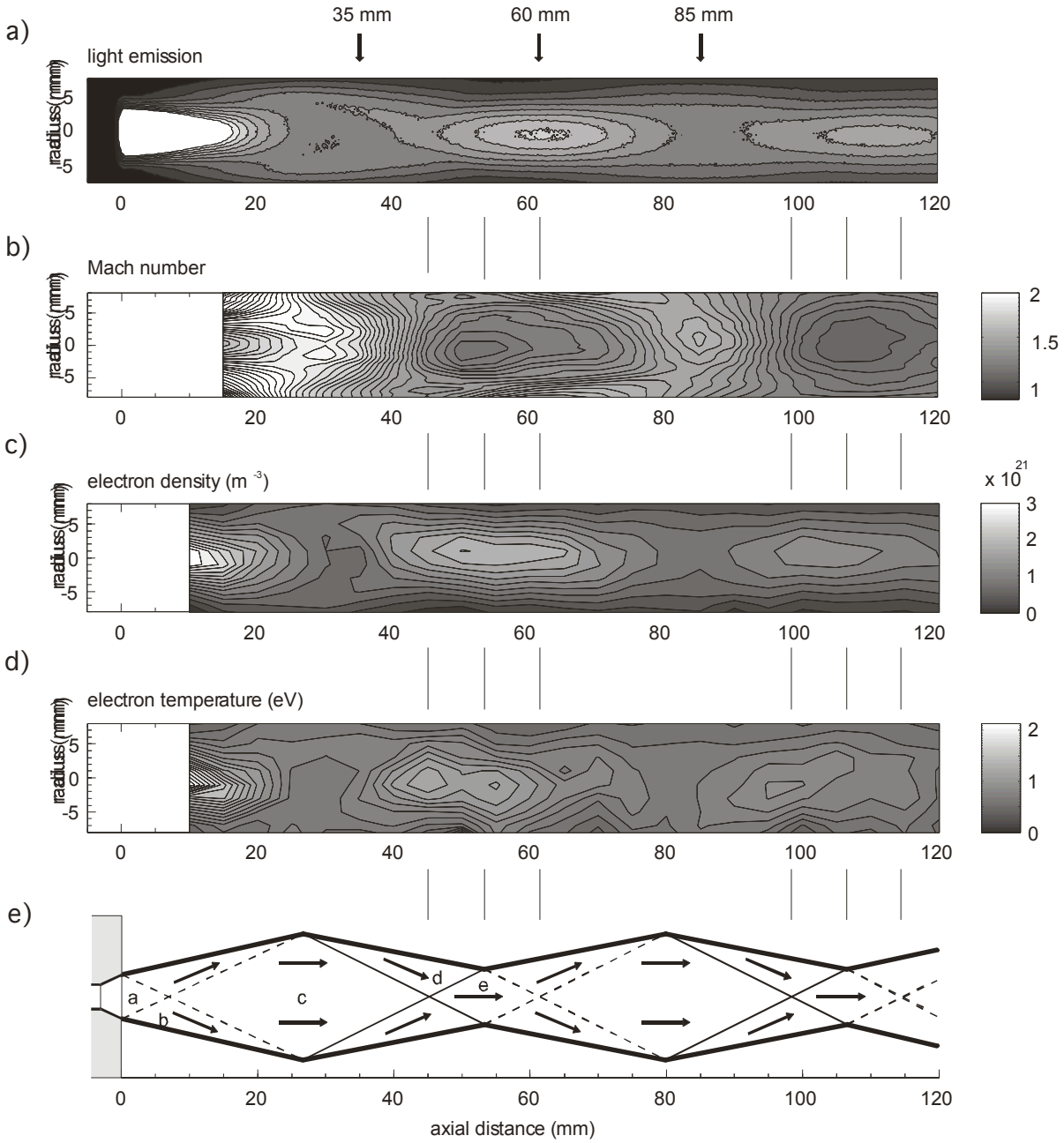

Fig. 2.6.3 *Contour plots of the total light emission a), Mach number iso-contours b), electron density iso-contours c), electron temperature iso-contours d) and the corresponding scaled shock structure of the plasma jet e). Chamber pressure 10mbar, 400A, 40SLPM Ar flow.*

The Mach number mapping shows that the region centered at z=110mm corresponding to the local minimum of the Mach number in the second compression zone is wider than in the first compression zone. Oblique shock structures are also shown up by the contour plots in the expansion zone at z=85mm.

In order to equilibrate the pressure difference at the nozzle exit, the expansion waves are created from the edges of the nozzle towards the jet axis which are then reflected in the direction of the plasma jet fringes. These expansion waves direct the flow towards the edge of the plasma jet, creating a radial expansion in region "b" in

addition to the axial expansion in region "c", where the local pressure is reduced. The edges of the first expansion zone are brighter than on axis because of the reflection of the expanding flow by the cold dense surrounding gas. This leads to the creation of so-called barrel shocks, visible on the plasma jet image. They correspond to a region where the density is slightly increased.

2.6.3 Design of a new large-area high density RF plasma source (HDS)

Capacitively-coupled parallel plate RF reactors are commonly used for plasma enhanced chemical vapour deposition (PECVD) and dry etching of thin films such as amorphous silicon or silicon oxide. Large area (>1m^2) reactors are used for the production of photovoltaic solar cells and thin film transistors for flat screens. These industrial applications typically require a uniformity in film thickness to better than 10%.

The non-uniformity considered is due to finite wavelength effects associated with high frequencies in large area reactors, such that the reactor size is comparable to, or larger than, a tenth of the free space wavelength at the excitation frequency. Non-uniform RF plasma potential will generally result in non-uniform power dissipation and consequently non-uniform deposition or etch rates. Many other phenomena can give rise to non-uniform deposition or etching in RF parallel plate reactors, including imperfect contact of the substrate with the electrode inappropriate gas flow distribution, clouds of dust particles, and various edge effects due to fringing fields, electrode asymmetry etc.

Fig. 2.6.4 *KAI 1000 plasma reactor at the CRPP*

The lens shaped design of the electrode is intended to compensate the standing wave effect by creating a uniform electrical field over the whole plasma volume. To be uniform, the plasma requires not only a constant electrical field, but also a constant plasma thickness. The plasma was therefore confined between parallel boundaries by a dielectric plate - a glass plate in these experiments - placed on the profiled electrode. A cylindrical reactor was used to facilitate comparison with the two-dimensional cylindrical vacuum theory. It was proven experimentally that the concept of the lens-shaped electrode works in the case of the cylindrical reactor.

This year was devoted to the proof of principle of the lens concept in an industrial rectangular large area reactor. A commercial KAI 1000 reactor was obtained from

UNAXIS Display which can coat substrates of $1m^2$, was installed at the CRPP (Fig. 2.6.4). Considerable effort by the CRPP was invested into the infrastructure of this large device, in particular the vacuum system, gas supply and the optical plasma diagnostic. The ground electrode was machined to the calculated shape expected to suppress the standing wave effect at 67.80MHz. The plasma diagnostics installed onto the KAI 1000 reactor were optical diagnostics and electrical probe measurements. 24 fibre optics were installed in the ground electrode in order to monitor the optical uniformity of the plasma. The fibre optics were led via vacuum feedthroughs to photodiodes and arrayed in multiplexers and a high performance digital multimeter in a PXI crate with embedded controller and Labview software. A calibration procedure of the whole fibre optic system has been developed.

The standing wave effect at typical industrial frequencies (13.56MHz, 27.12MHz, 40.68MHz, 67.80MHz, 100MHz) was measured in the conventional flat electrode reactor design with and without plasma. Figures 2.6.5 and 2.6.6 show normalized light intensity measurements in the KAI 1000 at 13.56MHz and 40.68MHz. This measurement clearly demonstrates the standing wave effect at 40MHz whereas at 13.56MHz the flat profile indicates that the standing wave effect is not dominant. The 100MHz operation of the reactor required the construction of a triple stub tuner, which is an original way of impedance matching at VHF.

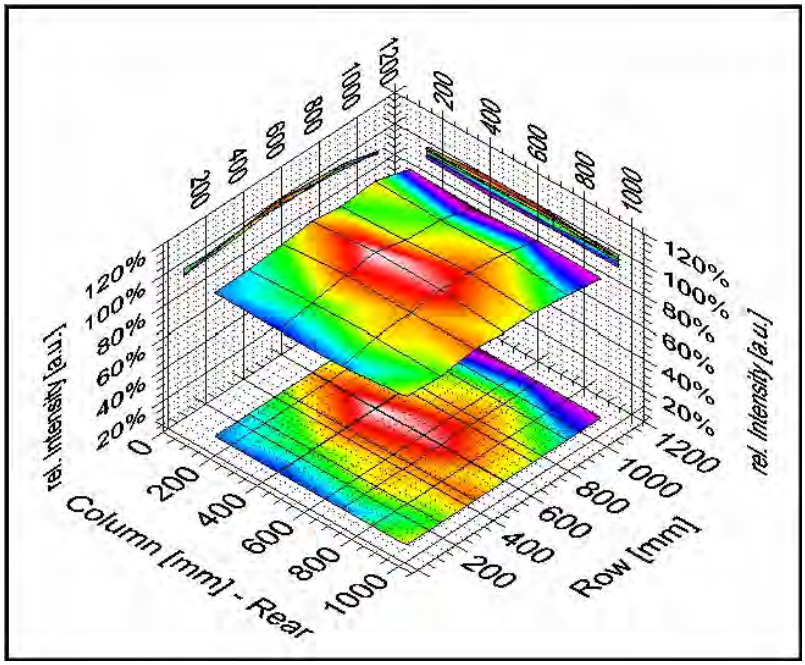

Fig. 2.6.5 *Normalised light intensity in the KAI 1000 at 13.56MHz in an Argon plasma at 1Torr*

During the last part of the year the reactor has been equipped with the novel rectangular lens design, which is supposed to suppress the standing wave effect at 67.80MHz. First experiments have started and are promising to show that the lens concept is a powerful technique to compensate the standing wave effect in an industrial large-area RF plasma reactor.

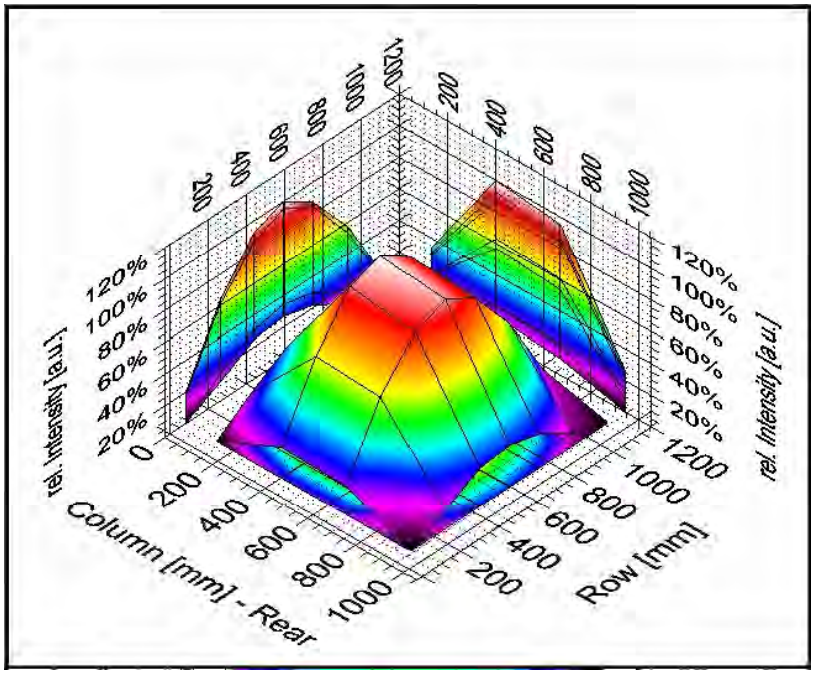

Fig. 2.6.6 *Normalized light intensity in the KAI 1000 at the 40.68MHz in an Argon plasma at 1Torr*

2.6.4 Reactive Low Energy Plasma Source for SiGe processing

Industry needs plasma sources capable of driving high deposition rate processes for high quality coatings. In particular, the semiconductor industry needs high deposition rates in epitaxial processes in order to decrease the production costs of the devices.

The underlying physical principal of the Low Energy Plasma (LEP) is that an intense low energy plasma can be generated by sustaining a low energy arc discharge by a large electron current emitted from a hot filament. The plasma source (see Fig. 2.6.7) contains a tungsten filament heated by a current. The plasma is sustained by applying a voltage of about 20-30V between the grounded chamber walls and the hot filament. Discharge currents in the range 10-100A can easily be obtained. The low energy electrons ionise and excite the argon as well as the admixed gases creating a dense reactive plasma in the chamber. The main advantage of the low energy plasma is the low energy (<12eV) ion bombardment of the substrate leading to interesting industrial applications such as the epitaxial growth of layers such as SiGe. In the case of the present project, plasma physics, chemistry and diagnostics are needed to finalise design and optimise the low energy plasma source for industrial applications.

The first successful applications of the low energy plasma source showed up several difficulties that are directly related to plasma physics and chemistry and to the technology of the plasma source design. It is the aim of the present project to identify and to obtain industrial solutions to these problems. One major problem inherent in the principle of the plasma source is the influence of the design of the ionisation source on the resulting plasma. Process stability and film inhomogeneity are two other topics that need to be clarified before successful industrialisation of the reactor and process. Therefore, diagnostics of the resulting plasma are needed in order to optimise the process plasma from the point of view of deposition rate and uniformity. For semiconductor applications, the process development for the

plasma cleaning and for solving the problem of the reactor self-cleaning has to be investigated. During the year an LEP plasma reactor was installed at the CRPP and first experiments have been started.

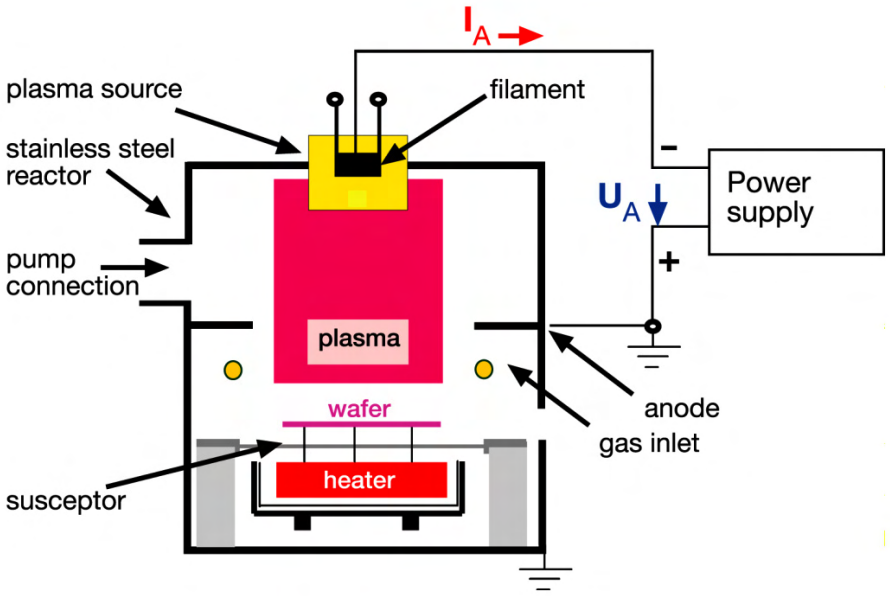

Fig. 2.6.7 *Schematic of the LEP plasma reactor*

2.6.5 A new reactor for thin film solar cell applications

At present capacitively-coupled RF discharges operating at 13.56MHz are the most popular plasma tool for the production of large area films used for flat displays and for thin film solar cells. Higher plasma excitation frequencies have been shown to be a better choice since high device quality at industrially interesting deposition rates could be obtained with this process. An attractive way to achieve high density plasmas, and therefore high deposition rates, consists of using very high excitation frequencies (VHF) while keeping the design similar to the parallel plate reactor design. In addition, since the sheath voltage decreases rapidly with increasing excitation frequency, we can couple much higher RF power into the plasma while keeping a moderate sheath voltage thus preventing the substrate from damage. However since the quarter wavelength of the excitation frequency becomes comparable to the reactor size, at least for the dimensions of the latest generation reactors, the film uniformity of 5-10%, an important issue in both mentioned applications, is difficult to achieve. In a previous CTI project, the theoretical and experimental proof was made that in a reactor with adequately shaped electrodes the so-called wavelength or standing wave effect can be compensated. The previous studies were undertaken in well-diagnosed large area reactors and mostly in non-reactive gases, and only a few substrates were coated with this new type of reactor.

The production of thin film solar cells is the first straightforward application of this new reactor type. The reasons are that higher plasma excitation frequencies are required for this type of application. Higher deposition rates together with moderate to high material quality can most probably only be obtained with such a process. In addition, the higher excitation frequency also allows the industrial deposition of microcrystalline or micromorph layers, requested by the photovoltaic (PV) industry for future solar cells. On the other hand, the commercial KAI plasma box concept has been proven to be adapted to PV applications and, coupled together with higher

plasma excitation frequencies, could be of benefit for the production of amorphous and microcrystalline silicon for application in solar cells. The new high density reactor generation could therefore be the most appropriate for thin film solar cell production.

The scientific and technological aim of the present project is to apply the newly-developed technology of the high density reactor to the production of large-area solar cells. This new reactor should represent the second generation of reactors in the PV equipment production line of UNAXIS Solar.

Besides these more technical problems, the development of the process for amorphous and microcrystalline silicon deposition in this new device is necessary and will therefore be a large part of the project. Microcrystalline or micromorphous silicon are the materials for future solar cells and therefore their production must be industrially possible using the next generation PV production equipment. Particular care will be taken regarding the electronic quality of the layer including roughness and film density as well on the deposition rate and the uniformity of the layer over the whole 1x1m^2 glass substrate. A scientific aim of the present project is to develop an industrial process for the deposition of these highly demanded PV materials.

The aim is to have at the end of a project a high density RF reactor operating at an elevated plasma excitation frequency allowing industrial high rate deposition of amorphous and microcrystalline (micromorph) silicon with a homogeneity of 5-10% on solar cells on large area substrates, typically around 1m^2.

2.6.6 Plasma diagnostics for the electrical discharge machining (EDM)

Electrical Discharge Machining (EDM) has been a well-known machining technique for more than fifty years. Nowadays it is widely used of a large number of industrial areas, mainly to produce moulds, dies and finished parts with complex shapes.

This technology uses the eroding effect of electric spark discharges on the electrodes. Thus, the machining consists in successively removing small volumes of electrode material, which are molten or vaporised during the discharge. The electrical discharges are created between the conductive workpiece and a shaped electrode (die-sinking machine) or a metallic wire (wire cutting machine). Thus EDM can be used to machine any material that conducts electricity, whatever its hardness may be. The sparks are created in a flowing dielectric fluid, generally water or oil. It guarantees a high plasma pressure and therefore a high removing force on the molten metal when the plasma collapses, it solidifies the molten metal into small particles, and it also enhances the flushing of these particles.

Figure 2.6.8 shows a schematic drawing of the experimental set-up, a small and versatile die-sinking EDM machine as installed by Charmilles SA at the CRPP. The dielectric, the electrode and the workpiece can easily be changed. We used pure water, mineral oil and liquid nitrogen as dielectric, copper, tungsten and graphite electrode; and W300 steel workpieces.

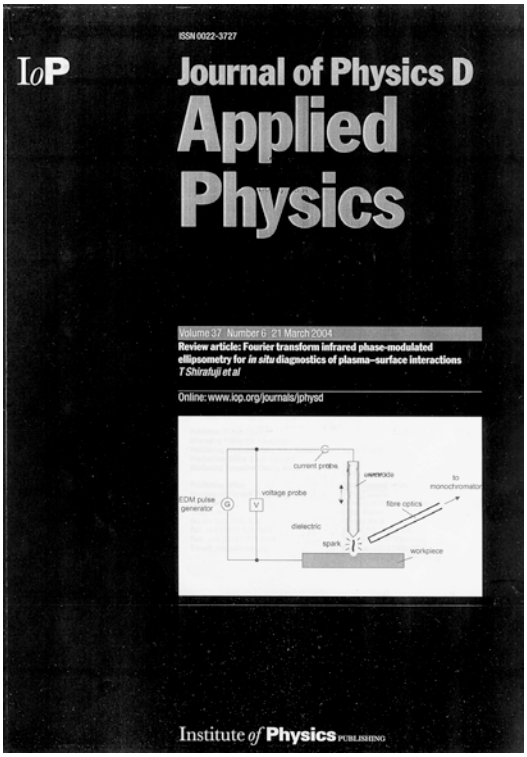

Fig. 2.6.8 *Schematic drawing of the EDM experimental set up at the CRPP, exceptionally used in the front page of the Journal of Physics D; Applied Physics*

Figure 2.6.9 is a close-up image of the electrodes during machining. These images were obtained with an endoscope composed of 10'000 fibres coupled to a CCD camera. The plasma is clearly visible, along with gas bubbles created by the discharge.

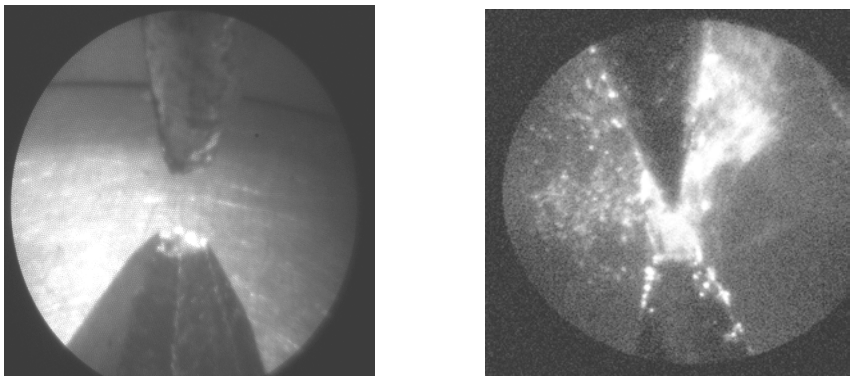

Fig. 2.6.9 *Image of an EDM discharge in a) water and b) oil obtained with an endoscope*

These gas bubbles are created at the cathode and move towards the anode. They are only observed if water is used as dielectric. Even at large electrode distances of up to a few centimetres, gas bubbles can be observed. By means of the CCD camera and laser light extinction measurements the velocity and size of the gas bubbles has been determined. The velocity of the gas bubble is in the range of cm/s and depends on the applied electric field. The size of the bubbles has been estimated to be between 30-100 micrometers.

Of particular interest is the pre-breakdown of the discharge in the water and oil dielectric as used in electrical discharge machining. First investigations showed that the pre-breakdown in the two oil and water dielectrics is fundamentally different. In the case of water, a pre-discharge current in the order of a mA is observed before the main breakdown of the discharge. The time duration of this current pulse is about 10ns. These indications strongly suggest that in the case of water a streamer is formed, which propagates with a velocity of about several km/s. The conductivity of the water influences the current and the number of streamers. Fast light intensity measurements might show light emission from streamers. However no pre-breakdown current and light is observed for discharges in clean or contaminated oil. From these observations it is concluded that the pre-breakdown in the two dielectrics is different.

Spectroscopy is a straightforward plasma diagnostic method for investigating the discharge during EDM. In the previous project phase the light emitted from the discharge was collected by a quartz fibre immersed in the dielectric, located a few millimetres from the spark to optimize the collected light intensity and to reduce absorption from the dielectric. However this arrangement allowed no spatially-resolved measurements of the emitted light. In order to obtain spatial resolution the image of the endoscope was projected by means of a lens on to a bundle containing 16 in-line fibres. This bundle was connected to the monochromator equipped with a fast CCD camera. With this experimental arrangement an estimated spatial resolution of 30-50 μm per fibre was obtained. For typical discharges 6-8 fibres had enough light intensity if the bundle was used along the discharge axis.

The plasma is contaminated by impurities and so several lines of atomic copper and chromium from the electrode are present in the emission spectrum. The spatially-resolved emission spectroscopy measurement showed that the chromium line increases towards the steel electrode whereas the copper line remained constant. First results from electron temperature measurements using the Boltzmann plot technique showed that the electron temperature is constant along the discharge.

Again, as in the non-spatially-resolved spectra, the dominant line within the spectra is the Balmer H_α line emitted by atomic hydrogen, which comes from the cracking of the dielectric molecules. Although the H_α line is dominant, the remaining Balmer series lines such as H_β or H_γ are not observed indicating a high electron density. Furthermore, the H_α line is strongly broadened. The Stark broadening of the H_α line depends strongly on the electron density and can be used to evaluate it.

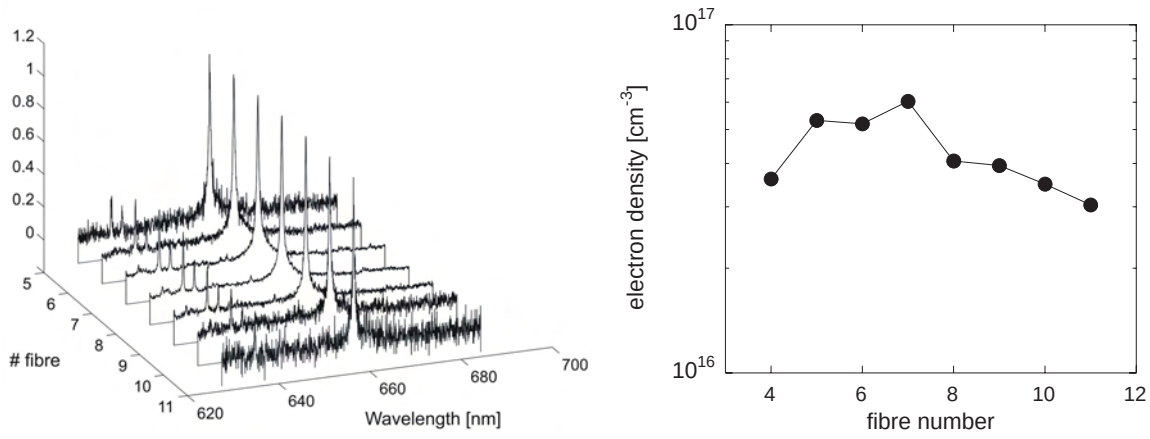

Fig. 2.6.10 *a) Spatially-resolved H_α lines b) spatially-resolved electron density obtained from the H_α Stark broadening.*

The results show electron densities in the order of 10^{16}-$10^{17}cm^{-3}$ and a maximum of the density in the centre of the discharge.

The effort during the year to obtain new information on the discharge used in EDM showed the experimental difficulties. In particular the small size and the non-reproducibility of the discharges are the main difficulties in investigating the discharge. The measurement of weak light emissions during nano-second periods is an additional problem. The study of the pre-breakdown is hindered by electrical interference and as well in this case by the non-reproducibility of the discharge.

2.6.7 Atmospheric plasmas for thin film coating

Avoiding vacuum technology for depositing coatings on polymer films is certainly one possible route for cost reduction. Vacuum technology has several economic drawbacks. The process for coating deposition is not continuous, the machine has to be stopped and opened for the loading and unloading of film reels, and pump down time is tightly linked to the pumping speed and cleanliness of the pumping system. The maintenance of equipment in production status is costly and time consuming. Plasmas at atmospheric pressure are thought to be an alternative way for the production of coatings for various applications.

However, there are various problems related to the process by RF plasmas operated at atmospheric pressure. First of all, the applied RF voltage must be in the kV range, giving rise to considerable problems in the design and construction of the RF generator, circuit and of the RF electrodes. RF plasma discharges at this pressure often show a discharge consisting of many different discharge filaments similar to the one observed in the so-called silent discharges. However, under certain conditions a uniform plasma can be obtained, as required for uniform film deposition. The control of the discharge type is one of the difficulties in atmospheric RF plasma applications. The control parameters for the discharge transition are the plasma excitation frequency and the electrode gap distance.

A preliminary study of the glow discharge in different neutral gas mixtures (He, N_2, Ar) as a function of the pressure (10^3 to 10^5 Pascal) has been made in order to determine the basic characteristics of the plasma. The diagnostics used for this study were optical emission spectroscopy and electrical measurements (discharge current and voltage, gas voltage...). Three kinds of discharges have been found: glow, multi-peak and filamentary. This study highlighted the role of metastables and of the dielectric surfaces for the establishment and the stabilisation of the glow discharge mode. It also permits determining the operation domain of the glow discharge according to the working pressure, voltage and frequency. Some work has been done in N_2/O_2 and N_2/N_2O gas mixtures according to the pressure and concentration of oxygen or nitrous oxide. These gases limit the formation of the glow due to their electronegativity and to their efficient quenching of N_2 metastables. Time-resolved spectroscopy has been used to determine the evolution of metastable molecules within one discharge cycle at different pressures in N_2 and He.

The addition of hexamethyldisiloxane (HMDSO) for SiO_x deposition on polymer films completely modifies the discharge. A few ppm of HMDSO are sufficient to induce a transition from glow to filamentary mode. The coating obtained at atmospheric pressure is inhomogeneous because of the geometry of the discharge cell ($60x60mm^2$) : the chemistry is changing along the gas flow direction. There are two different regions observed: one where surface reactions dominate and the other

where volume reactions (powder formation and redeposition) are predominant. The next step is the understanding of these processes and the characterisation of the coating for different gas mixtures, power and frequencies.

2.6.8 Nano powder synthesis by thermal plasmas

The goal of this project is to monitor the process of nano-particle formation in the thermal RF plasma by various *in-situ* particle diagnostic methods. The aim is to understand the nano-particle synthesis and growth mechanism and to develop *in-situ* process monitoring for nano-particle processing in inductively coupled RF thermal plasmas. In the framework of TOPNANO 21, a project has been started on the nano-powder synthesis in thermal plasmas in collaboration with EMPA in Thun. The project intends to contribute to the understanding of nanometer-sized powder formation and production in RF thermal plasmas through a multidisciplinary approach involving material scientists (EMPA-Thun) and plasma physicists (EPFL-CRPP).

The melting and/or evaporation zone of the injected powder below the torch nozzle exit was diagnosed by the enthalpy probe. This diagnostic can be used to optimise the thermal plasma with respect to enthalpy which is related to the distribution of available RF power in the plasma-powder reaction zone. Various plasma parameters such as gas mixtures and different gas flow rates have been varied in order to find the most appropriate process parameters for nano powder formation. In addition, analysis of the sampling gas of the enthalpy probe by a mass spectrometer makes the plasma chemical composition.

Several in-situ powder and plasma diagnostics have been designed, constructed and are available for the study of the plasma processing of nano-powders. Extinction measurements simultaneously available at two different distances from the torch exit allow the monitoring of the amount of non-evaporated, primary powder. In order to obtain high quality mono-dispersive nano-powder, no primary particle should pass the reaction zone untreated . The chemical composition of the primary particles and the plasma source (including various gas flows) and in addition the powder feeding rate, must be optimised to obtain complete evaporation of the primary particles. In the melting and evaporation region chemical reactions take place as well as the nucleation phase leading finally to the nano-particle formation. An additional diagnostic, optical emission spectroscopy, is applied simultaneously with the extinction measurements to the same location. The emission spectroscopy can be used to obtain basic information on the plasma chemistry, in particular concerning the plasma composition. The use of a digital camera gives qualitative information on plasma flow and powder flow pattern.

The usefulness of the plasma and in-situ particle diagnostics is also well documented by finding an influence of the powder feeder carrier gas and the precursor feed rate on the enthalpy and the plasma temperature, respectively.

It was found that the central gas flow of the RF torch has an important influence on the melting and evaporation of the primary particles. For low central gas flow rates, the flow pattern is laminar and the powder flow remains in the hot central part of the plasma jet. High central gas flows lead to turbulent gas and powder flow patterns. Furthermore, a higher enthalpy was measured for low central gas flow rates. The influence on the nano-particle formation is shown by the fact that at low particle/carrier gas flow rates, a higher volume fraction of finer particles and a lower fraction of untreated particles have been measured by the ex-situ powder characterisation methods.

Optical emission spectroscopy showed that the intensity of the Al emission lines is a reasonable monitor for the vaporisation of the Al_2O_3 precursor particles. The maximum in the Al emission intensity as a function of the powder feeding rate indicates that for low feed rates, a precursor deficient regime is reached. The Al emission intensity also decreases for higher feed rates indicating that an energy deficient regime is obtained (overloading of the plasma jet by cold particles). These observations are consistent with the laser extinction measurements showing the correct dependence on the RF power and which are mostly sensitive to the large precursor particles. The maximum volume fraction of large particles might reach a few tens of percent at these locations and for the highest feed rates. The figure of merit for particle vaporisation is the ratio (unit "enthalpy") of the RF power (kW) to the powder feed rate (kg/s) by analogy with a similar parameter which plays an important role in plasma spraying and polymerisation. This relation shows that in order to optimise the precursor treatment, the enthalpy in the plasma must be maximised.

Two sampling stations allow extraction of samples for ex-situ characterisation. Ex-situ characterisations by various methods such as SEM, TEM, XRD, BET of the produced powders showed consistent results with the above mentioned process behaviour.

2.6.9 Plasma induced surface modifications for biomedical applications

Various studies on surface modifications for biomedical application have been performed in projects in collaboration with the Laboratoire de Métallurgie Chimique (LMCH) of the STI-EPFL.

Plasma surface treatments are potentially very useful for the covalent incorporation into polymer surfaces of extraneous reactive groups suitable for participation in further, conventional chemical reactions at the surface. The plasma modification can be carried out in the presence of specific gases, such as O_2, Ar, He, NH_3, N_2, and H_2. This results in the generation of active species, which can activate and modify the material depending on the nature of the gaseous medium.

Besides surface modifications as studied in preceding projects, plasma deposition is used to modify polymer surfaces for biomedical applications.

Pseudomonas aeruginosa is one of the most prevalent bacterial strains in clinical environments, responsible for 30% of pneumonia cases occurring in intubated patients. Colonisation of the intubation tubes can lead to death, despite antibiotic therapy. Silver is currently used as an antibacterial agent in several medical applications. The project aimed to develop a strategy to reduce bacterial adhesion by plasma-depositing Ag/Teflon-like coatings, consisting of Ag clusters embedded in a teflon-like matrix.

Ag/Teflon-like coatings were deposited on PVC substrates in a mixed RF PECVD/sputtering process, employing a silver cathode in a RF reactor, C_2F_6 or C_3F_8 as a monomer, H_2 as a carrier gas and Ar as a buffer gas. Additional depositions have been performed by adding N_2 into the discharge to study its effect. A systematic study of the deposition parameters using XPS analysis to investigate the chemical nature of the coating has been made. For both monomers tested, it was determined that an increase in Ar flow rate and RF power increased cross-linking of the Teflon-matrix and Ag-content was measured. The greatest Ag content of 14.4% was achieved for C_3F_8-H_2-Ar discharges containing 20% N_2 gas feed.

2.6.10 Uniformity study in large-area showerhead reactors

In collaboration with UNAXIS, a project on the modelling of industrial plasmas has been defined. Until now, the development of the next large-area PECVD reactor generation has essentially been done empirically, based on the experience acquired with the preceding reactor generations. Due to the rapid increase of the substrate size, which now reaches more than $1m^2$ in the flat display industry, the development of PECVD reactors used for the fabrication of thin film transistors (TFT) becomes more and more costly and difficult especially if technological innovations have to be tested and introduced to reach the required specifications.

Although PECVD processes using capacitively-coupled RF plasma reactors remain the first choice for thin film deposition (e.g. silicon nitride, amorphous silicon or silicon oxide), they are complex and are affected by a large number of process parameters such as reactor geometry, gas injection distribution, powder contamination, voltage non-uniformity, and perturbations due to reactor edges. Therefore, in order to design even larger plasma reactors, a better understanding of the different sources of non-uniformity of the deposited layers is needed.

The different aspects that have to be treated in the development of the model are first the simulation of the gas flow distribution across the porous showerhead rf electrode, and then the development of the neutral chemistry model which has to be coupled to the plasma physical model (fluid description). It has been decided to use a commercial software package (CFD-RC ACE+) and to adapt it to our specific reactor geometry and process conditions.

The non-uniform deposition of silicon nitride in the UNAXIS KAI-1 800 Plasmabox reactor can not be reproduced by taking into account only the standing wave effect, whereas a good agreement is found when the local power dissipation into the plasma accounts for both the electrode dimension effect (standing wave) and electrode edge asymmetry (telegraph effect). The experimental observations show two distinct deposition profiles in the rf and ground sheath which cannot be explained by the standing wave effect alone, which imposes the same electrical power distribution in both sheaths. The telegraph effect instead provides different distributions in each sheath, which give the sources for the different deposition rates on each electrode. The results of the present work are also compared with the outcomes of the two-dimensional model elaborated previously to demonstrate the importance of electromagnetic non-uniformities in film deposition. It must also be pointed out that the deposition profiles of each electrode have been measured in two different experiments and a new experimental campaign is underway to verify these results.

2.6.11 Influence of a weakly ionised boundary layer on air flow

During 2004, a project which involves a close collaboration between the Laboratoire de Thermique Applique et de Turbomachines (LTT) and the Laboratoire d'Ingénierie Numérique (LIN) of the Energy Institute (ISE) from the EPFL Faculty of Engineering (STI) and the CRPP has been started.

The goal of the project is to study the effect of ionized gases in the proximity of leading edge surfaces on the shape, strength and absorption of the shock envelopes present within oncoming air flow in transonic and supersonic regimes. The project

proposes an experimental investigation of the modification and dispersion of shocks that arise in transonic and supersonic flow by use of a weak ionisation of the gas generated by a surface discharge. The modification of the flow structure and shock wave structure with the ionised air will be investigated and compared with the model and the former experiments without the plasma layer. The investigations will also include studies on the effect of the surrounding flow on the stability of the glow discharge.

The experiments will consist of an installation of a typical wing section in one of the Laval nozzles at LTT. The Laval nozzle available at the LTT produces an outlet Mach Number that can be regulated between 0.2 and 1.6. An atmospheric uniform glow discharge shall be used as plasma source to obtain the required plasma layer covering the necessary wing surfaces. This surface plasma source consists of a parallel arrangement of electrode strips on a suitable dielectric between which the plasma is created. Up till now, different electrode design, geometries and arrangements have been tested. Yet none of the different plasma sources so far made out different electrode materials and various qualities of dielectric can withstand the reactive air plasma conditions for a long enough time.

2.6.12 Micro-Plasma

Recently, micro-discharge devices that permit the generation of plasmas at length scales of the order 10-100μm havefound great interest. This interest is based on the fact that such micro-discharges can be used in a variety of applications that exploit their small scale, their ability to generate radical species and the ability to generate intense radiation. However, there is very little knowledge about the plasma structure and dynamics in micro-discharges and a clear understanding is precluded by difficulty in diagnosing the plasma at small length scales.

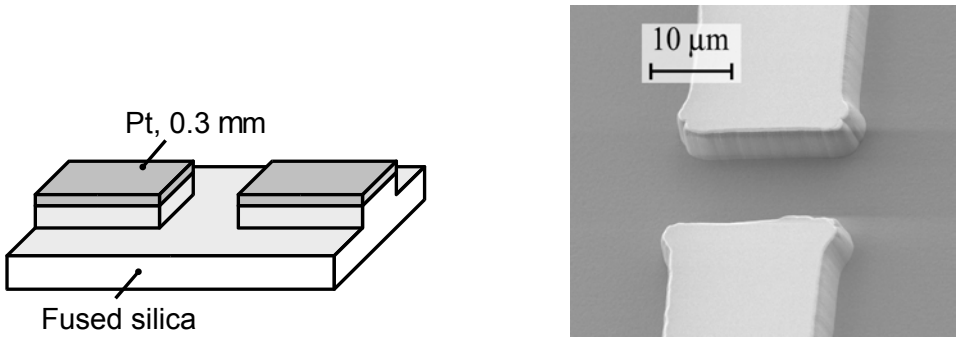

Fig. 2.6.11 *a) Schematic drawing of microelectrode structures; b)SEM image of electrode structures*

For the micro discharge experiments we used thin film Pt electrodes on fused silica substrates as shown in Fig. 2.6.11. The substrate was dry etched to a depth of 5 to 10μm to achieve electrodes that are elevated from the substrate. In this way, the field strength of the edges exposed to the gas is higher, and the leakage current path is lengthened. The electrodes are 20μm wide. The gap between the electrodes was initially 10 to 12μm and increased by a few μm during discharges due to erosion, causing an increase in breakdown voltage. For some of the experiments the cathode was partly insulated with photoresist. Once the discharge has started and a glow has developed, the glow spreads partly across the cathode. The gas pressure

and the applied voltage determine the expansion of the glow. While the glow is confined to a volume between the electrodes and near the gap at high pressure, the glow spreads more and more over the cathode at reduced pressure. In our experiments with DC microdischarges in Ar, N_2 and air, we observed oscillations of the circuit current. With a simple electric circuit, the influence of a number of discharge parameters on an oscillating glow discharge was modelled. However the final goal to find a conclusive explanation for the observed oscillations has not yet beenreached.

In plasma technology, the miniaturisation of plasma will lead not only to the development of novel applications such as material processing, but also to explorations of new scientific fields. The present project was made in collaboration with the Centre for Micro- and Nano-technology (EPFL-CMI), where the microdevices were fabricated.

2.6.13 Helyssen SA, a start-up company at the CRPP

Helyssen SA, a young start up company, has installed a test bed in the laboratories of the industrial plasma group to evaluate the performance of an innovative plasma source based on the Birdcage Antenna. The performance of this plasma source will be benchmarked with standard Helicon plasma sources. The magnets and the necessary equipment for benchmarking and infrastructure has been given to Helyssen SA by the CRPP. This particularly includes experience and equipment for plasma diagnostics in order to quantify the performance of the two RF plasma sources. The collaboration has been established with the help of the Service de Relations Industrielles (SRI) of the EPFL.

2.6.14 New or planned projects

From conventional Plasma Spraying to Reactive Thermal Plasma CVD

The plasma torch is one of the most elementary plasma sources used in industrial applications. The plasma torch brought atmospheric thermal plasma spraying to commercial and economic success. Many daily applications would not be possible without this widespread industrial process. However the applications are limited to relatively porous and thick coatings with respect to vapor deposition techniques, and the spray materials are restricted to substances with a convenient melting point.

A few years ago, operation of the plasma torch under controlled atmosphere and at reduced pressure opened the way towards new technologies and applications, in particular to processes where oxidation has to be controlled. Recently the plasma torch has been operated and investigated at very low pressures. The low pressure plasma spraying (LPPS) operates down to pressures in the mbar range and more and more approaches thin film technology which is mainly dominated by conventional RF plasma sources. This broad operation range has a large potential for a wide variety of industrial applications and will widen the traditional market of plasma spraying and plasma spray equipment.

The plasma torch up till now is the only plasma source which successfully allows the use of solid, liquid and gaseous precursors. This great advantage is due to the high enthalpy content of the plasma jet. The existing plasma torch shall be the basis for a new technology of reactive thermal plasma CVD. In reactive thermal

plasma CVD, the evaporated solid or liquid precursors and the gaseous components contribute to a complex plasma chemistry which leads to film deposition. With reactive thermal plasma CVD, the residual porosity of the plasma spray coatings could be suppressed and dense layers at high deposition rate should be obtained. However, this needs a completely new development of processes and deeper understanding of the underlying plasma physics and chemistry, the main aims of the present project. A particular scientific challenge is the diagnostic of the physico-chemistry of the plasma. The chemistry within the plasma jet shall be diagnosed by means of space-resolved optical emission spectroscopy and mass spectrometry.

Low Energy Plasma Processing for Wear Resistant Coatings

Existing technologies for wear resistant coatings have their limitations. Thermal CVD technology is not flexible enough in the selection of the precursors for a determined temperature range to compete with PVD and the thermal load is limiting the free choice of substrate material. Existing technology for plasma-enhanced CVD for the wear resistant coatings has mainly been developed for diamond and diamond-like deposition. In the case of diamond deposition, plasma helps to dissociate the precursor and to produce atomic hydrogen, which is necessary to form and stabilize this extremely hard but metastable phase of carbon. In the case of diamond-like carbon, the plasma is used to crack the hydrocarbon precursor to form a carbon-hydrogen layer with high hardness, but only stable up to about 200°C. Both processes are dedicated developments for these market segments, and are not sufficiently flexible to form graded interfaces necessary for excellent adhesion as produced by thermal CVD.

The objective of the project is the deposition of wear resistant coatings on metallic and insulating substrates by a new plasma-enhanced CVD process. The new process approach will combine the advantages of existing technology. The process is based on a DC arc discharge. The discharge operates at high currents and at low voltages. All gases fed to the discharge are more or less completely dissociated. The operating pressure is orders of magnitudes lower than in conventional CVD and also lower than in PECVD for diamond. The DC arc discharge is also used for heating, etching and deposition purposes. The whole process sequence consists of a plasma pre-treatment of the substrates, deposition and substrate cool-down. In the pre-treatment, the substrates are usually heated in a reactive plasma environment and sputter cleaning is performed.

Arc Phenomena for a Space Environment and Equipment

Arc phenomena provide one of the oldest topics in plasma physics. In the beginning of plasma physics, quite intensive research on arcing was made and a convenient knowledge base was built up. Later in the development of modern plasma physics, arcing and related phenomena have been less investigated since fusion research started to be a priority. However arcing is a key issue in the application of plasma in industry and also, as in the present case, in space environment and space equipment. Arcing starts to be the limiting factor in several applications of plasmas triggering intense research and development on this topic. In the present proposal to ESA in collaboration with Mecanex SA in Nyon and ONERA in Toulouse, the necessary fundamentals of the arcing shall be established and be applied to the space equipment in order to reduce or suppress arcing in space environment and equipment.

In order to investigate arcing a micro-plasma device will be mounted in a small UHV vacuum chamber where a controlled atmosphere will be created. Various gases at

pressures from ultra high vacuum up to several mbar pressure shall be used for the different arcing experiments.

Such an arrangement has the advantage that the discharge can be ignited and sustained with relatively small voltages. The sustaining voltage of such a discharge should be similar to the one encountered in the slipring on the spacecraft. The electrode material and conditions are more easier controllable than in the classical point and plane situation. In addition this geometrical arrangement is closest to the situation in space equipment. Furthermore, the plasma is accessible for further plasma characterisations, an important point for advancing the understanding of the arcing phenomena in the space environment.

2.6.15 Other collaborations and industrial mandates

Numerous industries consulted us during the last year and this resulted in many small experiments and tests which have been performed on the existing plasma reactors at the CRPP.

At this point it should be added that the collaboration with industry is excellent and a high degree of confidence between the collaborating industry and the plasma processing group exists. This working atmosphere is extremely stimulating for the different members such as PhD students and senior physicists.

3 TECHNICAL ACHIEVEMENTS OF THE CRPP IN 2004

3.1 TCV Operation

During 2004, TCV underwent a major maintenance and upgrade period, with an opening from the 3rd November 2003 to the 12th May 2004. This was, in terms of the number of modified ports, the most important TCV opening to date. This period was followed by two blocks of scientific exploitation ending the 1st October 2004, giving a total of 15 weeks (5 days each) of operation. At this time, the machine was again opened for further internal installations and Gyrotron and ancillary system repair and maintenance. The most important tasks carried out during the major opening are listed below, with some described in more detail later in this section.

- Repair Langmuir probes
- Installation of new Langmuir probe arrays
- Installation of the ECE wave guide
- Installation of the new Compact NPA
- Installation of the new AXUV cameras
- PF coil support modifications for AXUV
- Tile modifications for AXUV
- Tile modifications for EC sniffers
- Displacement of the infra-red camera
- Vertical PHA calibration
- SPRED calibration
- Replacement of the X2 launchers by redesigned simplified launchers
- Mechanical maintenance of the X2 lateral launchers
- Mechanical maintenance of the X3 upper launcher
- Maintenance of the machine cooling system
- Maintenance of the motor generator

3.2 Diagnostics

3.2.1 Introduction

As usual, the maintenance and upgrading of the diagnostic systems on TCV represents a large fraction of the human resources expended. A large quantity of the experimental information derived from TCV is the result of the introduction of new or improved diagnostic capability that was inspired from a previous observation that could not be completed. This ebb and flow of experimental observation and diagnostic development is still, and will likely remain, one of the main activities on TCV.

In the following paragraphs, some of the major changes in TCV's diagnostics are described.

3.2.2 DNB-source improvements

In order to increase the diagnostic neutral beam (DNB) full energy fraction the RF-plasma source of the present DNB system was re-conditioned to reduce cumulated metal coating. The Budker Institute of Nuclear Physics, Novosibirsk, Russia performed this cleaning operation and installed a set of Faraday shields in an RF plasma box. This resulted in an increased equivalent current at full energy beam fraction in TCV plasmas by a factor of 1.5-1.7.
The beam fraction components of the DNB are largely determined by the ions extracted from the source. A contract has been placed with the Budker Institute to replace the RF-plasma source with an "ARC" device, which, together with improved ion optical grids, is expected to increase the beam purity and a reduction of beam divergence resulting in a higher ion neutral density on the line of sight of the DNB spectroscopy.

3.2.3 DNB-Ocean

It was noticed that the conditioning of the DNB RF source has a strong effect on the beam energy fractions. A compact high-resolution "Ocean Optics HR 2000" spectrometer was installed to observe the light emitted from the beam in the plasma. An example spectrum is shown in Fig. 3.2.1 where the separation into different peaks is caused by the Doppler shift of each beam component that travels at a different velocity. This system will soon be installed on the DNB to monitor the actual beam fraction for every TCV discharge.

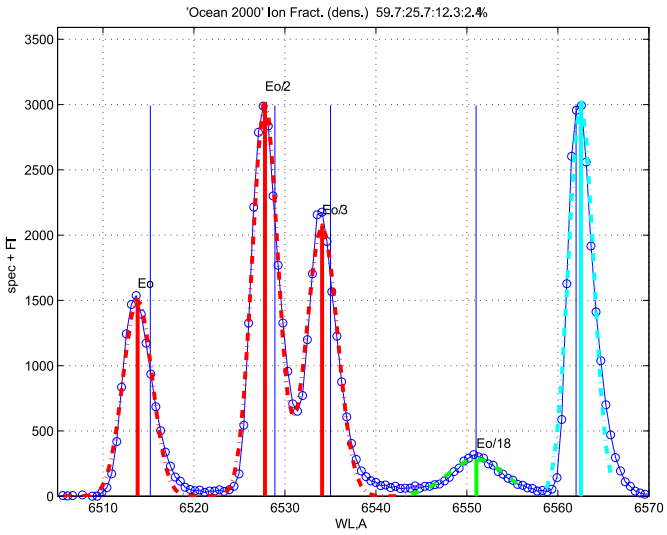

Fig. 3.2.1 *Beam fraction measurement with "Ocean" spectrometer (the H+ fraction which corresponds to the peak on the left is ~60% of the total current)*

3.2.4 Compact NPA

In addition to the existing 5 channel electrostatic Neutral Particle Analyzer, used at the CRPP since 1982, a Compact Neutral Particle Analyzer from the A.F. Ioffe Physical-Technical Institute, St.-Petersburg, Russia has been procured and

installed on TCV, Fig. 3.2.2. This device features electromagnetic mass and energy separation. In normal operation, the spectrometer is configured to disperse hydrogen and deuterium neutral fluxes from the plasma onto separate arrays of channeletron detectors. The CNPA is currently mounted on a horizontal TCV port intersecting the diagnostic neutral beam for preliminary "active" NPA measurements. This system was used to study particle transport by measuring characteristics of accumulation, propagation and relaxation of hydrogen ions in deuterium background with the artificial injection of hydrogen gas into an nominally deuterium plasma.

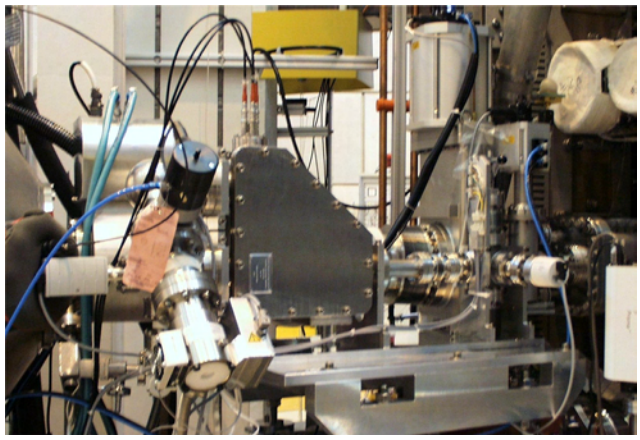

Fig. 3.2.2 *CNPA on TCV: The device is shown without its magnetic shielding that turns out not to be required for all plasma configurations. The relatively small size of the spectrometer makes it possible to envisage changing the port location for particular experiments.*

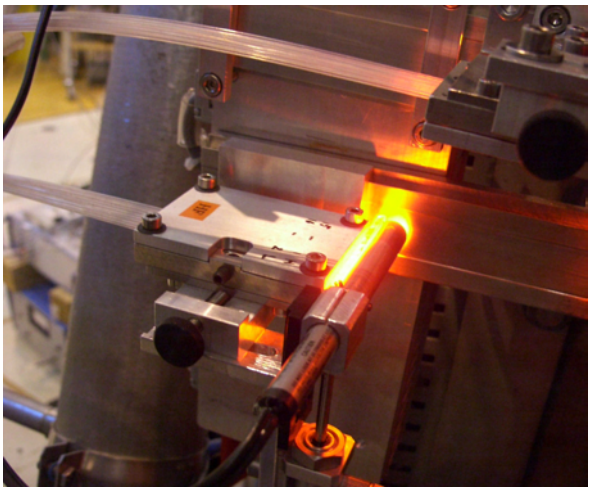

Fig. 3.2.3 *Showing the details of the Ne pen lamp inserted in front of the collection fibres using a pneumatic translator*

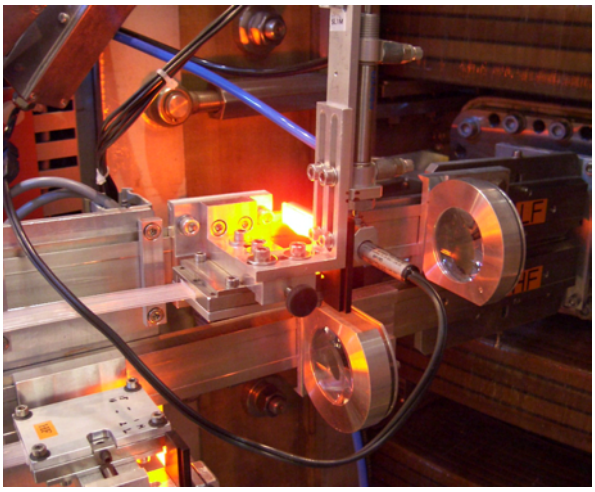

Fig. 3.2.4 *Showing the complete observation cameras with the upper Ne pen lamp operational. Note the fibres take the light to the left of the image to the spectrometers*

3.2.5 CXRS Charge eXchange Recombination Spectroscopy

The CXRS diagnostic can provide profiles of ion temperature, toroidal velocity rotation and density profiles of a given impurity species. The present configuration allows T_i measurements from the CVI (n=8->7) line (5291Å) in plasmas with average densities up to $8x10^{19}m^{-3}$. While T_i profiles are ordinarily worked out discharge by discharge, for v_i and n_i more delicate analyses are needed, and work was performed to establish appropriate calibration and data analysis methods.

A wavelength calibration procedure has been established that permits the measurement of the rotation velocity profiles. Three known spectral lines from a Ne spectral lamp are acquired after each plasma discharge. The lamp illuminates the fibres that transmit the light from the plasma to the spectrometers through a glass diffuser plate to ensure a homogenous distribution, Figs 3.2.3, 3.2.4.

Software was developed which uses the calibration Ne spectral shape to de-convolve the spectrometer instrumental functions simultaneously for all acquired channels. In this way we recover the spectrum, with the same wavelength calibration for all the channels, which can be used to obtain the corrected velocity profile.

An absolute intensity calibration of the system is in progress (taking advantage of the autumn 2004 opening) by means of a calibrated lamp of known emissivity which will be introduced inside the vessel. This may then be used to calibrate an impurity density profile that may be compared to the working gas density profile to look for transport and accumulation effects, Fig. 3.2.5.

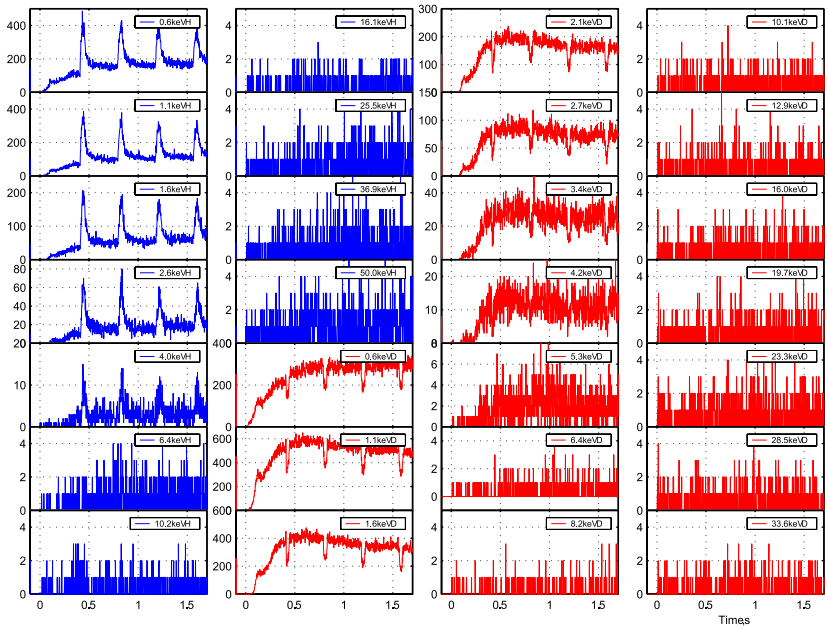

Fig. 3.2.5 *CNPA counts for TCV shot (27115) with H-puff: In red are the counts at increasing energies from the Deuterium working gas whereas in blue are the energy resolved signals from the injected H_2 gas. The isotope replacement (from D to H) has been observed to cumulate, probably due to wall retention during a sequence puffing of H_2 gas into the D plasma*

3.2.6 *Duplex Multiwire Proportional X-ray detector*

A new soft X-ray detector (DMPX) has been installed on TCV and replaces the initial detector prototype (MPX). The new detector consists of two superposed wire chambers separated by 1cm of air. Both detector chambers are similar to the previous MPX wire chamber, with 64 sensitive wires in each, other than, in the lower chamber, the wires are connected in pairs to increase the signal to noise ratio, Figs 3.2.6, 3.2.7. By employing the "differential absorber" method a temperature profile with high spatial and temporal resolution may be obtained (8mm at the equatorial plane and 200kHz, respectively). Additional absorbers may be inserted between the two detector chambers to move the energy range observed by the lower chamber towards higher energies, thus increasing the instrument's electron temperature dynamical range. Instrumental ratio curves have been calculated for different additional absorbers (Al, Be,...) and chamber gas (Ar, Xe, Kr) up to photon energies of 200keV. An additional four absorber holder, remotely controlled, is placed in front of the two chambers to be able to adapt the DMPX to various plasma emissivity conditions, allowing, for example, a steepening of the emissivity gradient to reveal a particular mode activity, or to focus on soft or hard X-ray emission.

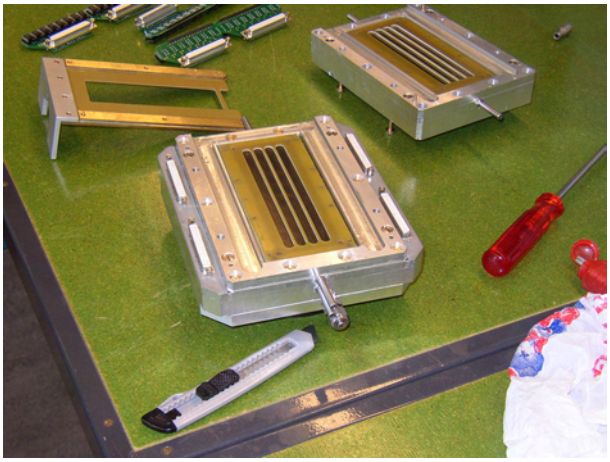

Fig. 3.2.6 *The two multiwire chambers before assembly*

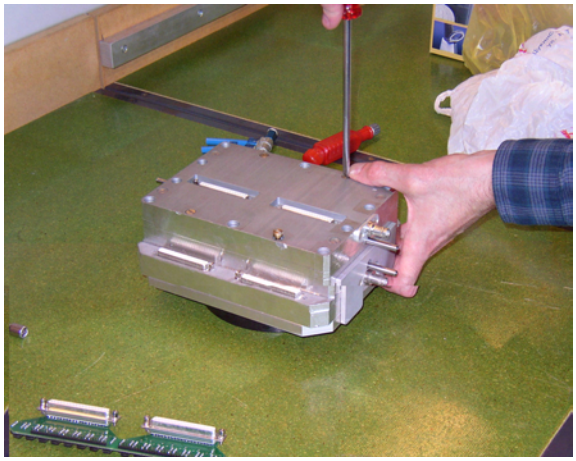

Fig. 3.2.7 *The same chambers now assembled ready for mounting on TCV*

3.2.7 *Tangential X-ray detector array*

A new tangential X-ray diagnostic is being designed in collaboration with RRC-Kurchatov Institute (Moscow, Russian Federation) and is planned for TCV installation by the middle of 2005. The diagnostic will feature three movable, tangentially viewing CdTe detectors to provide fast (10μs) and radially localized (2cm) measurements of 2-200keV bremsstrahlung emission in the direction parallel to the magnetic field, from any chosen location in the plasma. These measurements are expected to provide insight into the physics of magnetic island formation, of runaway electron production and of electron acceleration associated with electron cyclotron current drive.

3.2.8 HIBP

A comprehensive study of the relative merits of a Motional Stark Effect and a Heavy Ion Beam Probe diagnostic was performed for TCV. It was concluded that, with the present port access, an HIBP was more likely to provide useful information on the TCV plasma current profile and other plasma parameters such as turbulence and has been preliminarily chosen for installation on TCV. Before what will become a major project, the exact components may be designed, experiments are underway inside the TCV vessel to determine the feasibility of the various electrostatic beam configurations and their compatibility with TCV operation.

3.2.9 ECE Low Field Side Radiometer

The installation of an ECE observation chord at z=+21cm was completed (in-vessel components, including scalar feed horn were installed during the 2003-2004 opening). Further to this, a third line was connected to the gyrotron launcher #1 allowing oblique ECE measurements, EBE study, poloidal and toroidal angle sweeps during the discharge (ECE tomography and Doppler shift measurements). The system features a motorised remotely controlled RF switch that permits the choice of the ECE setup most appropriate for the next TCV discharge, Figs 3.2.8, 3.2.9.

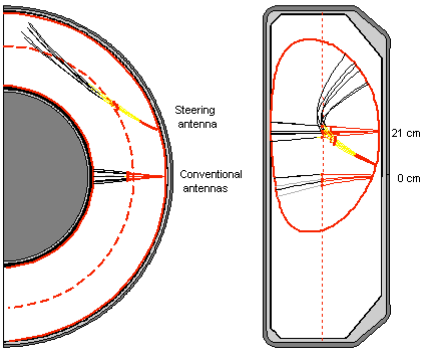

Fig. 3.2.8 *Showing a top and side view of the trajectory of microwave radiation in plasmas with medium density. The observation at z = +21cm provides better access to the plasma core.*

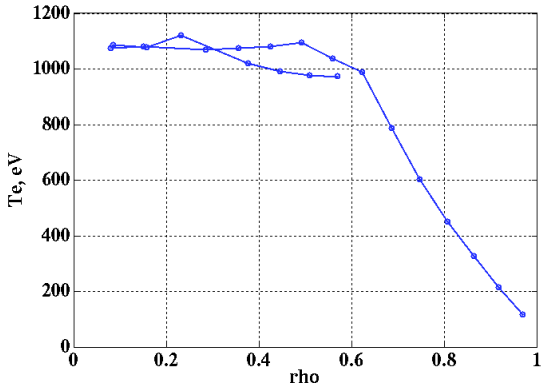

Fig. 3.2.9 *Te profile in plasma rho co-ordinates. The HFS and LFS spectrometers are plotted together and with good agreement at the plasma centre where they overlap.*

3.2.10 Development of the Xtomo and Lyalpha systems

The seven 20 channel X-ray Tomography and Lyman Alpha cameras have completed the chord optimisation phase, and been calibrated absolutely for diode response and light of sight before installation on TCV. They will be equipped with the new DTAQ-196 acquisition modules providing high time and spatial resolution energy emission and Lyman alpha tomography systems for TCV. It is hoped, at a

later date, that the algorithms developed to invert the Xtomo data may be coded into a real-time controller to enhance the DSP based plasma control described later.

3.2.11 In vessel sample-holder

To monitor the effect of plasma on materials and to monitor the parameters of machine conditioning during Boronisation a sample is placed at near the same level as the machine wall tiles and exposed to the plasma. In recent years, the legacy system installed on TCV has become too cumbersome for regular use. A flange equipped with a gate valve and a long vertical bellows is being installed under TCV to allow the insertion and withdrawal of plasma facing samples without the admission of air into TCV. The exposed samples will, as before, be analysed with the help of our colleagues from Basel University who are also interested in the behaviour of materials exposed to high temperature plasmas.

3.2.12 Fast reciprocating Langmuir probe and new LFS Langmuir probes

Edge physics experiments on TCV have made extensive use in recent years of a mid-plane mounted, fast reciprocating Langmuir probe equipped with 5 graphite single probe tips in a boron nitride matrix. The probe head was modified in 2003 to allow measurements of the parallel flow in the scrape-off layer. This first version was shaped to match the poloidal contour of the standard TCV single-null lower diverted plasma in which the majority of edge physics experiments are performed. A third design (Fig. 3.2.10) follows the same principle for Mach flow measurements – a raised bar separating pins on either side. The three central pins are used in the usual way to obtain temperature and density profiles and measurements of turbulence in density and electric potential. This new head has a flat contour and has been successfully employed in 2004 to study the extent to which outboard ballooning transport influences SOL flow.

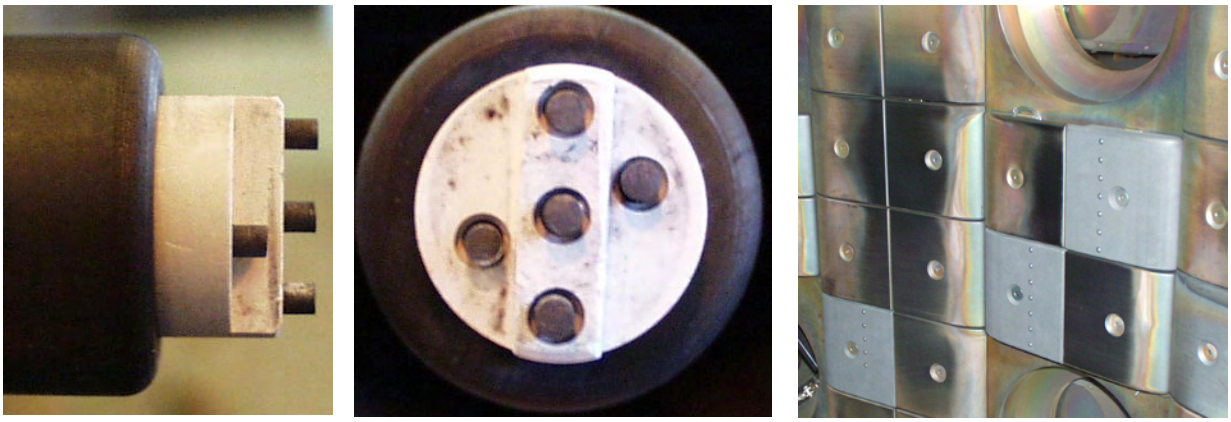

Fig. 3.2.10 *Left and centre: the new fast reciprocating Mach probe head with flat profile for study of the effect of ballooning transport on SOL flow. Right: the array of low field side fixed Langmuir probes installed during the 2004 shutdown. The three new tiles with embedded probes can be easily distinguished amongst the older components covered with re-deposited layers.*

In an attempt to investigate the perpendicular transport of ELM driven particle fluxes, a small array of tile-mounted, fixed Langmuir probes (Fig. 3.2.10) has been installed on the outboard side, vertically disposed approximately either side of the magnetic axis of the most common SNL equilibria used for ELM studies. These probes represent one of the first attempts to make such measurements in a Tokamak and have functioned very successfully in first experiments in 2004. They are of similar design to existing probes in TCV – domed, graphite single probe tips with diameter 4 mm and protruding to a maximum of 1 mm above the tile surface.

3.2.13 Vertical PHA diagnostic

The electrically cooled X-ray detector has been equipped with a pair of real-time servo filter wheels for installation on TCV, Fig. 3.2.11. It is hope that the acquisition of PHA spectral information from this diagnostic will be interpreted in real-time by a DSP circuit that will also control the filter wheel position to account for the large intensity dynamic range of X-ray plasma emission from TCV.

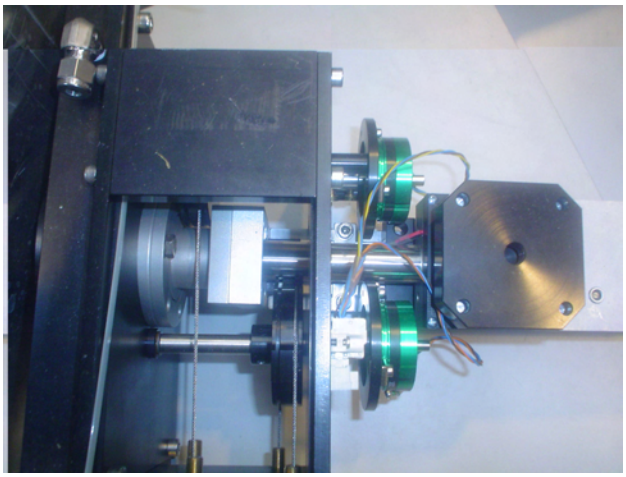

Fig. 3.2.11 *Showing the PHA diode with the two filter wheels. The green potentiometers on the ends of the drive shafts are used to servo the filter position to a 0-10V signal provided by the control system,*

3.3 Control and Acquisition

3.3.1 Data acquisition and analysis

For the period of this report, there have been ~1600 TCV shots, each generating around 250MB of data stored to disk.

All the TCV data, acquired and calculated, are kept on-line on hard disks, for immediate access, and in the case of the analysed results file, updating. At the end of 2004 these files occupy over 650GB of disk space. The backup system has been upgraded to account for this increase.

This year has seen a new multi-channel acquisition module from DTACQ in which each board features 96 channels and the ability to sample at a rates of up to 400 Msamples/s with 14-16 bit data resolution. The boards are no longer directly controlled by a host PC in their housing crate, but are controlled and read-out through their onboard Ethernet network interfaces. At present two boards have been delivered and integrated into experiments at the CRPP, and several more are foreseen. They are particularly useful for multi-chord diagnostics such as the new AXUV and Lyman-Alpha cameras mentioned below. Since each board is able to

generate over 80 MB of data per discharge, it has become necessary to be more careful in deciding which data are significant and have to be stored: filtered, windowed (limited to "interesting" episodes), selected by relevance, etc. In an attempt to avoid “losing” important data, we are storing the complete data set for each discharge on temporary staging disks where, should the need arise, it is possible to decide, up to several weeks after the data have been acquired, to store the data stored permanently.

The computational resources have been strengthened by the replacement of the 4-processor IBM computer by an 8-processor unit, also IBM, with roughly ten times the computing power. Virtually all the TCV data analysis is carried on this machine. Although the purchase cost of such a system is higher than the purchase of a park of comparatively cheaper hardware, the maintenance time and the hosting of all users in the same environment is still considered to be a big advantage of this approach for TCV and the larger machine can tackle the jobs with no extra multi-thread coding required by the users.

3.3.2 Plasma control system

NTPC - New TCV Plant Control

The control system for TCV diagnostics has increasingly, over the years, suffered from software limitations. Moreover, the sequential nature of the system was not adapted to the growing number of controlled systems. Together with this, several minor problems also arose from the integration of the inter-discharge glow system and the integration of the complex ECH control system. It was thus decided to redesign and implement a new TCV plant control environment.

The new system, called the New TCV Plant Control (NTPC), consists in a series of software sequences, running in parallel, that separately control the state of every part of the TCV plant, e.g. the motor generator, the data acquisition, the FIR and Thomson diagnostics. Although all the sequences are independent, they have an identical control structure and evolve in the same state machine. The integration of a new sequence to control another device will only require the definition of the requested actions to be performed for each of the given states and a cloned software sequence.

To control these sequences, two levels of master sequences summarise the state of one section of the plant, (all diagnostics for instance), and the overall master the whole TCV plant. The sequences corresponding to these masters have exactly the same structure and evolve in the same state machine as the individual one sequences described above. With the introduction of a unique control sequence it is expected that software maintenance will be greatly facilitated and that the structure will scale naturally for the control of additional systems.

A fraction of the whole TCV plant has been successfully controlled with the NTPC since July 2004. The remaining systems will be incorporated piecemeal in the coming year until the old system will effectively no longer be controlling any of the plant and may thus be withdrawn.

Plasma control algorithms

The TCV plasma control system employs pre-programmed waveforms as feedforward inputs for all the coil currents and for the gas feed valve, calculated by

a free boundary equilibrium code on the basis of the requested plasma parameters. In addition, linear feedback algorithms are employed to minimise the deviations from their references for a number of crucial observers, such as the plasma current, positions and density. Since the shaping flexibility of TCV is one of its unique features and in view of the expanded calculation possibilities that will soon be possible with the coming DSP-based control system core, we have launched a programme to study and compare shape control algorithms. In the initial phase, the elongation feedback system has been put into routine use and a preliminary comparison of different elongation observers has been performed where the previous algorithm has been modified to better decouple the shape from the position feedback loop.

This feedback system has already been a strong asset in experiments with intense and variable off-axis electron cyclotron heating, designed for studying the dependence of electron energy transport on shape. For a constant quadrupole field, the strong current profile changes associated with ECH lead to pronounced elongation variations that often interfere with the purpose of the experiment. The enhanced feedback system keeps the elongation constant typically to within 5% even when other shape parameters, such as triangularity, are varied. This work is ongoing and will be extended to more complex shape parameterisations.

EC system operation

Continual improvements are made to the overall EC operating system. Testing of an automated conditioning routine is planned for the end of the year. The goal is to allow one operator to easily control all 9 gyrotrons and 7 launchers. At present 2 operators are required.

Hardware

The CRPP has based a large fraction of the dedicated electronics for TCV and other experiments on the BitBus field bus. This bus is driven from the TCV control computers to read plant parameters such as temperature, pressures, alarms etc. and to upload control and timing information around the TCV plant for plasma discharge operation. With the increasing number of diagnostics and the age of these components, the electronics group are looking at ways of modernising the field bus to not only maintain the existing systems but to also allow our designed hardware to be used outside the TCV environment. A new TCV controller is being developed using Ethernet for the data transport but emulating the legacy BitBus controller so that, with the appropriate software layer, newer systems can use the internet to control devices without having to rewrite the already developed control software.

In the same spirit, we are integrating an Ethernet based RS232 controller featuring up to 16 RS232 serial ports on the same module together with the control software to emulate the system already in use on TCV. The result will not only be better performance and the ability to locate these devices anywhere where the standard computer network is available, but also the introduction of intelligent controllers that read and interpret information from the controlled hardware before presenting it to the TCV plant control. This modernisation into a “distributed” control system is much more upwardly scalable that the current “centralised” system and feature a potentially greatly improved performance.

The same approach is being continued for commercial products that require some kind of control PC. This approach, which is becoming very popular with the advent of cheap PC hardware, means that although the PC controls the hardware, as

defined by the manufacturer, that it is also able to provide control and acquired information to the TCV control and acquisition system again using an Ethernet connection. In this way, a lot of the subsystems on TCV are now only linked by Ethernet connections that are available virtually everywhere using cheap and very reliable commercial hardware.

3.4 Heating Systems

3.4.1 X2 heating system

Gyrotrons

Gyrotrons 3 and 5 were repaired at the factory and will pass acceptance tests at CRPP scheduled during the autumn opening. Five weeks of testing and recalibration/realignment are expected.

Launchers

All the X2 launchers of cluster A were removed during the 2003/4 winter shutdown and upgraded to simplified launchers with fully ceramic support frames. In this arrangement, there is no longer any PEEK ceramic in these launchers that was found to have been partially melted during injection of high-power X3 ECH in high-density plasmas during 2003. Two new simplified launcher mirror assemblies were also installed at this time (Fig. 3.4.1 shows the open launcher in front of a new simplified launcher).

Two launchers have been equipped, at different times, with a window allowing transmission of low power radiation from the plasma. The ECE radiometer has been modified to measure of this radiation permitting the first measurements of electron-Bernstein emission (EBE) from TCV. This provides an ideal system for preparation of the electron-Bernstein Heating experiments, as the receiver beam aiming optics is identical to that of the launchers.

Fig. 3.4.1 *An old X2 launcher in front of the new modular launcher with features fewer components..*

3.4.2 X3 heating system

Gyrotrons

Two X3 gyrotrons were regularly available during the 2003 operational period. At the end of this period, one of the X3 magnets began to consume increasing quantities of liquid He. Extensive testing has been carried out in collaboration with the manufacturer to determine the origin of the problem. At present, the third gyrotron is also operational with its cryostat being continuously pumped (the other systems are initially pumped and then sealed).

Real time feedback control on X3 launcher

Previous experiments using X3 heating have shown a strong dependence of the X3 absorption on the poloidal injection angle. The real time feedback control system on the X3 launcher, whose development started in 2003, has been successfully used on L-mode plasmas. The main element of the developed feedback system consists in the synchronous demodulation of a harmonic perturbation of the plasma response (line-integrated emissivity of a central soft-X ray chord), where the harmonic perturbation is generated by sinusoidally varying the launcher injection angle. A schematic of the layout of the feedback system is shown in Fig. 3.4.2b. A study of the frequency response of the system composed by the mirror mechanical system and the mirror motorisation obtained the optimum frequency (f = 13Hz) for the sinusoidal perturbation.

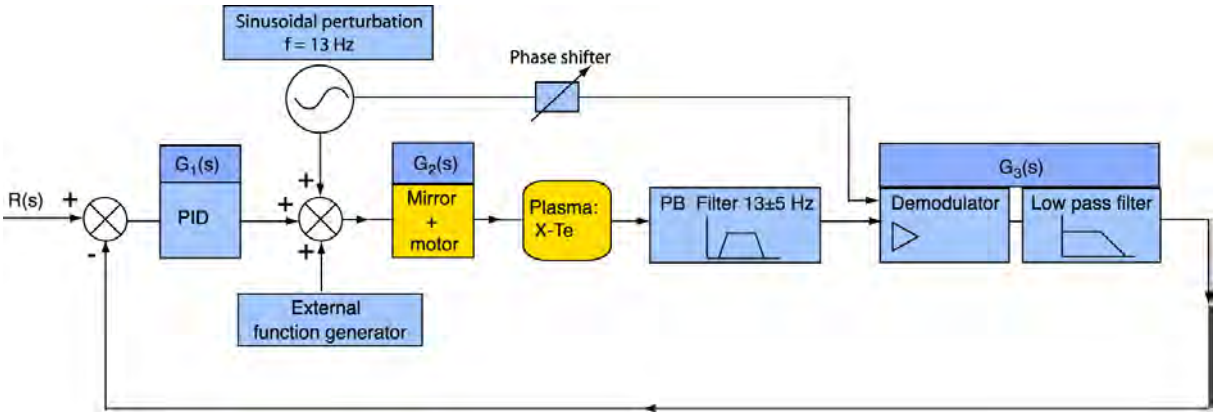

Fig. 3.4.2 *Schematic of the complete closed-loop feedback system. The harmonic perturbation at 13Hz is used both for applying the sinusoidal perturbation on the launcher mirror and also as an input of the synchronous demodulator which is placed after a pass-band filter centred at 13Hz±5Hz. At the output of the demodulator the AC component is filtered out by a low-pass filter with the resulting signal being proportional to the derivative of the plasma response function, $dT_e/d\theta$ where T_e is the electron temperature and θ is the mirror poloidal angle. The dynamic response of the closed-loop system can be adjusted by the parameters of the PID regulator.*

In a first series of experiments only the proportional term of the PID controller was used. After an experimental optimisation of the different parameters in the system, a stable real-time control of the optimum injection angle of the X3 launcher was obtained for a wide variety of L-mode plasma configurations.

The closed loop characteristics of the real-time feedback are shown in Figure 3.3b. In this discharge the mirror poloidal angle was pre-programmed to perform a linear sweep across the angular region of optimum heating (green line). The feedback control of the mirror (red line) was able to attain the optimum angle more quickly than the pre-programmed sweep and once the optimum angle was reached (t = 1.1s), it reacted so as to maintain this optimum angle despite of the external ramp reference that was programmed to sweep away from it.

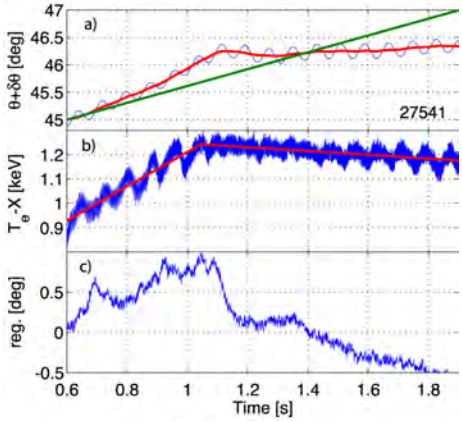

Fig. 3.4.3 *Real-time control of the mirror in a L-mode plasma phase. In this discharge the mirror angle was programmed with a linear sweep across the optimum injection angle which occurs at t =1.1s. The error signal that is fed to the proportional controller is shown on trace c. On trace b), the time-trace of the central plasma temperature demonstrates that once the optimum launcher angle is obtained, the feedback controls the launcher so as to maintain optimum absorption.*

In this way, it has been possible to obtain high power EC-heating in ELMing H-mode discharges for the first time, using 1.35MW (all three gyrotrons). Further development of this real time control system is required for H-mode discharges where the perturbations associated with the presence of ELMs, together with rapid density variations, strongly perturbed the feedback loop. A modelling of the complete system will allow us to further optimise the dynamic response of the real-time control to further improve the feedback system's response. Once the Advanced Plasma Control System of TCV will be operational it is also planned to transform this analogue controller to a digital one that could, for instance, compensate changing plasma parameters by changing the scanning amplitude.

3.5 Upgrades to the TORPEX device

The construction the main elements of TORPEX was completed in 2003. During 2004, several upgrades were implemented. Minor upgrades include completion of the security infrastructure for the machine area, and improvement to the existing diagnostic systems and the relevant data analysis packages. Major upgrades to the power supply installation, the vacuum vessel, and a new diagnostic system are described in what follows.

Power Supply

A power supply to drive the TORPEX ohmic circuit and the poloidal field coils in the cusp field configuration has been installed and is ready for testing at the end of 2004. The ohmic drive will allow us to investigate the change in the character of the electrostatic turbulence in the presence of closed flux lines, while the cusp field configuration can be used in the future to investigate instabilities and turbulence around a magnetic X-point and their role in magnetic reconnection phenomena.

Movable sectors

Two movable sectors of the vacuum vessel have been constructed, one of which has been installed to accommodate the new HEXTIP diagnostic, described below. An additional mechanical support and assembly has been designed and fabricated `in house', which allows a quick and easy exchange of certain sectors of the vacuum chamber and associated toroidal field coils and cooling system (Fig. 3.5.1). Different movable sectors are available, each one equipped with a particular set of diagnostic to be used for specific experimental campaigns. Testing and fitting diagnostic components can then be carried out in parallel with plasma operations, minimising machine down time.

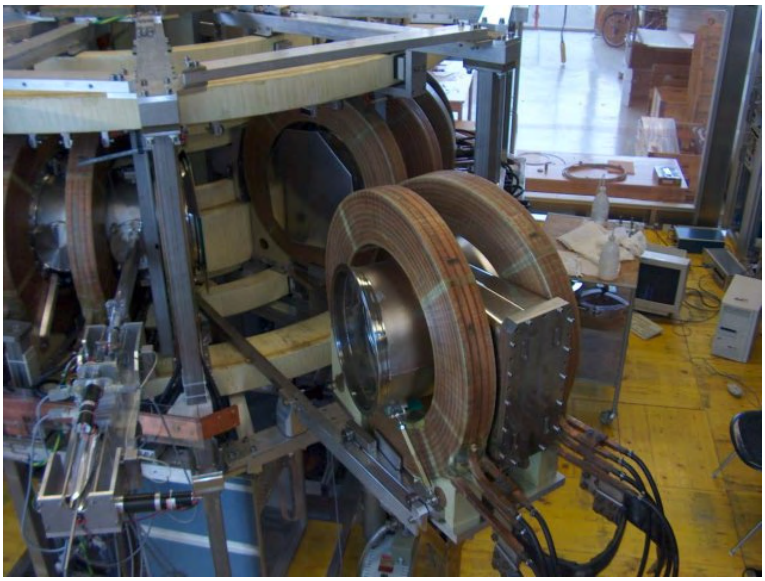

Fig. 3.5.1 *Picture showing a new "movable" sector being incorporated into the rest of the TORPEX machine. The structure for sliding it into place is visible as well as the wide access port*

92 tip Langmuir probe array, HEXTIP

Turbulent structures are observed to form and propagate in the poloidal cross-section (see Section 2.3.5). To determine the physical mechanism that drives these structures, information can be drawn from the relationship between the phase of the density fluctuations and the plasma potential, as well as the relationship between parameters such as the coherence length `perpendicular' and `parallel' to the magnetic field. Existing data indicates that the perpendicular coherence length can be between 2 and 10cm and in the parallel direction it is approximately 10cm.

In order to characterise the structures, i.e. wavelength, coherence lengths, frequency, speed and statistical properties, a diagnostic with a sufficient spatial and temporal resolution is necessary. For this reason an array of 92 Langmuir probes covering one poloidal section has been constructed and installed on TORPEX. Based on the values above, an hexagonal array of 92 Langmuir probes has been chosen, maximising the number of closest neighbours for the cross-section. The array covers the entire plasma cross-section (diameter = 40cm) at one toroidal location with a spatial resolution of 3.5cm. The additional data acquisition unit (96 channels @ 250kHz) yields a temporal resolution of 4μs. Final testing is about to be completed and data collection will begin soon.

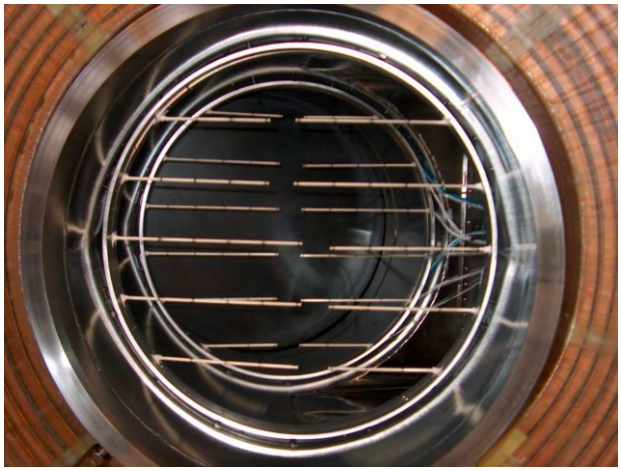

Fig. 3.5.2 *Lay out of the HEXTIP array*

Ultra Fast Langmuir probe (FMP)

To complement the above new array, another `Ultra fast' Langmuir probe system is in fabrication. The probe consists of four tips in close proximity to each other and will measure plasma density and potential fluctuations. Unique feature of this probe is that it is able to move radially and vertically (on a shot to shot basis) mapping out one poloidal section at an acquisition frequency of 10MHz, toroidally separated from the probe array above. The probe will be mounted on a mechanical system capable of being displaced along both radial and vertical directions, to cover the whole cross-section.

3.6 Superconductivity

3.6.1 The SULTAN facility

In 2004 the SULTAN facility was operated successfully during the whole year except between 21.11.03 and 19.03.04, when the activity was interrupted due to the burnout of the current lead of the 9 T coil. The burnout was caused by extended operation at maximum current with insufficient cooling of the leads, due to insufficient pressure in the liquid helium cryostat of SULTAN. In the slow, thermal runaway due to the insufficient cooling, the local temperature most likely reached 700-800°C, vaporizing the epoxy insulation, before sufficient heat was conducted to the (protected) superconducting busbar which eventually triggered the quench and the fast discharge of the coils. despite the insulation damage, no short circuit occurred during the coil dump. The state of the current lead and its environment in the SULTAN tank after the burnout is shown in the few pictures below.

Fig. 3.6.1 *The damaged (burn-out) current lead inside the SULTAN vacuum tank. Observe the massive deposition on the 80K shield by condensation of the gases produced by the heat developed during the burn-out.*

Fig. 3.6.2 *The damaged current lead. The burned region is situated in the upper one third of the current lead. The Silver coating diffused into the thin Coper wires at about 700-800°C.*

The manufacturing of a new current lead, based on the CRPP design was started. The most challenging and time consuming activity was the preparation of the current carrying elements of the current lead, the thin, wiggled copper wire. The residual resistance ratio (RRR) of copper wires sold on the market is higher (RRR=120) than the optimum required for a current lead (RRR=70). Therefore a machine tool was used to prepare the copper wire with reduced RRR. Before entering in the wiggler part, the copper wire undergoes a number of bendings, which by mechanical effect decreases the RRR. An RRR factor of 90 was reached after four bendings.

A novelty for this new generation of SULTAN current leads was the presence of voltage taps to measure the voltage drop along the non-superconducting part. This will permit a more precise monitoring of the current lead and contribute

substantially to an increased safety in operation. The plan is to extend this monitoring to all other SULTAN current leads and include it in the SULTAN control system. The manufacturing of the current lead is illustrated in Fig. 3.6.3. The the new current lead was installed in SULTAN on 11.02.04. The cool-down of the SULTAN facility was restarted on 25.02.04.

A particularly work intensive activity was the cleaning of all internal surfaces of the SULTAN facility from the depositions created during the burnout accident.

Fig. 3.6.3 *The heat exchanger and current carrying part of the new SULTAN current lead during insertion in the outer steel jacket. The bundle of 70'000 very fine (0.1mm dia) wiggled silver coated copper wires, is pulled-up in the steel jacket.*

3.6.2 The JORDI Facility for Resistance Distribution Test on Joints

Due to the late availability of the sample and the very right manpower schedule for 2004, the completion of JORDI (Fig. 3.6.4) project was delayed. The cryostat is now completely prepared for insertion into the vacuum shroud and starting the cryogenic commissioning. For the cryogenic commissioning two steps are foreseen. First the cool-down test and then the steady state operation including helium liquefaction with simultaneous return of cold gas to the KAIII refrigerator and warm gas through the current leads in both current and current-less conditions.

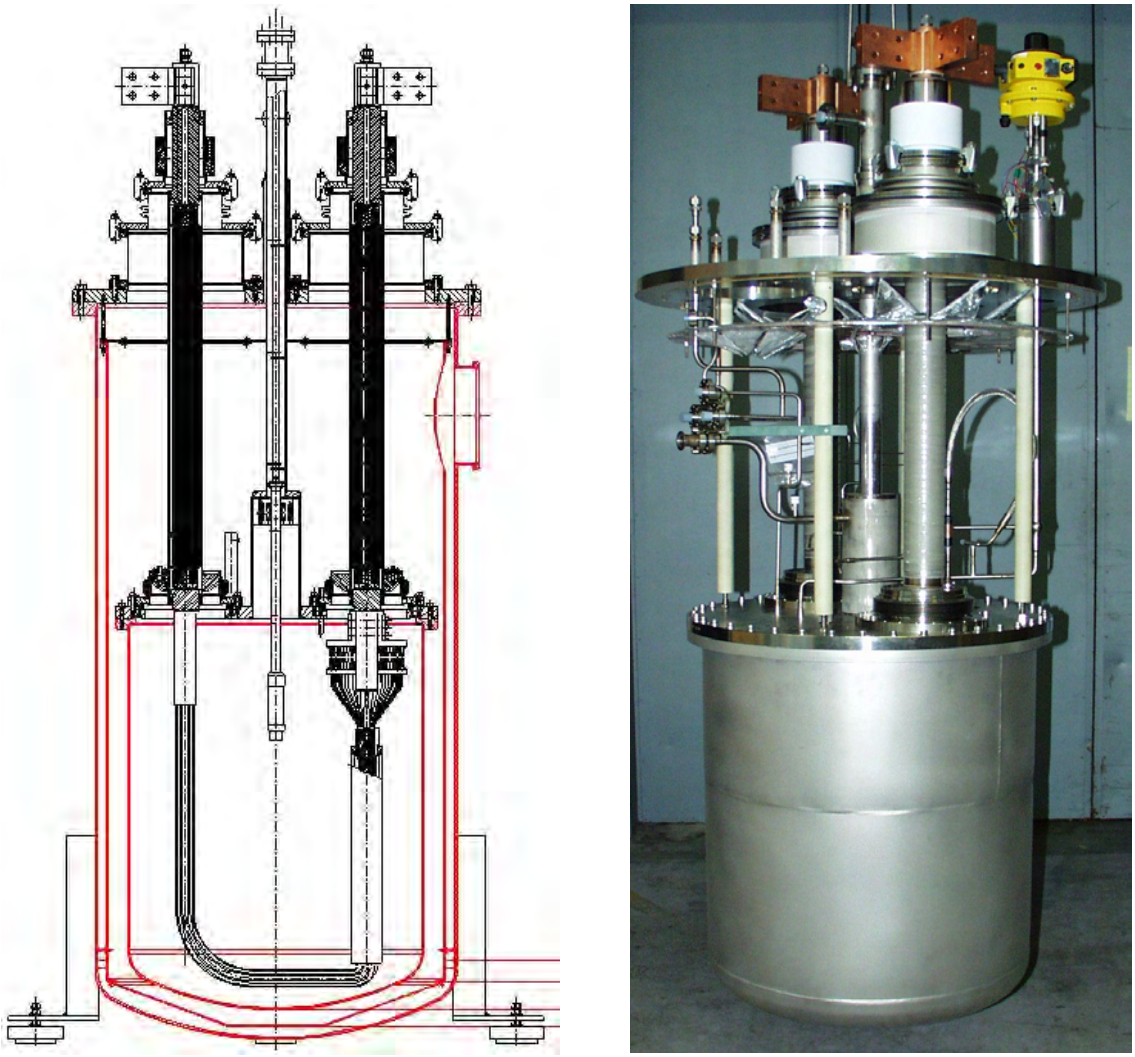

Fig. 3.6.4 *Schematic and view of the JORDI facility cryostat. The joint sample is mounted inside the liquid helium vessel and connected to two conventional, forced cooled current leads.*

The measuring system is composed of a sensitive digital nano-voltmeter and the main current source is a 10kA/2V power supply. The 96 shunts divide the main current in 96 individual currents of a maximum of 104A each. The voltage drop along the shunts is a measure of the real current flowing in the element. For each element (super-strand), the voltage drop between the upper part of the element and the equipotential (superconducting) surface of the joint is also measured. These voltages divided by the measured individual current give the contact resistance in the joint. The 2x96 voltage signals from the sample are multiplexed and delivered to the nano-voltmeter. The whole system is controlled by a LabView™ 7.0 application. The control and monitoring system for the cryogenics is also included in the upgraded data acquisition system.

As a preliminary signal to noise ratio analysis has shown, due to the low resistance of the current injection circuit (copper bus-bars, current leads and sample), the existing power supply at the second floor of the SULTAN Hall (12kA, 32V) will operate at a very high noise level due to the firing of the thyristors operating at practically zero voltage. Another power supply capable of delivering 10kA at a maximum of 2V was therefore installed in place of the 32V power supply and successfully commissioned. First test results are expected by the end of 2004.

3.7 ITER 170GHz gyrotron and test facility

For the electron cyclotron wave system of ITER the European Party plans to deliver 2MW CW sources at a frequency of 170GHz. Compared with the reference design of ITER based on 1MW sources, a high power unit source (2MW) allows a lower system cost. In 2003 the physics design of the main items was completed and a call for tender for the construction of the tube was carried out. CRPP members participated regularly in meetings with EFDA and other participating Associations concerning all elements of the project.

3.7.1 Gyrotron components

A Technical Evaluation Group (TEG), in which the CRPP was represented, evaluated the tenders and reported their recommendation to the EFDA leader. Subsequently, contract negotiations were carried out and the technical specifications of the contract were written. The contract for the manufacture of the gyrotron was signed in May 2004 by both the European Commission and the industrial partner, Thalès Electron Tubes Devices. The gyrotron delivery at the CRPP test-stand is foreseen by the end of November 2005. This industrial project will be supported by a group of Associations (CRPP, FZK (Germany) and TEKES (Finland)) with the CRPP being the leading Association. The CRPP will provide the scientific assistance to industry during the final design and construction phase of the tube.

The ITER gyrotron modelling constitutes the first use of the e-beam tracing code DAPHNE for the design of a coaxial gyrotron. Extensive simulations have been performed to study how the beam parameters (mainly the pitch-ratio α and its spread $\delta\alpha$) depend on discretisation of the quantities used in the code. The results confirm previous cross-code tests with conventional cavity gyrotrons showing that care must used in the discretisation. These results will be used as a basis for creating a more user-friendly, automated interface for gyrotron design.

Magnet

In relation to the issued call for tender for the gyrotron superconducting magnet (Tender EFDA 03/961), two offers were evaluated by a second TEG, in which the CRPP was represented. A report with recommendations was sent to the EFDA Leader in December 2003. After having received a formal authorisation, negotiations for placing a contract with the selected company was started in March 2004. A final technical specification and related contractual documents were agreed by both parties by July 2004. The contract was signed by the supplier in September 2004 and the formal contract signature is expected before the end of 2004.

RFCU (RF conditioning unit)

At the end of 2003 the internal launcher of the gyrotron was redesigned to minimize the stray diffracted radiation inside the gyrotron. This resulted in a change of the output beam pattern compared with that used for the design of the RFCU. The effects of this change were studied. Starting with the calculated rf power distribution at the gyrotron window (phase and amplitude provided by FZK) a study of the diffraction losses inside the RFCU and the relative HE11 mode purity inside

the corrugated waveguide has been carried out. The study shows that with the present RFCU mirror layout, using only quadratic phase correcting mirrors, a significant level of stray rf power is to be expected inside the RFCU. The level of HE11 mode purity should be further improved. Further analysis is presently underway.

3.7.2 C-GT170 Test Facility

A test facility for the CW 2MW 170GHz ITER gyrotron is under construction at the CRPP to incorporate elements provided by industrial suppliers and other Associations. The CRPP is the lead association within EFDA for the project.

Power supplies

The main component after the gyrotron and the magnet is the high power installation. At the beginning of the year, the tenders from several European companies for the three main objects composing the power structure (Main High Voltage PS, Body PS, High Voltage Solid State Switch) were received. A TEG was formed, in which the CRPP was represented, and the offers were evaluated. Several companies were asked both to complete their offers and to provide more details concerning some particular points. In June the final choice, proposed by the TEG, was approved by the European committees (AFAC, CCE-FU). The contract will be submitted to the Commission for signature in Novemeber.

Infrastrucutre

Working with the EPFL's architect, an overhead crane has been installed to insert/extract the gyrotron from the cryomagnet. Holes have been drilled in the floor for cooling pipes to pass from the pump room (in the basement) to the gyrotron. Installation of the ground plane has been completed. The false floor and security barrier around the gyrotron are being ordered and will be installed by the end of 2004.

Cooling water system

The Cooling Water System (CWS) for the GT 170GHz test stand has been outlined in terms of functional elements, space requirements and fluid routing and the major hardware and software components have been identified. The technical cooling specifications for the gyrotron components and the microwave load are available. Several options for the heat removal from the primary cooling circuit to the environment (lake or atmosphere) are under consideration by the CRPP and the plant department of the EPFL, such as an intermediary lake water storage facility or water to air heat exchanging equipment. Cost of installation and maintenance are the important factors for a desicion to be taken in autumn 2004. The design of support structures for cooling components located at level 0 of the building has been initiated. As soon as results from transient and steady state thermal response analysis are available, hardware such as pumps, tubing, valves and heat exchangers will be ordered to comply with the cooling needs of the first short pulse (1s) high power test programme planned for spring 2006.

Cryogenics

The yearly liquid helium consumption of the EPFL is as high as 80'000 l with the CRPP consumption being of the order of 35'000 litres. The EPFL management decided to finance a new helium liquefaction and recovery system with a capacity compatible with total EPFL consumption. The main elements of this system (liquefier and high-pressure recovery system) will be sited at the CRPP premises. With a strong participation by CRPP, a Call for Tender for this system has been written and was issued at the end of September 2004. The evaluation of the offers will be made in November 2004 and the placement of the contract by the EPFL is expected before the end of 2004.

Transmission line

An international Call for Tender for the evacuated waveguide elements for the transmission line between the gyrotron and the CW load was issued in spring 2004. The Call for Tender also included elements to be used by the Dutch Association FOM for testing the prototype ITER remote steering launcher. After both the CRPP TEG and FOM evaluated the responses, General Atomics was awarded the contract in July 2004. Delivery of all elements is scheduled for the end of 2004. The components delivered initially to FOM will be re-used by the CRPP for eventual long pulse testing of the launcher at the Test Facility in 2007.

Data acquisition and control

A call for tender for the data acquisition system was issued in Spring 2004 and several responses were received. A TEG was formed within the CRPP. Following clarification of some points with several tenderers and comparison of the offers, a contract was placed at the end of July 2004 for delivery in November 2004. The control state machine structure is being defined with a working draft planned for the end of this year, allowing at least 8 months for construction of the detailed elements.

4 INTERNATIONAL AND NATIONAL COLLABORATIONS

4.1 *Exploitation of the JET facilities*

4.1.1 Collisionality and shear dependences of particle pinches in JET

Results from an extensive database analysis of JET density profiles show that the broadness of the density profile, $<n_e>/n_{e0}$ (inverse peaking factor) in JET H-modes decreases from near *0.8* at high collisionality to around *0.6* as the plasma collisionality decreases towards the values expected for ITER (Fig. 4.1.1). The density peaking behaviour of L modes is remarkably different from that of H modes, scaling with overall plasma shear as $<n_e>/n_{e0} \sim 0.6/li$, where *li* is the internal inductance, independently of collisionality (Fig. 4.1.2). H-mode density profiles show no shear dependence, except at the lowest collisionalities. These differences in behaviour are theoretically challenging and may help elucidate the underlying anomalous convective mechanisms. Evidence for L_{Te}, L_{Ti}, ρ^* or β dependences has been obtained neither in L nor in H-modes. Carbon impurity density profiles from Charge Exchange Spectroscopy are always less peaked than electron density profiles and usually flat in H modes. The investigation on impurity behaviour is being extended to heavy impurities in collaboration with *Consorzio RFX* and *UKAEA*. The peaking of the electron density profiles, together with the flatness of the impurity density profiles, are favourable for fusion performance, if they can be extrapolated to ignited conditions. In particular, peaked density profiles may alleviate a recently expressed concern that the density limit may be insufficient for obtaining the expected fusion performance in ITER.

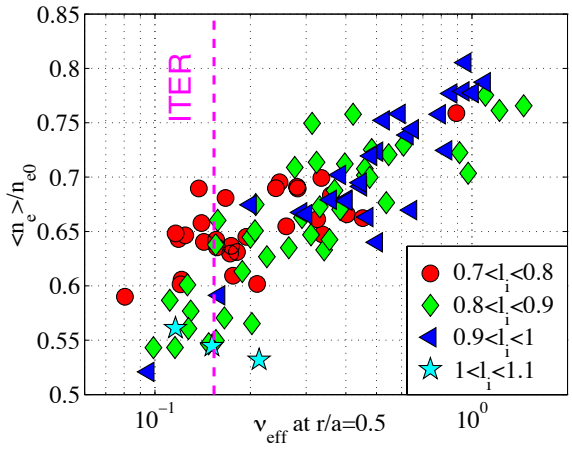

Fig. 4.1.1 *Dependence of density profile peaking on effective collisionality parameter ν_{eff} at r/a in ELMy H-modes.*

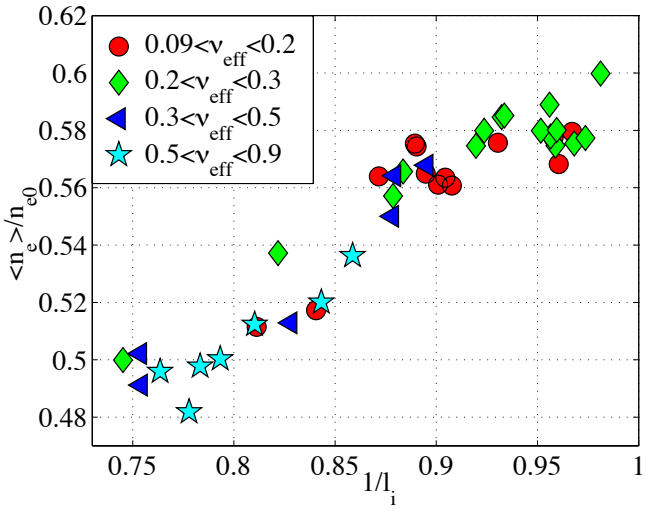

Fig. 4.1.2 *Dependence of density profile peaking on internal inductance in Lower Hybrid Current Driven L-mode plasmas.*

4.1.2 Collaboration with the JET-EFDA Task Force E (Exhaust)

Strong support of the Task Force Exhaust (TF-E) facilities has continued through 2004, with the CRPP representative in place as Deputy Task Force Leader for Campaigns C8-C14 are nominated as full Task Force Leader in June 2004 with mandate until the end of 2006.

Analysis of data obtained during the two week experimental campaign with reversed toroidal field, B_φ, executed in 2003 (Campaign C9, during which the TFE activities were coordinated in large part by CRPP) continues to yield a wealth of important information on the physics of drift flows and divertor asymmetries. An example is shown in Fig. 4.1.3(a), where the divertor energy deposition asymmetry, E_A, is plotted as a function of the total input energy to the SOL, P_{SOL}. At low P_{SOL}, the energy asymmetry is similar for both field directions and favours the outer target, reflecting the well known tendency for preferential energy transport (ballooning) on the outboard (low field side) and the obvious geometrical factors afforded by the toroidal configuration. With increasing P_{SOL}, E_A decreases in reversed field (ion BxVB drift direction upwards) and increases in forward field. If drift flows (which reverse with field direction) are at the origin of this behaviour of E_A, the effect should scale approximately as P_{SOL}/n_e with n_e the upstream SOL density. The rather surprising absence of a theoretically expected inverse B_φ dependence in this scaling arises because the power e-folding length, λ_q, which is also an important parameter in determining the strength of drift flows, is known, in JET, to scale as $1/B_\varphi$, thus cancelling the direct B_φ dependence which enters through Larmor radius considerations. This is shown particularly clearly in Fig. 4.1.3(b) and constitutes the first direct proof in a large tokamak that field dependent drift terms determine the energy asymmetry over and above that given by cross-field transport and toroidal geometry effects.

A retarding field analyser (RFA) built by CRPP as part of a JET diagnostic enhancement project in 2002-03 and mentioned in last year's Annual Report, continued to produce interesting data in 2004. Given the mounting concern, and evidence for, strong interactions with the main chamber walls in tokamaks during Type I ELM events, the RFA has recently been used to capture individual ELMs as they arrive in the wall vicinity. A key open question is the magnitude of the ELM ion

energy deposition since ion fluxes and energies determine the extent of material sputtering and it is in any case known that the ELM induced electron temperature rise is relatively small. Figure 4.1.4 is an example of the first ever direct ELM ion energy measurement on any tokamak and demonstrates that ions expelled by the ELM do indeed reach the wall radius and do so with energies characteristic of those in the pedestal region of the H-mode edge transport barrier. The burst of ion current seen on the RFA collectors during the ELM event in Fig. 4.1.4 has been produced by ions with energies exceeding a retarding potential of 400V.

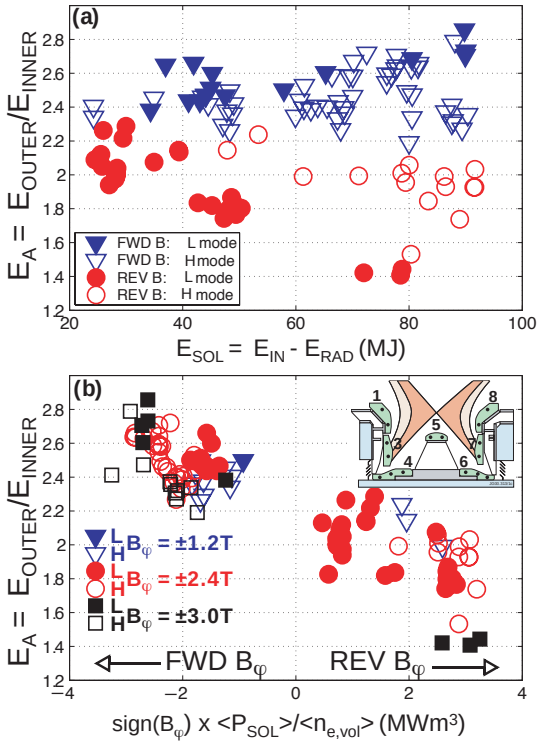

Fig. 4.1.3 *(a) Dependence of outer to inner divertor target energy asymmetry on power into the SOL for forward and reversed toroidal field in JET. (b) Scaling of E_A with P_{SOL}/n_e demonstrating clearly that drift flows (which reverse with the direction of B_φ) are responsible for the changes in E_A as P_{SOL} is increased. The inset shows the locations of tile embedded thermocouples which are used on JET to compute an unambiguous value of the integrated energy deposition during any particular discharge.*

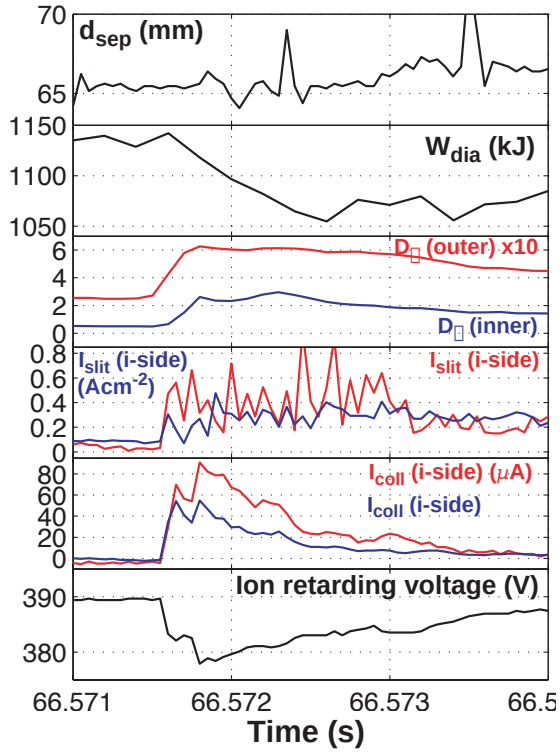

Fig. 4.1.4 *First ever demonstration in a tokamak that ions arriving in the far SOL (top frame – probe is located ~65 mm from the separatrix) during an ELM event do so with high energies. In this example, from a hydrogen plasma with (I_p,B_φ)=1.2MA,1.2T, the ELM plasma energy loss is ΔW_{dia} ~100 kJ and provokes a strong burst of current on the RFA slits (the device is bi-directional – seeing current from both ion and electron drift sides along the magnetic field). This current burst is also observed at the RFA ion collectors, despite a 390 V retarding voltage (lower panel). Ions reaching the collector must have at least this energy parallel to the magnetic field.*

4.1.3 Collaboration on Alfven Waves and Fast Particle Studies

The study of Alfvén waves and their interaction with fast particles is an important topic in the JET programme. A number of dedicated experiments have been performed within the framework of the Task Force activities during this period. This work has mainly concentrated along the following lines:

- studying the dependence of the frequency and damping rate of stable, externally driven, Alfvén Eigenmodes (AEs) with low toroidal mode number upon the value of the safety factor on axis, the bulk plasma rotation and the direction of the ion ∇B-drift;
- studying the instability threshold for AEs driven by resonant fast particles as function of the plasma density for the second harmonic ICRF heating scheme.

Further to the experimental work, we have been involved in various aspects of design, installation and commissioning for some new diagnostic systems that are to be installed ion the JET tokamak during the 2004-2005 shutdown. The main focus of this work has been the design, installation and commissioning of a new dedicated antenna system for the excitation of AEs with high toroidal mode number, CRPP being directly responsible for this project. Furthermore, we have also contributed to the installation and commissioning (hardware/software) of a new fast data acquisition system as well as to the design, installation and commissioning of a new set of high frequency magnetic probes.

The following sections present the main results of these activities.

Measurement of the damping rate of low-n AEs

One of the main purposes of the AE studies on JET is to validate the existing theoretical models and identify the dominant damping mechanisms for global AEs, with the aim of obtaining accurate predictions for future burning plasma experiments such as ITER. As an example of this work, we have investigated the role of the central safety factor q_0, of the plasma rotation and of the direction of the ion ∇B-drift on the AE stability in plasmas with a monotonic q-profile. Due to the strong increase of the damping rate for low-n AEs at high edge elongation ($\kappa_{95}>1.6$) and triangularity ($\delta_{95}>0.35$), which makes it difficult to measure low-n AEs in such configurations, our experimental work has mainly focused on plasmas with low κ_{95} and δ_{95}, to assess the contribution of additional damping mechanisms in regimes much closer to the marginal stability limit of low-n AEs.

Considering ohmic plasmas with $\kappa_{95}<1.5$ and $_{95}<0.3$, we find that for $q_0>1.1$ the damping rate of n=1 Toroidal AEs does not exceed $\gamma/\omega\approx1.5\%$ for a variety of electron density and temperature profiles and for different values of the plasma current and magnetic field. Conversely, with $q_0\approx1$, we find that in the same experimental conditions γ/ω can rise to $\gamma/\omega\approx5\%$. This could indicate a link between the stability of low-n TAEs and the redistribution of the plasma current associated with reconnection events such as sawteeth.

Theoretical modelling and direct measurements indicate that low-n AEs are global modes, i.e. modes whose radial profile extends over a large fraction of the plasma cross-section. It is thus important to study the effect of a sheared rotation on the stability of such modes. Comparing discharges with similar level of Neutral Beam power (P_{NBI}), we notice that for $P_{NBI}\leq5$MW the shear in the plasma rotation has no

clear effect on the damping rate of n=1 TAEs. Only for P_{NBI}>6.5MW can a general trend be identified in the database, namely that the damping rate of n=1 TAEs is ≈50% larger in discharges with a higher rotation shear.

The direction of the ion ∇B-drift is an important parameter in determining the accessibility conditions for the high-confinement regime known as H-mode. Therefore, it is important to study the effect of the ion ∇B-drift direction on the value of the background plasma damping of low-n TAEs. By comparing similar discharges with the ion ∇B-drift directed towards or away from the divertor, we have inferred that γ/ω for n=1 TAEs is a factor ≈2 smaller when the ion ∇B-drift is directed towards the divertor. This significant difference could be used to test the prediction of these different classes of modelling, hence motivating further theoretical developments.

Measurement of the instability threshold of AEs with intermediate and high-n.

The measurement of the instability threshold of fast-ion driven AEs gives information not only on the modes themselves, but also on some properties (energy, spatial profile) of the fast ion populations driving the modes.

Operation at high density is required to reach the burning plasma regimes in ITER. The DT fusion cross section has a broad peak around $E_D \approx E_T \approx 70$keV/amu, and the temperature of the bulk plasma ions has to reach comparable values in order to maximise the fusion yield. Therefore, in view of possible extrapolations of the minority ICRF heating schemes used in JET to the heating of the fuel ions in ITER, it becomes important to study the stability of fast ion driven AEs as a function of the plasma density for otherwise similar plasma conditions. First, the most obvious effect of plasma density on ICRF-driven fast ions comes from the dependence of the fast ion slowing down time, $\tau_S \sim T_e^{3/2}/n_e$. Second, the RF diffusion coefficient goes to zero at lower fast ion energy for increasing plasma density due to the larger perpendicular wavenumber of the ICRF wavefield, effectively preventing a formation of a tail in $f_{FAST}(E)$ above a certain energy. This critical energy decreases with the harmonic number, from >3MeV for 1st harmonic heating to ≤1MeV for 2nd and higher order harmonics. In order to test this theoretical result and thus benchmark existing ICRF code calculations, a series of experiments was performed using the 2nd harmonic H(D) ICRF heating scheme. The ICRF power P_{ICRF}=5.2MW, the electron temperature profile and the shape of the electron density profile were very well matched between the various discharges, allowing a direct comparison of T_{FAST} as a function of the electron density in the plasma core, n_{e0}. The measured fast ion temperature is almost double at low plasma density, $T_{FAST} \approx 200$keV at $n_{e0} \approx 3\times10^{19}$m^{-3}, whereas $T_{FAST} \approx 120$keV at $n_{e0} \approx 4\times10^{19}$m^{-3}. Correspondingly, much weaker q=2 TAEs are excited for similar values of P_{ICRF}, thus indicating a much lower drive at the mode location.

Design of new AE antennas

The present antenna geometry limits the active AE excitation to low toroidal mode numbers, n=0÷2, whereas intermediate or high toroidal mode numbers characterise the most unstable AEs, which are already detected in JET and are similarly predicted for ITER. A direct excitation and tracking of the same modes is therefore of clear interest for preparing the next step experiment. For this purpose, an antenna structure optimised for the excitation and detection of AEs with n≈10-15 has been designed and built, and it is being installed during the current JET shutdown.

The new antenna system comprises two assemblies of 4 toroidally spaced coils, situated at opposite toroidal locations. The self-inductance of each coil is L≈15μH, similar to that of the saddle coils. Each coil is made using 18 turns of 4mm Inconel 718 wire, covers an extent of ~(20×20×15)cm^3, and is individually insulated from the supporting frame with Shapal-M spacers. The first turn sits ~40mm behind the poloidal limiters. The coils are mounted on a 3mm-thick open Inconel 625 structure, to avoid a closed path for disruption-induced currents. This structure is attached to the poloidal limiters and the remains of the saddle coil brackets through four attachment points isolated with Shapal-M spacers, bypassed with 3mΩ resistive straps to provide a known and reliable current path and optimise the mechanical load distribution (Fig. 4.1.5a). The frame is further protected by CFC tiles. To comply with the "As Low As Reasonably Possible" system for manual in-vessel access, the new antennas will be almost entirely installed by Remote Handling (RH). Hence many components and jigs had to be specially designed to be compliant with the requirements of the RH installation.

To simplify the ex-vessel installation, only four of the eight antennas will be actively driven, and the four "passive" ones will be used as additional detectors, together with magnetic pick-up coils and internal measurements such as ECE and reflectometry. The maximum antenna current and voltage used for the AE excitation experiments are of the order of 10A and 700V, producing a very small antenna-driven magnetic field, $|\delta B/B|<10^{-5}$. Any combination of 4 out of the 8 antennas can be chosen to excite different n-spectra, up to n~20. Code calculations also demonstrate that this arrangement provides a coupling to the plasma for a n=5 Toroidal AEs (TAE) that is of the same order as that achieved with the present, much bigger, saddle coils for an n=2 TAE for the same JET equilibrium. Thus, it is foreseen that the real-time tracking capabilities of the old saddle coil system will be maintained and, possibly, control of the marginal stability limit could be envisaged for the intermediate n-modes driven by the new antennas.
The design of all the antenna components was completed in April 2004. All the support brackets have been delivered to JET. The two antenna frames are currently in the final stage of manufacturing (Fig. 4.1.5b), together with all the other major parts (ceramic spacers, coils, tiles). The finally antenna assembly and the electrical testing will take at CRPP between October and November 2004. The delivery to JET of the new antenna system (in- and ex-vessel components) is planned for the beginning of December 2004, with the remote handling in-vessel installation currently scheduled for the end of January 2005.

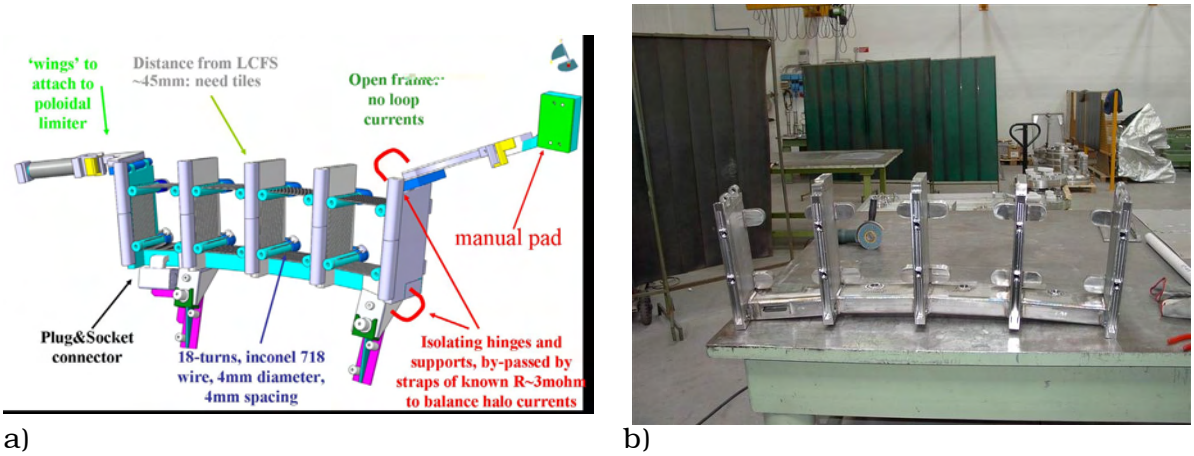

a) b)

Fig. 4.1.5 *a) The final antenna design (April 2004), b) The antenna frame (September 2004).*

Contributions to the installation and commissioning of a new fast digitiser data acquisition system.

In collaboration with MIT (USA), a new fast digitiser system (2MHz, 32 channels, 16sec, 14bit) has been installed in JET to provide high resolution magnetic and internal (soft X-rays, reflectometry and electron cyclotron emission) fluctuation measurements. This work is linked to the installation and commissioning of a new set of high-frequency magnetic pick-up coils. The CPPP contribution to these activities includes the preparation of the technical specifications for this new diagnostic system, participation in the initial commissioning and calibration phase and the production and maintenance of a general-purpose data analysis software, to be released for the use of all JET staff.

Contributions to the design, installation and commissioning of a new set of high frequency coils.

In collaboration with ENEA and the CREATE consortium (Italy), a new set of high frequency pick-up coils has been designed and is being installed on JET to improve the equilibrium reconstruction and the measurement of MHD activities. The CPPP contributions to these activities include participation in the design of the coil array and its positioning, the initial commissioning and calibration phase and the production and maintenance of general-purpose data analysis software to study MHD instabilities, to be released for the use of all JET staff.

4.2 ITER

The CRPP continues to place a high priority on work directly related to ITER, some of which is described here.

4.2.1 International Tokamak Physics Activities (ITPA)

H-mode transitions

The International H-mode Threshold Power DataBase, managed by a member of the CRPP, gathered data from JET, ASDEX Upgrade, MAST and Alcator C-Mod. The database was then updated, checked and new analyses were performed. Particular attention was given to the data selection. For instance, when selecting data from the best divertors from each tokamak, 'best' in terms of low H-mode threshold power, the RMS error in the power law scaling calculated to estimate this threshold power is significantly reduced. The threshold power for ITER was then predicted using the different fits and a comparison between the estimations was made.

MHD, disruptions and plasma control

The CRPP is also represented in this topical group, both for its experience of MHD and of plasma control.

Confinement DataBase and Modeling

A CRPP staff member is now coordinating the information on Joint Collaborations in the framework of the international collaboration experiments under the IEA.

ITER Physics Basis

All ITPA Topical groups are presently preparing a complement to the ITER Physics Basis for publication in 2004.

4.2.2 ITER ECRF 170GHz gyrotron development

The test facility for the CW 2MW 170GHz ITER gyrotron is under construction at the CRPP to incorporate elements provided by Industrial suppliers and other Associations. The CRPP is the lead association within EFDA for the project. This work, and other work carried out in the field of the development of the gyrotron sources for ITER is reported in Section 3.7

4.2.3 Upper launcher design

In collaboration with EFDA-CSU Garching, ITER-IT, and the Associations ENEA-CNR-Milano, FOM, FZK, IPP-Garching, IPF-Stuttgart, the CRPP participates in the design of the remote steering ECW upper launcher of ITER. CRPP is also responsible for defining the methodology and guidelines in incorporating new designs in the CATIA database.

CRPP performed a preliminary design of an alternative front steering system (moveable mirrors positioned near the plasma rather than outside of the neutron shielding as for the remote steering concept) for the ECW upper launcher of ITER. The study concluded that a front steering system offers a significant improvement in stabilising the neo-classical tearing mode (a factor of 2.7 increase) plus a larger steering range (factor of 1.6 increase). Due to the increased potential performance, EFDA-CSU is now supporting CRPP to advance the launcher design to a level equivalent to the remote steering design.

4.2.4 Development of feedback control for combating power supply saturation

This project described in detail in the 2003 report was completed with a demonstration of improvements in a linear model and with the final studies of implementational details. The underlying mathematical basis and analysis is therefore complete. A brief attempt at implementing the method in the non-linear free-boundary DINA-CH environment demonstrated that the implementational details had been covered, but the controller was less globally stabilising than expected. Work will now have to be started on understanding the results of the non-linear simulations to expose any weakness. Current thinking is that the linearised model used is not applicable, in which case the issue of robustness will have to be addressed.

4.2.5 Superconductivity

A large number of specific R&D tasks were dedicated to studies of different superconductivity issues, mostly described in detail in section 2.5, partly funded by EURATOM preferential support. These are summarised as:

TW4-TMSC-SULT, Operation of the SULTAN facility and conductor test
TW3-TMSC-HTSCL, Test of high temperature superconducting current leads, in collaboration with FzK, Karlsruhe
TW4-TMSC-ASTEST, Test of advanced Nb3Sn strands
TW3-TMSC-SULSAM, Preparation and test of two Nb3Sn subsize samples in collaboration with MIT
TW2-TMSC-LCJOIN, Adaptation for testing of two full size NbTi sample and test of a low cost NbTi joint sample
TW1-TMC-JSPREP Deliverables 2 and 4, Fabrication of NbTi and Nb3Sn joint samples for contact resistance distribution and test in the JORDI facility.
TM-G02.01, M29, Development and manufacture of a low cost NbTi full size joint sample
TW4-TMSF-HTSCOM, Conceptual Design of External HTS Busbars

4.2.6 Materials

A large number of specific R&D tasks were dedicated to studies of different fusion material issues, described in detail in section 2.4. These studies are partly funded by EURATOM preferential support, summarised as:

Tasks "Long Term"

TW0-TTMI-003 deliverable 3: Small specimen test technology - Development of experimental fracture testing devices to be used in a hot cell environment and constraint loss assessment on sub-sized compact specimens of EUROFER 97
TW1-TTMS-001 deliverable 3 : Proton irradiation of EUROFER 97 up to 1 dpa of plate, for He effect testing
TW1-TTMS-002 deliverable 20 : Tensile and fracture toughness of EUROFER 97, punch testing
TW2-TTMS-006a deliverable 3 : Creep testing at RT-750°C on the two improved ODS batches
TW2-TTMS-006a deliverable 6 : Tensile testing at RT-750°C on the two improved ODS batches
TW2-TTMS-004b deliverable 3 : Development and testing of coatings to improve the corrosion resistance vs Pb17Li at T>450°C
TW2-TTMS-005b deliverable 6 : Small-scale fracture mechanics - Modelling of brittle and brittle to ductile transition behaviours using appropriated theories. Formation of rules for transferability to standards and fusion components
TW3-TTMA-002 deliverable 2 : W coating onto RAFM alloys
TW3-TTMS-005 deliverable 1 : Low cycle fatigue testing of EUROFER 97
TW3-TTMS-005 deliverable 2 : Investigation (tensile and Charpy testing) of PHT and PWHT to improve the design limits and to define the acceptable temperature range
TW3-TTMS-006 deliverable 3 : Study of the influence of Ti addition on the mechanical properties (Charpy, tensile) with characterisation of the full fabrication process
TW3-TTMS-007 deliverable 8 : Irradiation in SINQ
TW3-TTMS-007 deliverable 10 rev.1 : MD simulations of effects of cavities

TW4-TTMA-002 deliverable 2 : Development of W-based materials for future divertor application using electrodeposition
TW4-TTMS-005 deliverable 4 : Support in development of design rules for structural materials with low ductility
TW4-TTMS-006 deliverable 2 : Literature study on ferritic ODS steels for HT application
TW4-TTMS-007 deliverable 7 : Molecular dynamics simulations of grain boundaries

Tasks "Next Step"

TW1-TVV/Titan : Titanium alloy irradiation testing
TW3-TVM-TICRFA : Effect of low dose neutron irradiation on Ti alloy mechanical properties
TW5-TVM-COMADA: Investigation of the effect of creep fatigue interaction on the mechanical performance and lifetime of CuCrZr

4.3 Collaborations on other tokamak experiments

Collaboration with ASDEX Upgrade, Germany

The ELM triggering technique developed on TCV has been tested in ASDEX Upgrade. A sinusoidal perturbation was applied to the vertical plasma position feedback control loop. It resulted in an oscillation of the current flowing in the coils used for the vertical control, which, in turn, generated an oscillating displacement of the plasma magnetic axis. The amplitude of the displacement was scanned between 6 and 12mm and the perturbation frequency between 33 and 80Hz, the limits being imposed by hardware constraints.
In most cases the ELM frequency was changed from its natural value to the externally imposed value, as show by Fig.4.3.1. In these first experiments, the ELM frequency was successfully controlled in a range of 0.75 to 1.8 times the natural ELM frequency.

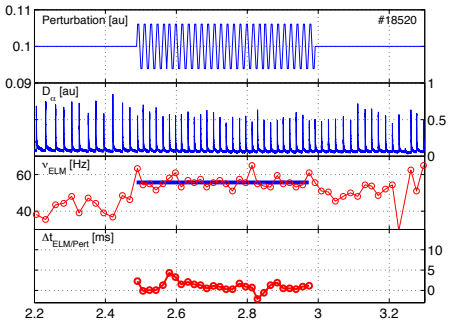

Fig. 4.3.1 *Change of the ELM frequency by vertical position toggling*

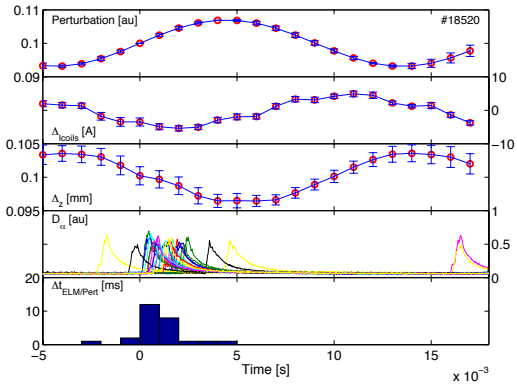

Fig. 4.3.2 *Synchronisation of the ELM timing with the drive signal*

The synchronisation of the ELMs with the perturbation cycle is shown in Fig.4.3.2. ELMs are triggered when the plasma moved down, towards the X-point. This result is opposite to experiments done in TCV. This discrepancy is currently being analyzed. In the amplitude scan, the synchronisation of ELMs to the perturbation was found to be better at low amplitude.

Perturbations were also applied during a scan of the additional power. The frequency and the type of the ELMs changed during this power scan. Therefore, synchronization was significantly affected by the level of additional power.
ELM control with edge ECH and ECCD was also tested. These preliminary experiments showed a dependence of the ELM frequency on the direction of the current driven at the plasma edge. Modulation of the edge ECH induced a synchronization of the ELM cycle. More experiments are planned to investigate this promising new technique to control ELMs.

Work has also continued on identifying the chaotic nature of ELMs in ASDEX Upgrade.

The NTM marginal beta limit on ASDEX Ugrade was investigated in a collaboration which also involved studies of the effect of tailoring sawteeth.

Collaboration with MIT-PSFC, USA

This collaboration constitutes the natural continuation of a programme on the physics of fast particles and their interaction with waves in the Alfvén range of frequencies in the high magnetic field, high density, T_e=T_i plasmas produced in the Alcator C-Mod tokamak. Recently, a localized antenna for the excitation and detection of Alfvén Eigenmodes (AEs) has been installed on Alcator C-Mod. The first experimental results indicate that AEs with intermediate mode numbers can be driven and detected, and that their damping rate can be measured, as shown in Fig. 4.3.3.

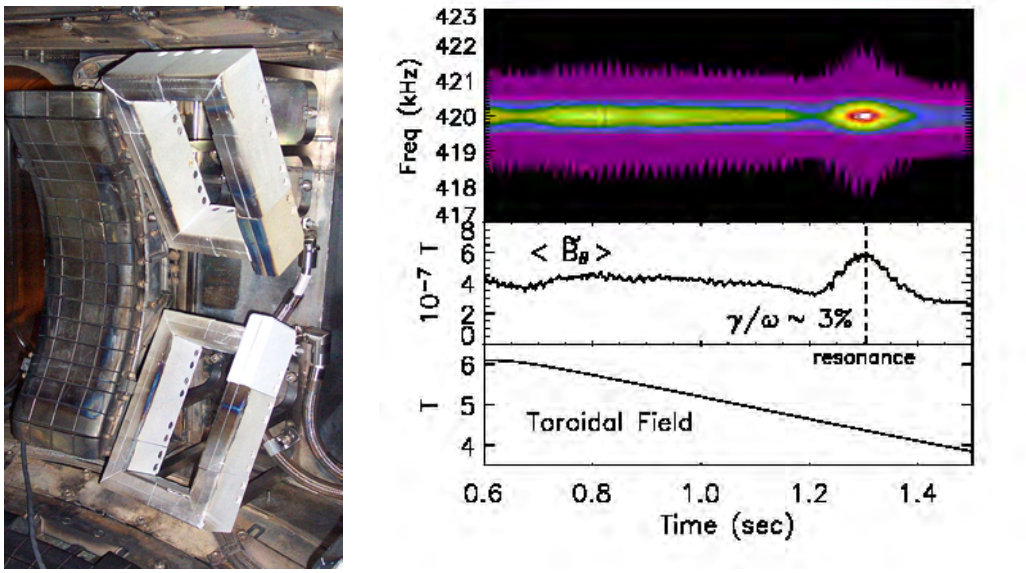

Fig. 4.3.3 *The antennas for the external excitation of Alfvén Eigenmodes in Alcator C-Mod (left), and the measurement of the damping of a Toroidal AE (right). The toroidal field is varied linearly in time, so that the TAE frequency crosses the antenna frequency, which is kept constant* (courtesy of J.Snipes).

4.4 *Plasma-surface interaction, in collaboration with the University of Basel*

Metallic mirrors are being tested in different tokamaks such as TEXTOR, JET and Tore Supra. All these experiments aim to study the evolution of the optical properties as a function of the exposure conditions. We are supporting these studies by means of our surface and optical analysis techniques.

Large polycrystalline molybdenum mirrors were mounted on an inclined target holder (20° inclination to the toroidal direction) and exposed in the scrape-off-layer of TEXTOR, one in the erosion dominated zone, the other in the deposition dominated zone. Total and diffuse reflectivity were reproducibly measured under almost normal incidence in the wavelength range 250-2500nm at about 50 locations on the mirror's surface before and after exposure by means of a spectrophotometer (Varian Cary 5). After plasma exposure, a decrease in the reflectivity is found in the areas where the deposition is noticed (by about 35%). Surprisingly, the reflectivity increases in eroded zones (by about 15%). The reason for this increase is still to be clarified.

Six metallic mirrors of 20mm diameter were installed on the high field side of the Tore Supra vessel for a long term exposure. Materials used for mirrors are single-crystalline molybdenum, copper and stainless steel. Reflectivity and ellipsometry measurements were made on virgin and exposed samples, as well as XPS measurements on exposed molybdenum and copper mirrors. After exposure a decrease of reflectivity was found for all the mirrors. XPS measurements showed up the oxidation of the bulk material at the surface. Impurities like carbon and boron are also present.

A large number of metallic mirrors will be installed in different locations in JET. Two materials have been chosen: stainless steel and molybdenum. Fifty samples were pre-characterised in July, total and diffuse reflectivity were measured in the range 250-2500nm. Spectroscopic ellipsometry was applied in the range 300-850 nm so as to determine the optical constants of the mirrors. Since the mirrors will be contaminated by beryllium and tritium after exposure, it was decided to purchase and install a reflectivity measurement setup in JET. Different companies have been contacted and different solutions are going to be tested.

"Mirror testing" experiments will be performed in TCV. Samples will be mounted on a modified version of the boronisation sample manipulator used for previous collaborations between CRPP and the University of Basel. Molybdenum, tungsten and vanadium samples will be exposed. Pre and post-characterizations with different surface analysis techniques (reflectivity measurements, photoelectron spectroscopy…) will be made.

To somehow model the intermixing effect observed when carbon diffused into molybdenum, we have focused on the co-deposition of Mo and C by magnetron sputtering, and have studied both the influence of the composition of the layer on the optical properties and the formation of molybdenum carbide. In all cases, XPS measurements revealed that the films are made of a mixture of Mo, C and MoC. The optical constants of the films were found to be strongly dependent on the composition, first attempts of interpretation using an effective medium approximation have been made.

4.5 Socio-Economic Studies

Long Term Electricity Supply Scenarios Worldwide : Quantitative Assessment with a Least Cost Electricity System Planning Model (PLANELEC-PRO)
(Work performed by the LASEN (EPFL) for the Association on behalf of EURATOM)

The ultimate objective of this study is to explore the potential role of fusion power in future electricity supply mixes in global scale and to quantify its advantages and possible drawbacks. The main tasks consist in performing general assessment of the electricity systems in different world regions at their current and anticipated state, estimating generic technical and economical performances of existing and prospective power generation technologies, and building on this basis consistent multi-regional electricity markets scenarios for the time horizon 2100. Various types of scenarios are examined, including "business as usual" and several explorative scenarios presuming different market shares of fusion, nuclear fission and clean coal with CO_2 capture and sequestration. Evaluation of different technology mixes is carried out from technical, economical and environmental (CO_2) points of view.

The research makes use of the PLANELEC-PRO least cost electricity systems planning model, developed by LASEN / EPFL. It determines the expansion plans of the power generating system, which adequately meet electricity demand at minimum cost while respecting constraints given by the user, such as CO_2 emissions and quality of service. When comparing alternative expansion patterns, the objective function to be minimized is the present value of total costs, including investment cost, operation & maintenance costs, and fuel cost. Competitiveness of fusion power generation is estimated through two indicators: the impact of various market shares of fusion power on the levelised electricity production cost and the total accumulated CO_2 emissions along the period of study.

For the work undertaken in 2003-2004, Western Europe was chosen as benchmark study. It is found that deployment throughout the period 2040 – 2100 of total 90 GW of fusion power in Western Europe is capable to reduce approximately up to 10 % of the total system CO_2 emissions by the end of the century. This limited introduction of fusion power causes a slight increase of the system levelised electricity production cost of the order of magnitude € 0.001/kWh. The estimated incremental CO_2 abatement cost of fusion power is € 11.5 / t CO_2. These results, however, are significantly dependent on the assumptions of future fuel prices and parameters of the candidate power generation technologies.

4.6 Collaborations with other EURATOM Associations

The Swiss Association has an active approach to external collaborations and works together with many other EURATOM Associations on specific research topics. A full list of these collaborative activities has been reviewed and endorsed by the EFDA Scientific and Technical Advisory Committee. The following list gives specific themes where such collaboration occurred. Those marked (*) are the subject of specific preferential support by EURATOM and are cross-references where specific mention is made in this report.

A. Alfier, P. Nielsen, R. Pasqualotto, G. Manduchi, Consorzio RFX, Padova, Italy, *"Thomson scattering from the edge plasma of TCV"*

C. Angioni, M. Maraschek, A. Mück, G. Pereverzev, F. Ryter, H. Zohm, IPP Garching, Germany, *"Sawtooth tailoring experiments for NTM control" (* See 4.3)*

J-F. Artaud, V. Basiuk, Association EURATOM-CEA, France, *"Integration of CRONOS and DINA-CH"*

J. Bakos, KFKI Budapest, Hungary, *"Laser ablated impurity transport using Nickel"*

F. Castejon, CIEMAT, Spain, *"Electron Bernstein Wave Current Drive in Stellarators (and Tokamaks)"*

G. Cunningham, G. McArdle, Association UKAEA Fusion, UK, **J. Qin**, Imperial College, London, UK, *"Comparing the plasma equilibrium control of tight and conventional aspect ratio tokamaks" (* Work with a UKAEA PhD student, not explicitly reported)*

A. DellaCorte, P. Gislon, Association EURATOM-ENEA, Italy, **D. Ciazynski and L. Zani**, Association EURATOM-CEA, France, *"Test in SULTAN of the PFIS samples" (* See 2.5.1)*

V. Grandgirard, CEA, France, *"Semi-Lagrangian gyrokinetic code development" (* See 2.2.1)*

R. Heller, Association EURATOM-FzK, Germany, *"EFDA task on design of high temperature superconducting current leads" (* See 2.5.4)*

R. Heller, Association EURATOM-FzK, Germany, *"Conceptual design of external HTS bus-bars (ITER)"*

Y. Igithkhanov. T. Andreeva, C. Beidler, J. Kisslinger, H. Wobig, Max Planck Institut für Plasmaphysik, Greifswald, Germany, *"Bootstrap Current Effect on Stability in a 4-Period Helias Reactor"*

Y. Ilyin and A. Nijhuis, University of Twente, Holland, *"The assessment of current distribution results from test in SULTAN"*

P.T. Lang, F. Ryter, IPP Garching, Germany, *"Experiments on ELM control using positional modulation and edge ECCD/ECH"*

T. Madeira, **P. Amorim**, CFN/IST, Lisbon, Portugal, *"X-ray spectroscopy of the TCV plasma" (* Regular diagnostic information on TCV)*

M. Maraschek and S. Guenter, IPP Garching, Germany, *"NTM marginal beta limit on ASDEX-Upgrade Tokamak" (* See 4.3)*

D. Mazon, Association EURATOM-CEA, France, *"Temporary installation of imaging hard-X-ray camera"*

J. Nührenberg, A. Koenies, V. Kornilov, A. Mishchenko, S. Sorge, IPP Greifswald, Germany, **A. Peeters**, IPP Garching, Germany, **R. Hatzky**, Rechenzentrum MPG Garching, Germany, *"Linear and nonlinear gyrokinetic code developments and simulations" (* See 2.2.1)*

J. Nuehrenberg, IPP Greifswald, *"Optimisation of Advanced Stellarator Systems"*

V. Piffl, IPP Prague, Czech Republic, *"Ultra Soft X-ray spectroscopy using a multi-layer mirror to observe He- and H-like emission from Boron, Carbon, Nitrogen and Oxygen" (* Regular diagnostic information on TCV)*

L. Popova, Institute of Mathematics and Informatics, Bulgarian Academy of Sciences, Sofia, BG), **S. Kuhn and D. Tskhakaya** (Association Euratom-OAW, Innsbruck, Austria, **A. Loarte** (EFDA-CSU Garching), *"PIC simulations of ELM-produced particle and energy pulses and their effect on the SOL"*

M.E. Puiatti, M. Valisa, Consorzio RFX, Padova, Italy, *"Modelling of the transport of laser ablated impurities"*

A.P. Rodrigues, L.A. Pereira, CNF/IST, Lisbon, Portugal, *"A DSP-based system for the TCV Advanced Plasma Control System" (* See 3.3.2)*

F. Ryter, IPP Garching, Germany, "*Inter-machine comparison of electron transport*"

F. Volpe, B. Lloyd, Association UKAEA Fusion, Culham, UK, "*Installing the ray tracing code ART and the Fokker-Planck code Bandit-3D at the CRPP and participation in the planning of EBW experiments in TCV*"

G. Zvejnieks, Institute of Solid State Physics, University of Latvia, Latvia, **O. Dumbrajs, V. Hynönen,** Helsinki University of Technology, Finland, **W. Suttrop, H. Zohm**, Max-Planck-Institut fuer Plasmaphysik, EURATOM-Association, Germany, *"Dynamical properties of Edge Localised Modes (ELMs) occurring in the ASDEX-Upgrade and TCV experiments" (* See 4.3)*

4.7 Other international collaborations

J. Egedal, W. Fox, M. Porkolab, PFSC, MIT, USA, *"Investigation of the physics of magnetic reconnection in the collisionless regime in a dedicated laboratory device, the Versatile Toroidal Facility"*

R.W. Harvey, A.P. Smirnov, CompX, San Diego, CA, USA, "*Modelling of electron cyclotron wave propagation and electron cyclotron emission in TCV*"

W. Heidbrink, H. Boehmer, UC Irvine, USA, "*Sources for energetic ions for a simple magnetized torus*"

V.E. Lukash, RRC Kurchatov, Institute of Nuclear Fusion, Moscow, Russia, **R.R. Khayrutdinov**, **V. Dokuka**, TRINITI, Troitsk, Russia, *"Simulation of TCV experiments using the non-linear DINA code"*

G. Manfredi, Laboratoire de Physique des Milieux Ionises et Applications, Université Henri Poincare, Vandoeuvre-les-Nancy, France, *"Development of the gyrokinetic semi-Lagrangian code CYGNE"*

M. Mikhailov, A. Subbotin, V.D. Shafranov, M.Yu. Isaev, M. Samitov, RRC Kurchatov Institute, Moscow, Russia, *"Optimisation of Advanced Stellarator Systems"*

J. Minervini, PFSC, MIT, USA and **N. Martovetski**, LLNL, USA, *"Preparation and test of two subsize Nb3Sn cable-in-conduit superconductors"*

A. Shushkov, A. Razumova, RRC Institute, Russia, *"Study of electron heat transport and non-local phenomena in transient processes following switch on/off in L-mode regimes with improved confinement".*

J. Snipes, R. Parker, M. Porkolab, J. Freidberg, J. Sears, PFSC, MIT, USA, *"Fast particle physics, Alfven waves, and active MHD mode excitation on the Alcator C-Mod tokamak plasma"*

Wendelstein Group, IPP Greifswald, Germany, *"Test of 2 W7X conductor joint samples"*

S.Yu. Medvedev, A.A. Martynov, A.A. Ivanov, Keldysh Institute of Applied Mathematics, Moscow, Russia, **M.Yu. Isaev, V.D. Shafranov, A.A. Subbotin**, RRC Kurchatov Institute, Moscow, Russia, *"Equilibrium and Stability of 2D and 3D plasma configurations"*

E. Valeo, PPPL, Princeton University, USA, "*Development of numerical methods for kinetic simulations*"

K. Yamazaki, K. Y. Watanabe, S. Okamura, T. Yamaguchi, Y. Narushima, H. Yamada, S. Sakakibara, C. Suzuki, National Institute for Fusion Science, Toki, Japan, **S.P. Hirshman**, Oak Ridge National Laboratory, USA, *"Model Anisotropic Pressure Equilibria in Stellarators with Tangential Neutral Beam Injection"*

M.Yu. Isaev, RRC Kurchatov Institute, Moscow, Russia, *"Development of the VENUS-df Code for Bootstrap Current and Neoclassical Transport in Stellarators"*

E. Zapretilina, Efremov Research Institute Of Electrophysical Apparatus (NIIEFA), Russian, *"Electromagnetic behaviour of the large NbTi cable-in-conduit conductors for the ITER Poloidal Field coils"*

4.8 Other collaborations within Switzerland

Ph. Mullhaupt, D. Bonvin, B. Srinivasen, Laboratoire d'Automatique, EPFL, *"Development of saturating controller algorithms for ITER"*

S. Siegmann, Jong-Won Shin, EMPA Thun, Top Nano 21 project: *"In-situ monitoring of the synthesis of nano-powders by an RF thermal plasma".*

P. Ott, S. Pavon, Laboratoire de Thermique Appliquée et Turbomachines, EPFL, **P. Leyland**, Laboratoire d'Ingénierie Numérique, EPFL, Swiss National Science Foundation Project: *"Influence of a weakly ionised boundary layer on transonic and supersonic air flows"*

5 THE EDUCATIONAL ROLE OF THE CRPP

The CRPP plays a role in the education of undergraduate and postgraduate students, particularly in the Faculté des Sciences de Base (Faculty of Basic Sciences) of the EPFL. Advanced education and training in fusion physics and technlogy and plasma physics topics is carried out as part of the research activities of the Association. Section 5.1 presents the 5 courses given to physics undergraduates and to engineering undergraduates. In their fourth and final year, physics undergraduates spend time with a research group at the EPFL, typically 12 hours per week for the whole year. During this period, they perform experimental or theoretical studies alongside research staff, discovering the differences between formal laboratory experiments and the "real" world of research. After their final examination at the end of the 4th year, physics students are required to complete a "diploma" work with a research group, lasting a full semester. This diploma work is written up and defended in front of external experts. The CRPP plays a role in all of these phases of an undergraduate's education, detailed in Sections 5.2 and 5.3.

As an academic institution, the CRPP supervises many Ph.D. theses, also in the frame of the Physics Section of the EPFL. 4 PhDs were awarded in 2004. At the end of 2004 we have 29 Ph.D. students supervised by CRPP members of staff, mostly in Lausanne but also 5 at the PSI site in Villigen. Their work is summarised in Section 5.4.

5.1 Undergraduate courses given by CRPP staff

S.Alberti, *Chargé de cours – "Plasma Physics I"*
This course is an introduction to plasma physics aimed at giving an overall view of the essential properties of a plasma and at presenting the approaches commonly used to describe its behaviour. We study single particle motion, the fluid description and the kinetic model. The relation between plasma physics and developing a thermonuclear reactor is presented and illustrated with examples.

N. Baluc, *Chargée de cours – "Material Physics"*
Basic course on material physics, presented as an option to 4th year Physics students. The course covers the theory of diffusion, dislocation and plasticity as well as the characterisation of materials. Ways of production, physical and mechanical properties and applications are presented for pure metals, intermetallic alloys, steels, superalloys, quasicrystals, metallic glasses, gels, liquid crystals, shape memory alloys, ceramics, composites and polymers.

A. Fasoli, Assistant Professor Tenure Track– *"Plasma physics II"*
One semester option course presented to 4th year Physics students, introducing the theory of hot plasmas via the foundations of kinetic and magnetohydrodynamic theories and using them to describe simple collective phenomena. Coulomb collisions and elementary transport theory are also treated. The students also learn to use various theoretical techniques like perturbation theory, complex analysis, integral transforms and solution to differential equations.

A. Fasoli, Assistant Professor Tenure Track– *"General Physics II"*
This course completes the introduction to mechanics provided in the first semester with the basic concepts of statics, oscillations and special relativity. It also covers the whole of thermodynamics, from the introduction to heat, temperature and

kinetic theory to the first and second principles, including entropy and thermal engines, ending with a treatment of transport and non-equilibrium phenomena in open systems.

J.B. Lister, *Chargé de cours – "Plasma Physics III"*
An introduction to controlled fusion, presented as a one semester option to 4th year Physics students. The course covers the basics of controlled fusion energy research. Inertial confinement is summarily treated and the course concentrates on magnetic confinement from the earliest linear experiments through to tokamaks and stellarators, leading to the open questions related to future large scale fusion experiments.

L. Villard, *Maître d'Enseignement et Recherche (MER) – "General Physics III-IV"*
Full year course given to students in their 2nd year Mechanical and Electrical Engineering. The course covers fluid dynamics, electromagnetism, waves and an introduction to quantum mechanics.

5.2 Undergraduate work performed at the CRPP

EPFL 4th year students (2004 Summer semester)

Olivier PISATURO: *"Design and construction of a Mach probe for the TORPEX experiment"*
Following the work performed during the previous semester, in this laboratory work the student completed the implementation of the Mach probe diagnostic system for measuring plasma flows in TORPEX. A remote mechanical control system for positioning the probe has been installed and commissioned. A full calibration for estimating the absolute values of the flows was performed. In addition, a study of the feasibility of measurements of drift wave fluctuations in the TORPEX plasmas by optical emission diagnostics was performed. A two-channel system based on photomultiplier tubes is suitable for the detection of TORPEX fluctuations, the measurements of their spectra, their statistical properties and correlation functions. First calibrations of a one-channel prototype system were also performed.

Martin PYTHON: *"Design and construction of an optical probe for the TORPEX experiment"*
This laboratory work aimed at conceiving, building and installing a movable optical probe for the local detection of visible light emission in the magnetised TORPEX plasma. A movable shaft was used to support an optical fibre, which views a small plasma volume, of order of 1cm^3 through a lens,. This volume is defined by a fully reflecting mirror, supported by the same shaft. The light collected locally is directed on a spectrometer to extract information on the TORPEX plasma. First measurements of the light emitted locally by electron collisional excitation in argon plasmas were obtained, along with a radial profile of plasma emissivity.

Jonathan ROSSEL: *"Analysis of the magnetic field structure and current formation during breakdown in TCV"*
The aim of the work was to contribute to the understanding of the plasma breakdown on TCV by studying the electromagnetic field structure during this phase. A finely tuned linear regression was developed to produce robust reconstructions of magnetic field maps, even with low accuracy in the measurements. The plasma current during the initial part of the current ramp up and the trajectory of its centre of gravity is also modelled. Statistical analysis of spatial correlations between the minima in the magnetic field modulus, the integral

of the electric field over the wall connection lines, the initial plasma current position and the breakdown failure or achievement are presented.

External students

Xavier LAPILLONNE, from the Ecole Nationale Supérieure de Physique de Grenoble, France: "*Statistical study of ECCD efficiency in TCV* "
The detailed dependence of local electron cyclotron current drive (ECCD) efficiency on plasma parameters has been experimentally determined only to a limited degree. Mr. Lapillonne, on a 2-month summer internship at the CRPP, has built a database of fully non-inductive TCV discharges with the aim of studying this dependence with a statistical approach. He carried out a preliminary study of the database with regression techniques. The complexity of the functional dependence was increased gradually to gain insight into the problem. The ultimate form for proper comparison with theory entails a multivariate nonlinear dependence with uncertainties on both the dependent and independent variables, and its resolution requires appropriate optimisation techniques and considerable computational power. The conclusion of the internship work offered preliminary approximate fits as well as useful recommendations on approaches for solving the general problem.

Janos MARKI, from the University of Budapest, Hungary: *"Laser ablated impurity experiments"*
A physics student from the University of Budapest spent three months at CRPP to complete his diploma work on a statistical analysis of some 200 impurity transport experiments by injection of laser ablated Silicon and Aluminium into TCV plasmas with a large range of plasma shapes. He revisited nearly the entire database of experiments accumulated since the installation of the laser ablation system on TCV several years ago. Some of the previous results were corrected by an improved method of subtracting the X-ray background, leading to a reduction of the scaling of impurity confinement time with elongation with respect to previously presented results. The impurity confinement times obtained from the analysis were compared to the very few such analyses performed on different devices, in particular Tore Supra, JET and Alcator. There is a factor-of-two agreement with these scaling laws with positive and negative deviations. Regressions based on TCV data only, despite allowing for additional parameters, only marginally improved the situation.

Paul SHEEHAN, from University of York, UK: *"DMPX development"*
A new double layer soft X-ray detector (DMPX) has been recently commissioned on TCV to determine of the electron temperature profile by the absorber method with high spatial and temporal resolution, covering a large range of densities, including above ECE cut-off. An existing program has been extended to include the required absorber elements, including the different noble gases of the detectors, with all the different material absorption characteristics extended to 200keV. The DMPX has been designed to adapt to the various operational regimes of TCV, from Ohmic to eITB plasmas (typically 0.5 – 20keV), by changing or inserting additional absorbers. The programme has allowed us to determine the different absorber thicknesses needed to obtain instrumental functions with an adequate dynamical range over different temperature ranges.

Vivek Kumar SINGH, from the Indian Institute of Technology, Delhi, India: "*Electron Bernstein wave heating and emission in TCV* "
Electron Bernstein waves (EBW), not subject to density cutoffs, can be used both to heat and to diagnose plasmas that are overdense to O- and X-mode ECRH. These electrostatic waves can be excited or detected by exploiting a double O-X and X-Bernstein conversion that can occur under particular propagation conditions. Mr. Singh, during his two months at the CRPP as a summer intern, developed a front-

end graphical user interface to the newly acquired GENRAY ray tracing code and employed it, in appropriate combination with the ART ray-tracing code, to determine the target and launching parameters for the EBW heating experiments planned for the current TCV campaign. In parallel with this work, Mr. Singh also participated in the design of the experimental setup for the first measurement of EBW emission in TCV and analysed the first successful results.

5.3 EPFL Diplomas awarded in 2004

Lukas DERENDINGER: *"Experimental investigation of the Telegaph effect in a large area plasma reactor and comparison with a 2-D numerical simulation"*
Capacitively-coupled parallel plate RF reactors are commonly used for plasma enhanced chemical vapour deposition and dry etching of thin films such as amorphous silicon or silicon oxide. Large area (> 1 m^2) reactors are used for the manufacture of photovoltaic solar cells and thin film transistors for flat screens. These industrial applications typically require a uniformity of film thickness to better than ± 10%, and therefore a corresponding uniformity in plasma parameters over the whole substrate area. The plasma non-uniformity considered in this diploma work is due to perturbations in the RF potential caused by electrode edge asymmetry. The damping length of the perturbation can be determined with the Telegraph equation. The non-uniform RF plasma potential in presence of the uniform DC plasma potential leads to non-ambipolar DC currents circulating through the plasma and along conducting surfaces. The diploma work measured the 2-dimensional non-ambipolar DC current flow and DC voltage pattern in a large area rectangular reactor using the installed array of 82 surface probes and multiplexer acquisition system. The measurements compared well with a numerical solution of the Telegraph equation.

Chong DING*: "Experimental study of dielectric barrier discharges operated at various pressures using optical emission spectroscopy and electrical characterisation"*
The dielectric barrier discharge (DBD) is a type of self limiting plasma discharge which is sustainable at atmospheric pressure without a transition to an arc. Because of its simplicity and usefulness it is becoming a widely used tool in industrial applications. However the operation regime is filamentary in most cases which prevents its use for processes which may suffer from local high energy density deposition. It has been shown that DBD can be operated in a so-called "glow" regime where the discharge is more uniform and diffuse. The working pressure and gas composition play a key role in the operation mode. In this work, DBDs in a parallel plate configuration are investigated using time resolved electrical measurements of the voltage and current and also by optical emission spectroscopy. Several operating parameters are investigated such as the working pressure (40 – 1000 mbar), the gas composition (N_2, Ar, He), and the supplied voltage. The operating mode (filamentary or glow) of the DBD has been characterised by its signature on the current waveform and a change in the discharge topology. Operation diagrams in parameter space have been constructed which show a transition between the different regimes. An indirect measurement of the voltage across the electrode gap has allowed us to determine the breakdown voltage, which shows a strong dependence on the pressure and gas composition but does not follow a Paschen law.

Sébastien JOLLIET: *"Résolution des equations gyrocinétiques en utilisant des coordonnées généralisées" ("Resolution of gyrokinetic equations in curvilinear coordinates")*

The aim of this work was to formulate and solve the time dependent gyrokinetic equations in a toroidal curvilinear coordinate system characterised by its ability to accurately represent low frequency perturbations driven by equilibrium gradients (drift type instabilities). The radial coordinate is a function of the poloidal magnetic flux. The poloidal coordinate is such that magnetic field lines are straight in the space of poloidal and toroidal coordinates. The gyrokinetic equations have a singularity in this system at the magnetic axis. An original formulation that completely avoids this problem was made, successfully implemented in the global linear code LORB5, and benchmarked: the new version gives correct results and is about 25% faster, because it avoids interpolations from the magnetic to cylindrical coordinates. The scheme is applicable to the nonlinear problem as well and will be implemented in the future.

Nicolas MELLET: *"Détermination des surfaces magnétiques résonantes d'Alfvén dans des configurations 2D et 3D" ("Determination of Alfvén resonant magnetic surfaces in 2D and 3D configurations")*
In this work, the dispersion relation for shear Alfvén waves has been solved in cylinder, tokamak, mirror, and fully 3D toroidal magnetic configurations (stellarators). The partial differential system of equations is solved with a Fourier decomposition in poloidal and toroidal Boozer coordinates. The equilibrium is computed with the VMEC code, then the TERPSICHORE code is used to obtain the metric coefficients in Boozer coordinates that are necessary to solve the shear Alfvén dispersion equation. The new code gives the frequencies of shear Alfvén resonances for each magnetic surface. The results have been compared with analytical expressions where available and to computations of a full wave code (LEMan, PhD thesis Pavel Popovitch). The agreement is excellent in all cases. Various geometrical couplings (toroidicity, elongation, helicity, mirror symmetry and fully 3D) have been studied and the corresponding gaps in the Alfvén continuum have been investigated.

Samantha PAVON: *"Caractérisation électriques, optiques et par spectrométrie de masse d'un arc DC à basse pression utilise comme source plasma pour la croissance épitaxiale de couches semi-conductrices" (" Electrical and optical characterization of a DC arc at low pressure used as a plasma source for epitaxial growth of semiconductor films")*
Low pressure DC arc plasma has been proven to be a serious alternative to the usual chemical vapour deposition technique for the growth of epitaxial semiconductor thin films. In this work, the low pressure DC arc plasma was investigated using Langmuir probes, emission spectroscopy and CCD imagery. Electron density and temperature profiles of the plasma column were determined for a wide range of parametes. These results have shown the importance of the operation pressure and of the magnetic field used for the plasma confinement; electron densities up to two orders of magnitude higher were obtained when the electron are magnetised compared to unmagnetised cases. During this work, the development of a numerical fluid model for the DC arc plasma in argon was also started. This model solves the current continuity, electron density continuity and electron energy continuity equations, including the anisotropy induced by the external applied magnetic field. The preliminary results of this model qualitatively reproduce the experimental results. The experimental results and the numerical model obtained in this work give a better understanding of the DC arc plasma, which should help to improve the design of the next plasma source for thin film epitaxial growth.

Karin SCHOMBOURG: *"Transport studies in TORPEX plasmas"*
Transport phenomena were studied in the low temperature, low density TORPEX plasmas by means of electrostatic probes. Two kinds of experiments have been performed. First, the mechanisms related to the disappearance of the plasma after

the switch off of the microwave power, the source of plasma production, have been investigated. Density structures appear to be generated by the abrupt stop of the microwave power and to move along with the ExB drift. Second, the plasma response to the perturbation caused by modulating the microwave power has been analyzed. The transfer function between the microwave power and the plasma density was reconstructed over the plasma cross-section. The plasma density response is maximal at the spatial location corresponding to the upper hybrid resonance. This confirms the fundamental role that the upper hybrid resonance plays in the plasma formation process, and indicates the structure of the source term that needs to be included in transport analyses.

Diploma studies presently underway (Winter semester 2004)

Olivier PISATURO: *"Investigation of plasma fluctuations via optical diagnostic techniques in the TORPEX device"*
Optical diagnostic methods complement measurements by electrostatic probes by providing information on fluctuations and the associated turbulence, such as the frequency spectrum, the spatial distribution and the probability distribution function, without perturbing the plasma. The candidate operates and is upgrading existing installations on the TORPEX magnetized toroidal plasma experiment, in particular a radially viewing telescope for line-integrated measurements and an in-plasma telescope for localized measurements in the equatorial plane. The candidate is contributing to conceiving and implementing space resolving optical techniques, using photodiode arrays or a fast CCD camera. The optical data will be interpreted in terms of theoretical models of plasma light emission and compared with data from electrostatic probes. Such comparison will provide information on the perturbative effect of the probe measurements and, more generally, on the nature of the plasma turbulence in the TORPEX device and on its possible influence on plasma transport.

Jonathan ROSSEL: *"Soft-X emissivity profile inversion in quasi-axisymmetric equilibria"*
In TCV (Tokamak a Configuration Variable), the measurements of the soft-X emissivity of the plasma are integrated along lines of sight. To obtain local values, it is necessary to inverse these measurements. This is often only possible by making certain assumptions on the emissivity of the plasma; e.g. assuming constant emissivity on the flux surfaces of the plasma. When MHD perturbations are present, the plasma equilibrium is not axisymmetric anymore. To obtain information on these perturbations, an inversion combining non-axisymmetric information must be developped; e.g. using measurements from other sources or using a model of the MHD instabilities. The aim of the project is to set the basis of such an inversion and to apply it to the measurements of the DMPX (Dual Multiwire Proportional X-ray Camera).

5.4 Postgraduate studies

Postgraduate courses given in 2004

Kurt APPERT, Stefan BRUNNER, Jean-Marc MORET: "*Advanced theory of plasmas*" (course PY-08 of the EPFL doctoral school)
Objectives: complete the theoretical knowledge acquired before the post-graduate studies. Contents: kinetic theory of gas and plasma, relaxation processes in a fully ionised plasma, classical transport, waves in inhomogeneous plasmas, non linear phenomena

Nadine BALUC, Robin SCHAUBLIN, Philippe SPÄTIG: *"Multiscale Approach of Plastic Deformation of Metals and Alloys"*
This 28-hour course is part of the EPFL Doctoral School in Materials Science and Engineering (PY-16 course). It is aimed at introducing the fundamental phenomena of plastic deformation of metals and alloys, and at providing the necessary background to understand the multi-scale nature of the plastic deformation from the atomistic scale up to the continuum one. The course is divided into eight chapters: 1) elasticity, 2) plasticity, 3) finite element simulations, 4) dislocations, 5) strain hardening model, 6) molecular dynamics simulations, 7) kinetic Monte-Carlo simulations, 8) discrete dislocation dynamics simulations.

Jean-Marc MORET, Antoine POCHELON, Olivier SAUTER, Henri WEISEN: "*Physics of magnetically confined plasmas*" (course PY-09 of the EPFL doctoral school)
Objectives. provide the physics basis of magnetics fusion. Contents: magnetic confinement, transport in magnetically confined toroidal plasmas, kinetic therory of waves in a magnetised plasma, heating and current drive by RF waves and neutral beam

Doctorate degrees awarded during 2004

Alberto BOTTINO: *"Modelling of magnetically confined plasmas" (Thèse No. 2938(04))*
In this thesis we have investigated the effect of magnetic shear and applied radial electric field on the linear stability of electrostatic microinstabilities, namely the ion temperature gradient (ITG) and trapped electron modes (TEM), using the new global electrostatic linear particle-in-cell (PIC) code LORB5. In LORB5, the ion dynamics are described by a gyrokinetic model based on a Vlasov-Poisson system in which the fast ion cyclotron motion has been averaged out. The model includes the effect of an equilibrium ExB flow. Trapped electrons are modelled using drift-kinetic equations. Passing electrons are considered to respond adiabatically to the perturbation.
Simulations of ASDEX Upgrade and JET discharges show that several physical mechanisms contribute to the stabilisation of electrostatic modes in the presence of an ion internal transport barrier (ITB). In particular, reverse magnetic shear and the local value of the electron to ion temperature ratio can cause the complete stabilisation of modes in the negative shear region even in the absence of ExB flow. Nevertheless, the ExB flow stabilisation is required if the ITB is partly localised in the positive shear region.
Electron ITBs in fully non-inductive TCV discharges are characterised by weak toroidal rotation. Global simulations show that the reverse magnetic shear has a very strong stabilising effect on trapped electron modes, found to be the dominant instability for these equilibria. This suggests that current profile modification alone can explain the presence of an ITB.
Moreover, the local value of the ion temperature appears not to have a significant role in the formation of the barrier. In addition to this, an important contribution has been provided to the development of the global nonlinear PIC code ORB5 leading to remarkable particle and energy conservation properties of the numerical scheme.

Jean-Yves FAVEZ: *"Application of modern control methods to a tokamak plasma"* (Thèse No. 3034(04))
The control of the current, position and shape of an elongated cross-section tokamak plasma is complicated by the instability of the plasma vertical position. In this case the control becomes a significant problem when voltage saturation of the

power supplies is considered. In practice, during large plasma disturbances, such as sawteeth, ELMs and minor disruptions, voltage saturation of the power supply can occur and as a consequence the vertical position control can be lost. If such a loss of control happens the plasma displaces vertically and hits the wall of the vessel, which can cause damage to the tokamak. The consideration and study of voltage saturation is especially important for ITER. Due to the size and therefore the cost of ITER, there will naturally be smaller margins in the Poloidal Field coil power supplies implying that the feedback will experience actuator saturation during large transients due to a variety of plasma disturbances.
The thesis was focused on the following main objectives: i) the stability analysis of the tokamak considering voltage saturation of the power supplies and ii) the proposition of a new nonlinear controller which enhances the stability properties of the tokamak under voltage saturation and iii) the proposition of a controller which takes into consideration the problem of reducing the AC losses in superconducting coils. Furthermore, we focus on the application of the proposed new controller to tokamaks. Since this controller is a state feedback controller one of the major problems is linked to the state reconstruction. Other pertinent topics are: i) the study of the effect of the disturbances on the closed-loop system stability, ii) the problem inherent to the nature of a state feedback controller when we want an output of the system to track a reference signal and iii) the discussion of the detrimental effects on stability if a pure time delay or a limited bandwidth are added to the closed-loop system, as is the case in reality.
For the purpose of the analysis, synthesis and validation of the new proposed controller we introduced and discussed the properties of the linear tokamak models RZIP and CREATE-L and the nonlinear tokamak code DINA.
The validation of the proposed controller was carried out by means of simulations. We presented results for ITER-FEAT and JET using the linear tokamak model CREATE-L. Finally, we began validation for the case of TCV using the nonlinear DINA-CH code.

Malko GINDRAT: *"Experimental study of the behaviour of a DC plasma spraying torch operated at low pressure" (Thèse No. 3120(2004))*
Low Pressure Plasma Spraying (LPPS) processes use a DC plasma jet expanding at low pressure for fast deposition of dense coatings in a controlled atmosphere. Low pressure plasma jets present unconventional properties such as low collisionality, large dimensions and supersonic flow. Therefore specific diagnostics have to be adapted to these conditions.
Imaging has been used to allow a qualitative description of the plasma jet topology for different pressures and torch parameters. It has been shown that different types of flow regimes with respect to the chamber pressure exist: below 45mbar the jet is under-expanded and above 45mbar the jet is over-expanded.
The enthalpy probe diagnostic tool, extensively applied on atmospheric plasma jets, has been modified to allow gas sampling from the plasma jet at low pressures. A shock wave appears in front of the probe when it is immersed in a supersonic plasma jet, making the interpretation of enthalpy measurements more difficult. However, determination of the free-stream enthalpy, Mach number and temperature were possible on over-expanded jets using two different interpretation methods.
Measurement of plasma jet properties such as the Mach number, electron density and temperature were performed using double Langmuir probes and Mach probes. In particular, under-expanded jets are studied in detail by performing complete mappings of plasma jet properties at pressures below 10mbar. These results show that the measured physical properties are consistent with the jet flow phenomenology, such as the presence of periodic expansion and compression zones, the effect of the pressure and the location of the shocks.
Boltzmann plots have been used to evaluate the deviation from local thermodynamic equilibrium (LTE) as a function of the working pressure and the

location in the plasma jet. It has been shown that the plasma jet is closer to LTE in the compression zones and close to the axis. Measurements of spectral line broadening due to the Stark effect allowed us to determine the electron density for under-expanded jets and give similar results to electrostatic probe measurements. On the other hand, excitation temperatures are systematically lower than the electron temperature for the same plasma conditions.
These results contribute to the understanding of the supersonic plasma jet behavior at low pressure and can be used to quantify the deviation from LTE. The extensive mapping of the measured physical properties of the jet will also serve as input for modeling.

Petri NIKKOLA: *"Simulations of electron cyclotron wave propagation in TCV" " (Thèse No. 3048(04))*
The main objective of the thesis was to understand electron cyclotron current drive (ECCD) experiments with very high microwave power density, the operational regime of TCV. Various types of plasmas were analysed with a Fokker-Planck code including fully ECCD driven discharges, plasmas with ECCD and inductive current components as well as plasmas with an electron internal transport barrier (eITB). The ECCD efficiency in this operational regime was found to be dominated by an interplay between quasilinear effects and radial transport. Without radial transport the simulation results were in strong disagreement with the experimentally measured global ECCD efficiency which is known with good accuracy in TCV. However, the observed efficiencies could be reproduced with transport levels in agreement with an experimental lower limit. In addition, the measured total plasma energy could be reproduced only using radial transport. Since radial transport also causes the wave driven current to diffuse radially it also affects the current density profile which can not be measured in TCV. In particular, the simulated current profiles show that in plasmas with an eITB the current density profile is hollow and its maximum is located in the region of the eITB.

Pavel POPOVITCH: *"Electromagnetic wave propagation in 3D plasma configurations" (Thèse No. 3063(04))*
We have developed and applied a new full-wave solver for 3D plasmas. The code determines a global solution for the propagation of the small-amplitude perturbations excited by antenna currents in a stellarator geometry. No assumption is made on the smallness of the wavelength in comparison with the characteristic gradient scale of the plasma properties. The potential formulation of the Maxwell's equations is used to avoid spurious solutions in the spectrum. The discretisation with finite elements radially combined with Fourier decomposition in the poloidal and toroidal directions makes the code a particularly efficient tool in the Alfvén frequency range. The code is implemented in Boozer magnetic coordinates and uses VMEC equilibria recalculated with TERPSICHORE. A full cold plasma model with finite electron inertia is implemented for the plasma description. Special care is taken to treat the magnetic axis and to ensure the unicity of the numerical solution and the energy conservation. A modification of finite elements near the axis helps to improve the convergence and to avoid an unphysical energy sink. Successful comparisons have been made with the existing LION code as well as with the experimental measurements of the TAE frequencies in a JET discharge. The code has been applied to the LHD stellarator geometry in the Alfvén frequency range. Energy is conserved with an accuracy of <0.05% for these calculations. Wave propagation in the ion cyclotron range of frequencies in tokamak and mirror geometries has been analysed. The position of the antenna (low- or high-field side) has similar effects in these two configurations with different symmetries.

External Students

Ph.D. Theses supervised by CRPP staff at the end of 2004

Laura ABRARDI: "*Study of density fluctuations in JET*"
We developed a software code to analyse the spectral and correlation properties of density fluctuations, particularly for application to reflectometry measurements on the JET tokamak. The software was applied to selected JET discharges, in order to determine the behaviour of edge turbulence during ELMs. The project was completed in April 2004.

Paolo ANGELINO: "*Gyrokinetic model for electron and ion dynamics in axisymmetric plasma configurations*"
The physical model implemented in the global nonlinear electrostatic PIC code ORB5 has been extended and improved. The work focused on the inclusion of the flux surface average component of the electrostatic potential in the quasi-neutrality equation. This term arises from the adiabatic response of the electrons on the magnetic surfaces. This term is crucial for a correct simulation of the zonal component of the electrostatic potential in global non linear simulations.
The geometrical mode coupling induced by toroidicity has to be taken into account. Therefore, the computation of the Vlasov equation requires us to solve an integro-differential problem. The algorithm has been implemented in ORB5 and successfully tested. Benchmarks against simplified cylindrical models have been performed. The resulting code has been used to study the effects of the toroidicity on the nonlinear turbulence suppression induce by zonal flows. These simulations were performed also in realistic shaped MHD plasmas, including reconstructed equilibria of the TCV discharge 21655. The latter showed the unique capability of the resulting code of simulating experimental plasmas. Therefore ORB5 is now a useful tool for physical investigation of plasma turbulence and heat transport.

Gilles ARNOUX: *"Plasma heating at the 3rd harmonic of the electron cyclotron frequency"*
TCV is the only tokamak which uses a 1.35 MW 3rd harmonic X-mode (X3) EC heating. The RF beam is launched from the top of the vessel to obtain full single pass absorption whereas other beams systems can be launched from the lateral side of the Tokamak. The fact that full single pass absorption is not guarantee and that the beam is launched from the top constitutes a specific field of research.
The experiments performed in 2003 showed that the X3 power absorption strongly depends on the injection angle and led us to install a real time feedback control system on the X3 launcher. The feedback signal is obtained using a synchronous demodulation technique and X3 mirror control is fed through a PID controller. It has been demonstrated this year that the system is able to lock the launcher on its optimal angle in typical plasma configurations. Further studies are underway to improve the system and extend the possibilities of use.
The real time feedback control system has allowed further absorption studies. The absorption dependence on the electron temperature and density has been measured varying the injected power up to 1.35 MW. Full single pass absorption has been measured when the maximum available power is injected and the central electron temperature has been increased by a factor 3. The optimal launching angle dependence on the electron temperature and density has also been measured using the feedback control system. These measurements are systematically compared with simulations performed by a linear ray-tracing code called TORAY-GA. And TORAY-GA results are compared with the results produced by the beam-tracing code ECWGB developed in CNR Milano.
For the first time, a clear change in the ELM type has been seen in H-mode in the presence of X3 heating.

Raul BONADÉ: "A *study of the constitutive behavior and fracture behavior of ferritic and martensitic alloys"*
In order to assess the size/geometry effect on fracture toughness in the transition from the ductile to brittle mode, we simulated the stress/strain fields at the crack tip by finite element analysis. A two dimensional model with ABAQUS 6.3-4 was built to evaluate the in-plane constraint loss for bend bars and compact tension specimens. The crack tip was modeled with an initial root radius ρ_o to allow blunting. For cleavage conditions, the effect of specimen size/geometry on fracture toughness can be quantified in the transition by defing a cleavage criterion related to the attainement of a critical stress stress σ^* encompassing a critical area A*. The size/geometry effect on fracture means that for different size/geometry various different critical appplied stress intensity factors K_c (or critical energy relase rate J_c) are required to reached the σ^*-A* criterion. If the dimensions of the specimen are large with respect to the those of the process zone in which cleavage is initiated, then fracture toughness can be regarded as a material property. To simulate these so-called small scale yielding (SSY) conditions, we also developed our own modified boundary layer model, For the bend bar geometry, we calculated the actual to SSY ratio J/J_{ssy} (J being the energy release rate) require to produce the same critical area A* at a normalized maximum principal stress contour σ^* as a function of the applied J itself. We have also investigated the influence of moderate variations in the constitutive behavior on fracture toughness and shown that this last parameter is highly sensitive to the constitutive behavior.
As far as the constitutive behavior is concerned, we have identified two distinct temperature ranges where the relationship between the flow stress and the dislocation density is different. One corresponds to that where the Peierls stress controls the mobility of the dislocations and the second one corresponds to the high temperature regime where the dislocation motion is similar to that of the fcc metals.

Alessandro BORTOLON: *"Charge eXchange Recombination Spectroscopy"*
The Charge eXchange Recombination Spectroscopy diagnostic can provide radial profiles of ion temperature, toroidal velocity rotation and density profiles of a given impurity species. While Ti profiles are ordinarily evaluated by each pulse (observing the CVI 529.1 nm line), for v_i and n_i a more delicate analysis is needed. A wavelength calibration procedure has been established: a known Ne spectrum is acquired after each plasma discharge by means of two Ne lamps. Each lamp is provided with a glass diffuser which ensures the uniformity of illumination of fibres and their complete filling. Furthermore a new analysis program has been developed allowing the deconvolution of the instrumental function (determined by the Ne the calibration spectrum) for all acquired channels, recovering a correct vertical alignement of all the channels.
Extended measurements of C rotation profiles in different plasma conditions has been performed, with typical uncertenties of the order of 10%.

Yann CAMENEN: *"Confinement studies in shaped and extremely shaped plasmas heated by electron cyclotron waves"*
Electron heat transport experiments were performed in 2003 at two plasma triangularities, δ=0.2 and δ=0.4, using radially localised electron cyclotron (EC) heating to vary the normalised electron temperature gradient R/L_{Te}. During this present year, these experiments have been analysed in detail. Local gyro-fluid (GLF23) and global collisionless gyro-kinetic (LORB5) linear simulations have been performed to determine the micro-instabilities responsible for anomalous heat transport in these plasmas. Ion temperature gradient (ITG) and trapped electron (TE) modes are found to be unstable. TE modes are the most unstable modes, except at the lowest R/L_{Te} values where they are stabilised and where ITG modes dominate. In all these plasmas, the high $Z_{eff}T_e/T_i$ values in these plasmas lead to a complete stabilisation of the electron temperature gradient (ETG) modes. Experimentally, a strong dependence of the electron heat diffusivity χ_e on the

electron temperature is observed. No such clear dependence of χ_e is observed on R/L_{Te} and R/L_{ne}, in contrast to the results from GLF23 simulations. The plasma collisionality ν_{eff} is found to reduce strongly the electron heat transport, which is consistent with the stabilisation of TE modes while increasing ν_{eff} in the simulations. However, the variation of ν_{eff} with δ prevents us from concluding a dependence of χ_e on δ. To answer this question, new experiments have been carried out keeping ν_{eff} constant while varying δ from –0.4 to 0.4. The analysis is proceding.
Concerning the diagnostic part of this thesis, a new soft X-ray detector (DMPX) which consists of two superimposed wire chambers has been commissioned, replacing the single layer detector prototype (MPX). The observation of the soft X-ray plasma emission in two energy ranges will allow us to compute the electron temperature profile with both high spatial and temporal resolution. A first step in this direction has been made inverting the line integrated plasma emissivity observed by the DMPX to give local emissivity values. This has allowed us to show that the formation an eITB is very radially localised.

Emiliano CAMPITELLI: "*Study of the relation between irradiation-induced microstructure and mechanical properties in Zircaloy*"
An assessment of the plastic anisotropy and of the neutron irradiation hardening in Zircaloy was performed. This was done with non-standard mechanical tests, namely the small ball punch tests. With the aid of a finite element (FE) model, it is possible to evaluate the irradiation-hardening. First, our FE model, initially designed for isotropic materials, had to be further developed to take into account the effects of the sample plastic anisotropy. Within the framework of Hill's theory for anisotropic yield function, an approximate description of the mechanical anisotropy of Zircaloy was implemented in the FE model. In particular, it was shown that transversal anisotropy can be as good as planar anisotropy in reproducing the force-deflection curves up to the maximum load, however the second case is more expected on a microstructural basis. Small punch test results were carried out on Zircaloy cladding tube material that was neutron irradiated in service at a Light Water Reactor during 3 reactor cycles (~10dpa). An assessment of the irradiation hardening was consistently done resulting in a yield stress increase of 300 ± 20MPa. We mention that the model was also applied to other materials, in particular the EUROFER97, to assess the strain-hardening at large strain as well as the irradiation-hardening.
Another FE model to describe ring tensile tests was developed. It was possible to reconstruct the first part of the load-elongation curves but the anisotropic model does not allow reconstruction of entire curve. This suggests that not only the anisotropy of the yield function has to be considered but also that of the strain-hardening.

Lukas DERENDINGER: "*Design of low-energy plasma sources*"
Recently it was shown that the low-energy plasma (LEP) technique allows high rate epitaxy of strained Si and SiGe. The low-energy plasma source is a novel way towards modern industrial plasma sources design. Its simplicity and its effectiveness make this source a promising candidate for processing various materials. However, before industrialisation of the plasma source and its process is reached, various physical and chemical problems have to be solved. The problems encountered are mainly related to the ionisation source, a key element in the design of the low energy plasma reactor. Film inhomogeneity and heavy metal impurities are strongly related to the design of the ionisation source and the discharge geometry. Detailed investigation of the physics of the ionisation source are foreseen to improve the performance with respect to film homogeneity, deposition rate, filament lifetime and material compatibility. For this reason, plasma diagnostics will be applied to an ultra high vacuum (UHV) LEP from Unaxis. In particular the gas pressure dependence of the plasma parameters will also be investigated. Modelling technical items such as gas flow in the reactor is foreseen as well as modelling of

the reactive LEP plasma itself. The aim is to have an industrial LEP reactor for epitaxy of SiGe by the end of the project.

Antoine DESCOEUDRES: *"Application of plasma emission spectroscopy to the electrical discharge during EDM"* (Top Nano 21 project n° 5768.2)
Electrical Discharge Machining (EDM) has been a well known machining technique for more than fifty years. Nowadays it is widely used in a large number of industrial areas. However, to improve on the performance of EDM, it is necessary to understand the electrical discharge in detail. Optical emission spectroscopy is used to diagnose the plasma created during the machining process. The plasma is cold (0.7eV), and extremely dense (electron density up to $2 \cdot 10^{18} cm^{-3}$ at the beginning of the discharge). Time-resolved spectroscopy shows that the density is decreasing afterwards with time. The low temperature and the high density measured prove that the EDM plasma is weakly non-ideal. In addition, an endoscope has been used to perform spatially resolved spectroscopy and imaging of the plasma. When using two different materials for the electrode and for the workpiece, an asymmetry in the plasma contamination is observed, proving the feasibility of spatially resolved spectroscopy on such small plasmas (typical gap is 100μm). Pre-breakdown phenomena are also studied, especially bubble creation and streamer propagation in the liquid dielectric. Short current pulses are measured before the breakdown (amplitude ~mA, duration ~10ns). Each pulse is associated with the propagation of a streamer and probably also with the creation of a bubble.

Emiliano FABLE: *"Simulation of plasma transport"*
The problem of FIR (Far InfraRed interferometer) signal inversion to obtain local density profiles has been solved with the singular value decomposition (SVD) method and the software has been developed for TCV.
The ASTRA code has been installed as a tool for transport simulation for TCV conditions, analysis of steady state profiles and evolutionary regimes. Coupled with the GLF23 turbulence model, it gives a reliable and powerful possibility to study advanced scenarios for TCV campaigns.
Work has started on a tool for the analysis of gyrotron operational scenarios (Bindslev-type diagrams).

Sergi FERRANDO i Margalet: *"Bootstrap Current and Stability in the Asymptotic Regime in Quasi-Symmetric Configurations"*
The relevance of the non-symmetric modes of the magnetic field structure on the calculation of the Bootstrap Current (BC) in reactor-size quasisymmetric stellarator devices is investigated. The BC effects on equilibrium and stability in reactor-like scenarios (i.e., high density, high temperature and high beta) for this kind of configurations has also been studied and shown to have a strong influence. For these cases a way to externally affect the rotational transform seems to be necessary. One way to do so is to use Electron Cyclotron (EC) waves with a frequency comparable to that of the electron (or its harmonics). Under some particular conditions the resonance between wave and electrons results in an asymmetric deformation of the electron distribution function, creating a net current inside the plasma. Under reactor-like conditions, however, the high density does not allow the EC waves to propagate due to a frequency cut-off. In those cases, however, the wave may undergo a mode conversion and continue to propagate as a purely electrostatic wave called an Electron Bernstein (EB) wave. In our present research, the use of EB waves to drive current inside reactor-like plasmas is investigated along with its effectiveness at to compensating the alterations caused by the inherent BC of the configuration.

Barbora GULEJOVA: *"Exploitation of the new AXUV diagnostic"*
A new system of 7 AXUV diode cameras has recently been installed on TCV. This diagnostic will give unprecedented poloidal coverage, at a single toroidal location, of

the distribution (after tomographic inversion) both of the total photonic plasma radiation (at energies in the range 10eV to ~6keV) and, by a separate array of filtered diodes, of the Lyman-alpha radiation at 120nm from excitation of hydrogenic atoms located in the cool plasma periphery. These diodes are extremely fast and their amplifier electronics has already been designed giving a system bandwidth in the range from DC to ~100kHz. The thesis will aim to investigate the physics of fast transient events (ELMs, disruptions) through their radiation characteristics and, in conjuction with modelling using the SOLPS5 fluid-Monte-Carlo code package, study the distribution of neutrals in the TCV edge, particularly during plasma detachment. The latter will also hopefully be facilitated by comparison of the AXUV data with that from an existing set of foil bolometer cameras, also measuring plasma radiation, but sensitive to both photons and the energy deposited by neutral particles.

Jan HORACEK: *"Measurement of edge electron temperature and turbulence in the tokamak plasma boundary"*
Continued analysis of data from 2003 has shown that plasma fluctuations in the TCV tokamak scrape-off layer (SOL) exhibit statistical properties which are universal across a broad range of discharge conditions. Analysis of the time series of density fluctuations from the separatrix to the plasma-wall interface, yields a probability density function (pdf) which conforms closely to a Gamma distribution. In the wall vicinity the density fluctuations exhibit clear evidence of self-similarity and are characterised by a pdf with a universal shape and with a standard deviation proportional to the mean density. It is also found that radial particle flux fluctuations scale solely with the mean density. Such findings, if confirmed elsewhere, indicate that it may be possible to improve the prediction of transport in the critical plasma-wall interaction region of future large scale tokamaks. Extensive new measurements of the parallel SOL flow have been performed using a newly designed probe head. Correlations with the turbulent driven radial particle flux have been studied, following recent suggestions in the literature that the anomalously strong SOL flows measured in all tokamaks might be partially generated by coupling of cross-field turbulence transport into parallel flow. The latter is indeed found to be very large and some evidence has been found for a qualitative link between the magnitude of the flow and the size of turbulent ExB driven fluxes.

Sébastien JOLLIET: *"Non-linear gyrokinetic simulations"*
Global particle-in-cell (PIC) simulations are a very useful tool for studying the time evolution of turbulence induced by ion-temperature-gradient (ITG) instabilities. Unfortunately, the linear code LORB5 and its non-linear version ORB5, which can simulate such instabilities, require high computational power. In order to study more sophisticated models, we need to optimize these codes.
In the original version of LORB5, the equations of motion are solved on a cylindrical grid, whereas the Poisson equation is solved on a polar grid. As a consequence, the code systematically goes from one grid to another, which implies losses of CPU time and precision.
Therefore, the gyrokinetic model has been implemented in LORB5 using a single magnetic coordinate system. First results show an improvement of the convergence and a gain of CPU time. This method would be very useful for the non-linear code ORB5, where a simulation can last several days. By reducing the simulation time, we will be able to add a drift-kinetic model for trapped electrons.

Sun Hee KIM: *"Full tokamak discharge simulations using DINA-CH"*
This recently started PhD thesis aims at full non-linear tokamak simulations using the DINA-CH free boundary evolution code. Integration of the Cronos transport and heat source modelling code will be part of the work, which will concentrate on features of tokamak modelling which are inadequately described by fixed boundary

or prescribed boundary transport simulations. Initial studies are focussing on understanding the ELM triggering seen on TCV and ASDEX-Upgrade tokamaks.

Igor KLIMANOV: *"Study of the electron distribution function during Electron Cyclotron Current Drive (ECCD)"*
The study requires the development of new diagnostic and analysis tools. A new 24-channel Low Field Side (LFS) radiometer has been built. Two antennas (at Z=0 cm and Z=21 cm) are installed and allow conventional Electron Cyclotron Emission (ECE) measurements. Third ECE LFS line was connected to the steering launcher that allowed oblique ECE and Electron Bernstein Emission (EBE) measurements. Poloidal and toroidal angle sweeps during the plasma discharge are possible as well, opening the way to ECE tomography and Doppler shifted ECE measurements (a rare possibility to get information about electron distribution function in the direction other than perpendicular to the magnetic field). A numerical module to simulate the ECE emission spectra at any angle for any distribution function has been developed. The code is combined with the best available plasma ray-tracing code TORAY-GA. The code is compatible with the Fokker-Plank code CQL3D. First experiments dedicated to the study of the electron distribution function during ECCD and during magnetic reconnection events (big amplitude sawteeth) were done on TCV.

Alessandro MARINONI: *"Study of edge fluctuations in JET"*
The goal of the work is to investigate density fluctuations in the edge region of the JET tokamak by microwave reflectometry, particularly the X-mode correlation reflectometer which can in principle yield the fine-scale spatial correlation structure of the turbulence. The applicability of advanced techniques such as wavelet analysis and coherent averaging is being studied, in particular for fluctuations during ELMs, on selected past discharges, with a view to proposing dedicated measurements in the next campaign. Future work will also include a feasibility study for fluctuation diagnostics in TCV.

Janos MARKI: *"Impurity transport in TCV and JET"*
This thesis will concentrate on comparing the transport of heavy impurities in the TCV and JET tokamaks.

Mikhail MASLOV: *"Particle transport and confinement"*
This thesis will concentrate on the physics underlying the transport of the working gas species in all tokamaks.

Andrei MARTYNOV: *"MHD activity of tokamak plasmas"*
Detailed analysis of TCV experiments on the effect of the plasma triangularity on the sawtooth period have shown that the ideal growth rate of the internal kink is much higher at slightly negative triangularity than the usual values in present experiments. This explains why the sawteeth are expected to be triggered by ideal internal kink rather than resistive modes. It also explains the qualitative and quantitative agreement of the observed experimental behaviour and the predictions with the KINX calculations. A review of the analytical contributions to the ideal internal kink growth rate, or equivalently to the potential energy, has been performed to compare with our scaling and with the experimental results. Even with the inclusion of higher order terms and new shaping terms recently published, the combined analytical formula cannot reproduce the experimental observations. It is also shown that it cannot reproduce correctly the growth rates calculated by KINX when the inverse aspect ratio is larger than 0.2-0.3, thus for present tokamak conditions.
The n=1 ideal kink mode responsible for disruptions or minor crashes in electron internal transport barrier discharges in TCV has been identified to correspond to infernal modes. However they depend both on the pressure and on the current

profile, as expected in general geometry and equilibrium. These modes are also similar to the ones responsible for plasma disruptions in reverse shear scenarios in other tokamaks, when they are not stabilised by rotation. Therefore the operation limits studied in eITBs on TCV are similar to the operation limits studied in resistive wall modes experiments, with regards to the ideal stability limits.

Nicolas MELLET: *"Extension of the LEMAN code to include finite temperature effects in the dielectric tensor to resolve singular mode structures and study effects of mode conversion without having to include gyroradius effects as in the PENN code"*
The inclusion of finite electron mass already allows conversion to the quasielectrostatic mode. The investigation of finite temperature effects on Afven eigenmodes in cylindrical, axisymmetric, helical, mirror and fully 3D geometries and application of the LEMAN code to the ion cyclotron resonance range of frequencies to investigate the propagation and absorption properties in 2D and 3D confinement systems, in particular the LHD device, constituting the main objectives of this thesis. This may require a modification of the LEMAN code, to adapt parallel processor solvers to invert a matrix equation because the memory requirements to obtain converged solutions is expected to be very large (>30GB). Eventually this will be interfaced with the VENUS-df code to examine the impact of the wave fields on particle orbits and distribution functions.

Stefan MUELLER: *"Basic investigation of turbulence and transport in toroidal plasmas"*
The plasma confinement mechanism by superimposing a small vertical magnetic field over the dominant toroidal field has been studied in the TORPEX experiment. A two-fluid model taking into account the main effects of the spiral-like magnetic field geometry has been developed and tested against experimental results, showing good general agreement.
A new system of Langmuir probe arrays, dedicated to turbulence imaging, has been installed on the TORPEX device. Covering the whole poloidal cross-section with 86 tips forming a hexagonal grid with a grid constant of 35mm, the project represents the first attempt at simultaneous imaging the whole cross-section of a plasma column. The first operational tests were passed successfully.

Gennady PLYUSHCHEV: *"Turbulence studies in TORPEX"*
This work, within the TORPEX basic experimental plasma group, focuses on the problem of the development of drift wave turbulence and on its effect on the particle and energy cross-field transport. We will start a new line of investigation by comparing the character and the effect of turbulence in cases with open and closed flux surfaces in the TORPEX toroidal magnetised plasma.

Mario PODESTA: *"Experimental studies of transport properties in toroidal plasmas"*
TORPEX is a toroidal device where plasmas of Argon and Hydrogen are generated and heated by microwaves in the electron cyclotron range of frequencies. In the last year, the basic processes leading to ionisation of the neutral gas have been investigated, along with the resulting plasma parameters (density, electron temperature and plasma potential). The role of electron cyclotron and upper hybrid frequencies in the resonant absorption of the injected waves has been experimentally confirmed by looking at the response of the density to a modulation of the injected power. The possibility of modifying the density profile by changing the level of the injected power has been explored. An expression for the global particle balance as a function of the absorbed microwave power, based on the power absorption and ionisation mechanisms, has been derived. It allows us to predict the global response of the plasma to different values of absorbed microwave power and the range of achievable parameters. The spatial profile of the particle source has also been investigated and modelled on the basis of a comparison between the experimental data and the results of a simple numerical code.

Francesca Maria POLI: *"Study of fluctuations and turbulence in toroidal plasma"*
The 2004 experimental TORPEX campaign has focused on the characterisation of drift waves in both Argon and Hydrogen plasmas. The power spectra of density fluctuations exhibit peaks at low frequency (less than the ion cyclotron frequency), whose width and amplitude appear to depend on the density gradient. Different regimes have been explored to quantify the effect of a radial electric field on the phase velocity. Linear and nonlinear properties of the waves have been studied through higher order spectral analysis including wavelet analysis. A new Langmuir Probe for the study of both density and potential fluctuations has been designed and is under development. The new probe will provide the measurement of the phase shift between density and potential fluctuations, which is necessary to completely identify the nature of the instabilities. The probe has been mounted on a shaft that provides radial displacement into the plasma and a more complete system to move the probe radially and vertically direction is under design.

Amuthan RAMAR: *"Effects of oxide dispersion on the microstructure and mechanical properties of a reduced activation ferritic/martensitic steel"*
The upper operational temperature of the reduced activation ferritic/martensitic (RAFM) steels, like EUROFER 97, is presently limited by a drop in mechanical strength at about 550°C. It has been recently shown that it can be significantly increased to about 650°C by the addition of a fine dispersion of strong particles. However, this increase in strength is accompanied by a strong decrease in fracture toughness of the alloy. The first part of this thesis is aimed at producing and characterising a batch of the EUROFER 97 RAFM steel reinforced with 0.3wt.% Y_2O_3 particles and containing a small amount of Ti in an attempt to improve the fracture properties of the alloy. A first ingot has been produced by powder metallurgy (ball milling and hot isostatic pressing). Transmission electron microscopy (TEM) observations revealed a martensitic morphology, with lathes and a high dislocation density. Large particles, between 10 and 500nm in diameter, have been observed. Their distribution is heterogeneous, which is in principle detrimental to mechanical properties. In-situ TEM chemical analyses revealed that the large particles are made of a titanium-yttrium oxide. Tensile tests showed that the material has an ultimate tensile strength in the GPa range from room temperature to about 400°C but with very limited plasticity (the total plastic strain is below 1%). Above 400°C, the strength starts to decrease and reaches 350MPa at 600°C, with a total plastic strain of 3 to 5%. Charpy impact tests revealed that the material is brittle over the temperature range from room temperature to 500°C.

Andrea SCARABOSIO: *"Studies on MHD activity as a function of plasma shape in standard TCV scenarios and MHD phenomena in advanced scenarios"*
During the last campaign a series of experiments was performed in order to systematically study the dependence of the toroidal rotation velocity profiles on major plasma parameters, like the direction and intensity of the plasma current, electron density and plasma shape. All experiments were performed in quasi-stationary Ohmic L-mode. Although the Ohmic L-mode has the lowest performance of all tokamak regimes, it constitutes a test for any momentum transport theory. Experiments with positive and negative plasma current clearly show that the carbon flows at all radii in the counter-current direction and the velocity profile symmetrically flips around zero velocity when changing the sign of I_p. The rotation profiles are normally monotonic in the outer part of the plasma and flat in the centre. This flat region corresponds to the region inside the q=1 flux surface and it is clearly connected with sawteeth activity. Other MHD modes present in the plasma reduce the velocity over all the cross section and in case of a locked-mode the plasma completely stops its toroidal rotation. The electron density has strong effects on the carbon rotation profile. Higher density results in a lower level of rotation. Similarly, for very low density ($<10^{19}$ m^{-3}), the velocity profile is usually

flatter. The comparison of carbon rotation with MHD rotation, all comparison with neoclassical theory and a simple model for momentum transport will be developed.

Christian SCHLATTER: *"Studies of the fast particle distribution in TCV and JET"*
The thesis is devoted to fast particles. Experimental data from the Neutral Particle Analysers (NPA) of TCV and JET for regimes involving both fast ions and electrons will be used to address the following topics:
Simulation of the ion neutralization probability with the aim of modeling the ion distribution function on TCV;
Characterisation of the slowing down of the fast ions by injection of neutrals using the Diagnostic Neutral Beam Injector (DNBI);
Study of the link between the fast ion tail of the ion distribution function and ECCD efficiency (TCV) or plasma rotation (JET) in discharges with ECH (TCV) or ICRH (JET);
Study of the radial transport of fast ions on both tokamaks and their relation to instability control.
In 2004 the neutralisation of fast ions has been studied at JET. On TCV the first measurements with the new Compact NPA in ohmic regimes have been carried out.

Hannes SCHMIDT: *"Characterisation of a high density, large-area VHF plasma source"*
The objective of this project is a feasibility study of a novel, large-area plasma-based thin film production technique. The successful "proof of principle" for a shaped electrode based on a cylindrical reactor design was given in 2003. The first half of 2004 was marked by setup, installation and diagnostic development activities for a rectangular industrial reactor design (vacuum system, gas supplies, data acquisition system for the optical uniformity measurement system). In the 3rd quarter the standing wave effect at typical industrial frequencies (13.56MHz, 27.02MH, 40.68MHz, 67.80MHz, 100MHz) was measured in a conventional, flat electrode reactor design (with and without plasma). The 100MHz required the construction of a triple stub tuner, which is a pioneering way of impedance matching at VHF. During the 4th quarter the reactor is being converted to the novel electrode design, which is to suppress the standing wave effect at 67.80MHz. The "rectangular proof of principle" is pending.

Karin SCHOMBOURG: *"Study of ELM dynamics"*
ELMy H-mode discharges are considered as the standard regime for ITER. Therefore the understanding of ELM physics and the development of ELM control schemes are very important. On TCV, experiments are carried out to control the ELM frequency by magnetic perturbations. It is well known that by increasing the frequency of the ELMs, their amplitude decreases.
The first studies have been devoted to the determination of the conditions for a successful ELM triggering. Another point is to determine whether the perturbation should be prompt or cyclic to trigger the ELMs. Practically this is done by applying series of pulses with different frequencies, or with random time delay. The reaction of the ELM on the perturbation provides information on their physical process. The interaction between the perturbation, the ELMs and the sawteeth is also studied.

Lukas STINGELIN: *"Beam Cavity Interactions in High Power Cyclotrons"*
Measurements and simulations of the beam-cavity interaction in the PSI 590MeV ring cyclotron were refined during the last year. The Higher Order Mode (HOM) spectra on the cavity and the newly installed radiation probe, located in the intermediate sector of the cyclotron, confirmed the presence of the simulated parasitic vacuum chamber modes, overlapping of HOMs and the temperature-dependence of their resonance-frequencies. In the frame of the collaboration with SLAC, it was possible to simulate the eigenmodes of the entire ring cyclotron with the parallel ESIL-solver in Omega3P, for the first time ever. The 280 calculated

modes were classified into 44 cavity, 18 vacuum-chamber and 218 mixed modes. Their effect onto the beam-quality was estimated from a calculation of the gap-voltages. The eigenmodes are then used in the mode-expansion for the simulation of the beam-excited fields in the particle-tracking from injection to extraction. The refined beam-cavity interaction simulation with OpenMP parallelisation indicated that the rf-phase of the fundamental modes induce a bending onto the proton-bunches and that space-charge effects induce a galaxy-like furling on very short bunches.

Raluca STOENESCU: *"Irradiation effects on the microstructure, mechanical properties and residual stresses in the heat affected zone (HAZ) of stainless steel welds"*
The objective of this thesis is to correlate the residual stress state induced by welding in the HAZ of two stainless steels with the microstructure and the mechanical properties after neutron irradiation in an experimental reactor, and to compare these results with those obtained for a similar material irradiated in a real fission reactor. During the last year, the material irradiated in a fission reactor to a maximum dose of 0.3dpa was investigated by means of tensile testing and transmission electron microscopy. A strong increase in the tensile yield strength and a decrease in the ductility of the irradiated material, with respect to the unirradiated one, have been evidenced. These phenomena were found to correlate well with the presence of irradiation-induced defects such as dislocation loops, black dots, and stacking fault tetrahedra. The investigation of the materials irradiated in the experimental reactor is in progress.

Benjamin STRAHM: *"A new large very high frequency reactor for high rate deposition of microcrystalline silicon for thin film solar cell application"*
A novel very high frequency (VHF) plasma source will be applied for large area ($1m^2$) deposition of amorphous (a-Si:H) and microcrystalline silicon (uc-Si:H) for thin film solar cell production. The use of plasma excitation frequencies up to 100MHz, higher than the standard 13.56MHz excitation frequency, allows us to substantially increase the plasma density and gas dissociation rates without the drawback of high ion energy bombardment of the substrate and consequently damaging. Therefore higher deposition rates at good device quality can be attained. The crucial problem in VHF plasma reactor, the non-uniform voltage on the RF electrode, is solved by using suitably shaped electrodes. The proof of principle of this new reactor has up till now only been made in non-reactive plasmas. In the present project, the novel RF reactor design will be used for the first time in applications, in particular for solar cell production. The aim is to have at the end of the project a high density RF reactor operating at elevated excitation frequencies allowing industrial high rate deposition of a-Si:H and uc-Si:H with a uniformity of –10% on large area substrates relevant for solar cells (typically 1 x $1m^2$).

Alban SUBLET: *"Study of RF atmospheric and near atmospheric pressure glow discharges"*
A preliminary study of the glow discharge in different neutral gas mixtures (He, N_2, Ar) as a function of the pressure (10^3 to 10^5 Pascal) has been done in order to determine the basic characteristics of the plasma. The diagnostics used for this study were: optical emission spectroscopy and electrical measurements (discharge current and voltage, gas voltage...). Three kinds of discharges have been found: glow, multi-peak and filamentary. This study highlighted the role of metastables and of the dielectric surfaces for the establishment and the stabilisation of the glow discharge mode. It also permits us to determine the operation domain of the glow discharge according to the working pressure, voltage and frequency. The same work has been done in N_2/O_2, N_2/N_2O gas mixtures according to the pressure and concentration of oxygen or nitrous oxide. These gases limit the formation of the glow due to their electronegativity and to their efficient quenching of N_2

metastables. Time resolved spectroscopy has been used to determine the evolution of metastable molecules within one discharge cycle at different pressure in N_2 and He.
The adjunction of monomer (HMDSO) for SiOx deposition on polymer films completely modifies the discharge. A few ppm of HMDSO are sufficient to induce a transion from glow to filamentary mode. The coating obtained at atmospheric pressure is inhomogeneous because of the geometry of the discharge cell ($60*60mm^2$) : the chemistry is changing along the gas flow direction. There are two different regions observed : one where surface reactions dominate and the other where volume reactions (powder formation and redeposition) are predominant. The next step is the understanding of these processes and the characterization of the coating for different gas mixtures/power/frequency.

Marco WISCHMEIER: *"Divertor detachment in the TCV and JET tokamaks"*
Efforts have continued in 2004 to understand, through SOLPS5 code simulations, the anomalous divertor detachment regularly observed in TCV single-null lower ohmic discharges. Research during 2003 eliminated two suspected candidates: molecularly enhanced recombination (MAR) assisted by the presence of D_2 molecules and geometry effects. Further refinement has now allowed the inclusion of CD_4 molecules which have been suggested in the literature as a possible strong mechanism by which MAR might reduce target ion fluxes, especially in the relative low density, high electron temperature plasma of the TCV outer divertor plasma. This represents one of the first ever attempts to include hydrocarbon MAR in a full fluid-Monte Carlo simulation of the SOL but has proved unable to account for the observed strong detachment. Strong intermittent ("bursty") cross-field transport, increasing with density has recently been observed in the TCV SOL (and in many other tokamaks). To date, however, the cross-field particle transport coefficient in SOLPS5 simulations has been assumed to be both constant in space (poloidally and radially) and with density. In an attempt to mimic experimental observation, an anomalous convective transport term has been added to the ordinary diffusive ansatz and switched on only in the low field side regions of the plasma equilibrium. Whilst the introduction of such a term does not itself enhance detachment, it turns out that the increased plasma-wall interaction that it provokes on the main chamber walls leads to increased impurity production which strongly influences the SOL energy balance (through radiation) and hence the power flux into the outer divertor. This establishes parallel temperature and density profiles along the outer divertor leg that make particle and momentum removal and hence early detachment possible. There are, in addition, indications that ion conversion processes (MAR) through both D_2 and CD_4 molecules do, under these conditions, seem to contribute to the total reduction in particle flux.

Zhongwen YAO: *"Mechanical properties and microstructure of irradiated metals"*
Nickel a model face centered cubic (fcc) metal being studied for radiation damage due to its still unexplained peculiar behavior under irradiation, contrary to fcc Pd and Cu whose behavior under irradiation is relatively well understood. Within this thesis, single crystalline specimens of pure Ni have been irradiated with high energy protons in the PIREX facility at various temperatures ranging between RT and 350°C to doses ranging between 10^{-3} and 1dpa. Transmission electron microscopy (TEM) observations showed that irradiation-induced defects include stacking fault tetrahedra (SFTs) and interstitial dislocation loops whose size increases with irradiation temperature. For a given dose, the defect densities decrease with increasing irradiation temperature. When examined as a function of dose, they reach a saturation level at about 0.1dpa. Voids appear after irradiation at 250°C and their size and density increase with irradiation temperature; at 350°C their size is about 5nm. A number of TEM image simulations were performed to clarify the problem of visibility of defects in TEM. Tensile mechanical testing showed that radiation hardening appears for a dose as low as 0.002dpa. SFTs were observed to

exhibit a strong pinning efficiency on moving dislocations in in-situ TEM straining tests. Molecular dynamics simulations were performed to investigate the damage accumulation in pure Ni. It was found that the values of physical parameters such as displacement threshold energy and stacking fault energy are of great importance for the evolution of atomic displacement cascades.

Gang YU: *"Small angle neutron scattering investigation of radiation damage in metals and alloys"*
This thesis is aimed at characterising nano-scale distributions of irradiation-induced features in terms of number density, size distribution and chemical composition by using the small angle neutron scattering (SANS) technique. SANS measurements were performed in a strong saturating magnetic field perpendicular to the incident neutron beam, on specimens of the EUROFER 97 RAFM steel following irradiation with high-energy protons in the PIREX facility at 250°C and 350°C to doses of 0.3 and 1dpa. SANS analysis was done assuming a single distribution of spherical nano-features. It was found that all the defect distributions peak below 1nm in size. The number density at a given irradiation temperature increases with dose but the number densities after the irradiations at 350°C are much lower than those at 250°C. Clearly, the sub-nanometer irradiation-induced defects tend to disappear with increasing irradiation temperature by enhanced recombination of point defects and possible coarsening of the clusters. It is also important to emphasise that the features described by these distributions have a size well below the TEM resolution limit.

Alexei ZABOLOTSKY: *"Particle transport in TCV"*
The accurate analysis of particle transport depends critically on the quality of the density profiles. In order to improve noisy JET density profile obtained from Thomson scattering measurements we developed two methods of density inversion of JET multichannel Far InfraRed (FIR) interferometer signals. One method uses top-hat base functions with weight coefficients found by minimization. The main advantage of piecewise functions is that it makes no further assumptions on the density profiles and it is therefore applicable to a large variety of cases. Nevertheless, the method is rather computationally inefficient and does not provide satisfactory results in the case of hollow density profiles or when the number of available interferometer chords is small. To overcome thes difficulties an SVD inversion (SVD-I) method based on singular value decomposition (SVD) was applied at JET. The SVD-I method adopts as base functions the topos provided by biorthogonal decomposition of a sequence of ~50 Thomson scattering profiles. Good agreement between the two methods was observed in most of the cases showing the applicability and reliability of the SVD-I method for JET density profile reconstruction.
Introduction of SVD-I method allowed us to extend the study of JET particle transport performed in 2003 to H-mode discharges. JET H-mode density profiles showed, in contrast to the L - modes, clear collisionality dependence and no l_i dependence, except for low ν_{eff}. No dependence of peaking on <ne>, P_{icrh}/P_{aux}, P_{nbi}/P_{aux}, L_{Te}, or L_{Ti} was found in agreement with observation on ASDEX-upgrade. The difference in behaviour between L– and H – modes was attributed to basic differences in the turbulence underlying the anomalous particle transport.

Costanza ZUCCA: *"Simulations of current perturbation effects on electron internal transport barriers in TCV"*
Internal transport barriers (ITBs) are regions in the plasma core characterised by stabilisation of turbulence, typically associated with local flattening or reversal of the plasma magnetic shear. New experimental results from TCV indicate that the strength of an electron ITB can be modified by adding small positive or negative surface voltage, thereby modifying only the current profile. The aim of the present work was to provide a better theoretical understanding of the evolution of the

current profile in the presence of an edge inductive current perturbation and its influence on steady-state eITB scenarios; this has been done by employing the ASTRA code for predictive/interpretative modelling of transport and current diffusion. The results provide a significant argument for the consistency of the current perturbation effect and the time-scales observed for the modification of the electron energy confinement time: an estimate of the plasma current redistribution time was obtained between 100-200ms. A study concerning the minimum amount of ECCD necessary to produce a zero-shear region has also been performed, with particular emphasis on the ECCD uncertainty. Finally, the relation between the effective current profile modification and the experimental observation that the more reversed the shear the better the confinement has been analysed by simulating plasmas fully sustained by ECCD to which we added the small surface voltage. If positive, this causes a peaking of the inductive current which eventually results in a monotonic safety factor, experimentally related to a weakening or even removal of the original eITB. On the contrary, when the voltage is negative, the counter-inductive current profile leads to a further reversal of the safety factor, which has been observed in strong eITB experiments. The centrally negative inductive current density is the only mechanism that drives the transition of the safety factor profile from monotonic to deeply reversed.

6 PUBLIC RELATIONS ACTIVITIES IN 2004

6.1 General outreach activities

An outreach activity presenting the progress in fusion and plasma science and their related activities was set-up for different levels of education: undergraduates, high school students, elementary school students, teachers at all levels, the general public and government officials. New brochures, posters and flyers were edited on fusion and plasma physics. We have been active via public colloquia, "round tables" and talks on energy issues especially on fusion energy.

We have been maintaining contact with the medias, through press releases and interviews, as well by participating in radio and TV broadcasts, mostly since Prof. M. Q. Tran became EFDA leader.

Organised visits to the CRPP

We welcomed about 800 visitors to the CRPP in Lausanne, mostly in groups of about 20 to 40 people. About 60% of the visitors came from schools, high schools or universities, 80% of the visitors were from Switzerland, the rest from different countries. Among the many visits in 2004 were:

Association of Apprenticeship instructors of Vaud Canton, 35 people
HES Yverdon, students in electronics, 20 people
Ingénieurs de la Côte, 25 people
Open day "jeune public", pupils (12-16 year olds), 220 people
CLUSTER workshop (participants from TU-Darmstadt, Politecnico de Turino and EPFL), 54 people
Classes from St-Gallen and Emmen High-schools
Classes from the Haute Ecole Spécialisée du Valais, 20 people
Association "Jeunes Entrepreneurs" from Luxembourg, 35 people
Catholic Church Committee of Ecublens, 20 people
Swiss Chapter Sigma Xi (Scientific Research Society), 20 people
Delegation from Crédit Suisse, 40 people
Association of the "Anciens élèves de la vallée de Joux", 20 people
"Oser tous les metiers", a day specifically for girls to discover science

During the summer holidays in 2004 we welcomed the regular so-called "Passeports-Vacances" for 45 13 -15 year olds who were able to visit different laboratories at the EPFL.

A talk on 'Fusion as the Energy for the Future' was given to the UNI-3 in Geneva, to a group of relatives at the CRPP and to kids in the frame of summer activities at the CRPP as well.

Talks and conferences

Many staff members of the CRPP presented their professional research activities at our research centre in Switzerland as well as abroad, listed in Appendix B.1.

A presentation by G. Tonetti, was made on 25 septembre at Luceram (Nice) for the Institut des Hautes Etudes pour la Defense Nationale région Côte d'Azur, entitled “La fusion thermonucléaire une solution aux problèmes énergétiques?”

Prof. A. Fasoli presented an educational course at CERN in October 2004: "New Trends in Fusion Research" as part of the CERN Academic Training program ("Applied Physics" and "Physics and Society"). He presented a second general audience talk in Stockholm, Sweden "Burning plasma physics: the new frontier of fusion energy science" as part of the EuroScience Open Forum 2004.

Starmakers

"The Starmakers" movie, for which Pierre Paris and colleagues won a prize in 2003, is now available in English, French, German, Italian, Portuguese, Spanish, Danish, Finnish, Basque, Hungarian and Korean. A version is now being made on DVD.

The 2004 NETS prize

The 2004 NETS prize (New Entrepreneurs in Technology and Science) was awarded to Dr. Irina Condrea, of the CRPP, for her project of science promotion amongst school students from Switzerland. In 2004 she founded Science Passion, a not-for-profit association with the mission of igniting passion for science and demystifying the image of science and of the scientist in schools. This prize is awarded annually by the Gebert-Ruf Foundation, as a part of the Swiss gouvernment program to encourage the entrepreneurial spirit amongst scientists from the Swiss universities and research institutes.

Web activities on http://crppwww.epfl.ch

The main CRPP website is regularly kept up to date, including links to other sites, mainly fusion oriented

APPENDICES

APPENDIX A Articles Published in Refereed Scientific Reviews During 2004

(see CRPP archives at http://crppwww.epfl.ch/archives)

Anghel A., Bruzzone P., *"Jordi, test facility for measurement of contact resistance in full-size conductor terminations"*, IEEE Trans. Appl. Supercond., 14(2), 1460-1463 (2004)

Ballutaud J., Bucher C., Hollenstein Ch., Howling A.A., Kroll U., Benagli S., Shah A., Buechel A., *"Reduction of the boron cross-contamination for plasma deposition of p-i-n devices in a single-chamber large area radio-frequency reactor"*, Thin Solid Films 468 (2004), 222-225

Baluc N.L., Schaeublin R., Spaetig P., Victoria M., *"On the potentiality of using ferritic/martensitic steels as structural materials for fusion reactors"*, Nucl. Fusion 44, 56-661 (2004)

Bonade R., Spaetig P., Victoria M., Yamamoto T., Odette G.R., *"Tensile properties of tempered martensitic iron-chromium-cabon model alloys"*, J. Nuclear materials 329-333 (2004)

Bottino A., Peeters A.G., Sauter O., Vaclavik J., Villard L., ASDEX Upgrade Team, *"Simulations of global electrostatic microinstabilities in ASDEX Upgrade discharges"*, Physics of Plasmas 11(1), 198-206 (2004)

Bottura L., Bruzzone P., Marinucci C., *"Analysis of current redistribution in a CICC under transient heat pulses"*, Advances in Cryogenic Engineering, American Inst. of Physics, 50B, 433-4400 (2004)

Brunetti M., Grandgirard V., Sauter O., Vaclavik J, Villard L., *"A semi-Lagrangian code for nonlinear global simulations of electrostatic drift-kinetic ITG modes"*, Comput. Phys. Comm. 163, 1-21 (2004)

Brunner S., Valeo E.J., *"Trapped-particle instability leading to bursting in stimulated Raman scattering simulations"*, Phys. Rev. Lett. 93, 145003 (2004)

Bruzzone P., *"The index n of the current voltage curve, in the characterization and specification of technical superconductors"*, Physica C, 401, 7-14 (2004)

Bruzzone P., Stepanov B., Wesche R., *"Coupling currents loss results from five NbTi CICC with layout variations"*, Advances in Cryogenic Engineering, American Inst. of Physics, 50B, 812-819 (2004)

Buttery R., Hender T.C., Howell D.F., et al., Sauter O., *"On the form of NTM onset scalings"*, Nucl- Fusion 44, 678-685 (2004)

Campitelli E.N., Spaetig P., Bonade R., Hoffelner W., Victoria M., *"Assessment of the constitutive properties from small ball punch test: experiment and modelling"*, J. Nucl. Materials, 2004

Cooper W.A., Ferrando i Margalet S., Allfrey S.J., Kisslinger J., Wobig H., Narushima Y., Okamura S., Suzuki C., Watanabe K.Y., Yamazaki K., Isaev M.

Yu., *"MHD stability of free boundary quasiaxisymmetric stellarator equilibria with finite boostrap current",* Fusion Science and Technology 46, 365-377 (2004)

Degeling A., Borg G., Boswell R., *"Transitions from electrostatic to electromagnetic whistler wave excitation",* Phys. of Plasmas 11(5), 2144-2155 (2004)

Degeling A., Lister J.B., Martin Y., et al., & ASEX Upgrade Team, *"Were the chaotic ELMs in TCV the result of an ARMA process?",* Plasma Phys. & Contr. Fusion 46(10), L15-L21 (2004)

Degeling A.W., Weisen H., Zabolotsky A., Duval B.P., Pitts R.A., Wischmeier M., Lavanchy P., Marmillod P., Pochon G., *"AXUV bolometer and Lyman-alpha camera systems on the TCV tokamak",* Rev. Sci. Instrum. 75, 4139 (2004)

Descoeudres A., Hollenstein Ch., Demellayer R., Waelder G., *"Optical emission spectroscopy of electrical discharge machining plasma",* J. Mater. Processing Tech. 149, 184-190 (2004) (proc. 14th Int. Symposium for Electromachining, Edinburgh, Scotland, UK, 30th March - 1st April 2004)

Descoeudres A., Hollenstein Ch., Demellayer R., Waelder G., *"Optical emission spectroscopy of electrical discharge machining plasma",* J. Phys. D: Appl. Phys. 37, 875-882 (2004)

Erents S.K., Pitts R.A., Fundamenski W., Gunn J.P., Matthews G.F., *"A comparison of experimental measurements and code results to determine flows in the JET SOL",* Plasma Phys. & Contr. Fusion, 46, 1757 (2004)

Erikksson L.-G., Mueck A., Sauter O., et al., *"Demonstration of the utility of localised current drive for destabilisation of long sawtooth free periods induced by the presence of fast ions",* Phys. Rev. Lett. 92, 235004-1 (2004)

Eriksson L.-G., Mueck A., Sauter O., Coda S., et al., *"Destabilization of fast-ion-induced lon sawteeth by localized current drive in the JET tokamak",* Phys. Rev. Letters 92(23), 235004-1 - 235004-4 (2004)

Eriksson L.-G., et al., Testa D., *"Plasma rotation induced by directed waves in the ion cyclotron range of frequencies",* Phys. rev. Lett. 92, 235001 (2004)

Ferrando i Margalet S., Cooper W.A., Allfrey S.J., Popovitch P., Isaev M.Yu., *"Bootstrap current and quasi-symmetry in ractor-size stellarators",* Fusion Science & Technol. 46, 44 - 53 (2004)

Ganesh R., Angelino P., Vaclavik J., Villard L., *"A full radius gyrokinetic stability analysis for large aspect ratio finite-beta tokamaks",* Phys. of Plasmas 11(6), 3106-3130 (2004)

Gindrat M., Dorier J.-L., Hollenstein Ch., Refke A., Barbezat G., *"Characterization of supersonic low pressure plasma jets with electrostatic probes",* Plasma Sources Science and Technology 13, 484-492 (2004)

Giunchi G., Raineri S., Wesche R., Bruzzone P., *"The voltage-current relations for MgB2 obtained by reactive liquid infiltration",* Physica C, 401, 310-315 (2004)

Graves J., *"Influence of asymmetric energetic ion distributions on Sawtooth stabilization",* Phys. Rev. Letters, 92(18), 185003 (2004)

Heller R., Aized D., Akhmetov A., et al., Wesche R., *"Design and fabrication of a 70kA current lead using Ag/Au stabilized Bi-2223 tapes as a demonstrator for the ITER TF-coil system",* IEEE Trans. Appl. Supercond. 14(2), 1774-1777 (2004)

Henderson M.A., Coda S., Goodman T.P., Nikkola P., Sauter O., and TCV team, *"Control of electron internal transport barriers in TCV"*, Plasma Phys. & Contr. Fusion 46, A275-A284 (2004)

Henderson M.A., Behn R., Coda S., Condrea I., Duval B.P., Goodman T.P., Karpushov A., Martin Y., Martynov An., Moret J.-M., Nikkola P., Porte L., Sauter O., Scarabosio A., Zhuang G., and , The TCV Team, *"Creation and control of eITBs in stable plasma conditions on TCV"*, Plasma Phys. & Contr. Fusion 46, A275 (2004)

Howling A.A., Sansonnens L., Ballutaud J., Hollenstein Ch., Schmitt J.P.M., *"Non-uniform rf plasma potential due to edge asymmetry in large-area rf reactors"*, J. Appl. Phys. 96(10), 5429-5440 (2004)

Hynoenen V., Dumbrajs O., Degeling A., Kurki-Suonio T., Urano H., *"The search for chaotic edge localized modes in ASDEX Upgrade"*, Plasma Phys. & Contr. Fusion 46(9), 1409-1422 (2004)

Kornilov V., Kleiber R., Hatzky R., Villard L., Jost G., *"gyrokinetic global 3D simulations of linear ion temperature gradient modes in Wendelstein 7-X"*, Phys. Plasmas 11, 3196-3202 (2004)

Kroll U., Bucher C., Benagli S., et al., Ballutaud J., Howling A.A., Hollenstein Ch., *"High-efficiency p-i-n a Si:H solar cells with low boron cross-contamination prepared in a large-area single-chamber PECVD reactor"*, Thin Solid Films 451-452 (2004) 525-530

Lang P.T., Degeling A.W., Lister J.B., Martyin Y.R., et al., & ASDEX Upgrade Team, *"Frequency control of type-I ELMs by magentic triggering in ASDEX Upgrade"*, Plasma Phys. & Contr. Fusion 46(11), L31-L39 (2004)

Litaudon X., et al., Sauter O., *"Status of and prospects for advanced tokamak regimes from multi-machine comparisons using the "International Tokamak Physics Activity" database"*, Plasma Phys. & Contr. Fusion 46, A19-A34 (2004)

Marinucci. C., Bottura L., Bruzzone P.,, Mitchell N., Stepanov B., Wesche R., *"Analysis and interpretation of Tcs tests of the ITER toroidal field conductor insert"*, IEEE Trans. Appl. Supercond. 14(2), 1523-1526 (2004)

Marmy P., *"In-beam mechanical testing of Cu-Cr-Zr"*, J. Nucl. Materials 329-333, 188-192 (2004)

Mayoral M.-L., et al., Coda S., Sauter O., *"Studies of burning plasma physics in the Joint European Torus"*, Phys. Plasmas 11, 2607 (2004) (Invited talk at the APS conference 2003)

McDonald D.C., Cordey J.G., Righi E., et al., Pitts R.A., and JET EFDA Contributors, *"ELMy H-modes in JET helium-4 plasmas"*, Plasma Phys. & Contr. Fusion 46, 519 (2004)

Mueller S., Fasoli A., Labit B., McGrath M., Poli F.M., *"Effects of a vertical magnetic field on particle confinement in a magnetized plasma torus"*, Phys. Rev. Lett. 93, 165003 (2004)

Nita N., Schaeublin R., Victoria M., *"Impact of irradiation on the microstructure of nanocrystalline materials"*, J. Nucl. Mater. 329-333, 953-957 (2004)

Odette G.R., Yamamoto T., Kishimato H., et al., Spaetig P., *"A master curve analysis of F82H using statistical and constraint loss size adjustments of small speciment data"*, J. Nuclear Materials 329-333 (2004), 1243-1247

Ongena J., et al., Sauter O., *"Towards the realisation on JET of an integrated H-mode scenario for ITER",* Nucl. Fusion 44, 124-133 (2004)

Panek R., Pitts R.A., Gunn J.P., Erents S.K., *"Particle-in-cell simulations of the impact of retarding field analyser probe head geometry on ion saturation current measurements",* Czechoslovak Journal of Physics, 54, Suppl. C, 150 (2004)

Pasztor G., Bruzzone P., Anghel A., Stepanov B., *"An alternative CICC design aimed at understanding critical performance issues in Nb3Sn conductors for ITER",* IEEE Trans. Appl. Supercond., 14(2), 1527-1530 (2004)

Pasztor G., Bruzzone P., *"Ic(B,T,strain) characterization of a Nb3Sn internal tin strand with enhanced specifications for use in fusion conductors",* Advances in Cryogenic Engineering, American Inst. of Physics, 50B, 458-465 (2004)

Peacock A.T., Barabash V., Daenner W., Linke J., Lorenzetto P., Marmy P., Merola M., Singh B., Taehtinen S., van der Laan J., Wu C., *"Overview of recent European materials R&D for ITER",* J. Nuclear Mater. 329-333, 173-177 (2004)

Piffl V., Weisen H., Zabolotsky A., and TCV team, *"Ultrasoft X-ray spectroscopy using multilayer mirrors on TCV",* Plasma Phys. & Contr. Fusion 46, 1659 (2004)

Sauter O., *"On the contribution of local current density to neoclassical tearing mode stabilisation",* Phys. of Plasmas 11, 4808 (2004)

Scavino E., Bakos J., Weisen H., and TCV Team, *"Effects of ECRH power and safety factor on laser blow-off injected impurity confinement in TCV",* Plasma Phys. & Contr. Fusion 46, 857 (2004)

Schlatter C., Testa D., Cecconello M., Murari A., Santal M., and JET EFDA contributors, *"Error analysis and parametric study of the high energy NPA at JET",* Rev. Sci. Instrum. 75(10), 3547-3549 (2004) (Proc. 15th Topical Conference on High Temperature Plasma Diagnostics, San Diego, USA, 19-22 April 2004)

Schmidt H., Sansonnens L., Howling A.A., Hollenstein Ch., Elyaakoubi M., Schmitt J.P.M., *"Improving plasma uniformity using lens-shaped electrodes in a large area VHF reactor",* J. of Appl. Physics 95(9), 4559-4564 (2004)

Sharapov S., et al., Testa D., *"Monitoring Alfvén cascade eigenmodes with interferometry on the JET tokamak",* Phys. Rev. Lett. 93, 165001 (2004)

Siegrist M.R., Hawkes N., Weisen H., *"Feasibility of a motional Stark effect system on the TCV tokamak (I)",* Rev. Sci. Instrum. 75(9) (2004)

Siegrist M.R., Hawkes N., Weisen H., *"Feasibility of a motional Stark effect system on the TCV tokamak (II)",* Rev. Sci. Instrum. 75(10) (2004)

Silva C., Gon4alves G., Erents S.K., et al., Pitts R.A., *"Fluctuation measurements using a five-pin triple probe in the Joint European Torus boundary plasma",* Rev. Sci. Instrum. 75, 4314 (2004)

Spaetig P., Schaeublin R., Baluc N., Kohlbrecher J., Victoria M., *"SANS Investigation of Proton-irradiated EUROFER97",* J. Nucl. Materials 329-333, 289-293 (2004)

Stepanov B., Anghel A., Bruzzone P., Vogel M., *"Impact of impressed current imbalance on n-Index",* IEEE Trans. Appl. Supercond. 14(2), 1495-1498 (2004)

Testa D., Fasoli A., Borba D., deBaar M., Bigi M., Brzozwski J., deVries P., and JET-EFDA contributors, *"Alfvén mode stability and wave-particle interaction in the*

JET tokamak: prospects for scenario development and control schemes in burning plasma experiments", Plasma Phys. & Contr. Fusion 46 (2004) S59-S79

Villard L., Allfrey S.J., Bottino A., Brunetti M., Falchetto G.L., Grandgirard V., Hatzky R., Nuehrenberg J., Peeters A.G., Sauter O., Sorge S., Vaclavik J., *"Full radius linear and nonlinear gyrokinetic simulations for tokamaks and stellarators: Zonal flows, applied ExB flows, trapped electrons and finite beta"*, Nucl. Fusion 44(1), 172-180 (2004)

Villard L., Allfrey S.J, Angelino P., et al., Bottino A., Sauter O., Tran T.M., *"First principles based simulations of instabilities and turbulence"*, accepted for Publication in Plasma Phys. & Contr. Fusion

Weisen H., Zabolotsky A., Garbet X., Mazon D., Zabeo L., Leggate H., Valovic M., Zastrow K.-D., and contributors to the JET-EFDA work programme, *"Shear dependence of particle pinch in JET L-mode plasmas"*, Plasma Phys. & Contr. Fusion 46, 751 (2004)

Wesche R., Stepanov B., Anghel A., Huber S., Pasztor G., Vogel M., Bruzzone P., *"Self-field effect in NbTi Subsize cable-in-conduit conductors"*, Physica C, 401, 113-117 (2004)

Wesche R., Anghel A., Bruzzone P., Stepanov B., *"Sudden take-off in large NbTi conductors: not a stability issue"*, American Inst. of Physics, 50B, 820-827 (2004)

Wesche R., Anghel A., Stepanov B., Bruzzone P., *"DC performance of subsize NbTi cable-in-conduct conductors"*, IEEE Trans. Appl. Supercond. 14(2), 1499-1502 (2004)

Wischmeier M., Pitts R.A., Andrebe Y., Behn R., Coster D., Duval B.P., Fremaux N., Horacek J., Reiter D., Zabolotsky A., Zhuang G., *"The influence of molecular dynamics on divertor detachment on TCV"*, Contribution to Plasma Physics 44 (1-3), 268 (2004) (9th Int. Workshop on Plasma Edge Theory in Fusion Devices, San Diego, CA, USA, September 2003)

Yao Z., Schaeublin R., Victoria M., *"Tensile properties of irradiated Cu single crystals and their temperature dependence"*, J. Nuclear Mateirals 329-333, 289-293 (2004)

Zanino R., Bagnasco M., Bruzzone P., Ciotti M., Gislon P., Savoldi Richard L., *"Analysis of thermal-hydraulic effects in the testing of the ITER poloidal field full size joint sample"*, Advances in Cryogenic Engineering, American Inst. of Physics, 49A, 544-551 (2004)

APPENDIX B Conferences and Seminars

(see CRPP archives at http://crppwww.epfl.ch/archives)

B.1 Conference and conference proceedings published in 2004

Allfrey S.J., Brunner S., *"Generalised evolving background f-o for plasma deltaf Particle-in-cell simulations",* Sherwood Conference, Missoula, Montana, April 26-28, 2004

Andrew P., Coad J.P., Corre Y., et al., Pitts R.A., *"Outer divertor target impurity deposition during reversed magnetic field operation in JET",* 16th Int. Conf. on Plasma Surface Interactions in Controlled Fusion Devices, Portland Maine, U.S.A., May 24-28, 2004, accepted for publication in J. Nucl. Mater.

Anghel A., Bruzzone P., *"Measurement of contact resistance distribution in typical ITER size conductor termination",* SOFT 2004 Symposium, Venezia, Italy, September 2004

Anghel A., *"Stability of power-law cable-in-conduit superconductors",* arXiv, cond-mat/0402044, February 2004

Anghel A., *"Effect of strand longitudinal thermal conduction on take-off properties in cable-in-conduit superconductors",* arXiv, cond-mat/0403042, March 2004

Arnoux G., Alberti S., Porte L., *"Absorption properties of X3 top-launch ECH on TCV",* 13th Joint Workshop on Electron Cyclotron Emission and Electron Cyclotrron Resonance Heating, Nizhny Novgorod, Russia, May 2004

Balazs D.J., Strahm B., Triandafillu K., Dorier J.-L., Hollenstein Ch., Mathieu H.J., *"PE-CVD of Ag/Teflon-like coatings on medical-grade PVC to control bacterial adhesion",* Italian Vaccum Conference, Venice, Italy, July 2004

Blais A., Jodoin B., Dorier J.-L., Hollenstein Ch., Barbezat G., *"Supersonic plasma jet modelling at low pressure, and validation using recent advances of the enthalpy probe measurement technique",* Proc. Int. Thermal Spray Conference 2004, Osaka, Japan, May 2004

Boswell C., et al., Fasoli A., Testa D., *"Comparison between TAEs and EAEs using MHD spectroscopy",* 31st EPS Conference on Plasma Physics, Imperial College London, June 27-July 2, 2004

Bottura L., Bruzzone P., Kauschke M, et al., *"A Cable-in-Conduit Superconductor for Pulsed Accelerator magnets",* ASC-2004 Conference, Jacksonvill, USA, October 2004

Bruzzone P., Bagnasco M., Bessette D., et al., Stepanov B., Wesche R., *"Test results of the ITER PF insert conductor short sample in SULTAN",* ASC-2004 Conference, Jacksonville, USA, October 2004

Bruzzone P., Stepanov B., Zapretilina E., *"V-I characteristics with bumps in the medium size NbTi CICC cables",* SOFT 2004 Symposium, Venezia, Italy, September 2004

Bruzzone P., *"Selected results of conductor R&D from the SULTAN test facility"*, Progress in Electromagnetic Research Symposium, PIERS, Pisa, Italy, March 2004

Buttery R.J., Belo P., Brennan D.P., et al., Coda S., Graves J., Mueck A., Sauter O., *"Cross-machine NTM physics studies and implications for ITER"*, 20th IAEA Fusion Energy Conference, Vilamoura, Portugal, November 2004

Buttery R.J., et al., Sauter O., *"NTM metastability scaling towards ITER"*, 31st EPS Conference on Plasma Physics, Imperial College London, June 27 - July 2, 2004

Carey C., Furno I., Weisen H., *"Application of the singular value decomposition method for the inversion of innterferometer measurements in the TCV tokamak."*, 15th Topical Conference, High Temperature Plasma Diagnostics, 19-22 April, San Diego, USA

Chavan R., Henderson M.A., Sanchez F., *"An alternative front steering launcher for ITER's upport port"*, 23rd SOFT Conference, Venice, Italy, 20-24 September 2004

Ciazynski D., Zani L., Gilson P., Muzzi L., Bruzzone P., Wesche R., Stepanov B., Zapretilina E., Martovetsky N., Bessette D., *"DC performances of ITER NbTi conductors: Models vs. Measurements "*, ASC-2004 Conference, Jacksonville, USA, October 2004

Cooper W.A., Andreeva T., Ighitkhanov Y., Kisslinger J., et al., *"Bootstrap Current and MHD Stability in a 4-period Helias Reactor Configuration"*, 31st EPS Conference on Plasma Physics, Imperial College London, June 27 - July 2, 2004

Cordey J.G., et al., Martin Y., *"The scaling of confinement in ITER with beta and collisionality"*, 20th IAEA Fusion energy Conference, held in Vilamoura Portugal, Nov. 1-6, 2004

Corre Y., Andrew P., eich T., et al., Pitts R.A., *"Inner and outer power and energy asymmetries during L-mode power staircase pulses with forward and reversed magnetic field"*, 31st EPS Conference on Plasma Physics, Imperial College London, June 27 - July 2, 2004

Coster D.P., Bonnin X., Chankin A., et al., Pitts R.A., Wischmeier M., *"Integrated modelling of material migratin and target plate power handling at JET"*, 20th IAEA Fusion energy conference, held in Vilamoura Portugal, Nov. 1-6, 2004

Descoeudres A., Hollenstein Ch., Demellayer R., Waelder G., *"Optical emission spectroscopy of electrical discharge machining plasma"*, 14th International Symposium on Electromachining (ISEM XIV), Edinburgh, Scotland, March30-April 1, 2004

Eich T., Herrmann A., Pautasso G., et al., Pitts. R.A., *"Power deposition onto plasma-facing components in poloidal divertor tokamaks during type I ELMs and disruptions"*, Review paper to16th Int. Conf. on Plasma Surface Interactions in Controlled Fusion Devices, Portland Maine, U.S.A., May 24-28, 2004, accepted for publication in J. Nucl. Mater.

Fasel D., Tran M.Q., *"Availability of lithium in the context of future D-T fusion reactors"*, 23rd SOFT Conference, Venice, Italy, 20-24 September 2004

Fasoli A., *"Burning plasma physics: the new frontier of fusion energy science"*, ESOF Conference, Stockholm, Sweden, 26-29 August 2004

Fietz W.H., Fink S., Heller R., et al., Pasztor G., Wesche R., *"High temperature superconductors for the ITER magnet system and beyond"*, SOFT 2004 Symposium, Venezia, Italy, September 2004

Fietz W.H., Heller R., Zahn G., et al., Wesche R., Pasztor G., *"Use of high temperature superconductors for future fusion magnet system"*, 20th IAEA Fusion Energy Conference, Vilamoura, Portugal, November 2004

Fundamenski W., Andrew P., Erents K., et al., Pitts R.A., *"Effect of BxDB direction on SOL energy transport in JET"*, 16th Int. Conf. on Plasma Surface Interactions in Controlled Fusion Devices, Portland Maine, U.S.A., May 24-28, 2004, accepted for publication in J. Nucl. Mater.

Fundamenski W., Andrew P., Eich T., et al., Pitts R.A., *"Power exhaust on JET: an overview of dedicated experiments"*, 20th IAEA Fusion energy conference, held in Vilamoura Portugal, Nov. 1-6, 2004

Giroud C., Testa D., et al., *"Charge exchange spectroscopy measurement at JET"*, 16th Symposium on Plasma Physics and Radiation Technology, Lunteren, The Netherlands, 16-17 March 2004

Goodman T.P., Behn R., Bottino A., Coda S., Fable E, Henderson M.A., Nikkola P., Sauter O., Zucca C., *"Inductive current perturbations to steady-state eITBs"*, Proc. 31st EPS Conference on Plasma Physics, Imperial College London, June 27 - July 2, 2004, ECA Vol. 28G, Europhysics Conf. Abstracts O-2.05 (2004)

Gormezano C., et al., Sauter O., *"IHabrid advanced scenarios: Perspectives for ITER and new experiments with dominant RF heating"*, 31st EPS Conference on Plasma Physics, Imperial College London, June 27 - July 2, 2004

Heller R., Darweschsad M.S., Dittrich G., et al., Wesche R., *"Experimental results of a 70kA high temperature superconductor current lead demonstrator for the ITER magnet system"*, ASC-2004 Conference, Jacksonville, USA, October 2004

Henderson M.A., Camenen Y., Coda S., Fable E., Goodman T.P., Nikkola P., Pochelon A., Sauter O., Zucca C., and the TCV team, *"Rapid eITB formation during magnetic shear reversal in fully non-inductive TCV discharges"*, 20th IAEA Fusion energy conference, Vilamoura, Portugal, Nov. 1-6, 2004

Hogge J.-P., , *"Accurate gyrotron magnetic axis determination"*, IRMMW 2004/THz 2004 held in Karlsruhe, Sept. 27-28, 2004

Huber A., Rapp. J., Andrew P., et al., Pitts R.A., *"The effect of field reversal on the JET MkIIGB-SRP divertor performance in L-mode density limit discharges"*, 16th Int. Conf. on Plasma Surface Interactions in Controlled Fusion Devices, Portland Maine, U.S.A., May 24-28, 2004, accepted for publication in J. Nucl. Mater.

Hurd F., Sborchia C., Salpietro E., et al., Bruzzone P., *"Design and manufacture of a full size joint sample (FSJS) for the qualification of the poloidal field (PF) insert coil"*, ASC-2004 Conference, Jacksonville, USA, October 2004

Ilyin Y., Nijhuis A., Abbas W., Bruzzone P., Stepanov B., *"Reconstruction of the current unbalance in full-size ITEr NbTi CICC by self field measurements"*, ASC-2004 Conference, jacksonville, USA, October 2004

Ilyin Y., Nijhuis A., Abbas W., Bruzzone P., Stepanov B., et al., *"Effect of cyclic loading and conductor layout on contact resistance of full-size ITER PFCI conductors"*, ASC-2004 Conference, Jacksonville, USA, October 2004

Karpushov A.N., Duval B.P., LaBombard B., *"Recovery of Ion Parameters from NPA Measurements on TCV"*, 31st EPS Conference on Plasma Physics, Imperial College London, June 27 - July 2, 2004

Khayrutdinov R.R., Dokuka V., Duval B.P., Favez J.-Y., et al., Lister J.B., Moret J.-M., Weisen H., *"Evolution of the DINA-CH tokamak simulator"*, 31st EPS Conference on Plasma Physics, Imperial College London, June 27-July 2, 2004

Kirnev G.S., corrigan G., Coster D., et al., Pitts R.A., *"EDGE2D code simulations of SOL flows in JET"*, 16th Int. Conf. on Plasma Surface Interactions in Controlled Fusion Devices, Portland Maine, U.S.A., May 24-28, 2004, accepted for publication in J. Nucl. Mater.

Lehnen M., Finken K.H., Fundamenski W., et al., Pitts R.A., *"Helium exhaust studies at JET in reversed B"*, 31st EPS Conference on Plasma Physics, Imperial College London, June 27 - July 2, 2004

Lindau R., Moeslang A., Rieth M., et al., Baluc N., Schaeublin R., *"Present development status of EUROFER and ODS for application in blanket concepts"*, 23rd SOFT Conference, Venice, Italy, September 2004

Lister J.B., Saint-Laurent F., Dokuka V., Khayrutdinov R.R., et al., *"Drift-Free Eqilibrium reconstruction using magnetic probes"*, 31st EPS Conference on Plasma Physics, Imperial College London, June 27 - July 2, 2004

Lister J.B., Dokuka V., Lukash V.E., Khayrutdinov R.R., et al., *"Evolution of the DINA-CH Tokamak Full Discharge Simulator"*, 23rd SOFT Conference, Venice, Italy, 20-24 September 2004

Maraschek M., et al., Sauter O., *"Active Control of MHD Instabilities by ECCD in ASDEX Upgrade"*, 20th IAEA Fusion Energy Conference, Vilamoura, Portugal, November 2004

Maraschek M., et al., Sauter O., *"Scaling of the marginal of the (2/1) neoclassical tearing mode and NTM onset conditions with extreme profiles in ASDEX Upgrade, DIII-D and JET"*, 31st EPS Conference on Plasma Physics, Imperial College London, June 27 - July 2, 2004

Marinucci C., Bruzzone P., Della Corte A., Savoldi Richard L., Zanino R., *"Pressure drop in the ITER PFI cable-in-conduit conductor"*, ASC-2004 Conference, Jacksonville, USA, October 2004

Marmy P., *"Fracture toughness and tensile properties of two titanium alloys before and after proton and neutron irradiations at 150C"*, 16th Int. Conf. on Physics of Radiation Phenomena and Radiation Material Science, Alushta, Crimea, Ukraine, 7-12 September 2004

Martin Y.R., *"H-mode threshold power dependences in ITPA threshold database"*, 20th IAEA Fusion energy conference, held in Vilamoura Portugal, Nov. 1-6, 2004

Martin Y., Degeling A., Lang P.L., et al., *"Magnetic ELM triggering on ASDEX Upgrade"*, 31st EPS Conference on Plasma Physics, Imperial College London, June 27-July 2, 2004

Martovetsky N., Bruzzone P., Stepanov B., Wesche R., et al., *"Effect of the conduit material on CICC performance under high cycling loads"*, ASC-2004 Conference, Jacksonville, USA, October 2004

McGrath M.A., Fasoli A., Labit B., Mueller S., *"Plasma production, confinement and diagnostic developments on TORPEX"*, TTF Conference, 29 April - 2 May, Salt Lake City, USA

McGrath M., Fasoli A., Labit B., Mueller S., Podesta M., Poli F.M., *"Initial TORPEX results of plasma production, confinement and fluctuation studies"*, 31st EPS Conference on Plasma Physics, Imperial College London, June 27 - July 2, 2004

McGrath M., Fasoli A., Labit B., Mueller S., Podesta M., Poli F., *"Plasma production, confinement and diagnostic developments on TORPEX"*, US TTF Conference 29 April - 2 May, 2004, Salt Lake City, USA

Medvedev S. Yu, Ivanov A.A., Martynov A.A., et al., Degeling A., Lister J.B., Martin Y.R., Sauter O., Villard L., *"Edge kink/ballooning mode stability scalings and ELM triggering in plasma with Separatrix"*, 31st EPS Conference on Plasma Physics, Imperial College London, June 27 - July 2, 2004

Medvedev S. Yu, Galkin S.A., Martinov A.A., et al., Villard L., *"Modelling of equilibrium and stability in tokamaks with reversed current density"*, 31st EPS Conference on Plasma Physics, Imperial College London, June 27 - July 2, 2004

Melnikov A., Perfilov S.V., Krupnik L.I., Tonetti G., Siegrist M.R., Weisen H., *"Applicability of heavy ion beam probing (HIBP) for tokamaks with highly shaped plasmas by example of TCV"*, 15th Topical Conference High Temperature Plasma Diagnostics in San Diego, USA, April 19-22, 2004

Mikhailov M.I., Cooper W.A., Heyn M.F., Isaev M. Yu, et al., *"Comparison of the properties of quasi-isodynamic configurations for different numbers of periods"*, 31st EPS Conference on Plasma Physics, Imperial College London, June 27 - July 2, 2004

Moret J.-M., Alberti S., Andrbe Y., Appert K., Arnoux G., Behn R., Camenen Y., Chavan R., Coda S., Condrea I., Degeling A., Duval B.P., Fasel D., Fasoli A., Goodman T.P., Henderson M., Hogge J.-P., Horacek J., Isoz P.F., Joye B., Karpushov A., Klimanov I., Lavanchy P., Lister J.B., Llobet X., Magnin J.-C., marletaz B., Marmillod P., Martin Y., Martynov A., Mayor J.-M., Mueck A., Nikkola P., Paris P.-J., Pavlov I., Perez A., Pitts R.A., Pochelon A., Porte L., Sauter O., Scarabosio A., Siegrist M., Siravo U., Sushkov A., Tonetti G., Tran M.Q., Weisen H., Wischmeier M., Zabolotsky A., Zhuang G., *"Progress in the understanding and the performance of ECH and plasma shaping on TCV"*, Overview paper of the 20th IAEA Fusion energy conference, held in Vilamoura Portugal, Nov. 1-6, 2004

Nave M.F.F., Coda S., Galvao R., Graves J., and EFDA JET contributors, *"Small sawtooth regimes in JET plasmas"*, Proc. 31st EPS Conference on Plasma Physics, Imperial College London, June 27 - July 2, 2004, ECA Vol. 28G, Europhysics Conf. Abstracts P-1.162 (2004)

Piffl V., Zabolotsky A., Weisen H., and TCV team, *"Carbon impurity transport studies in the TCV tokamak using spatially resolvt ultrasoft X-ray spectroscopy"*, Proc. 31st EPS Conference on Plasma Physics, Imperial College London, June 27-July 2, 2004 (P-2-142)

Pinches S., et al., Fasoli A., Testa D., *"The role of energetic particles in fusion plasmas"*, 31st EPS Conference on Controlled Fusion and Plasma Physics, London, July 2004 (to appear in Plasma Phys. & Contr. Fusion)

Pitts R.A., Andrew P., Eich T., S.K. Erents, et al., *"Edge and Divertor Physics with reversed toroidal field in JET"*, Invited paper to 16th Int. Conf. on Plasma

Surface Interactions in Controlled Fusion Devices, Portland Maine, U.S.A., May 24-28, 2004, accepted for publication in J. Nucl. Mater.

Pochelon A., Camenen Y., Behn R., Bortolon A., Bottino A., Coda S., Duval B.P., Fable E., Goodman T.P., Henderson M.A., Karpushov A.N., Moret J.M., Mueck A., Nelson-Melby E., Porte L., Sauter O., Scarabosio A., Zhuang G., TCV team, *"Influence of plasma shape on electron heat transport the presence of extreme temperature gradient variations in TCV"*, 20th IAEA Fusion energy conference, held in Vilamoura Portugal, Nov 1-6, 2004, Oral EX/9-1

Pochelon A., et al., Sauter O., *"Effect of plasma shape on electron heat transport in the presence of extreme temperature gradients variations in TCV"*, 20th IAEA Fusion Energy Conference, Vilamoura, Portugal, November 2004

Poli F., Fasoli A., Labit B., McGrath M., Mueller S., Podesta M., *"Observation of low frequency electrostatic fluctuations on TORPEX"*, US TTF Conference 29 April - 2 May, 2004, Salt Lake City, USA

Porte L., Alberti S., Arnoux G., Goodman T.P., et al., Henderson M.A., Hogge J.-P., *"3rd Harmonic ECH on TCV using vertically launched 118GHz radiation"*, 31st EPS Conference on Plasma Physics, Imperial College London, June 27 - July 2, 2004

Salmi A., et al., Testa D., *"Experimental verification of the role of finite ion Larmor radius effects on the ICRF-resonant fast ion distribution"*, 31st EPS Conference on Plasma Physics, Imperial College London, June 27-July 2, 2004

Sansonnens L., Strahm B., Derendinger L., Howling A.A., Hollenstein Ch., Ellert Ch., Schmitt J.P.M., *"Measurements and consequences of non-uniform RF plasma potential due to surface asymmetry in large area RF capacitive reactors"*, AVS 51st Int.Symposium & Exhibition, Anaheim, USA, November 2004, submitted to J. Vacuum Sci. and Technol. A)

Sartori R., et al., Sauter O., *"Scaling study of Elmy H-mode global and pedestal confinement at high triangularity in JET"*, 20th IAEA Fusion Energy Conference, Vilamoura, Portugal, November 2004

Shafranov V.D., Cooper W.A., Heyn M.F., Isaev M.Yu., et al., *"Results of integrated Optimization of a N=9 Qasi-isodynamic Stellarator"*, 31st EPS Conference on Fusion Physics, Imperial College London, June 27 - July 2, 2004

Sharapov S., et al., Fasoli A., Testa D., *"Experimental studies of instabilities and confinement of energetic particles on JET and on MAST"*, 20th IAEA Fusion energy conference, held in Vilamoura Portugal, Nov. 1-6, 2004

Sips A.C.C., et al., Sauter O., *"Study of advanced tokamak regimes using the international tokamak physics activity database"*, 20th IAEA Fusion Energy Conference, Vilamoura, Portugal, November 2004

Sobbia R., Sansonnens L., Bondkowski J., *"Uniformity study in large-area showerhead reactors"*, AVS 51st Int.Symposium & Exhibition, Anaheim, USA, November 2004, submitted to J. Vacuum Sci. and Technol. A)

Solano E.R., Jachmich F., Villone F., et al, Pitts R.A., *"ELMs strike point jumps and SOL currents"*, 20th IAEA Fusion energy conference, held in Vilamoura Portugal, Nov. 1-6, 2004

Solano E.R., et al., Testa D., *"ELMs strike point jumps and SOL currents"*, 16th PSI Int. Conf. on Plasma-Surface Interaction, Portland, USA, 24-28 May 2004

Spaetig P., Campitelli E.N., Bonade R., Baluc N., *"Assessment of plastic flow and fracture properties with small speciments test techniques for IFMIF-designed specimens",* 20th IAEA Fusion Energy Conference, Vilamoura, Portugal, November 2004

Stepanov B., Bruzzone P., Vogel M., *"A low cost joint for the ITER PF coils, design and test results",* SOFT 2004 Symposium, Venezia, Italy, September 2004

Strachan J.D., Alper B., Corrigan G., et al., Pitts R.A., *"Methane screening in JET reverse field experiments",* 16th Int. Conf. on Plasma Surface Interactions in Controlled Fusion Devices, Portland Maine, U.S.A., May 24-28, 2004, accepted for publication in J. Nucl. Mater.

Strek A.B., Bonicelli T., Fasel D., et al., *"Pre-study results on high voltage solid-state switches for gyrotron protection",* 23rd SOFT Conference, Venice, Italy, 20-24 September 2004

Suttrop W., Hynoenen V., Kurki-Suonio T., et al., Pitts R.A., *"Studies of the Quiescent H-mode regime in ASDEX Upgrade and JET",* 20th IAEA Fusion energy conference, held in Vilamoura Portugal, Nov. 1-6, 2004

Testa D., Fasoli A., Bertizzolo R., Chavan R., Villard L., et al., *"The new Alfven wave active excitation system at JET",* 23rd SOFT Conference, Venice, Italy, 20-24 September 2004

Testa D., et al., *"Experimental studies of Alfvén mode stability and wave-particle interaction in the JET tokamak",* 20th IAEA Fusion energy conference, held in Vilamoura Portugal, Nov. 1-6, 2004, paper EX/P4-45

Texier M., Proult A., Bonneville J., Rabier J., Baluc N., Cordier P., *"Microstructural analysis of i-AlPdMn quasicrystals deformed between room temperature and 300C under confining pressure",* Scripta Materiala 49 47-52 (2003) (appeared in 2004)

Tran M.Q., Casci F., *"ITER, the major step towards fusion energy for the world",* WEC Conference, held in Sydney, Australia, Sept. 5-9, 2004

Turnbull A.D., Lao L.L, Cooper W.A., Fu G.Y., et al., *"Equilibrium and Stability for the ARIES Compact Stellerator Reactor",* 31st EPS Conference on Plasma Physics, Imperial College London, June 27 - July 2, 2004

Villard L., Allfrey S.J, Angelino P., et al., Bottino A., Sauter O., Tran T.M., *"First principles based simulations of instabilities and turbulence",* 31st EPS Conference on Plasma Physics held in London, June 28-July 2, 2004 (Invited Paper)

Watanabe K.Y., Sakakibara S., Narushima Y., et al., Cooper W.A., , *"Effects of global MHD instability on operational high-b regime in LHD",* 20th IAEA Fusion energy conference, held in Vilamoura Portugal, Nov. 1-6, 2004

Weisen H., Zabolotsky A., Giroud C., Leggate H., et al., *"Shear and temperature gradient dependances of particle pinches in JET",* 31st EPS Conference on Plasma Physics, Imperial College London, June 27-July 2, 2004

Weisen H., Angioni C., Bortolon A., Bourdelle C., et al., *"Anomalous particle and impurity transport in JET",* 20th IAEA Fusion energy Conference, held in Vilamoura Portugal, Nov. 1-6, 2004

Weisen H., et al., *"Multi-chord diagnostics on the TCV tokamak",* 2nd German-Polish Conf. on Plasma Diagnostics for Fusion and Applications (GPPD), Cracow, Poland, Septe. 8-10, 2004

Wesche R., Anghel A., Bruzzone P., Gislon P., Muzzi L., *"Analyses and implications of V-I characteristics of PF insert conductor sample",* SOFT 2004 Symposium, Venezia, Italy, September 2004

Yovchev I., Hogge J.-P., Goodman T., Alberti S., Tran T.M., *"Design of the ITER 170 GHz Gyrotron gun ",* IRMMW 2004/THz 2004, held in Karlsruhe, Sept. 27-28, 2004

Yu G., Nita N., Baluc N., *"Thermal creep behavior of the EUROFER97 RAFM steel and two European ODS-EUROFER97 steels",* 23rd SOFT Conference, Venice, Italy, September 2004

Zhuang G., Scarabosio A., Behn R., Camenen Y., et al., Goodman T.P., Henderson M.A., Klimanov I., Sauter O., Weisen H., *"MHD activity in EC-heated TCV plasmas with eITBs",* 31st EPS Conference on Plasma Physics, Imperial College London, June 27 - July 2, 2004

American Physical Society (APS)

Scarabosio A., Bortolon A., Bosshard P., Duval B.P., Karpuchov A., Pochelon A., *"Toroidal plasma rotation in TCV ohmic L-mode discharges",* APS Conference 2004, Savannah, Gorgia, USA, 15-20 November 2004 (oral presentation)

Société Suisse de Physique (SSP)

Descoeudres A., Hollenstein Ch., Demellayer R., Waelder G., *"Optical emission spectroscopy of electrical discharge machining plasma",* Socit Suisse de Physique, SPS Annual Meeting, Neuchtel, 4 mars 2004

Gindrat M., Dorier J.-L., Blais A., Jodoin B., Hollenstein Ch., Barbezat G., *"Diagnostics of low pressure supersonic plasma jets with enthalpy probes",* Socit Suisse de Physique, SPS Annual Meeting, Neuchtel, 4 mars 2004

Howling A.A., Sansonnens L., Schmitt J.P.M., Ballutaud J., Schmidt H., Hollenstein Ch., *"Elimination of electromagnetic non-uniformities in large-area RF plasma reactors used for thin-film deposition",* Socit Suisse de Physique, SPS Annual Meeting, Neuchtel, 4 mars 2004

Tran M.Q., *"ITER and the road map to fusion",* Socit Suisse de Physique, SPS Annual Meeting, Neuchtel, 4 mars 2004

B.2 Seminars presented at the CRPP in 2004

Dr. C. Angioni, IPP-Garching, Germany, *"Density response to central electron heating: theoretical investigations and experimental observations in AUG"*

A. Bortolon, Consorzio RFX, Padova, Italy, *"Modelling medium and high Z impurity transport in fusion experiments"*

Dr. J.-M. Moret, CRPP-EPFL, *"Développement et possibilités de l'Advanced Plasma Control System de TCV"*

E. D'Agata, Max-Planck-Institut für Plasmaforschung, ITER, Garching, Germany, *"Mechanical and thermal aspects of the divertor of the ITER machine"*

Dr. X. Garbet, DRFC, CEA-Cadarache, France, *"Physics of transport at JET"*

Dr. A. Manini, Max-Planck-Institut für Plasmaphysik, Garching, Germany, *"Electron heating transport in low density H-mode plasmas in ASDEX-Upgrade"*

Dr. A. Peeters, Max-Planck-Institut für Plasmaphysik, Garching, Germany, *"Effects of shearless flow on microinstabilities"*

P. Sheehan, Physics with Philosophy, Univ. of York, UK, *"Quantum computing and the interpretation of quantum mechanics"*

Prof. W.W. Heidbrink, Dept. Physics & Astronomy, Univ. of California, Irvine, CA, USA, *"Two new tokamak diagnostics"*

Dr. P. Browning, Dept. of Physics, UMIST, Univ. of Manchester, UK, *"Solar coronal heating by magnetic reconnection"*

M. Vettorazzo, ETH, Zürich, *"Confinement of quarks in lattice gauge theory"*

Dr. Y. Idomura, JAERI, Japan, *"Development of gyrokinetic toroidal particle code for ITG-TEM and ETG turbulence simulations in tokamaks"*

Dr. N. Noda, Director, NIFS, Japan, *"Large Helical device (LHD) project and its recent results"*

E. Fekete, Babes-Bolyai Univ., Cluj, Roumania, *"Transient MHD modes in the Wendelstein 7-AS stellerator"*

Z. Liye, Univ. of Science and Technology China, Hefei, China, *"Experiments with atmospheric pressure glow discharge and applications to sterilisation"*

Dr. C. Suzuki, NIFS, Japan, *"Analyses of MHD equilibrium and stability in CHS-qa"*

M.V. Maslov, Nuclear Fusion Institute, Kurchatov Institute, Moscow, Russia, *"Reduced transport in the core of the T-10 and TEXTOR plasma after off-axis ECRH switch-off"*

K. Schombourg, CRPP-EPFL, *"Phénomènes de transport dans le plasma de TORPEX"*

N. Mellet, CRPP-EPFL, *"Détermination des surfaces magnétiques résonantes d'Alfvén dans des configurations 2D et 3D"*

G. de Temmerman, Institute für Physik, Univ. Basel, Switzerland, *"Development of optical mirrors for analytical purposes in ITER"*

A. Marinoni, Politecnico di Milano, Dipt. Di Ingegneria Nuclear, CeSNEF, Milano, Italy, *"Power modulation experiments in JET ITB plasmas"*

G. Plyushchev, Kurchatov Institute, Moscow, Russia, *"Investigation of ECRH/ECCD influence on MHD instabilities in T-10 plasma. Testing of wire proportional X-ray detector prototype for ITER"*

B. Strahm, EPFL, *"Contrôle de l'adhésion bactérienne par co-déposition plasma d'un composite Ag/Teflon-like"*

Dr. F. Buclin, Univ. Bern, Switzerland, *"Heating and acceleration of heavy ions in the solr wind by Coulomb collisions and wave-particle interactions"*

B. Gulejova, Dept. of Plasma Physics, Faculty of mathematics, Physics and Informatics, Comenius Univ. Bratislava, *"A crossed beam high-resolution study of dissociative electron attachment and electron impact ionisation of dinitrogen pentoxide"*

E. Hemsing, Los Alamos National Laboratory, NM, USA, *"Magnetic reconnection driven by free-boundary filamentary shaped flux ropes"*

J. Ghosh, Institute for Research Electronics & Applied Physics, Univ. Maryland, College Park, MD, USA, *"Measurements of ion and neutral atom flows and temperatures in the inner and outer mid-plane scrape-off layers (SOL) of the Alcator C-mod tokamak"*

J. Markì, KFKI-Research Institute for Particle and Nuclear Physics, Budapest, Hungary, *"Laser blow-off impurity transport in TCV"*

Dr. G. Falchetto, DRFC, CEA-Cadarache, France, *"Effect of the collisional damping of zonal flows on flux-driven ITG turbulence"*

Prof. E. Lazzaro, IFP, CNR, Milano, Italy, *"ECE temperature fluctuations due to magnetic islands and real-time detection control of mode radial location and EC deposition layer"*

Dr. A.V. Melnikov, Institute of Nuclear Fusion, Kurchatov Institute, Moscow Russia, *"HIBP plasma potential study in stellarator TJ-II and tokamak T-10"*

I. Chavdarovski, Institute of Physics, Faculty of Natural Sciences & Mathematics, Skopje, Macedonia, *"Genetic algorithms - Theory and some examples"*

Dr. R.A. Pitts, CRPP-EPFL, *"Edge and divertor physics with reversed toroidal field in JET"*

S.H. Kim, Seoul National Univ. Seoul, Korea, *"Numerical simulations on internal transport barrier formation in reversed shear regime of KSTAR tokamak"*

Dr. M. Isaev, RRC Kurchatov Institute, Moscow, Russia, *"VENUS + df: A bootstrap current calculation module for 3D configurations"*

Dr. H. Weisen, CRPP-EPFL, *"Shear, temperature gradient and collisionality dependences of particle pinches in JET"*

M. Kogelschatz, LTM/CNRS, Grenoble, France, *"Diagnostics des plasmas $HBr/Cl_2/O_2$. Application à l'étude des interactions plasma-parois lors de la gravure du silicium"*

Dr. A. Fukuyama, Dept. of Nuclear Engineering, Kyoto Univ., Japan, *"Integrated tokamak modelling code TASK and its recent results"*

Dr. M. Kondo & Dr. Takagi, Research Center for Photovoltaics, Nat. Inst. Of Advanced Industrial Science and Technology, Umezono Tsukuba Ibaraki, Japan, *"Formation of nanocrystalline silicon and its control of the size using plasma CVD" & "Large area deposition of thin film silicon using VHF plasma CVD with array antenna"*

Prof. A. Fasoli, CRPP-EPFL, *"Burning plasma physics: the new frontier of fusion energy science"*

Dr. Y. Idomura, JAERI, Japan, *"Development of gyrokinetic PIC and CIP codes for micro-turbulence simulatins in tokamaks"*

S. Solbrig, Univ. Regensburg, Germany, *"Topological objects in gluodynamics, Chiral symmetry breaking and confinement"*

Dr. G.Y. Antar, Univ. of California San Diego, La Jolla, USA, *"Recent progress in understanding intermittency in the scrape-off layer of magnetic fusion devices"*

Dr. T.M. Tran, CRPP-EPFL, *"Le cluster Pléiades: présentation et mode d'emploi"*

F. Turco, Politecnico di Torino, Italy, *"Scrape-off layer modelling during edge localised modes in the JET tokamak"*

Dr. R. Olstad, General Atomics, San Diego, USA, *"ITER-relevant transmission line components and DIII-D ECH system"*

Dr. D. Testa, CRPP-EPFL, *"The accuracy on the inferred radial electric field in JET plasmas"*

A. Zhuchkova, Joint Institute of Nuclear Research, Dubna, Russia, *"Modern high energy physics. Preliminary results of the data analysis of the experiment NA48/2 (CERN) and some results of the detector's simulation for the space experiment NUCLEON (JINR)"*

J. Rossel, SPH-EPFL, *"La configuration magnétique lors du claquage"*

A. Scarabosio, CRPP-EPFL, *"Carbon toroidal rotation in TCV limited L-mode discharges"*

J.-Y. Favez, CRPP + STI Lab. D'automation, EPFL, *"Enhancing the control of tokamaks via a continuous non-linear control law"*

V.K. Yadav, Institute of Plasma Research, Bhat, Gandhinagar, India, *"Studies on ECR produced plasmas"*

Dr. A. Marinopoulos, Lab. Des solides irradiés, Ecole Polytechnique, Palaiseau, France, *"Determining properties of materials through first-principles and empirical calculations"*

Dr. V. Granata, CERN, Geneva, Switzerland, *"Radiation hardness of cryogenic silicon detectors: the Lazarus effect"*

S.M. Hafez Haghighat, Dept. of Materials Sci. and Engineering, Sharif Univ. of Technology, Teheran, Iran, *"Simulations of metals grain growth using the Monte Carlo Method"*

Dr. Z. Oksiuta, bialystok Technical Univ. Dept. of Materials Science, Poland, *"Porous materials base on Co-Cr-Mo alloy"*

L. Vermare, DRFC/SCCP, CEA-Cadarache, France, *"MHD and micro-turbulence measurements using fast sweep reflectometry on Tore Supra"*

J. Anderson, Chalmers Univ. of Technology, Div. Of Electronics Production, Mölndal, Sweden, *"Comparison of linear ITG-mode stability in tokamak and stellarator geometry"*

F. Sartori, JET, Culham, UK, *"Design, implementation and test of the extreme shape controller (XSC) in JET"*

L. Zabeo, JET, Culham, UK, *"Real-time development at JET q-profile reconstruction and control"*

B.3 Other external presentations in 2004

Martin Y., *EPFL-CRPP, 17 janvier 2004* , ""La fusion contrôlée - une énergie pour le futur""

Tran M.Q., *Haute Ecole Valaisanne (HEVs), Sion, Suisse, 2 avril 2004* , ""Le soleil sur terre: une option énergtique dans le cadre d'un développement durable""

Cooper W.A., Ferrando i Margalet S., Allfrey S.J., Popovich P., Mellet N., Isaev M. Yu., Mikhailov M., Subbotin A., Drevlak M., Merkel P., *CSCS User's Day, Mano, CH, 27-28 September 2004* , "Optimised advanced stellarator systems"

Baluc N., *Japan-EU Meeting on Refractory Alloys, Garching, Germany, March 2004*, "Development of W coatings for RAFM steels"

Baluc N., *IFMIF users group, Venice, Italy, September 2004* , "Recent progress in the interpretation of small speciment techniques with FEM"

Baluc N., *Warsaw, Poland, September 2004* , "Fusion technology at the CRPP"

Martin Y., *Université du 3e âge, Genève, 28 avril 2004* , ""La fusion contrôlée - une énergie pour le futur""

Ferrando i Margalet S., *NIFS, National Institute for Fusion Science, Toki, Japan, 6 October 2004* , "Bootstrap current compensation with electron Bernstein current drive in reactor-size Stellarators"

Ferrando i Margalet S., *Inst. of Advanced Energy, Kyoto University, Japan, 12 October 2004* , "Bootstrap current compensation with electron Bernstein current drive in reactor-size Stellarators"

Ferrando i Margalet S., *Dept. of Nuclear Engineering, Kyoto University, Japan, 13 October 2004*, "Bootstrap current compensation with electron Bernstein current drive in reactor-size Stellarators"

Ferrando i Margalet S., *JAERI, Dept. of Fusion Plasma Research, Naka Fusion Research Establ., Naka, Ibaraki, Japan, 15 October 2004*, "Bootstrap current compensation with electron Bernstein current drive in reactor-size Stellarators"

Schaeublin R., *Report on EFDA task TW3-TTMS-006 del 3, EFDA Materials Meeting, Garching, Germany, 27 April 2004*, "Study of the influece of Ti additions in ODS F/M steels for fusion"

Schaeublin R., *Report on EFDA task TW3-TTMS-007 del 9, EFDA Materials Modelling Meeting, Paul Scherrer Institute, Switzerland, 22 June 2004*, "Strength of a distribution of nanoscale defects in Fe: a simulatin study"

Schaeublin R., *University of Alicante, Spain, 21 October 2004*, "Dislocation-defect interaction in iron"

Poli F., McGrath M., *HELIMAK, Fusion Research Center, University of Austin, Texas, USA, May 2004* , "TORPEX: A presentation"

Degeling A.W., Weisen H., Zabolotsky A., Duval B.P., Pitts R.A., Wischmeier M., Lavanchy P., Marmillod P., Pochon G., *HTPD Meeting, San Diego, USA, April 2004*, "AXUV bolometer and Lyman-alpha camera systems on the TCV tokamak"

Weisen H., Baluc N., *Dept. of Material Sciences, Warsaw Technical Univ., 14 September 2004* , "The Centre de Recherches en Physique des Plasmas"

APPENDIX C External activities of CRPP Staff during 2004

C.1 National and international committees and ad-hoc groups

MEMBERSHIP

K. Appert	Member of the EFDA Steering Committee Member of the CCE-FU committee
N. Baluc	Scientific and Technical Advisory Committee, Euratom Symposium on Fusion Technology Organising Committee IEA Annex II Executive Committee Task Coordinator of the Subproject entitled 'Radiation Resistant Materials' within the EXTREMAT integrated project (IP) of the 6th European Framework Program. Task Coordinator of the EURATOM Task TTMS-003 “Compatibility of Steels with Hydrogen and Liquids, within the Tritium Breeding and Materials Programme of EFDA” IEA Fusion Materials Agreement Executive Committee PhD Committee “Microstructures et mécanismes de déformation des alliages quasicristallins AlPdMn et AlCuFe deformés aux hautes et basses températures” Michael Texier, Université de Poitiers, Futuroscope-Chasseneuil Cedex, France.
P. Bruzzone	International Magnet Technology Conference Organising Committee EFDA, Magnet Expert Group GSI Magnet Advisory Board
W.A. Cooper	PhD Committee 'Global wavemodes of dissipative fluid models in strongly three dimensional plasmas: Calculation and Interpretation', Ben MacMillan, Research School of Physical Sciences and Engineering, Australian National University, Canberra, Australia.
J-L. Dorier	Coordinator for Dusty and Low Temperature Plasmas in the 31st EPS Conference Programme Committee, London 2004
A. Fasoli	Scientific and Technical Advisory Committee, Euratom ASDEX Upgrade Programme Committee, Germany Scientific Expert for Switzerland at Fusion Power Coordination Committee of the International Energy Agency International Tokamak Physics Activities: Steady-State Operation and Energetic Particles Topical Group Member of ad-hoc group of STAC for the monitoring of 2003 activities and 2005 work program of JET Member of ad-hoc group of STAC for assessment of the progress in Research and Development of Lower Hybrid Current Drive.
Ch. Hollenstein	Conseil scientifique du Département Science pour l'Ingénieur du CNRS Scientific council of the Institute of Surface Modifications at Leipzig (Wissenschaftsgemeinschaft Gottfried Wilhlem Leibniz) Expert for a "Sonderforschungsbereich-Projekt" of the Deutschen Forschungsgemeinschaft.
J.B. Lister	International Tokamak Physics Activities: MHD, Disruption and Control Topical Group EPS-13, Bern 2005, International Core Programme Committee 31st EPS Conference Programme Committee, London 2004 32nd EPS Conference Programme Committee, Tarragona 2005 International Scientific Advisory Committee and Local Organising Committee for ICALEPCS, Geneva 2005

C. Marinucci	CHATS, Scientific Programme Committee Applied Superconductivity Conference 2004, Committee Member
R.A. Pitts	International Tokamak Physics Activities: Diagnostics Topical Group Member of the EFDA Plasma Edge Task Force
O.Sauter	Scientific Committee of the 11th European Fusion Theory Conference
R. Schäublin	Member of the board of the Swiss Society for optics and microscopy
P. Spätig	Member of an ad hoc expert group to evaluate the IFMIF Comprehensive Design Report
M.Q. Tran	Electron Cyclotron Wave Task Area Leader Chairman of the Electron cyclotron Wave-Coordinating Committee Consultative Committee for the Euratom Specific Research and Training Programme in the field of Nuclear Energy, Fusion (CCE-FU) CCE-FU Special Working Group on "The accompanying programme" EFDA* Steering Committee, in his role as EFDA leader Scientific and Technical Advisory Committee, Euratom Chairman of the Ad-hoc Group for the Monitoring of the project W7-X Standing Committee of the International Symposium on Fusion Nuclear Technology Scientific Committee of the IAEA Technical Meeting on ECRH Physics and Technology for ITER Expert on the IAEA International Fusion Research Council Member of a PSI technical committee to evaluate research on fusion materials Chairman of the Fusion Staffing Committee created by the CCE-FU Member of the committee on Energy Research in the CEPF Member of the Steering Committee for the 2008 Fusion Energy Conference Member of the Accompanying Programme Committee for the European Fusion Programme Expert member of the Helmhotz Senate-Commission “Energy” representing “Fusion” research; Member of the strategic evaluation committee on “Fusion” research; Reviewer for the “Impuls und Vernetzungsfonds” of the Helmholtz Association
L. Villard	Scientific and Technical Advisory Committee, Euratom Conseil Scientifique du Département de Recherche sur la Fusion Contrôlée – CEA, France Chairman, Ad-Hoc Group for the assessement of an application for a Cost-Sharing Action by the University of Sofia, Bulgaria
H. Weisen	International Advisory Board of the IPP Prague, Czech Republic Member of the Expert Working Group on JET diagnostics

PARTICIPATION

B. Duval	ICALEPCS 2005 International Scientific Advisory Committee Remote Participation Users Group, EFDA-JET
C. Marinucci	ITER TFMC Test and Analysis Group
J.B. Lister	PhD Committee ”Safety factor profile identification on the Asdex upgrade tokamak using the motional Stark effet and inverse problem methodology” Marcus Foley, University College Cork, Ireland

* EFDA: European Fusion Development Agreement

Y.R. Martin	International Tokamak Physics Activity: Confinement Database and Modelling Topical Group
R.A. Pitts	International Tokamak Physics Activity: SOL and Divertor Topical Group

C.2 Editorial and society boards

Ch. Hollenstein	Vice President of the Swiss Vacuum Society Committee "Union Radio-Scientifique Internationale" Editorial Board of Plasma Chemistry and Plasma Processing
J.B. Lister	Chairman of the European Physical Society Plasma Physics Division Deputy Editor of Plasma Physics and Controlled Fusion
Y.R. Martin	Chairman of the Association Vaudoise des Chercheurs en Physique
P.J. Paris	Fusion Expo Consortium Committee EFDA Information Network "Fédération Romande de l'Energie" Committee Chairman of the "International Association of Specialists in Energy" (AISEN)
L. Sansonnens	Committee of the Swiss Physical Society, Responsible for Applied Physics
M.Q. Tran	Board of Editors of Nuclear Fusion

C.3 EPFL committees and commissions

N. Baluc	Commission Ecole Doctorale en Science et Génie des Matériaux
J-L. Dorier	Commission du Doctorat de la Section de Physique, FSB-EPFL
A. Fasoli	Commission d'Enseignement de la Section de Physique, FSB-EPFL
Ch. Guillemin	Assemblée d'Ecole, EPFL
J-Ph. Hogge	Commission du Doctorat de la Section de Physique, FSB-EPFL
B.Marlétaz	Conseil de la Faculté des Sciences de Base, EPFL
O. Sauter	Commission d'Informatique, FSB-EPFL
M.Q. Tran	Commission du Doctorat de la Section de Physique, FSB-EPFL Member of the "Comité de sélection pour le Prof. d'Energie et Directeur du Centre de l'Energie de l'EPFL"
T.M. Tran	Groupe de travail technique du Comité de Pilotage HPC/MPC, EPFL
L. Villard	Commission d'Enseignement de la Section de Physique, FSB-EPFL Commission Scientifique du 3ème Cycle de la Physique en Suisse Romande Groupe de travail technique HPC (High Performance Computing) – EPFL

APPENDIX D Lausanne Reports (LRP)

(see CRPP archives at http://crppwww.epfl.ch/archives)

Ballutaud J., *"Study of radio-frequency plasma deposition of amorphous silicon for the improvement of solar cell production",* LRP 781/04

Scavino E., Bakos J., Weisen H., and TCV Team, *"Effects of ECRH power and safety factor on laser blow-off injected impurity confinement in TCV",* LRP 782/04

Furno I., Carey C., Weisen H., *"A new method for the inversion of interferometry data using base functions derived from singular value decomposition of local measurements in tokamak plasmas",* LRP 783/04

Descoeudres A., Hollenstein Ch., Demellayer R., Waelder G., *"Optical emission spectroscopy of electrical discharge machining plasma",* LRP 784/04

Weisen H., Zabolotsky A., Garbet X., Mazon D., Zabeo L., Leggate H., Valovic M., Zastrow K.-D., and contributors to the JET-EFDA work programme, *"Shear dependence of particle pinch in JET L-mode plasmas",* LRP 785/04

Bottino A., *"Modelling of global electrostatic microinstabilities in tokamaks: effects of ExB flows and magnetic shear (Thèse EPFL 2938(04))",* LRP 786/04

Brunetti M., Grandgirard V., Sauter O., Vaclavik J, Villard L., *"A semi-Lagrangian code for nonlinear global simulations of electrostatic drift-kinetic ITG modes",* LRP 787/04

Howling A.A., Sansonnens L., Ballutaud J., Hollenstein Ch., Schmitt J.P.M., *"Non-uniform rf plasma potential due to edge asymmetry in large-area rf reactors",* LRP 788/04

Heguedues F., Bruetsch R., Oliver B, Marmy P., *"Fracture toughness and tensile properties of the titanium alloys Ti6A14V and Ti5Al2.5Sn before and after proton and neutron irradiatins at 150C (EFDA TASK TW1-TVV/titan and TW3-TVM-TICRFA: Titanium Alloys Irradiation Testing)",* LRP 789/04

Henderson M.A., Camenen Y., Coda S., Goodman T.P., Nikkola P., Pochelon A., Sauter O., and TCV Team, *"Rapid and localized eITB formation during shear inversion in fully non-inductive TCV discharges",* LRP 790/04

Henderson M., Chavan R., Sanchez F., *"Front steering ECCD launcher study for the ITER upper port",* LRP 791/04

Favez J.-Y., *"Enhancing the control of tokamaks via a continuous nonlinear control law (thèse EPFL 3034(2004))",* LRP 792/04

Nikkola P., *"The effect of electron transport on electron cyclotron current drive in tokamak plasmas (thèse EPFL 3048(2004))",* LRP 793/04

Sauter O., *"On the contribution of local current density to neoclassical tearing mode stabilisation",* LRP 794/04

EPS Participants, *"Papers presented at the EPS Plasma Physics Conference, London, June-July 2004",* LRP 795/04

Popovitch P., *"Low frequency electromagnetic wave propagation in 3D plasma configurations (thèse EPFL 3063(04))"*, LRP 796/04

Arnoux G., Alberti S., Porte L., Nelson-Melby E., Hogge J.-P., and TCV Team, *"Thrid harmonic X-mode absorption in a top-launch configuration on the TCV tokamak"*, LRP 797/04

Gindrat M., *"Characterization of supersonic low pressure plasma jets (Thèse EPFL 3120(2004))"*, LRP 798/04

APPENDIX E The basis of controlled fusion

E.1 Fusion as a sustainable energy source

Research into controlled fusion aims to demonstrate that it is a valid option for generating power in the long term future in an environmentally, politically and economically acceptable way. Controlled fusion is a process in which light nuclei fuse together to form heavier ones: during this process a very large amount of energy is released. For a fusion reactor it is planned to use the two isotopes of hydrogen: deuterium (D) and tritium (T), which fuse together much more readily than any other combination of light nuclei according to the following reaction:

$$D^2 + T^3 \rightarrow He^4 + n + 17.6MeV$$

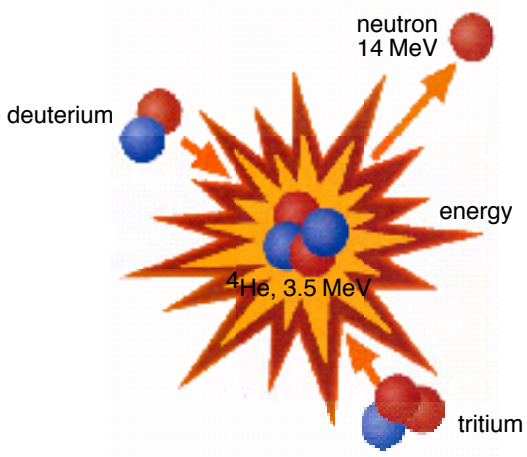

Fig. E.1 *Schematic of a fusion reaction between deuterium and tritium nuclei. The products are 3.5MeV ^4He, the common isotope of helium, and a 14MeV free neutron.*

The end products are helium and neutrons (n). The total energy liberated by fusing one gram of a 50:50% mixture of deuterium and tritium is 94000kWh, which is 10 million times more than from the same mass of oil. 80% of this energy is carried by the neutrons with an energy of 14MeV while the remaining 20% is carried by the helium nucleus. All this energy eventually becomes heat to be stored or converted by conventional means into electricity.

The temperature at which fusion reactions start to become significant are above a few tens of millions of degrees. For the D-T reaction, the optimal temperature is of the order of 70-200 million degrees. At such temperatures the D-T fuel is in the plasma state.

Deuterium is very abundant on the earth and can be extracted from water (0.034g/l). Tritium does not occur naturally, since its half-life is only 12.3 years, but it can be regenerated from lithium using the neutrons produced by the D-T fusion reactions. The two isotopes of natural lithium contribute to this breeding of tritium according to the reactions:

$$Li^6 + n \rightarrow He^4 + T^3 + 4.8MeV$$

$$Li^7 + n \rightarrow He^4 + T^3 + n - 2.5MeV$$

The relative abundance of the two lithium isotopes Li^6 and Li^7 are 7.4% and 92.6%, respectively. The known geological resources of lithium both in the earth and in the sea water are large enough to provide energy in an unlimited time.

E.2 Attractiveness of fusion as an energy source

The inherent advantages of fusion as an energy source are:

- The fuels are plentiful and their costs are negligible because of the enormous energy yield of the reaction;
- The end product of the reaction is helium, an inert gas;
- No chain reaction is possible; at any time only a very small amount of fuel is in the reacting chamber and any malfunction would cause an immediate drop of temperature and the reaction would stop;
- No after-heat problem can lead to thermal runaway;
- None of the materials required by a fusion power plant are subject to the provisions of the non-proliferation treaties.

Its further potential advantages are:

- Radioactivity of the reactor structure, caused by neutrons, can be minimised by careful selection of low-activation materials resulting in a manageable quantity of long lived radioactive waste;
- The release of tritium in normal operation can be kept to a very low level. The inventory of tritium in the breeding section of the reactor and on the site can be sufficiently small so that the worst possible accident could not lead to a harmful release to the environment requiring evacuation of the nearby population.

APPENDIX F Glossary

A general purpose glossary for the field of controlled fusion and plasma physics is provided in the CRPP Annual Report every two years. This report is an even year and the glossary is therefore not provided.

APPENDIX G Sources of Financial Support

The work carried out at the CRPP and presented in this annual report was financed from several sources. The major financial support is derived from the Ecole Polytechnique Fédérale de Lausanne (EPFL), EURATOM, the Paul Scherrer Institute (PSI), which hosts the supraconductivity and materials science activities, and the Swiss National Science Foundation. Other public and private organisations which contributed funding for our research in 2003 include, in alphabetical order: Balzers Tribology, Charmilles SA, the Swiss Commission pour la Technologie et l'Innovation (CTI), Fischer-Connectors, the Swiss Office Fédéral de l'Education et de la Science (OFES), Sulzer Metco AG, Tetra Pak SA and Unaxis Balzers.

The CRPP is the Host of a Euratom Fellowship, Dr. M. McGrath entitled *"Nonlinear structures in turbulent transport plasmas and methods of control".*

The Fonds National Suisse de la Recherche Scientifique provides a grant during this period for *"Basic plasma physics for fusion energy research",* which partly finances TORPEX and the CRPP-JET collaboration on Alfven waves and fast particles. Prof. A. Fasoli is supported by this grant as "Professeur Boursier du Fonds National".